Interpretation of UHF Signals Produced by Partial Discharges in Oil-filled Power Transformers

Thesis presented for the degree of Doctor of Philosophy in Electronic & Electrical Engineering at the University of Strathclyde.

Gerard Patrick Cleary, MEng, MIEE

May 2005

Department of Electronic & Electrical Engineering
University of Strathclyde
Glasgow
UK

Declaration

The copyright of this thesis belongs to the author under the terms of the United Kingdom Copyright Acts as qualified by University of Strathclyde Regulation 3.51. Due acknowledgements must always be made of the use of any material contained in, or derived from, this thesis.

ABSTRACT

Oil-insulated power transformers are key components of the electrical transmissi network. Knowing the state of their insulation is therefore of considerable interest utilities. Failure in transformers often occurs as a result of electrical breakdown in t insulation materials. Such breakdowns may occur following insulation damage caus over a substantial period of time by the cumulative adverse effects of partial dischar (PD) activity. Recognition of PD in power transformers in important because ear detection can allow utilities to take appropriate preventative measures in order that cost failures do not occur.

In this work, a range of on-line partial discharge (PD) measurement techniques a reviewed. Ultra high frequency (UHF) and measurements based on the Internatior Electro-technical Commission (IEC) standard 60270 are considered to be the mc suitable. UHF measurements have the advantage that PD can be located using time flight measurements, while IEC 60270-based measurements can be quantified in terms pC.

A test cell is designed, and PD current pulses are measured when the insulating oil at t tip of a sharp, conducting protrusion breaks down. Current pulses are recorded using tv different measurement circuits, and different pulse shapes are observed. The experiments are of fundamental significance because UHF signals are only excited wh discharges occur on timescales of around 1 ns or less. Results demonstrate that t

durations of current pulses in oil can be sufficiently short to cause the excitation of UH signals.

Characteristics of PD generated in air, new transformer oil and used transformer oil a compared. PD current pulses are measured simultaneously with both IEC 60270-bas and UHF measurements systems. Since IEC 60270-based and UHF measurement syster operate on very different principles their responses to PD current pulses of knov magnitude provides a useful basis for comparing the performance of both systems.

A range of insulation defects that would cause concern in an operational pow transformer are then investigated. Radiated UHF signals are measured simultaneous using two broadband electric field sensors. The spectral content and energy of rati measured using each sensor during both half cycles are shown to be useful methods assist with the understanding of discharge behaviour.

UHF PD signals are also measured in a phase-resolved form, and these are analysed ways that provide evidence of the physical differences between insulation defects. Fie tests are carried out on a 1000 MVA, 400 kV/ 275 kV power transformer, and resu demonstrate that the UHF measurement technique is a very promising approach for I monitoring. The research contributes to the knowledge base required for the developme of continuous monitoring systems for partial discharge and arcing in oil-filled pow transformers.

4. COMPARISON OF CONVENTIONAL AND UHF MEASUREMENTS

1. INTRODUCTION

1.1 Power Transformers: An Overview

Electrical utilities use transformers to step the high voltages generated at power stations down to levels which can be used by industrial and domestic consumers. In its most basic form, a transformer consists of two copper windings and a laminated steel magnetic core. The primary winding is connected to an AC power supply and the secondary is connected to a load. If a tap changer is part of the design then the voltage supplied to the load can be varied to suit the electrical demand. For a three-phase system, the transformer consists of three sets of windings together with a single magnetic core. The transformer must also have an insulation system, sets of leads and bushings to allow connection of the different circuits and a tank to contain the insulating medium (SF_6 gas or oil).

The main components of a transformer are shown in Figure 1.1. The magnetic circuit consists of three vertically mounted magnetic cores (limbs) which are connected using upper and lower horizontal sections of laminated steel (yokes). A set of primary and secondary windings are wrapped around each limb, the LV winding (secondary) is usually mounted between the HV winding (primary) and the core. Each of the winding sets and the magnetic circuit are clamped together to minimise vibrations when the system is energised at 50 Hz [1].

The LV winding is normally wrapped around a pressboard cylinder. This provides mechanical strength for the construction and can provide a cooling duct for the oil.

The windings are usually insulated using Kraft paper and are separated using cellulose spacers to help prevent short circuits from developing between adjacent turns.

Interface barriers are usually positioned between adjacent phases and can act as cooling ducts for the oil. The oil in a transformer will be circulated by natural convention, but pumps might also be used to force cooling during periods of high demand. External cooler banks can be used for cooling purposes.

The HV winding is usually mounted on the outside and this is more suitable for carrying out tap changing operations. The HV windings of a step-down transformer have more turns and carry less current than the LV windings and so the tap changer contacts will '*break*' a comparably smaller current. The arc which is drawn is less severe and so the procedure is safer and oil contamination is minimised.

The HV and LV bushings are usually positioned on the tank lid. These allow the windings to be connected to the power grid. The HV bushings are usually larger than the LV bushings due to insulation requirements. A neutral bushing might also be present but this is dependent on the vector grouping of the transformer.

Figure 1.1 shows inspection hatches located on the tank lid. These allow access for carrying out post-fault investigations and routine maintenance. However, as will be described in Section 1.3.3.2, they can also provide a convenient platform for mounting dielectric windows for UHF PD monitoring.

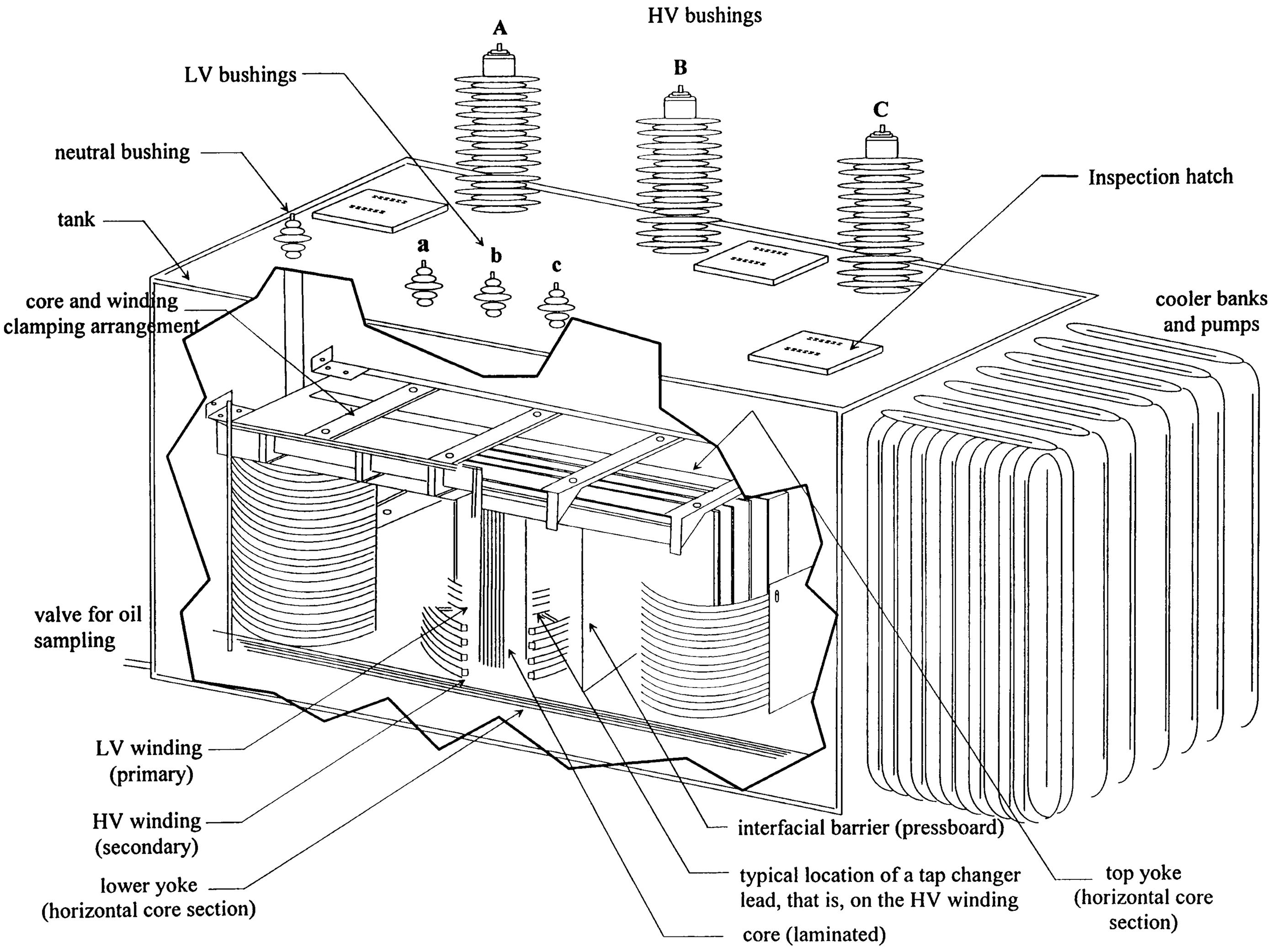

Figure 1.1 A simplified drawing showing the main components of a power transformer

1.2 Oil-filled Power Transformers and Partial Discharge

It is generally accepted that partial discharge (PD) occurs prior to the breakdown of electrical plant, and so its early detection is important to prevent catastrophic failure [2,3]. PD occurs when the electric field exceeds the dielectric strength of the insulation within a localised volume, and may be caused by temporary over-voltages, weaknesses in the insulation system from manufacture or ageing effects over the plant lifetime. The term partial discharge describes the condition when the ionised discharge path only partially bridges the gap between two conductors [2]. During its infancy, PD may be quite small, however it is by nature a damaging process and can cause degradation and erosion of materials leading to the eventual breakdown of the transformer [4,5]. Effective on-line monitoring of power transformers has the potential to reduce the incidence of catastrophic failure, as well as the financial, environmental and safety issues that may ensue [6,7].

In the most serious of cases, condition monitoring may help to prevent unfortunate incidents such as that shown in Figure 1.2 [2].

Figure 1.2 Example of a catastrophic transformer failure (photograph courtesy of Lee Lane).

In this chapter, a variety of defects that are known to cause undesirable electrical discharge activity in operational power transformers are described. As shown in Figure 1.3, protrusions may exist on HV conductors [8]. These may be introduced at manufacture stage or as a result of conducting flexing over a substantial period of time.

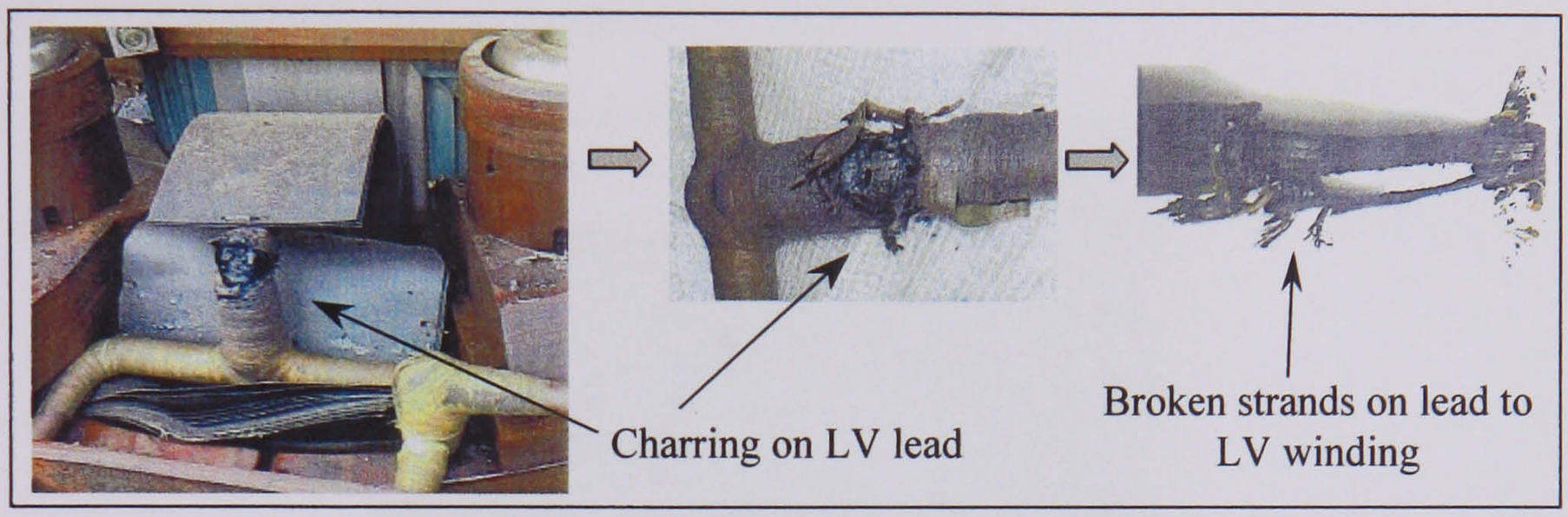

Figure 1.3 Example of damaged transformer components during disassembly.

During normal operation, the windings of a transformer will vibrate at twice the power frequency, but eventually this can result in fasteners becoming loose. Similarly, stress shields may not be properly bonded and this can result in loose connections. Figure 1.4 shows an example of free metallic particles that were found to lie on the upper yoke section of the magnetic circuit of a ScottishPower transformer. These may have been introduced by the failure of a mechanical component [9], or as a result of degradation between tap changer contacts. If the local electric field at these defects exceeds the breakdown strength of the insulating medium within a localised volume then PD will occur.

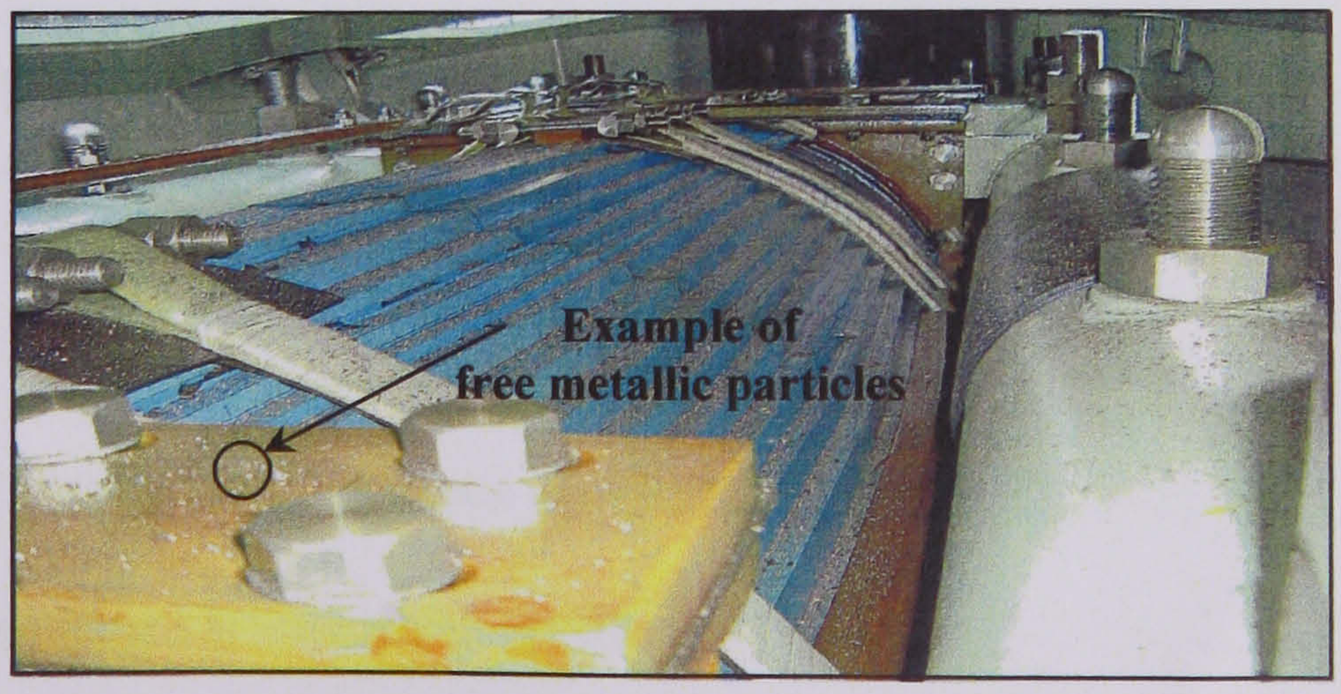

Figure 1.4 Example of free metallic particles.

It is generally accepted that increased moisture content has an adverse affect on the breakdown strength of oil and contributes to the deterioration of the paper/pressboard insulation [3,10]. Excessive moisture levels may occur due to degradation of the tank seals or the breakdown of cellulose [11, 12 and 13]. The presence of free moisture can lead to streaming electrification and surface discharges on cellulose surfaces [14]. An example of damaged cellulose is shown in Figure 1.5 [15].

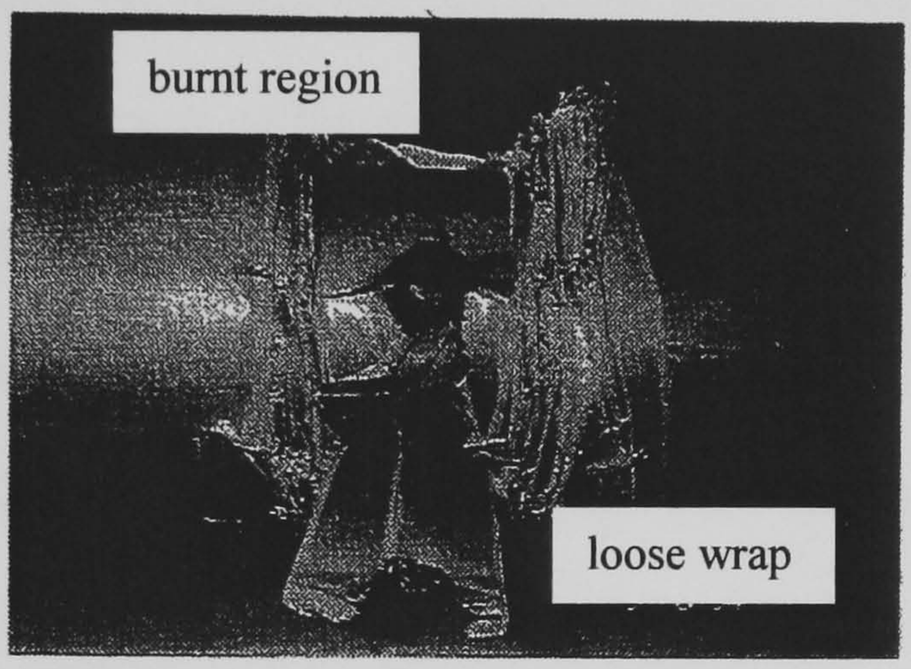

Figure 1.5 Example of damaged cellulose (photograph courtesy of Edgar Robles).

Although the failure rate of transformers is less than 1% in the UK, most of the units have been in service for more than 20 years [16]. These units were designed and manufactured using the best available techniques and materials at the time, but in comparison with those being manufactured and designed today are less efficient. Many of these existing transformers are approaching or have exceeded their predicted lifetime, but are still required to operate continuously. Therefore, the continuous monitoring of the condition of their insulation should be of considerable interest to utilities.

Several post-fault investigations have demonstrated that the aforementioned defect sources caused undesirable electrical discharge activity [16]. Although, PD tests are usually carried out on transformers at manufacture stage, it is not common practice to

carry out such tests in the field. However, due to an ageing transformer population there is a requirement for PD measurement systems in the field to assess insulation conditions.

It is generally accepted that the UHF technique is effective for continuous remote monitoring of gas-insulated substations (GIS) [17,18]. In a GIS, radiated UHF PD signals propagate along the busbar and can be extracted using UHF sensors. In order to provide adequate coverage of the complete GIS, sensors are fitted approximately 20 m apart. The UHF technique allows defects such as protrusions, particles and surface discharges to be detected [17,18]. The research described in this thesis is carried out to establish the applicability of the UHF technique for detecting PD in power transformers [2,8].

1.3 Partial Discharge Detection Techniques

1.3.1 Partial discharge

When the electric field exceeds the dielectric strength of an insulating medium ionisation will occur [19,20]. When electrons are liberated by ionisation they are accelerated resulting in a flow of electric current [21]. This current is quenched once the local electric field falls below the level required to sustain further ionisation [22,23].

A PD is therefore a current pulse that flows in what is normally an insulating medium [21]. Since PD can cause degradation in an insulating medium it can be detected using chemical techniques [24,25]. PD also causes the liberation of electrons and so it can be detected indirectly using optical measurements [20]. In addition, acoustic signals are generated by the rapid thermal expansion and contraction of the discharge channel at the PD site and so acoustic measurements can also be used for its detection [26].

PD causes the flow of current pulses that can be detected using an external measurement circuit. Discharge magnitudes can be quantified in terms of charge, usually in the pC or nC range [21]. When PD occurs on timescales of around one nanosecond or less, electromagnetic waves in the UHF range (300 – 3000 MHz) are excited [27,28].

This chapter describes a variety of measurement systems that exploit these fundamental physical and chemical processes to allow the detection of PD.

1.3.2 Non-electrical methods of PD detection

1.3.2.1 Dissolved gas analysis

Chemical techniques are at present the most commonly employed method for determining the state of oil insulation in operational power transformers, and have the advantage that measurement of chemical decomposition is not affected by spurious events such as electrical interference.

Gases are produced as a result of oil degradation at elevated temperatures from faults such as: overheated areas of the windings; bad connections that have high resistances; circulating core currents; and PDs and electrical arcing. The principal gases considered are hydrogen (H_2), methane (CH_4), ethane (C_2H_6), ethylene (C_2H_4), acetylene (C_2H_2), carbon monoxide (CO) and carbon dioxide (CO_2) [25,29].

Traditionally, dissolved gas analysis (DGA) has relied on oil samples being collected at intervals of typically 6 or 12 months. These are passed through a chromatograph in a laboratory to provide an indication of the relative percentages of gases present within the oil sample. More recently, on-line gas sensors such as Hydran units have been used to continuously monitor the oil insulation [30].

The relative concentrations of dissolved gases can be related to fault type and the rate of gas generation can be indicative of fault severity [31]. Interpretation techniques are outlined in the IEC 599 document, '*Mineral oil-impregnated electrical equipment in service – guide to the interpretation of dissolved and free gases analysis*'. The types of fault that can be identified are PD, low energy discharges, high-energy discharges and thermal faults [24]. The IEC 599 document serves as a guide for using Rodgers ratios and the Duval triangle [24,31,32].

Figures 1.6 and 1.7 shows how the concentration of gases can be related to fault type using Rodgers ratios and the Duval triangle methods respectively. With regard to the Rodgers ratios method, a particular DGA sample is analysed by plotting the relative concentrations of C_2H_2/C_2H_4, CH_4/H_2 and C_2H_4/C_2H_6 on a three-dimensional grid. As shown in Figure 1.6, different regions of the grid correspond to different fault types. The Duval triangle method also provides a graphical means to relate dissolved gas concentrations to fault type. The relative concentrations of CH_4, C_2H_4 and C_2H_2 are calculated and a perpendicular line is drawn from each axis at the appropriate position. The position at which the lines intercept on the triangle is marked and the corresponding fault type is found. However, the Rodgers ratio method and the Duval triangle method can lead to different classifications of a particular fault type, and so DGA can sometimes give inconclusive results. Since DGA databases can contain large amounts of data, intelligent software techniques have been developed to assist with the interpretation of measurements [33,34,35].

Before they are detected, dissolved gases must diffuse through the insulation from the discharge site to the measurement region and so a considerable time may pass between discharge inception and gas detection [36]. Gases may be accumulated from several different sources, and so discrimination of separate sources can be difficult. In addition, DGA methods are not suitable for defect localisation and are considered too insensitive for general PD monitoring.

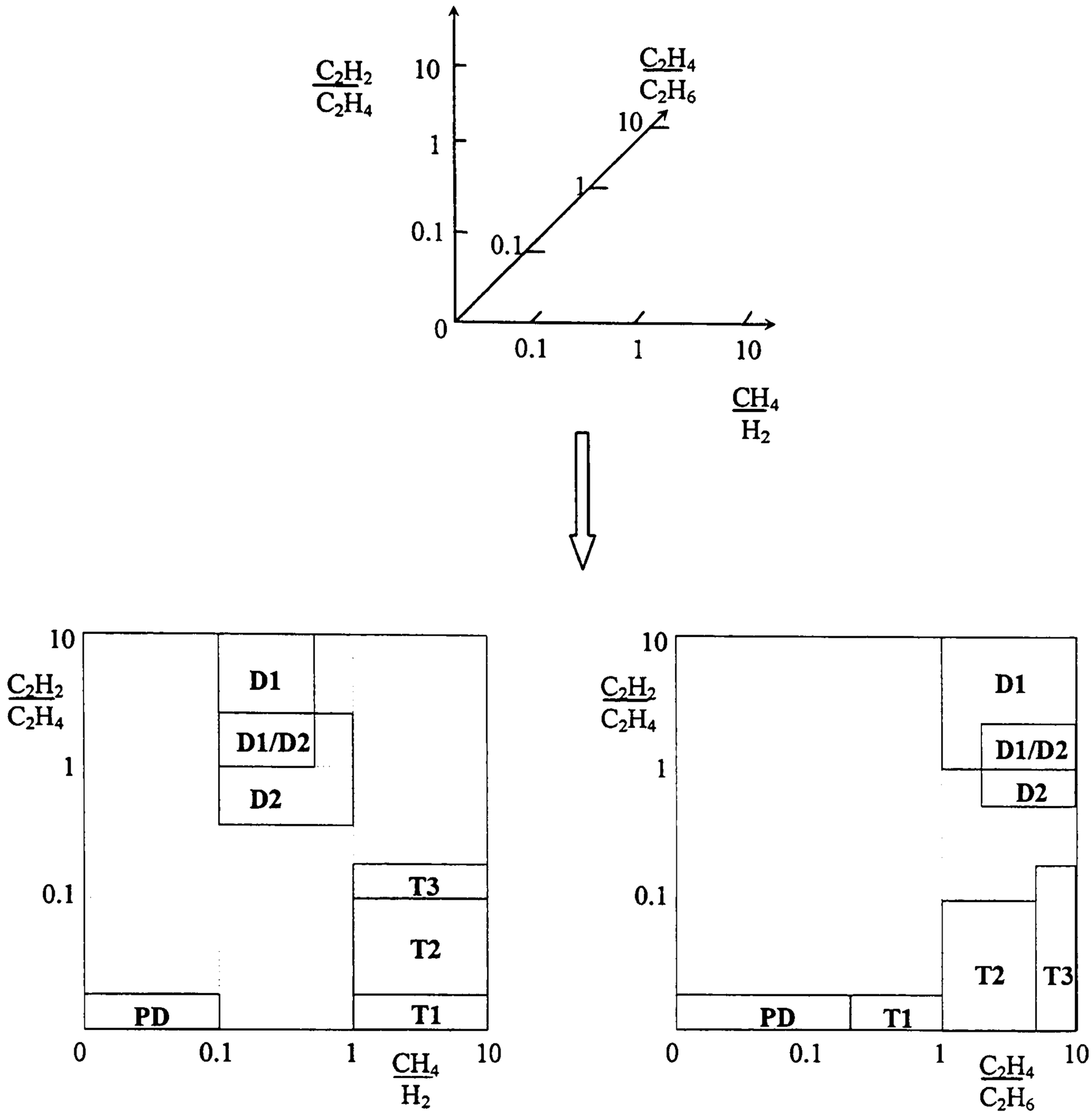

PD: Partial discharges
D1: Discharges of low energy
D2: Discharges of high energy
T1: Thermal fault, $t < 300^{\circ}C$
T2: Thermal fault, $300^{\circ}C < t < 700^{\circ}C$
T3: Thermal fault, $t > 700^{\circ}C$

The axis are limited to values of 10 for clarity, however, these can extend to unlimited values. The parameter t denotes temperate.

Figure 1.6 Graphical representation of DGA concentrations using the Rodgers ratio method.

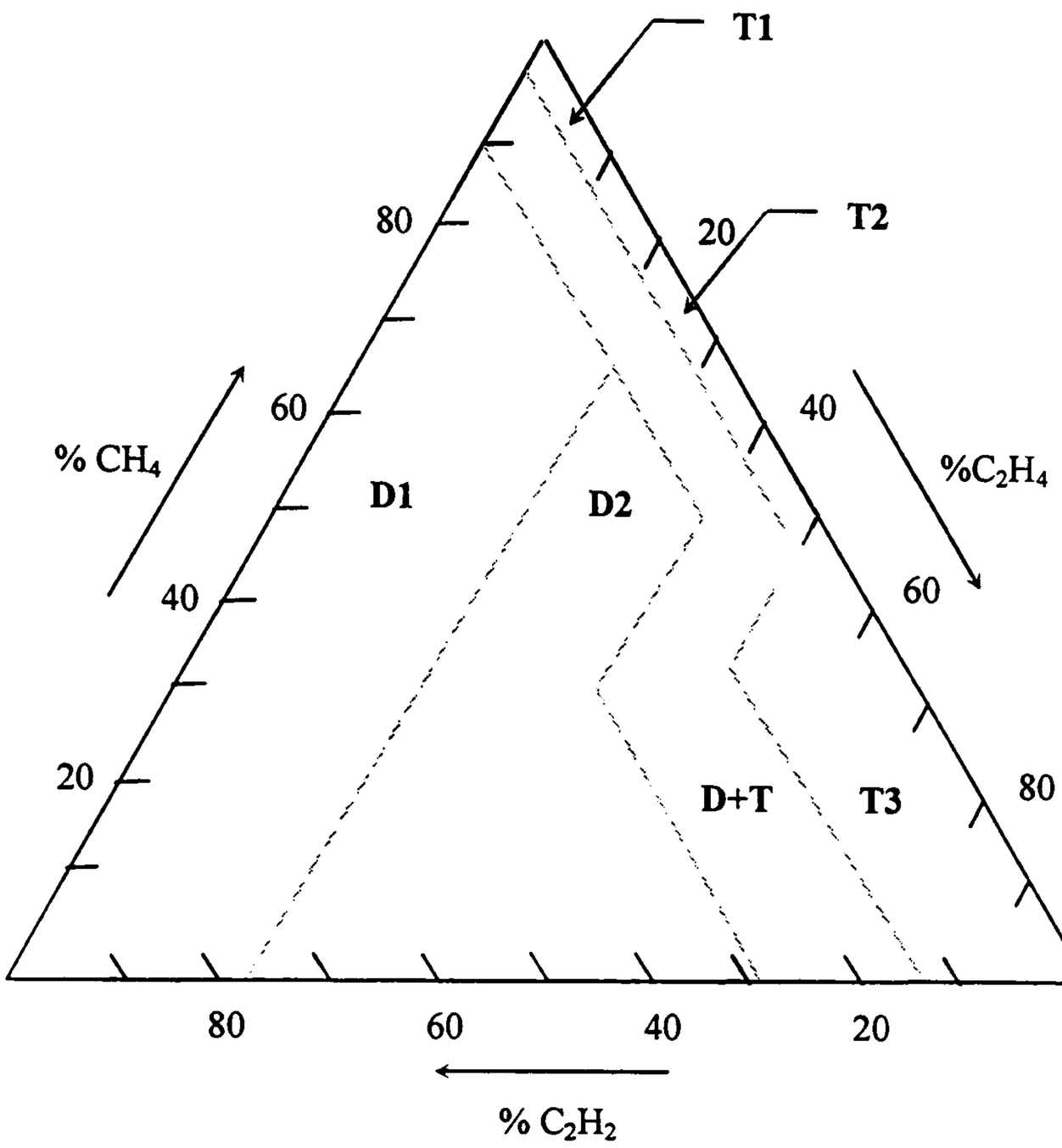

$$\% C_2H_2 = \frac{100x}{x+y+z} \quad \text{for } x = [C_2H_2] \text{ in micro litres per litre}$$

$$\% C_2H_4 = \frac{100y}{x+y+z} \quad \text{for } y = [C_2H_4] \text{ in micro litres per litre}$$

$$\% CH_4 = \frac{100z}{x+y+z} \quad \text{for } z = [CH_4] \text{ in micro litres per litre}$$

PD: Partial discharges
D1: Discharges of low energy
D2: Discharges of high energy
T1: Thermal fault, $t < 300$ °C
T2: Thermal fault, 300 °C $< t <$ 700 °C
T3: Thermal fault, $t >$ 700 °C

Limits of zones				
PD	98% CH_4			
D1	23% C_2H_4	13% C_2H_2		
D2	23% C_2H_4	13%C_2H_2	38% C_2H_4	29% C_2H_2
T1	4% C_2H_2	10%C_2H_4		
T2	4%C_2H_2	10%C_2H_4	50%C_2H_4	
T3	15%C_2H_2	50%C_2H_4		

Figure 1.7 Graphical representation of DGA concentrations using the Duval triangle method.

1.3.2.2 Furfuraldehyde analysis

Windings in a power transformer are usually insulated using Kraft paper. During normal operation of a transformer, the winding temperature will increase. As the temperature of the windings increases, the cellulose polymers in the Kraft paper will break down [3,37]. This has an irreversible effect on the mechanical and insulating properties of the cellulose material, so that the transformer is more susceptible to failure.

The degradation of cellulose material results in the release of furfuraldehyde (FFA) into the oil. The concentration of FFA can be used to provide an indication of the condition of the paper in terms of its degree of polymerisation, and the rate of change of FFA concentration can be related to the rate of ageing of the paper. These parameters are of interest because increased concentrations of FFA might be an indication that a transformer is reaching the end of its life.

The concentration of FFA in oil can be measured using high-performance liquid chromatography (HPLC) techniques or by chemical analysis in a laboratory remote from the transformer. Recently, novel solid-state opto-electronic sensors have been developed to allow the measurement of FFA fluorescence in oil to concentrations as low as 0.1 ppm [38,39]. The principal advantage of this technique is that the optoelectronic device could be utilised in a portable device and mounted on a transformer for continuous monitoring. The disadvantage is that such devices have not yet been extensively tested on-line, and only faults involving cellulose material can be identified.

1.3.2.3 Acoustic monitoring

Acoustic signals are generated by the rapid thermal expansion and contraction of the discharge channel. PD can result in a mechanical shock wave that can propagate through the tank. In an oil-filled power transformer, acoustic signals can have a wide spectrum extending from the audible range to ultrasonic frequencies in excess of 400 kHz [40]. Acoustic techniques have been used extensively to locate defects in operational power transformers. The advantage of this technique is that sensors are non-intrusive and offer some immunity to electromagnetic interference (EMI) [40,41].

The propagation of acoustic signals can be modelled if the internal geometry of the transformer is known. This typically involves dividing the transformer geometry into sub-modules, and analysing the propagation characteristics of the acoustic wave [42,43]. However, the complicated structure of a power transformer results in a multitude of different acoustic impedances, and so the path between the PD source and the sensor is often complex. The sensitivity of PD detection is affected by the geometric spreading of wavefronts, the division of waves among multiple paths, and propagation losses due to material absorption [44,45 and 46].

The propagation delay between the PD and reception at an acoustic sensor can represent a significant phase shift relative to the 20 ms (at 50 Hz) power cycle. Therefore, interpretation and classification of discharge activity can be difficult using phase-resolved measurements. In addition, acoustic techniques are not ideal for remote continuous monitoring because many sensor positions are required for maximum sensitivity [47].

1.3.3 Electrical methods of partial discharge detection

1.3.3.1 IEC 60270-based measurements

The IEC Publication 60270 [21] describes the principles of detecting PD using conventional electrical measurement circuits. The main advantage of this technique is that PD measurements can be calibrated in terms of charge, usually in pC. IEC 60270-based systems are commonly used for measuring PD under laboratory conditions [48], or for testing power transformers at manufacture stage [8].

Figure 1.8 shows a circuit representation that allows PD to be measured at the bushing tap of a transformer in accordance with IEC 60270 specification [21,49]. The principles of the IEC 60270-based method are explained further in Section 2.4.2.

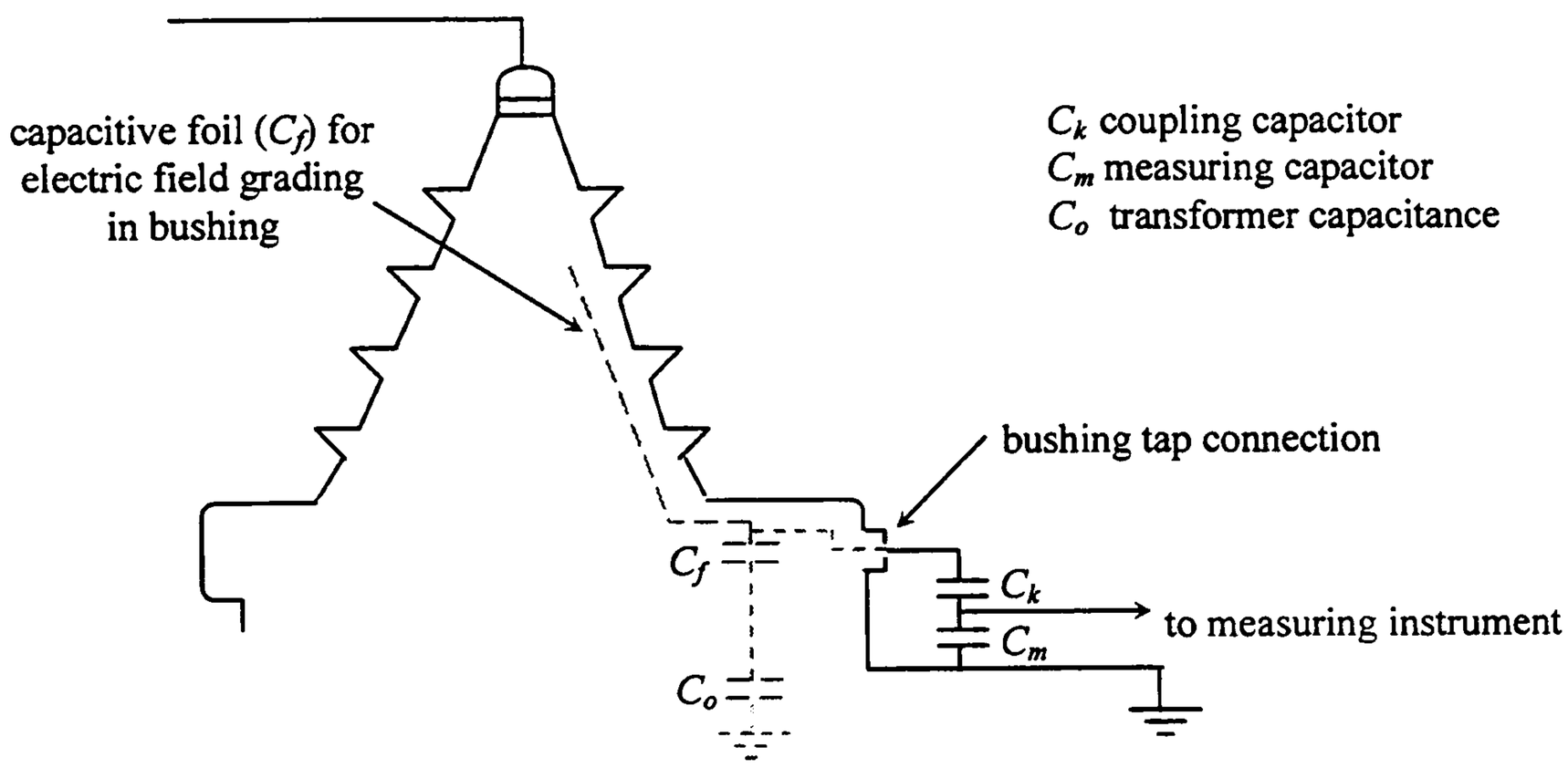

Figure 1.8 Schematic diagram of a bushing tap connection.

Rogowski coils can also be used to measure PD at the bushing tap [21,50], as shown in Figure 1.9. The Rogowski method does not require direct electrical contact and is therefore safer, but the method is less sensitive than the bushing tap method.

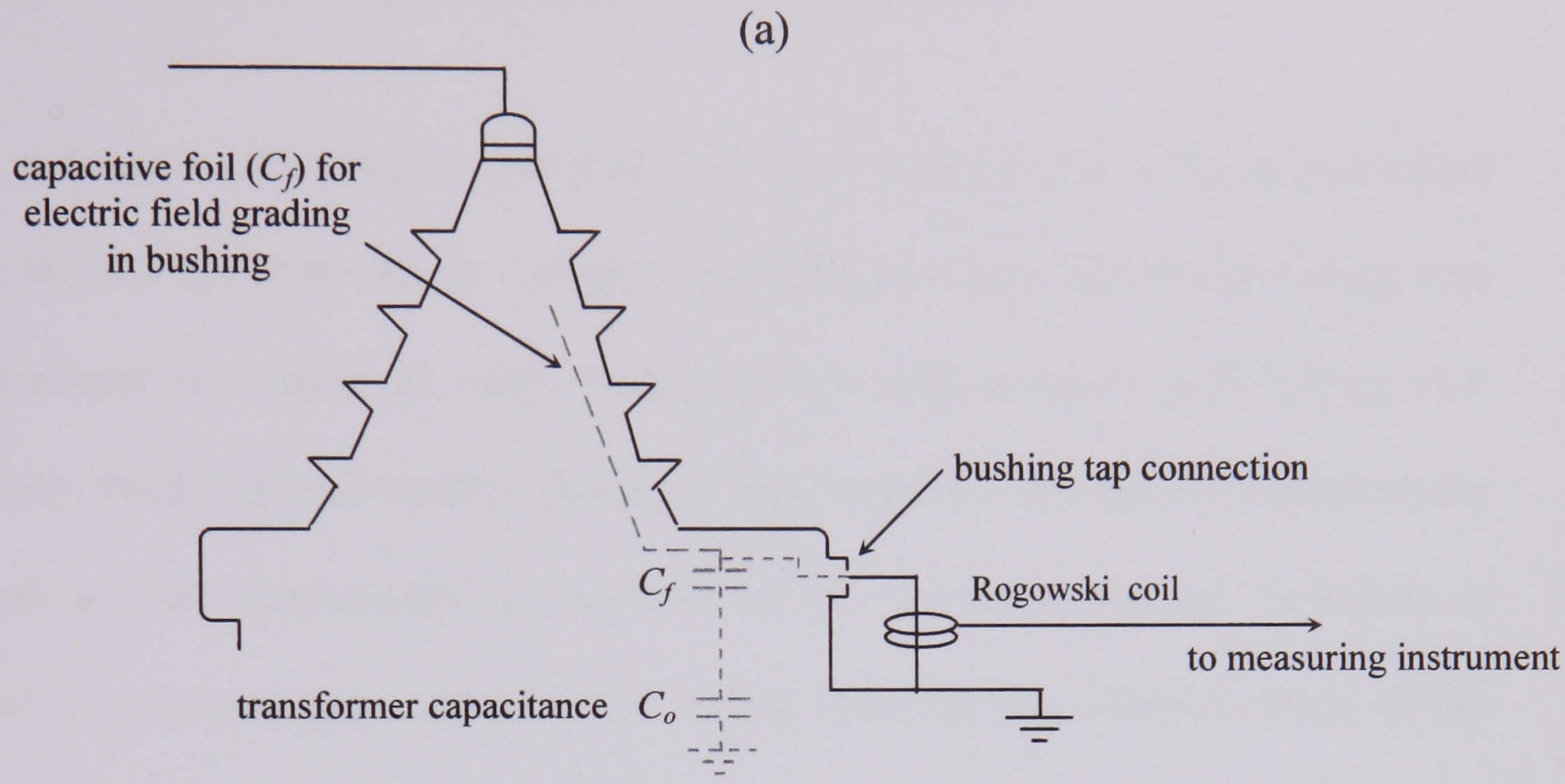

Figure 1.9 Rogowski coil measurement system, (a) schematic circuit and (b) installation (photograph courtesy of Zhongdong Wang).

Figure 1.10 shows a circuit schematic for measuring PD at the (resistively) earthed point of a star-connected transformer [50]. On the other hand, Figure 1.11 shows a convenient method that allows PD to be measured using three Rogowski coils. These are mounted externally on a set of neutral bushing terminals.

These techniques are based on the principle that a voltage will develop across the neutral resistor if PD occurs on a single phase. The technique has the advantage that measurements are made at earth potential, but measurements suffer from low sensitivity. Faults such as surface flashover may cause the potential at measurement terminals to rise momentarily to hundreds of kV, so that additional protection is required. A common approach is to use optical links for the interconnection of the coupling device and the measuring instrument [51,52,53].

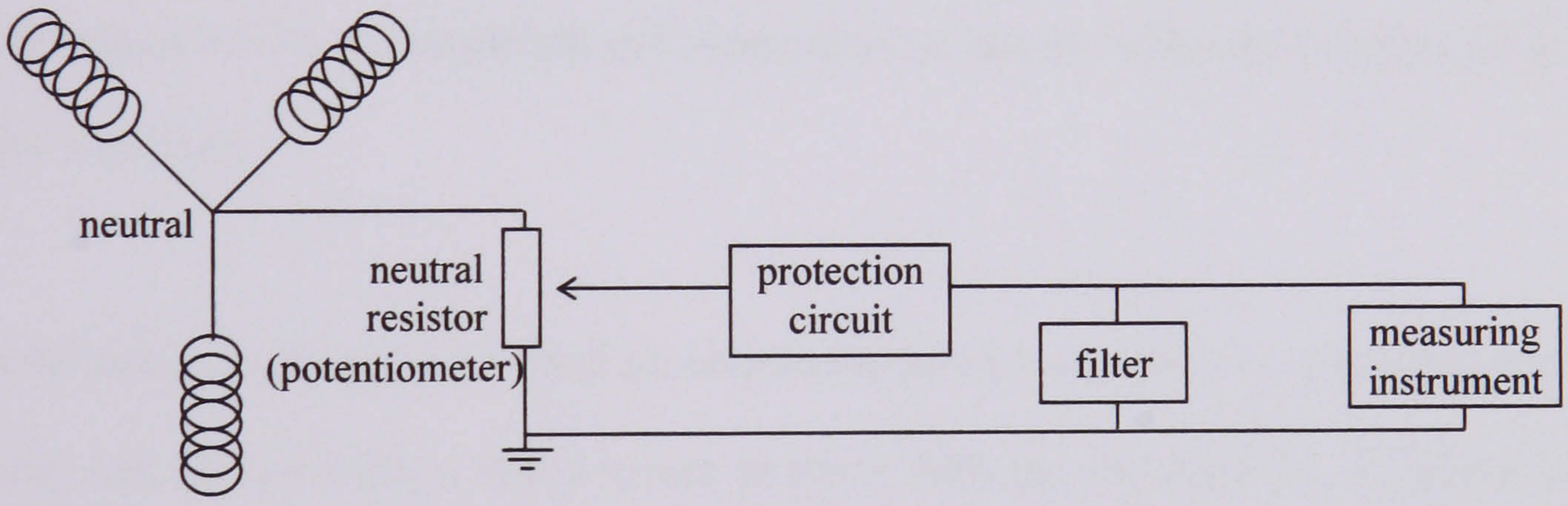

Figure 1.10 Schematic of neutral terminal

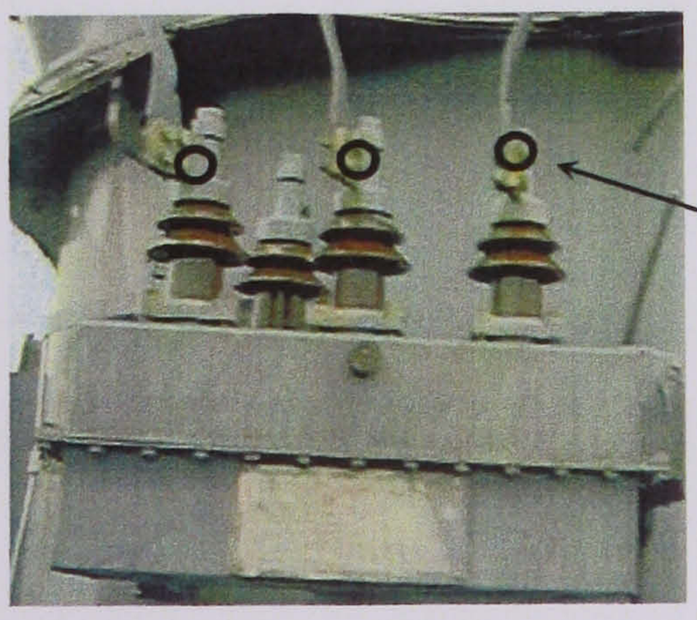

Figure 1.11 Measurement of PD at neutral terminals using Rogowski coils

The detection of PD using electrical techniques involves the use of either narrow-band or wide-band measurement systems [54,55]. In accordance with the IEC 60270 specification, a narrow-band measurement bandwidth is defined between 9 kHz and 30 kHz, and with a centre frequency up to 1 MHz [21]. Narrow-band techniques can have the advantage of increased sensitivity and noise rejection. However, the technique is inherently bandwidth limited, discharge location can be difficult, and measurements are generally only carried out 'off-line' [56].

In the case of wide-band techniques, the location of a PD source on a winding can be found by analysing the shapes of the measured current pulses [56]. For such a defect, current pulses must propagate through the distributed impedance system of the windings to get to a detector [57]. If the internal geometry of the transformer is known then the transfer function of the propagation path can be determined. This allows pulse shapes to be reconstructed and measurements can be calibrated in terms of pC [58,59 and 60].

Both narrow-band and wide-band measurements can be recorded in a phase-resolved form, and this provides a useful means to assist with the interpretation of discharge behaviour [61]. IEC 60270-based measurements are commonly carried out at manufacture stage because sensitive PD measurements can be carried out in laboratories that are shielded from EMI. However, in substation environments, the sensitivity of electrical PD measurements is reduced because of telecommunication signals and disturbances from power electronic devices [46]. Filtering methods are often required to obtain adequate sensitivity to PD [46,62,63].

1.3.3.2 UHF measurements

The UHF technique involves detecting electromagnetic waves in the band 300 MHz – 3000 MHz which are excited by PD pulses [64,65]. UHF measurement systems have the advantage that defects can be located and classified.

The main parts of a UHF monitoring system for locating defects are shown in Figure 1.12. By performing time-of-flight measurements, the location of a PD source can be found. This involves measuring the time difference (Δt) between UHF signals arriving at two sensors, and calculating the distance of the PD source from each sensor [66,67]. It is preferable to make measurements in the UHF range because the relative intensity of external air corona falls rapidly with increasing frequency.

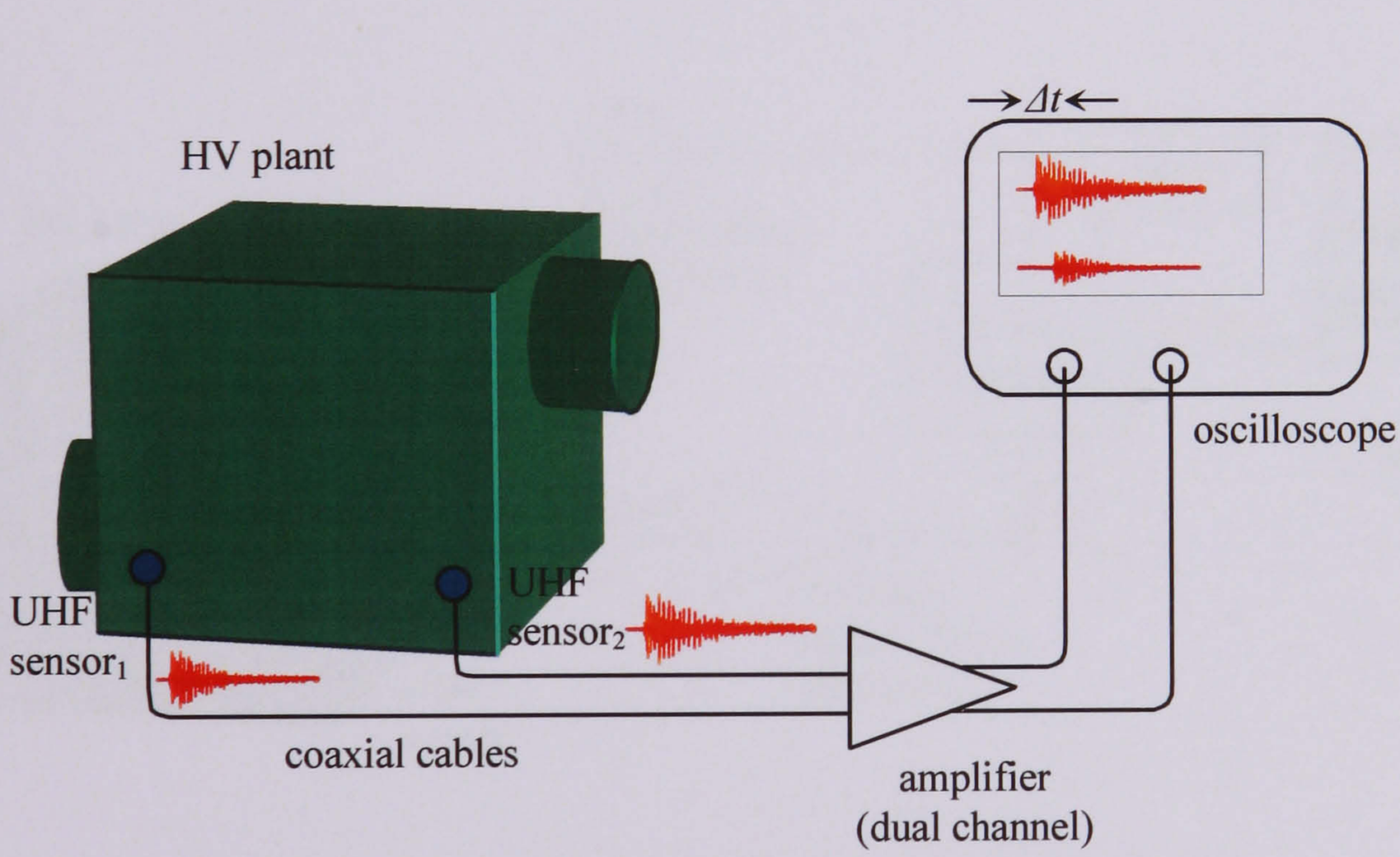

Figure 1.12 Overview of a UHF PD monitoring system for locating defects.

For defect classification, UHF PD signals are generally measured in 'phase resolved' form. An overview of such a measuring system is shown in Figure 1.13. Signals from one or more sensors are filtered, amplified and detected using hardware prior to being digitized. A phase signal derived from the power frequency waveform provides a reference for synchronising UHF PD signals. Each PD pulse recorded is placed within a data framework and associated with a particular time and 'point-on-wave'.

In contrast with acoustic PD detection, the velocity of electromagnetic waves in oil does not represent a significant delay relative to the duration of the power cycle. This property allows phase-resolved measurements to be used for interpreting PD activity [68,69,70 and 71]. These measurements can be analysed to provide information on whether PD is becoming more severe or is changing in character.

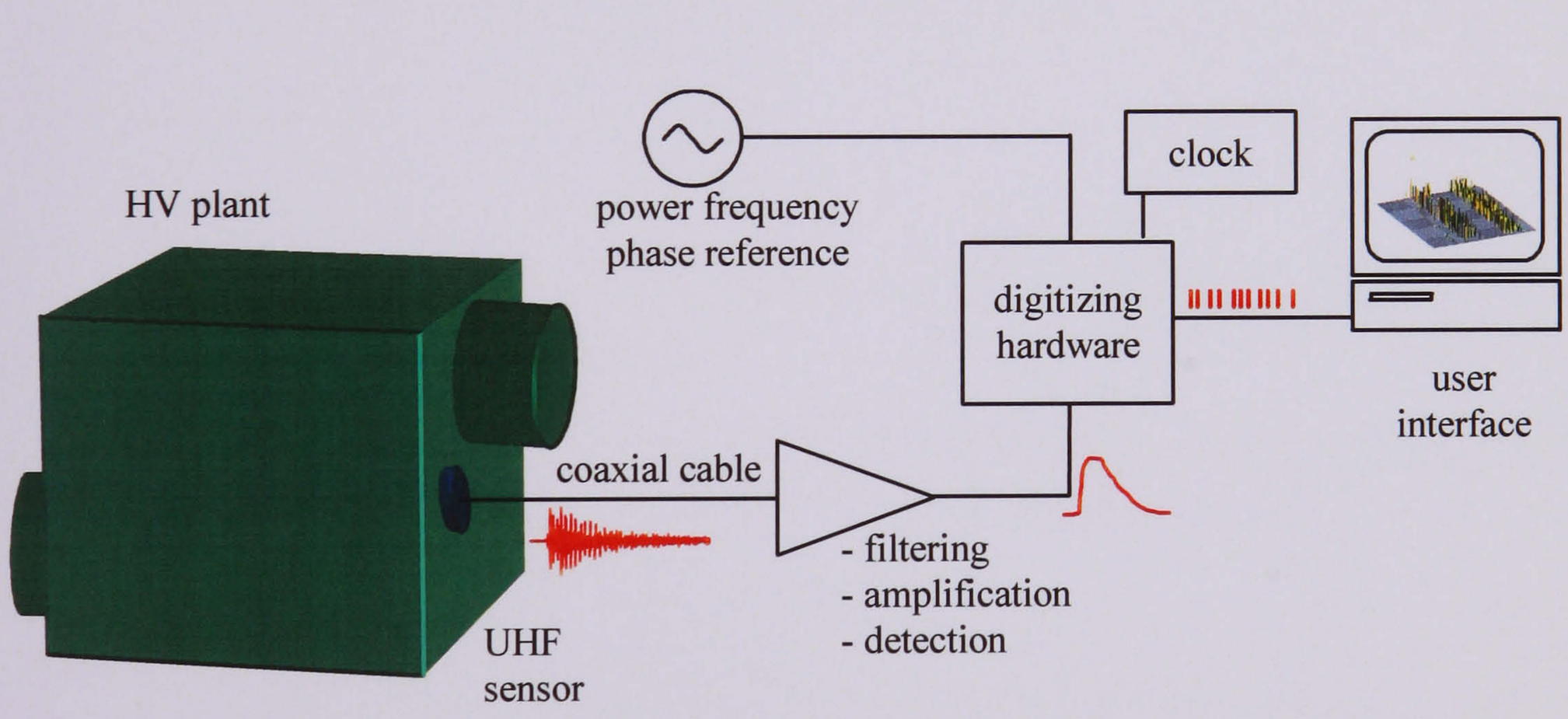

Figure 1.13 Overview of a UHF PD monitoring system for locating defects.

In this thesis, the UHF measurement technique is investigated for the detection of PD in oil-filled power transformers. In a preliminary laboratory experiment by Judd [28], it was reported that PD occurring in insulating transformer oil caused the excitation of UHF signals. A 'spark plug' was immersed in oil and radiated electromagnetic (EM) signals were found to have frequency content up to at least 1.5 GHz.

Based on the success of this experiment, two UHF sensors were designed and retrofitted to hatches at the top of a ScottishPower transformer (SGT4 at Neilston substation) [72]. UHF signals were detected while the transformer was re-energised and returned to full load. This confirmed that PD occurring in a power transformer could be detecting using the UHF technique. Rutgers et al [73,74 and 75] carried out similar investigations, and also concluded that the UHF technique should be considered further for PD monitoring.

1.4 Research Objectives

1.4.1 UHF PD detection for oil-filled power transformers

From Section 1.3, it is clear that DGA, FFA, acoustic monitoring and IEC60270-based measurement systems are not ideal for continuous remote monitoring of power transformers. The main limitation of DGA is that discrimination of separate discharge sources can be difficult and defect localisation is not possible. At present, there remains a lack of extensive field testing using portable on-line FFA measurement systems and only faults involving cellulose can be detected. Acoustic techniques are not ideal because many sensor positions are required for maximum sensitivity. In the case of IEC60270-based systems, measurements generally suffer from low sensitivity. On the other hand, preliminary investigations by Judd [28] and Rutgers [73,74] suggested the UHF technique should be considered further for the continuous remote monitoring of power transformers. The following questions summarise the basis of this research:

- What types of PD that can be detected using UHF measurements?
- What are the main types of defect that would cause concern in an operational power transformer?
- How can UHF signals be processed in ways to provide information that will assist with the interpretation of PD behaviour?

This thesis answers the above questions and provides the basis for the creation of a viable system for on-line PD monitoring of power transformers.

1.4.2 Overview of the research programme

The experimental arrangements and measuring equipment used to investigate PD activity are described in Chapter 2.

The work of Chapter 3 describes PD pulses recorded using different measurement circuits. At inception voltage, PD current pulses are measured using a high-frequency measurement system. At voltages well above inception, current pulses are measured using a high-frequency current transformer. These fundamental measurements are carried out to determine whether the rate of change of PD current pulses in transformer oil is sufficiently high to cause the excitation of UHF signals [76,77].

Chapter 4 describes and discusses current pulses simultaneously recorded with IEC 60270-based and UHF measurement systems. The influence that current pulse shapes have on both measurement systems is discussed, and it is recommended that field measurements might be enhanced by simultaneously recording UHF and IEC 60270-based measurements [78,79].

In the work of Chapter 5, PD is generated at a range of defect configurations that would cause concern in an operational power transformer. Radiated UHF PD signals are measured using two broadband electric field sensors, and the relationship between measured charge and UHF energy is investigated. The spectral energy and the relative energy measured using both sensors are also investigated. These techniques are shown to provide a useful means to assist with the interpretation of discharge behaviour [80,81].

Chapter 6 describes and discusses PD that is generated at a range of defect configurations and UHF signals are recorded in phase-resolved form. Experiments are carried out over a range of test voltages, and this allows a comprehensive database of results to be created. Results are analysed in ways that provide evidence of physical differences in the nature of each insulation defect [82,83].

In the work of Chapter 7, field tests are carried out on a ScottishPower transformer that was known to be discharging. UHF PD signals are recorded in both the time domain and in phase-resolved form. Analysis of the time domain data reveals the presence of two separate PD sources. Phase-resolved measurements are analysed in the light of Chapter 6 [84,85].

The significance of this research is discussed in Chapter 8. This chapter draws conclusions and makes recommendations for further research. In Chapter 8, the general requirements of a power transformer PD monitoring system are described.

2 GENERATION AND MEASUREMENT OF PD ACTIVITY

2.1 Introduction

In this chapter, the test apparatus that was designed for investigating PD in transformer insulating oil is introduced. The HV transformer, interconnection and the HV divider network that is used to monitor the profile of the AC waveform is also described.

The high-frequency current transformer is introduced. This is used to measure PD current pulses in transformer oil at test voltages well above inception. The current transformer affords electrical isolation between the PD source and the sensitive measuring equipment.

As will be described in Chapters 4, 5 and 6, PD is generated at a range of defect configurations. UHF PD signals are detected using a broadband electric field sensor, and these signals are pre-amplified or attenuated as necessary. The frequency response of the broadband electric field sensor, the pre-amplifiers and the attenuators are described. In the work of Chapters 6 and 7, UHF PD signals are recorded in a phase-resolved form using a partial discharge monitor (PDM). An overview of the PDM is provided here.

2.2 PD Test Arrangements

A test cell was designed to simulate a variety of PD sources in transformer insulating oil. Figure 2.1 shows a schematic of the test cell which was designed using materials that could easily be machined. The upper and lower plates of the test cell were made from insulating materials such as Tufnol and Nylon 6-6. A Perspex tube fits into a slot machined on both plates, and 'O'-rings are used for sealing purposes. The test cell is clamped together using insulating bolts.

The edges of the HV electrode have been machined with a generous radius to prevent the generation of unwanted PD, and it is energised via a brass connector with rounded corners. A sealed Sub Miniature Type-A (SMA) connector was attached to the centre of the lower plate of the test cell. A needle was soldered to the centre of the SMA connector to create a sharp protrusion. The typical diameter of the needles tested was 30 μm. This design of test cell allows external measurement of PD current pulses. The distance between the HV electrode and the tip of the protrusion can be varied using a threaded mechanism.

Figure 2.2 shows the PD test arrangement that was designed to allow a range of electrode configurations to be tested in an oil bath. The test arrangement was constructed mainly from polypropylene. The relative permittivity of this material is closely matched to that of mineral oil therefore electric field variations between the oil and the polypropylene interface were minimised [86]. Electrode protrusions, surface discharges, bad contacts, floating components and suspended particles were simulated using this test arrangement.

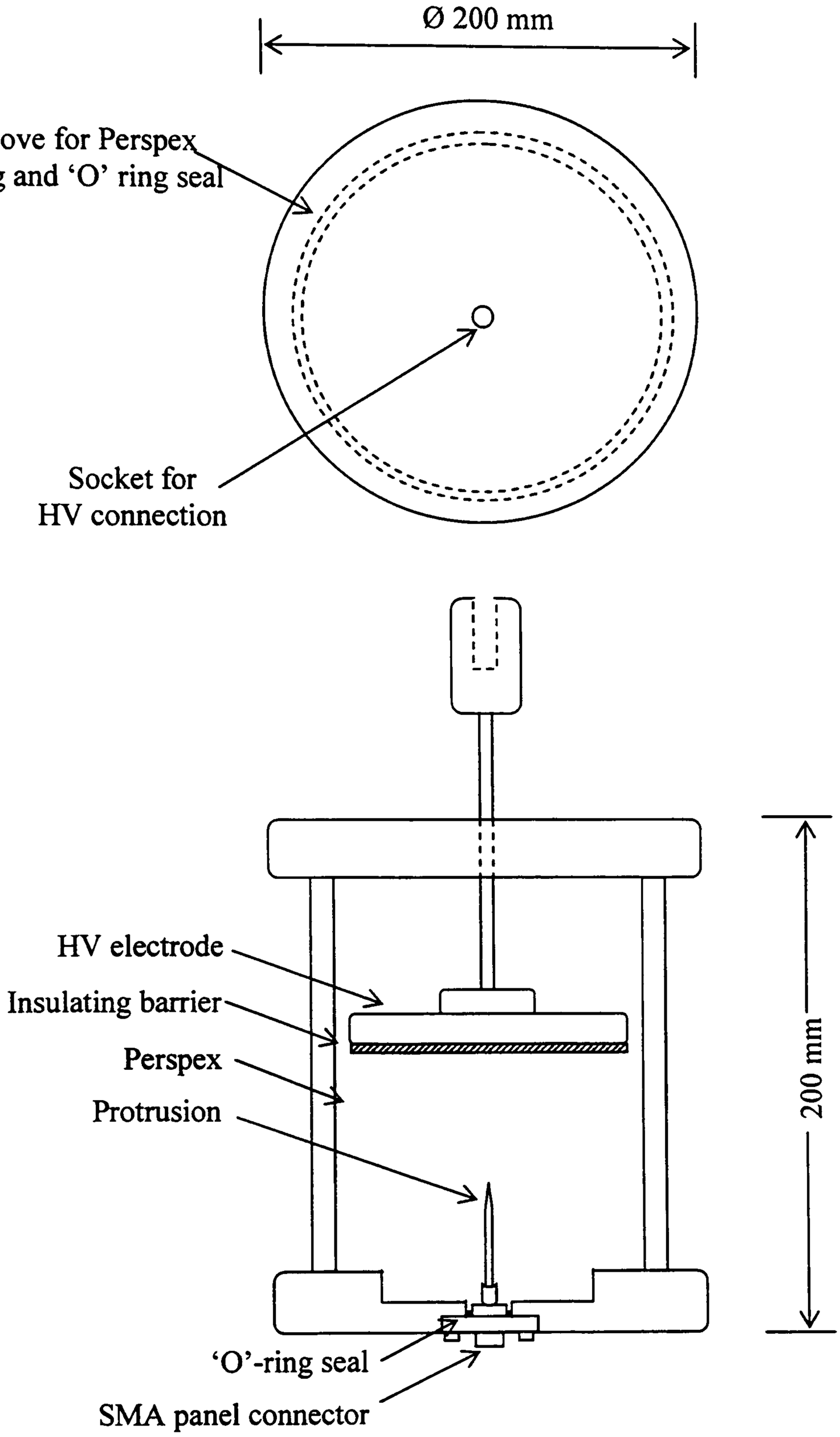

Figure 2.1 Test cell containing a point PD source with an SMA connector for external measurement of current pulses.

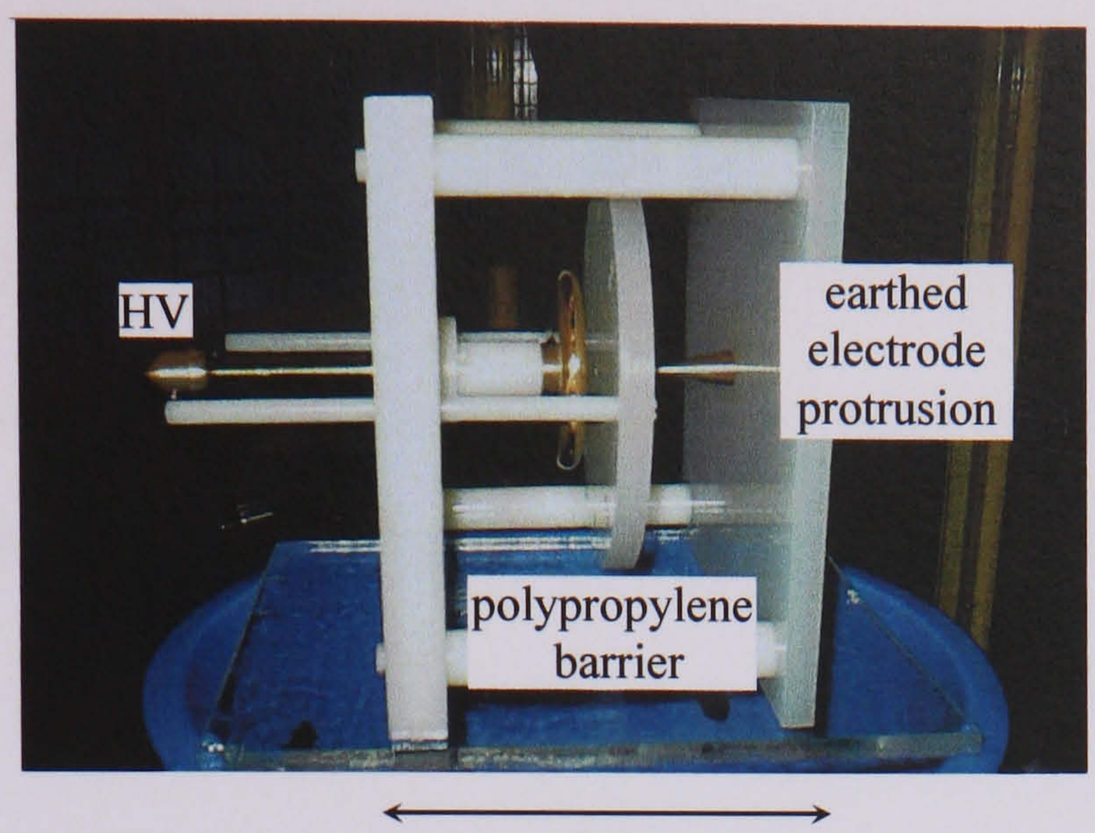

Figure 2.2 PD test arrangement.

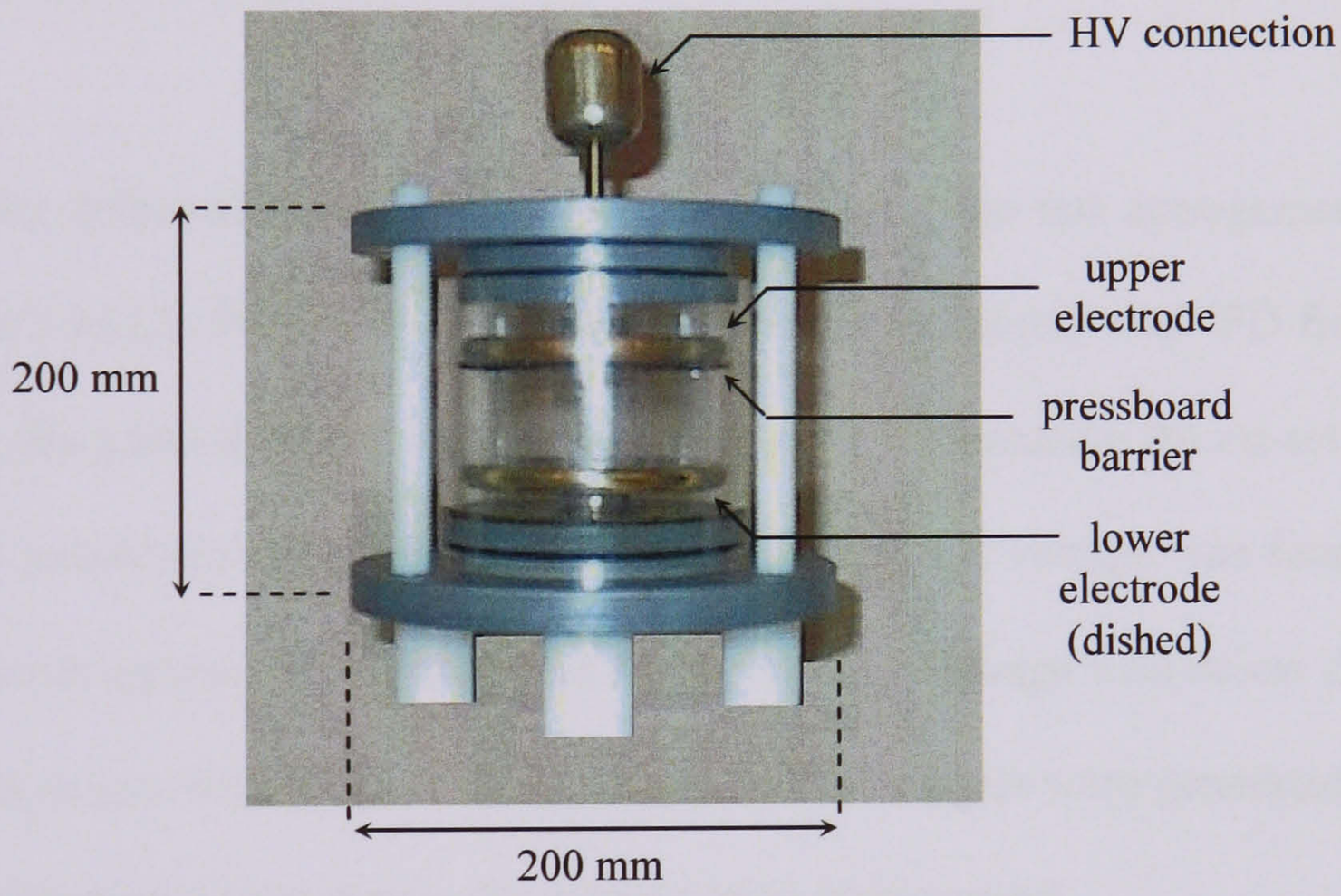

Figure 2.3 PD test cell.

Figure 2.3 shows the test cell used to investigate moisture contamination and a free metallic particle defect. A particle or a water droplet can be placed on the concave dished electrode prior to filling the test cell with oil. For these tests, an enclosed test cell was used to ensure that the defects remained in a region of high electric field stress.

For each test configuration, an insulating barrier was suspended between the electrodes to reduce the risk of flashover [87,88], which would damage the test equipment. Both the test arrangement and the test cell were energised using the HV transformer described in Section 2.3.2.

Before a particular defect arrangement was added to either of the test arrangements shown in Figures 2 and 3, the extent to which the experimental set-up was 'PD free' was investigated. By gradually increasing the test voltage and measuring the on-set of PD using a UHF measurement system an upper limit for the test voltage was found. PD was subsequently generated at each defect but using a test voltage well below this limit. This technique provided confidence that measured PD signals were generated at the defect site and not anywhere else in the experimental arrangement.

2.3 High Voltage Equipment

2.3.1 Safety precautions

All equipment that generates HV was located inside an earthed metal mesh cage and energised from a 230 V AC supply. A Castell interlock system ensured that HV equipment was automatically disconnected before the cage door could be opened. The cage was also fitted with an isolating safety switch to cut off the power supply to the cage in emergencies. When experiments were completed, an earthing rod was used to discharge any exposed parts of the experimental apparatus that may have retained a stored charge. The earth rod was left in contact with the main HV terminal while the equipment was not in use.

2.3.2 HV test equipment

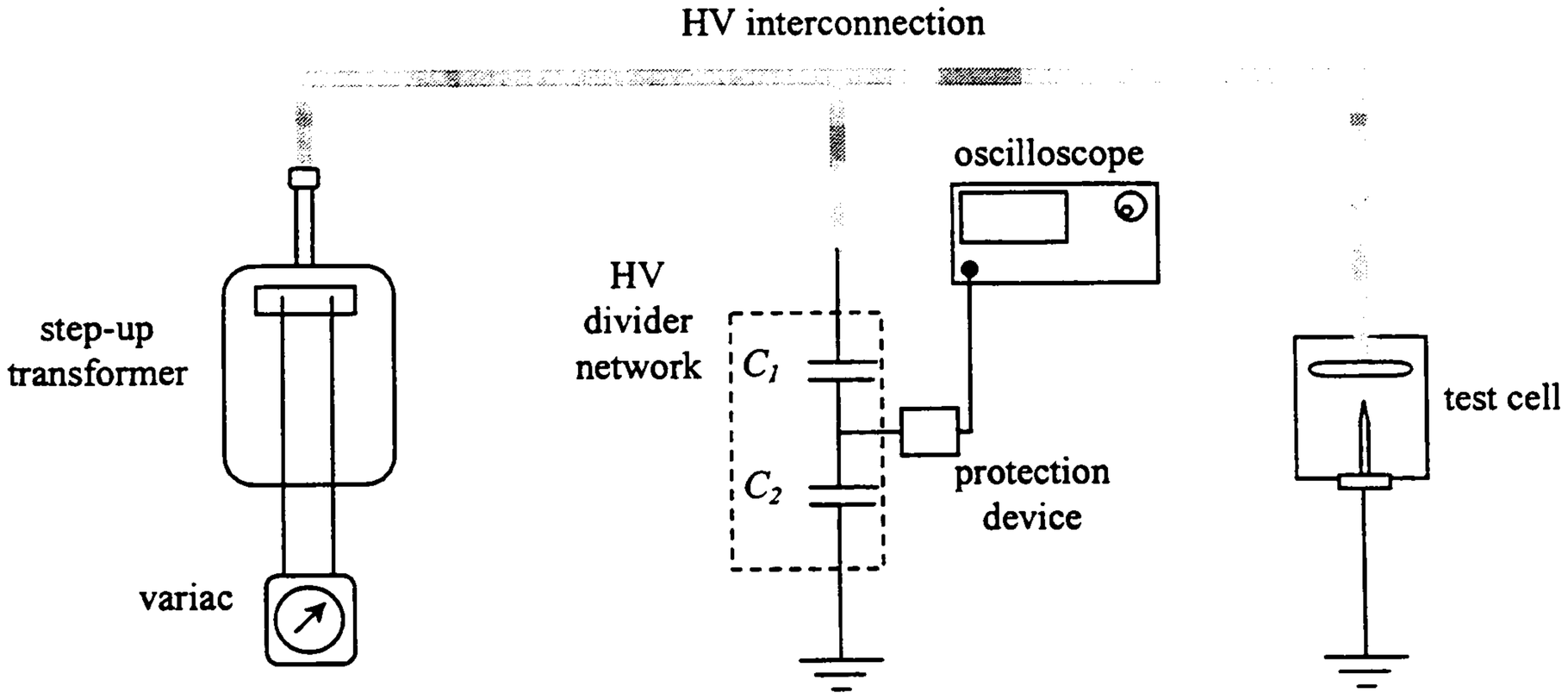

Figure 2.4 HV interconnection.

An overview of the experimental equipment used to generate PD is shown in Figure 2.4. A variac was used to control the mains voltage between 0 to 100% of AC mains voltage. A single-phase 230 V to 40 kV step-up transformer (Ferranti, Serial No. 161030) was used to generate high voltage.

An HV busbar was used to connect the step-up transformer, the HV capacitive divider network and the test cell. An oscilloscope was connected to the HV divider network via a protection circuit and this allowed the profile of the AC waveform to be monitored. PD was generated at a variety of defect types in the test cell.

2.3.3 HV busbar

A robust HV busbar system was configured using copper pipes that allowed interconnection of the step-up transformer, the capacitive divider circuit and the test cell. Care was taken to ensure that the radius of the busbar (r) was sufficiently high to prevent air corona from being generated at its surface. Figure 2.5 shows how the electric field at the surface of a busbar varies with r [89,90]. In this simulation the busbar voltage V was set to 50 kV because test voltages were always less than 50 kV.

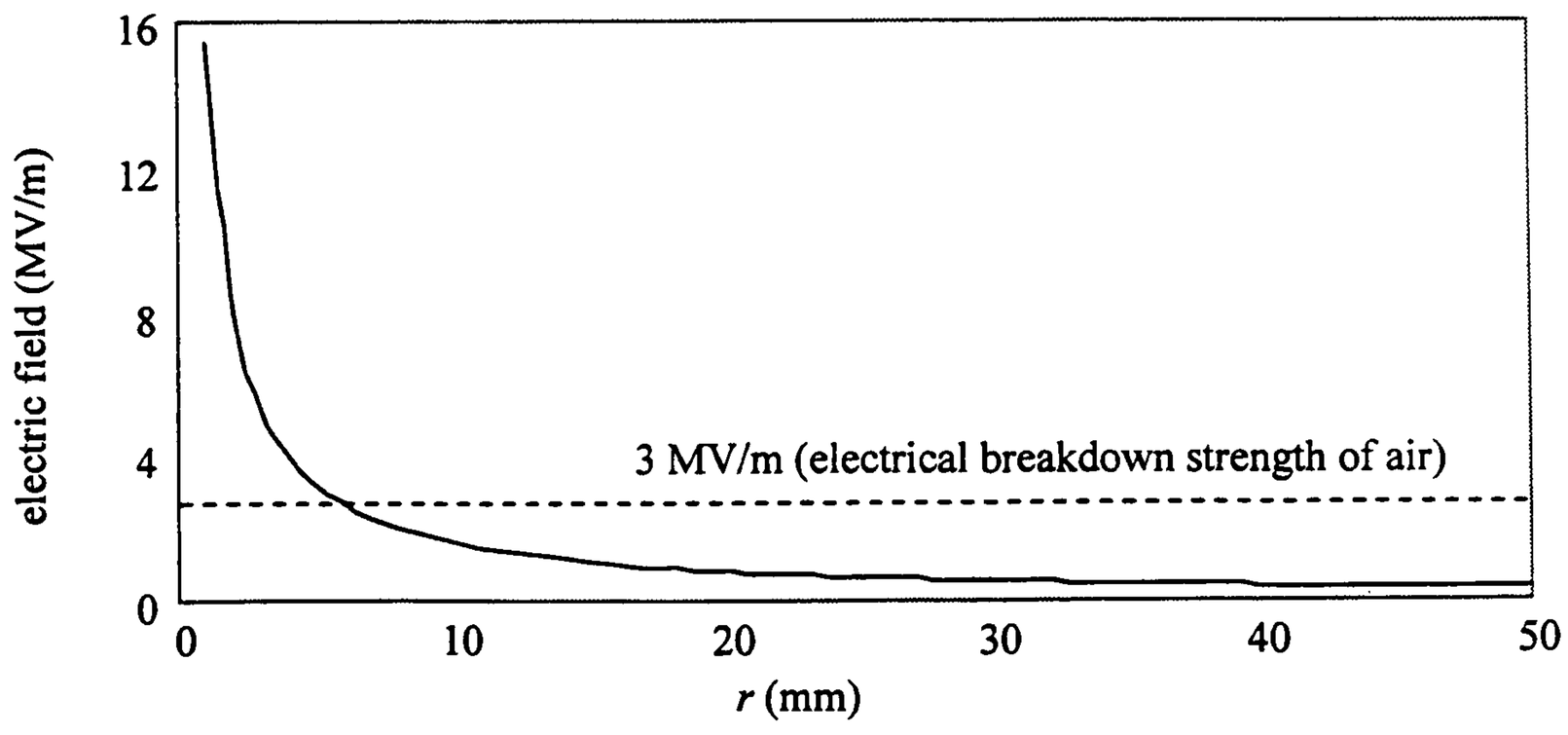

Figure 2.5 Electric field at the surface of the cylindrical busbar.

Since the HV interconnection network was air-insulated, the outer diameter of the copper pipe was chosen to ensure that the electric field at the surface of the busbar did not exceed 3 MV/m [91]. The chosen value for the busbar radius was a standard size of 28 mm. This provided a low-cost solution and gave a good safety margin. Electrostatic shields were used at the joints in order to prevent unwanted discharges.

2.3.4 HV divider network

As shown in Figure 2.6, the HV AC waveform was monitored at the output of a capacitive divider circuit by connecting an oscilloscope across C_2 via a protection circuit.

(a)

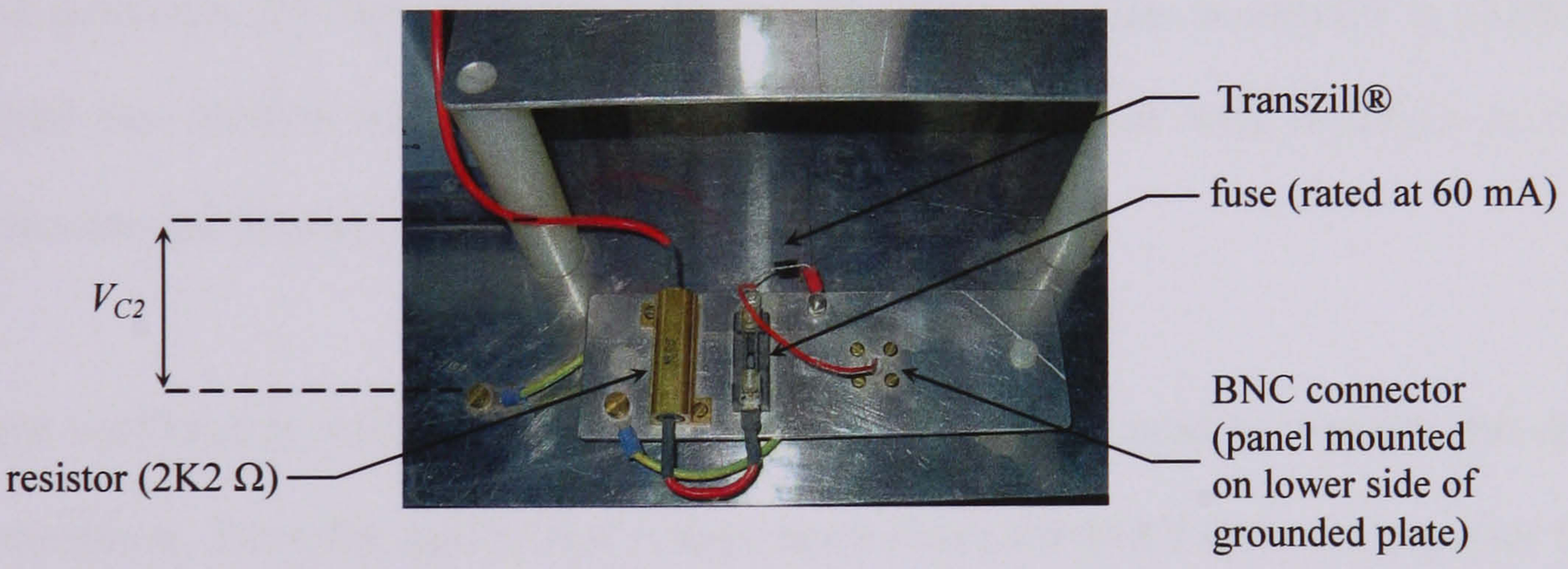

(b)

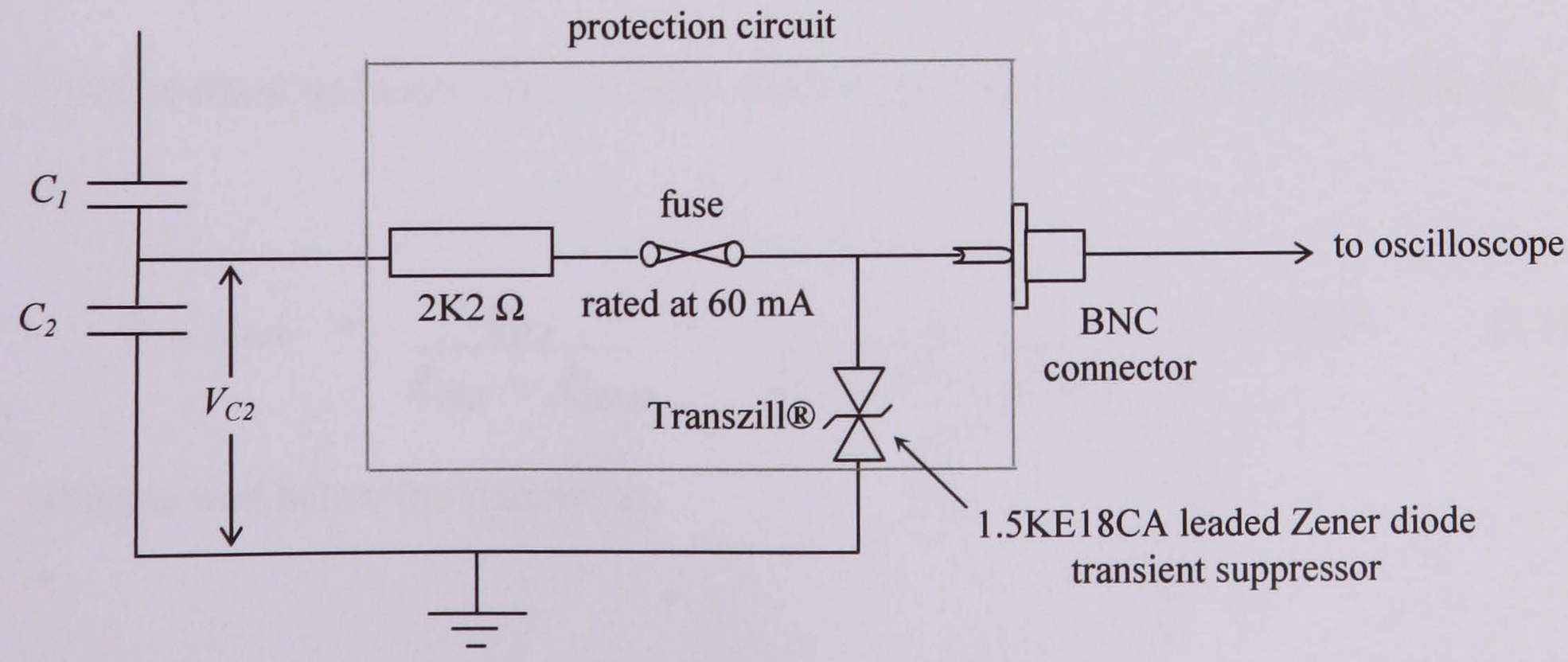

Figure 2.6 Protection circuit (a) expanded view of protection circuit and (b) equivalent diagram of capacitive divider network and protection circuitry.

The applied test voltage never exceeded 40 kV, and the values of C_1 and C_2 were chosen to limit the voltage at C_2 to 4V. The values chosen for C_1 and C_2 were 0.3 nF and 3 μF. This provided a division ratio of 10,000:1, although the manufacturing tolerance on these capacitances will affect this ratio. This high division ratio meant that almost all of the test voltage was dropped across C_1, and so C_1 was rated at the maximum test voltage. Under normal operating conditions, the voltage across C_2 should only be 1/10,000 of the test voltage. Therefore, an HV capacitor was not required for C_2 and this offered a lower cost solution.

Should breakdown occur in C_1, the oscilloscope would be at risk from high input currents. As a safety precaution, a protection unit was designed. A current-limiting resistor and a fuse were connected in series with the oscilloscope to provide a measure of protection for high currents. A Transzill® device was also connected in parallel with the oscilloscope to provide protection from transients with risetimes in the nanosecond duration.

An oscilloscope with a 1 MΩ input impedance (R_{in}) was used to measure the AC waveform. Since the applied test voltage never exceeded 40 kV the voltage across C_2 should not exceed 4V.

During normal operation, the maximum current drawn by the oscilloscope would only be

$$I_{steady\ state} = \frac{V_{C2}}{R_{2K2} + R_{scope}} = \frac{4}{(2.2 \times 10^3 + 1 \times 10^6)} = 3.99\ \mu A \qquad (2.1)$$

which is well below the fuse rating.

In the event of a short circuit occurring across C_1, the voltage across C_2 would rise to 40 kV. The maximum instantaneous current would be limited by the resistor to be

$$I_{fault} = \frac{V_{test}}{R_{2K2}} = \frac{40{,}000}{2{,}200} = 18.18 \text{ A} \qquad (2.2)$$

The Transzill® device will sink this current long enough for the fuse to 'blow'. The selected Transzill® device clamps the voltage to 25.2V, which will protect the oscilloscope input [92]. When the fuse 'blows' the oscilloscope is electrically isolated from the HV divider network. Figure 2.7 shows the complete capacitive divider and protection circuit.

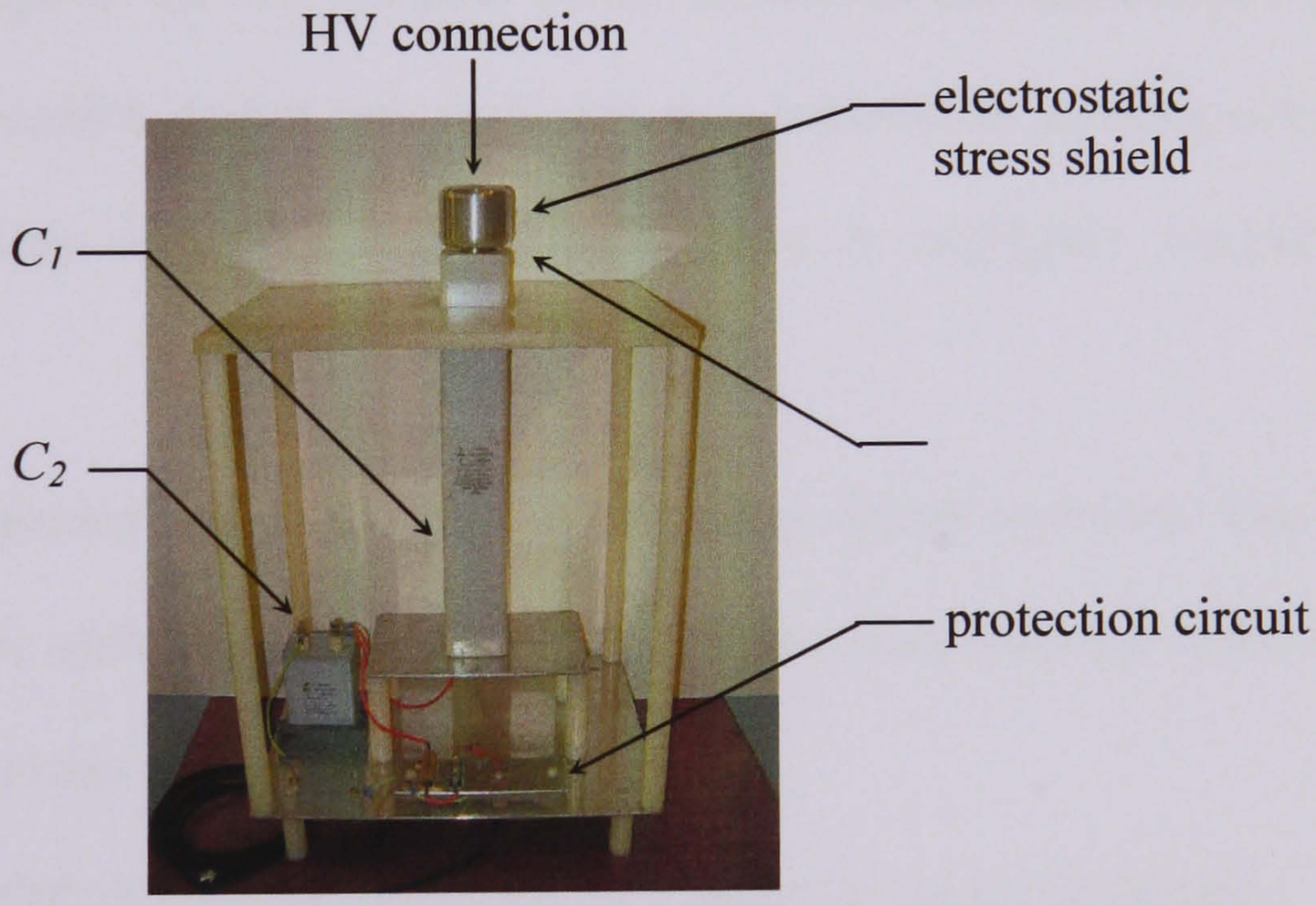

Figure 2.7 Experimental arrangement used to monitor the HV waveform.

2.3.5 Frequency response of HV AC measurement circuit

The frequency response of the HV AC measurement circuit was simulated to ensure that it is suitable for measuring frequencies around 50 Hz. The voltage measured by the oscilloscope can be expressed as

$$V_{scope} = V \left\{ \frac{1}{1 + Z_{C1} \left[\frac{Z_{C2} + R_2}{Z_{C2} R_2} \right]} \right\} \tag{2.3}$$

where,

$$R_2 = R_{in} + 2K2 \tag{2.4}$$

The parameters Z_{C1} and Z_{C2} correspond to the impedances of C_1 and C_2 respectively and V is the AC voltage at the HV terminal of the divider. In this calculation, the impedance of the Transzill® device was neglected as it behaved as an open circuit during normal operating conditions and its capacitance is negligible compared with C_2.

In Figure 2.8, the frequency response of the measurement circuit is shown. This is plotted on a logarithmic scale and demonstrates that the frequency response is flat for a broad range of frequencies around 50 Hz.

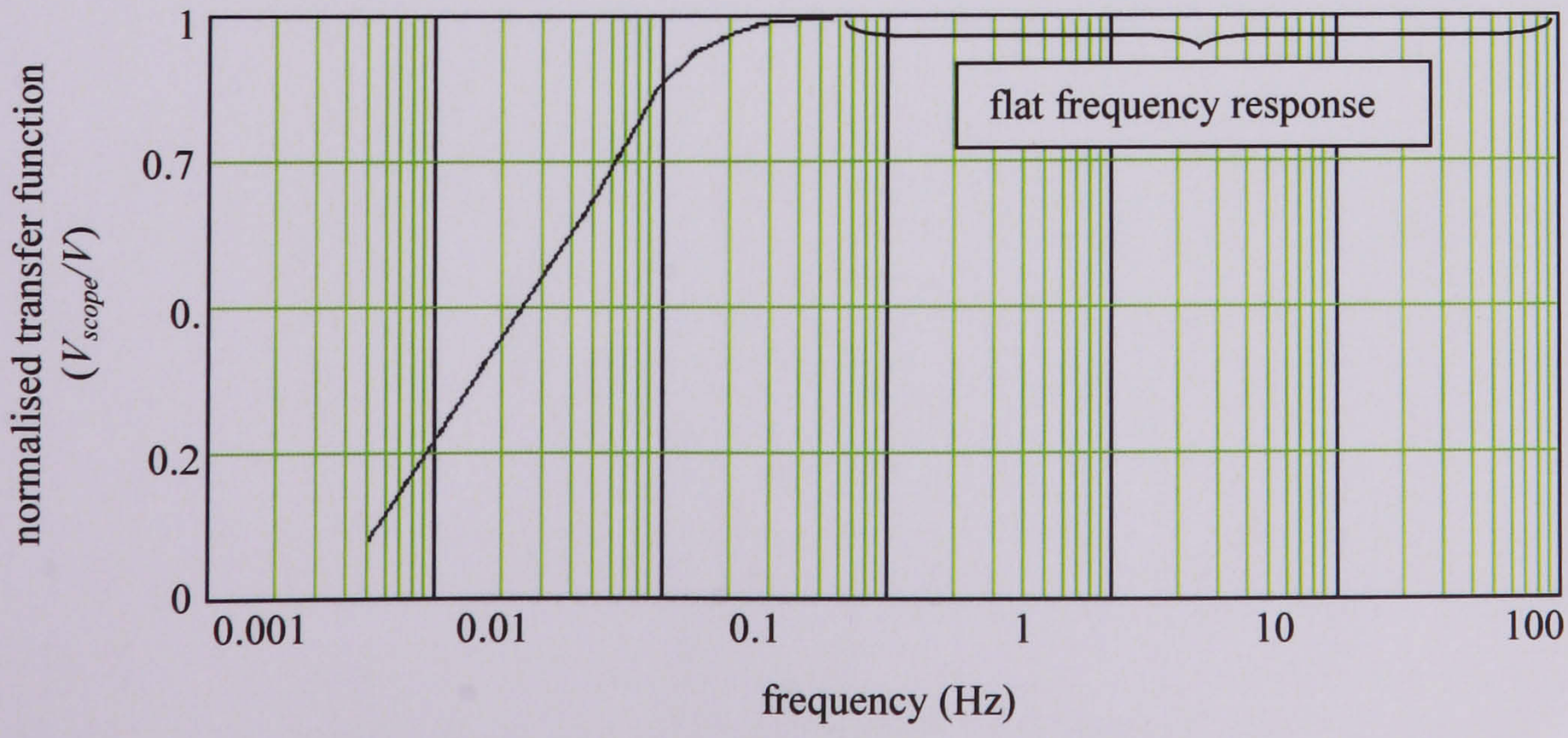

Figure 2.8 Frequency response of HV divider network and protection circuitry.

Figure 2.9 shows a profile of the HV AC waveform that was measured in the laboratory using the oscilloscope. Clearly, the waveform is not a pure sinusoid. As will be discussed in Chapter 6, this is likely to modify the phase position at which PD occurs.

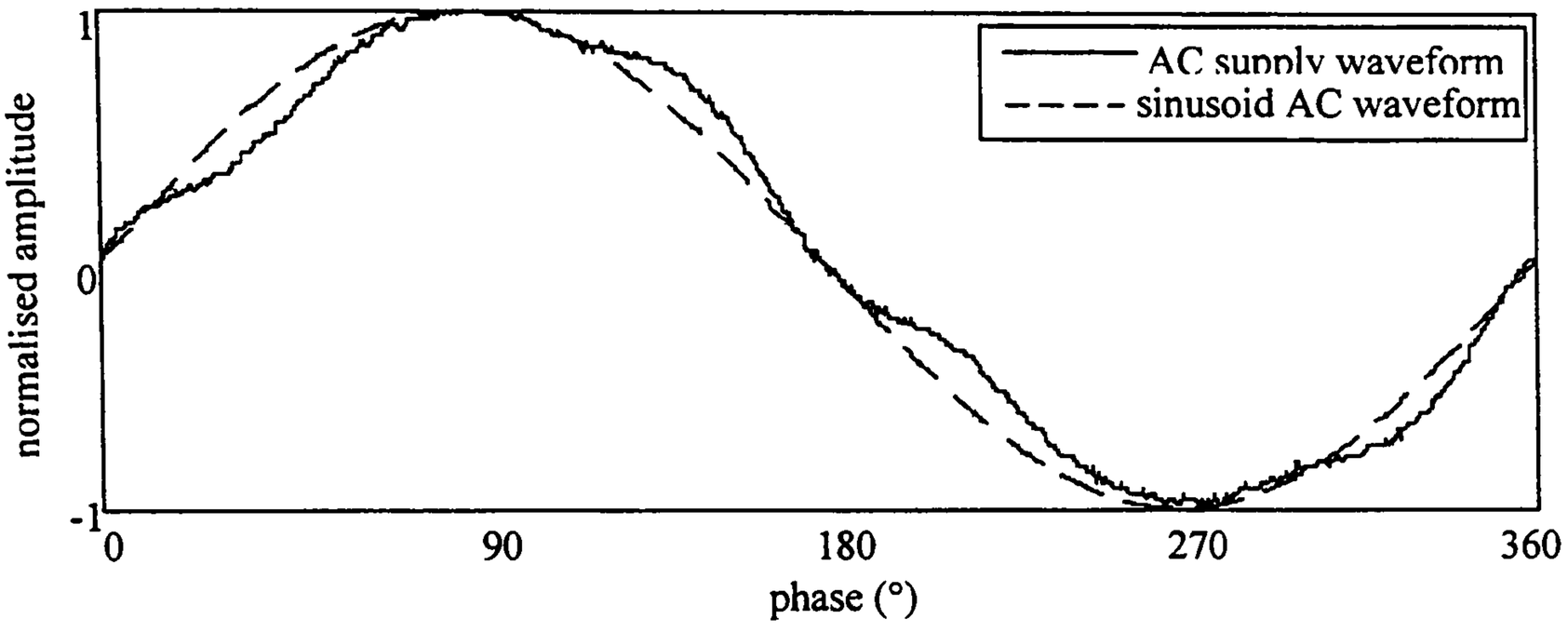

Figure 2.9 Profile of the experimental HV AC waveform.

2.4 Measurement Equipment

2.4.1 Current transformer

A high-frequency current transformer (Tektronix CT-1) was used to measure current pulses at test voltages well above inception [93]. The Tektronix data sheet states that the sensitivity of the current transformer is 5 mV/mA and its bandwidth is 25 kHz – 1 GHz. However, the current transformer could not be positioned around the protrusion because of the high electric field in this the region. Therefore, a 3 m length of RG405U cable was connected to the protrusion and current pulses flowing at the remote end were measured using the current transformer. This section is concerned with measuring the frequency response of this measurement system (Figure 2.10). A detailed view of the high-frequency current transformer, SMA type connector and the 50 Ω resistor are shown in Figure 2.11.

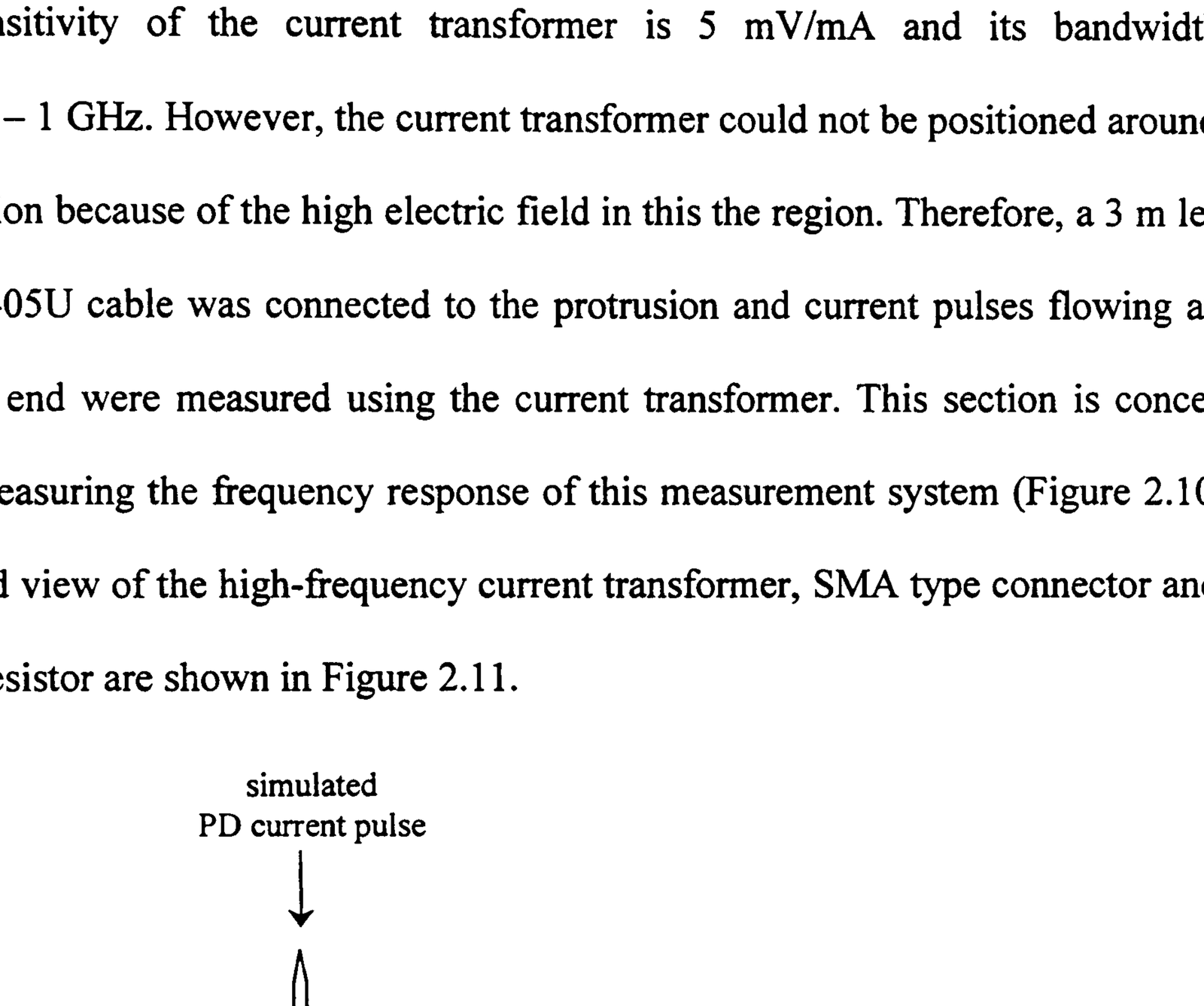

Figure 2.10 Schematic of PD current pulse measurement technique.

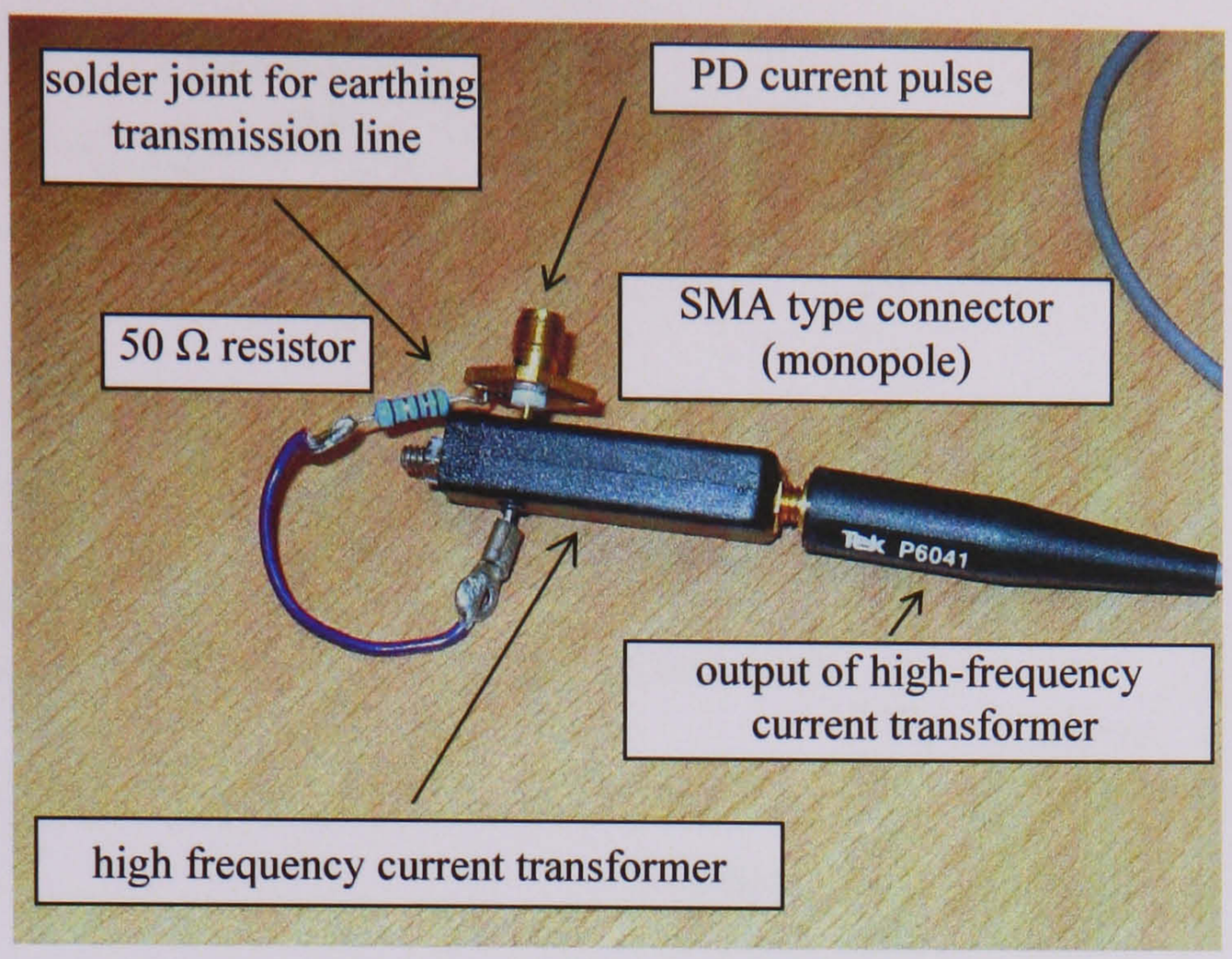

Figure 2.11 Broadband current transformer, SMA type connector and 50Ω resistor.

Determination of the frequency response is explained with reference to Figure 2.12. A repeatable current pulse with a 0.5 ns risetime was generated using a current pulse generator circuit [67], this pulse was attenuated by 20 dB.

Firstly, the arrangement shown in Figure 2.12(a) was connected and a reference pulse (I_{ref}) was recorded using the 3 GHz oscilloscope. The measurement system was then modified to include the current transformer (Figure 2.12(b)). The output of the current transformer was connected to the 3 GHz oscilloscope and the modified current pulse (I_{probe}) was measured. Both pulses were transformed into the frequency domain using a fast Fourier transform (FFT) and the frequency response was found by determining the ratio I_{probe} / I_{ref}. The frequency response of the measurement system shows that current pulses with frequency content in the UHF band up to 1000MHz can be measured.

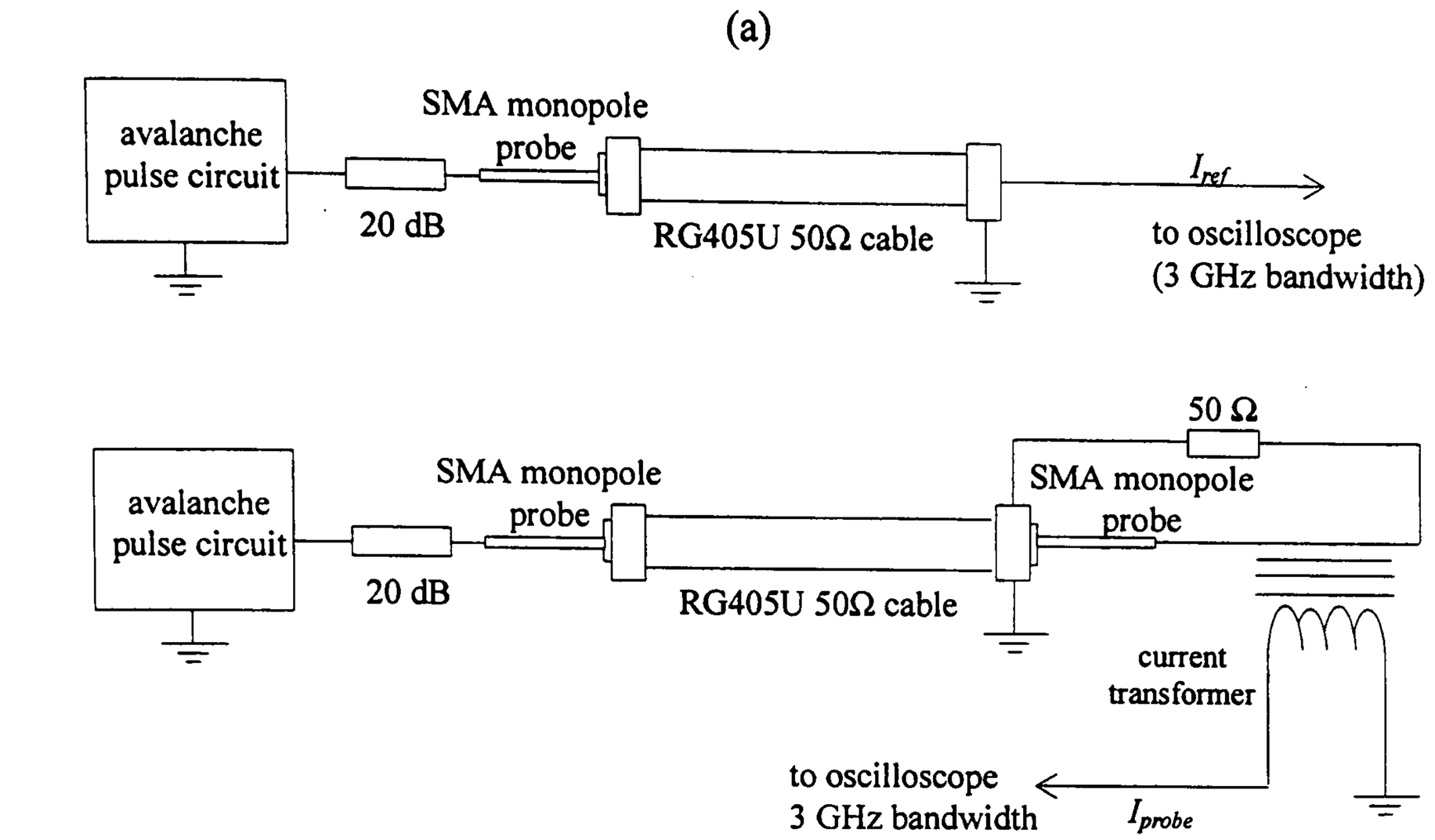

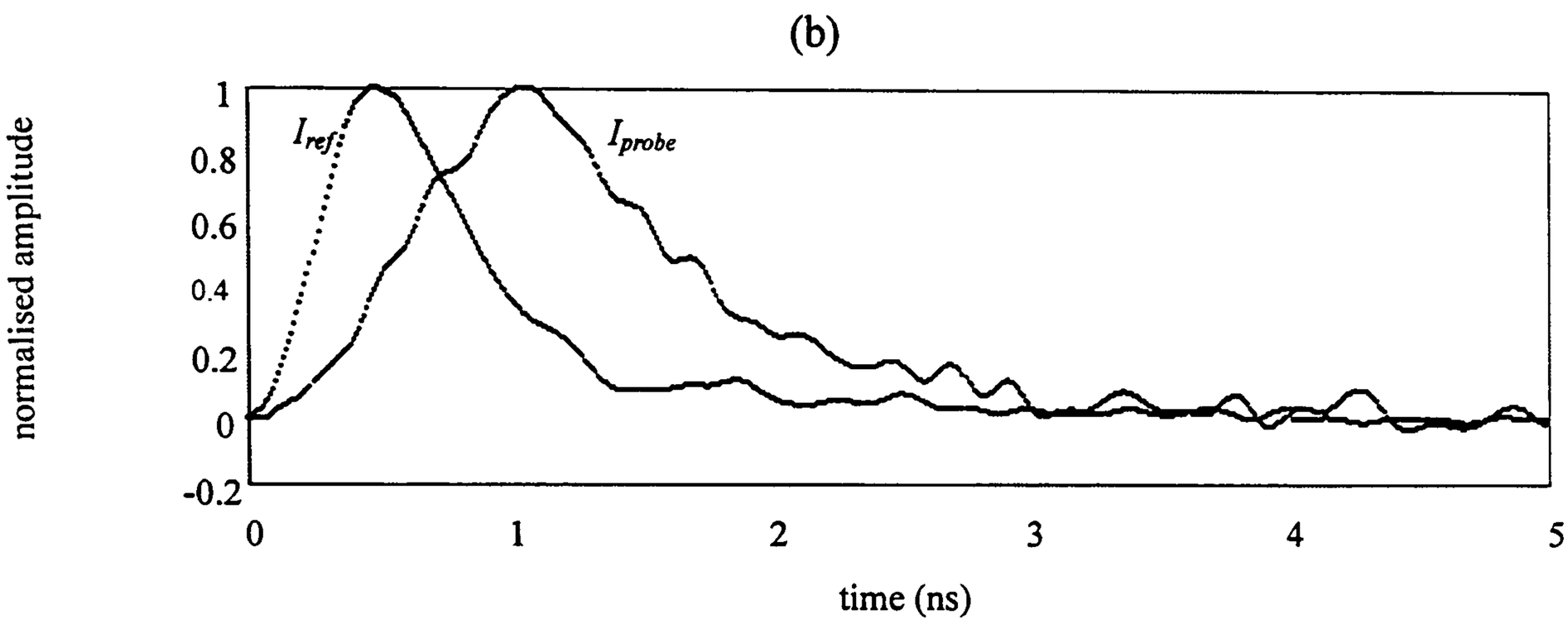

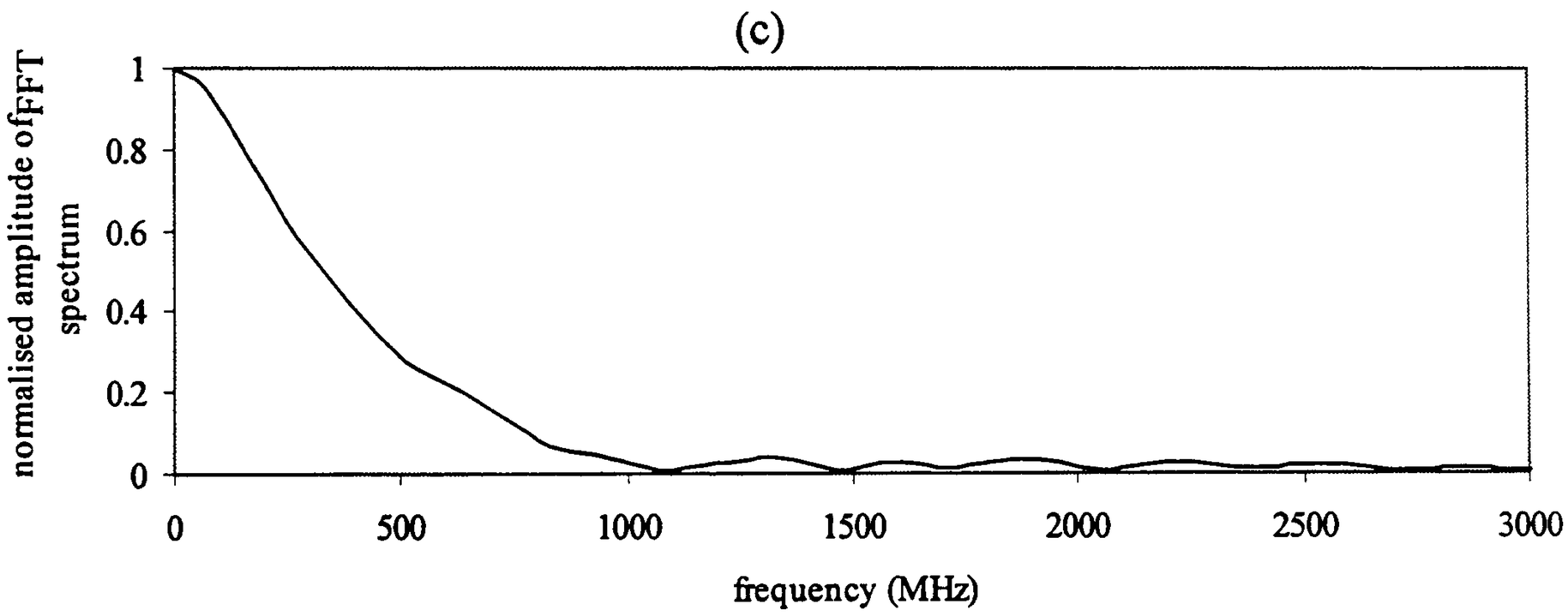

Figure 2.12 Technique for calibrating the high-frequency measurement system;
(a) arrangements for measuring current pulses,
(b) examples of measured pulses and
(c) measured frequency response.

2.4.2 IEC 60270-based measurement system

IEC Publication 60270 [21] sets out the principles for conventional PD measurement systems. In Figure 2.13, an example of a conventional PD measurement circuit commonly used under laboratory conditions is shown.

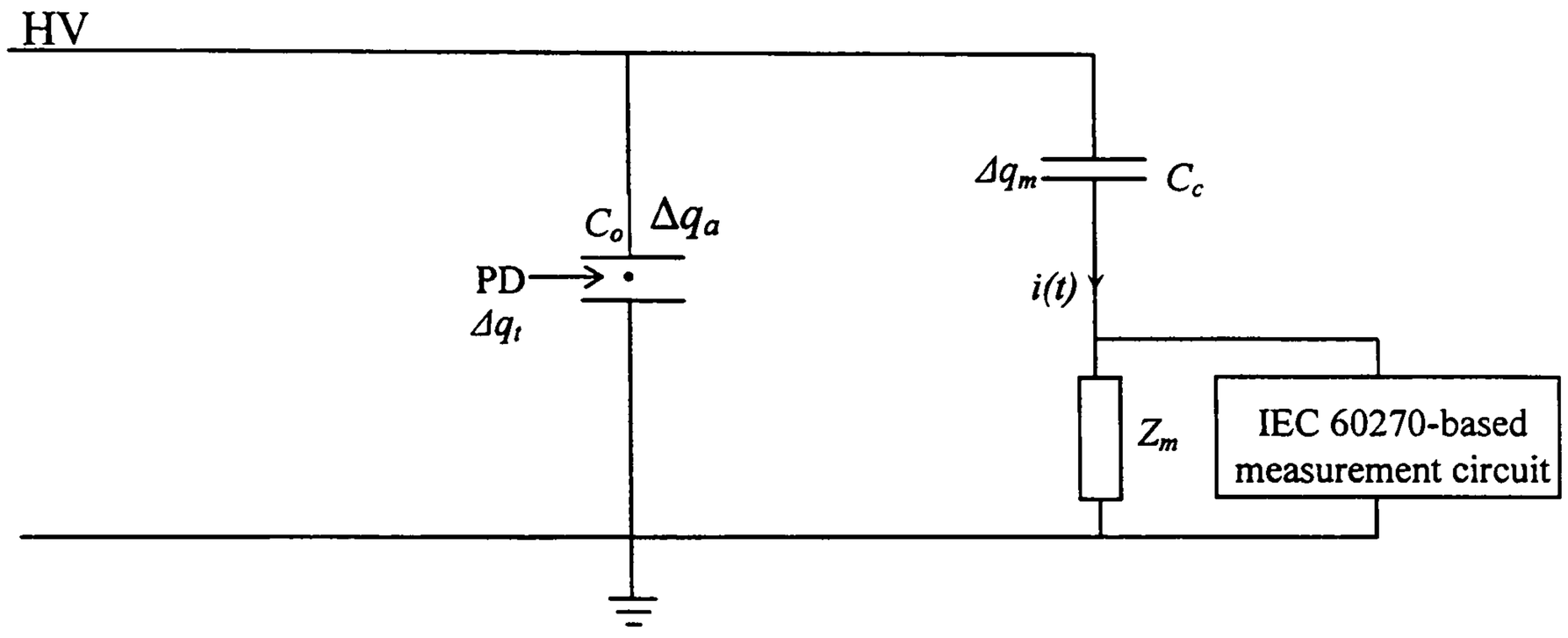

Figure 2.13 Schematic of a conventional PD measurement circuit.

An HV coupling capacitor (C_c) and a measurement impedance (Z_m) are connected in parallel with the test object (C_o). When PD occurs in the test object (Δq_t) there will be a redistribution of charge inside C_o and a transient current *i(t)* will flow through Z_m [94]. The *true charge* Δq_t corresponds to the charge transferred at the defect site. However, the *measured charge* Δq_m is released from C_c and is found by integrating *i(t)*.

If the values of C_o and C_c are known the *apparent charge* Δq_a can be determined using

$$\Delta q_a = \frac{\Delta q_m (C_o + C_c)}{C_c} \qquad (2.5)$$

The *apparent charge* refers to the charge induced on the terminals of C_o, whereas Δq_t is the *true charge*, which is transferred at the PD site.

The rapid rate of change of PD current allows it to be detected using a measurement system that offers suitable sensitivity, bandwidth and isolation from the HV source [50,51]. The measured waveform is shaped and amplified by the IEC 60270-based measurement circuit to provide a value that is proportional to the *apparent charge* quantity. The sensitivity of such a measurement system is calibrated by injecting a calibration pulse across the terminals of the test object.

The frequency response of the IEC 60270-based measuring circuit used in this work is shown in Figure 2.14. This circuit and its frequency response were provided by the School of Engineering, Science and Design at Glasgow Caledonian University. The frequency range of the circuit is 30 kHz – 3 MHz, the resonant frequency (f_o) is 750 kHz and the -3 dB bandwidth is 478 kHz.

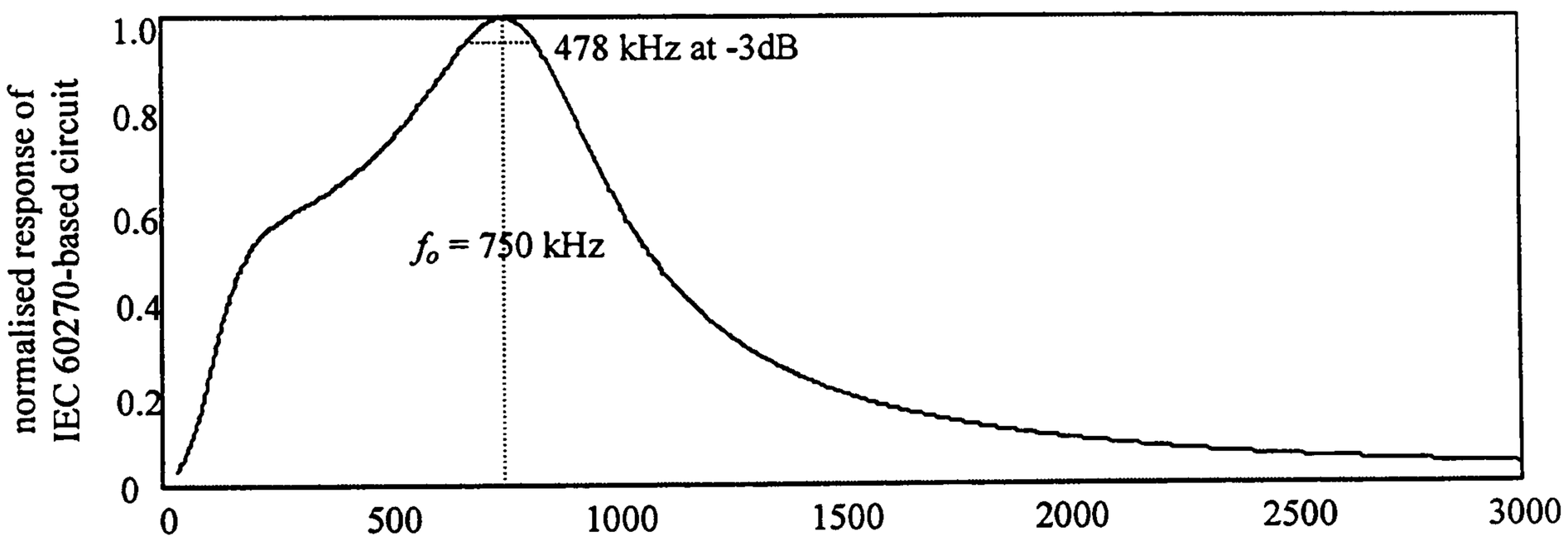

Figure 2.14 Frequency response of the IEC 60270-based measurement circuit (simulated using software).

Figure 2.15 shows an example of a waveform detected using an IEC 60270-based measurement circuit. This waveform was measured when PD activity was generated at an air-insulated protrusion [78]. The maximum voltage of the waveform (V_{pk}) is proportional to the *apparent charge* quantity.

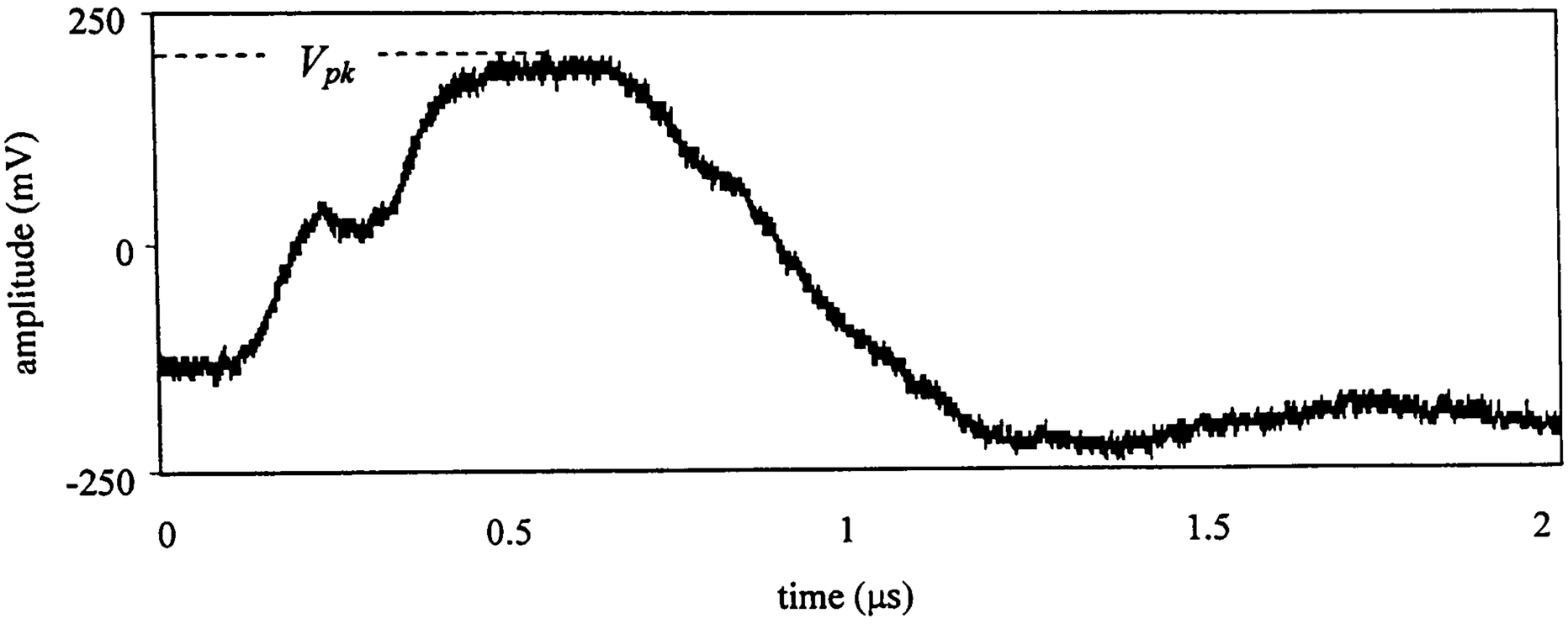

Figure 2.15 Example of a waveform detected using the IEC60270-based measurement circuit.

2.4.3 Broadband electric field sensors

In the experiments of Chapters 4, 5 and 6, radiated UHF PD signals are detected using passive broadband electric field sensors mounted inside a test chamber. In this investigation, a D-dot sensor was selected, an example of which is shown in Figure 2.16. This sensor converts the rate of change of electric flux density into a voltage that can be measured using an oscilloscope and was chosen because of its good impedance match to a 50 Ω measurement system. An example of a measured UHF signal is shown in Figure 2.17.

Figure 2.18 shows the frequency response of the D-dot sensor as measured using a pulsed GTEM (Gigahertz Transverse Electromagnetic) system [67]. This plot shows that the sensor is suitable for detecting frequencies in the range 200-2000 MHz with a sensitivity greater than 6 mV/Vm^{-1}[95]. Therefore, the sensor is suitable for the detection of UHF signals.

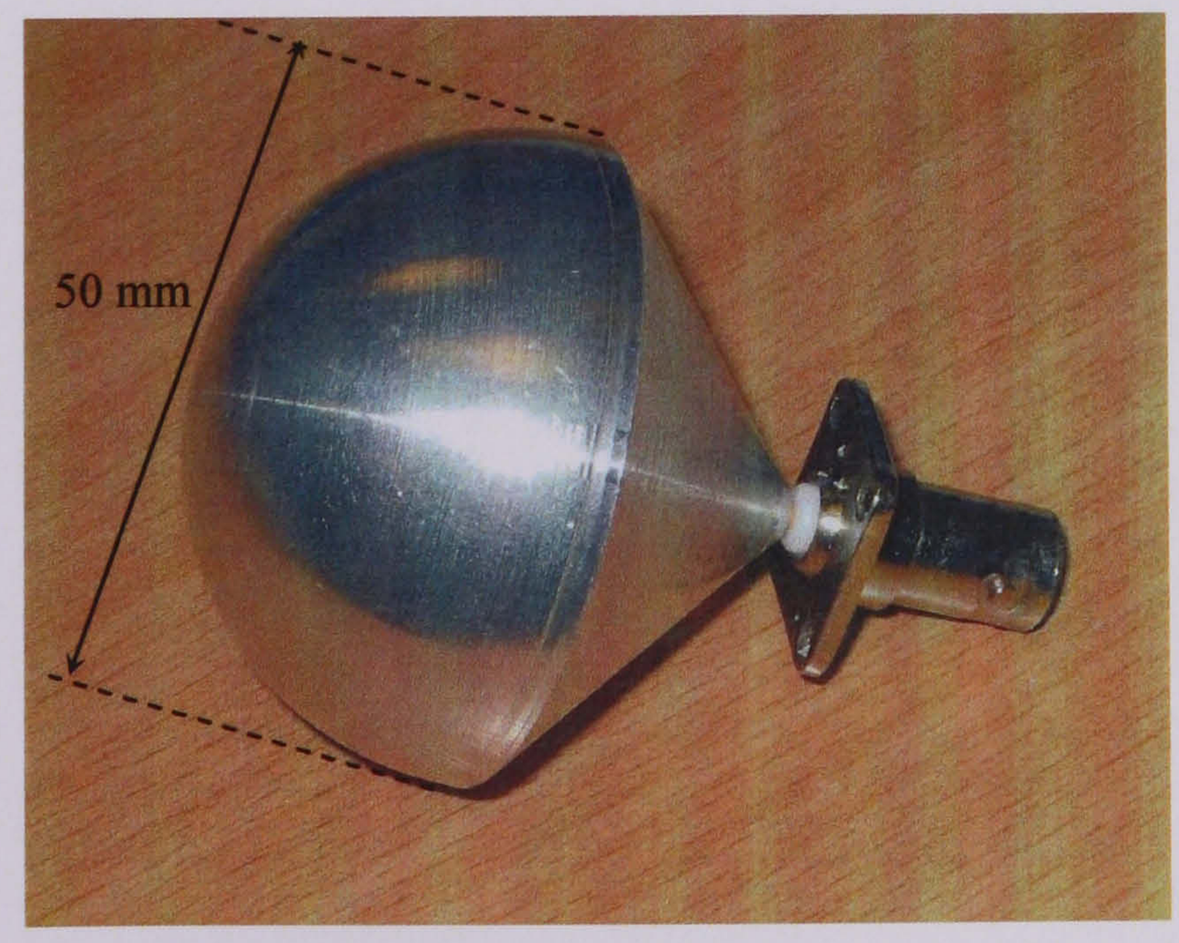

Figure 2.16 Example of a D-dot sensor and coaxial BNC-type connector.

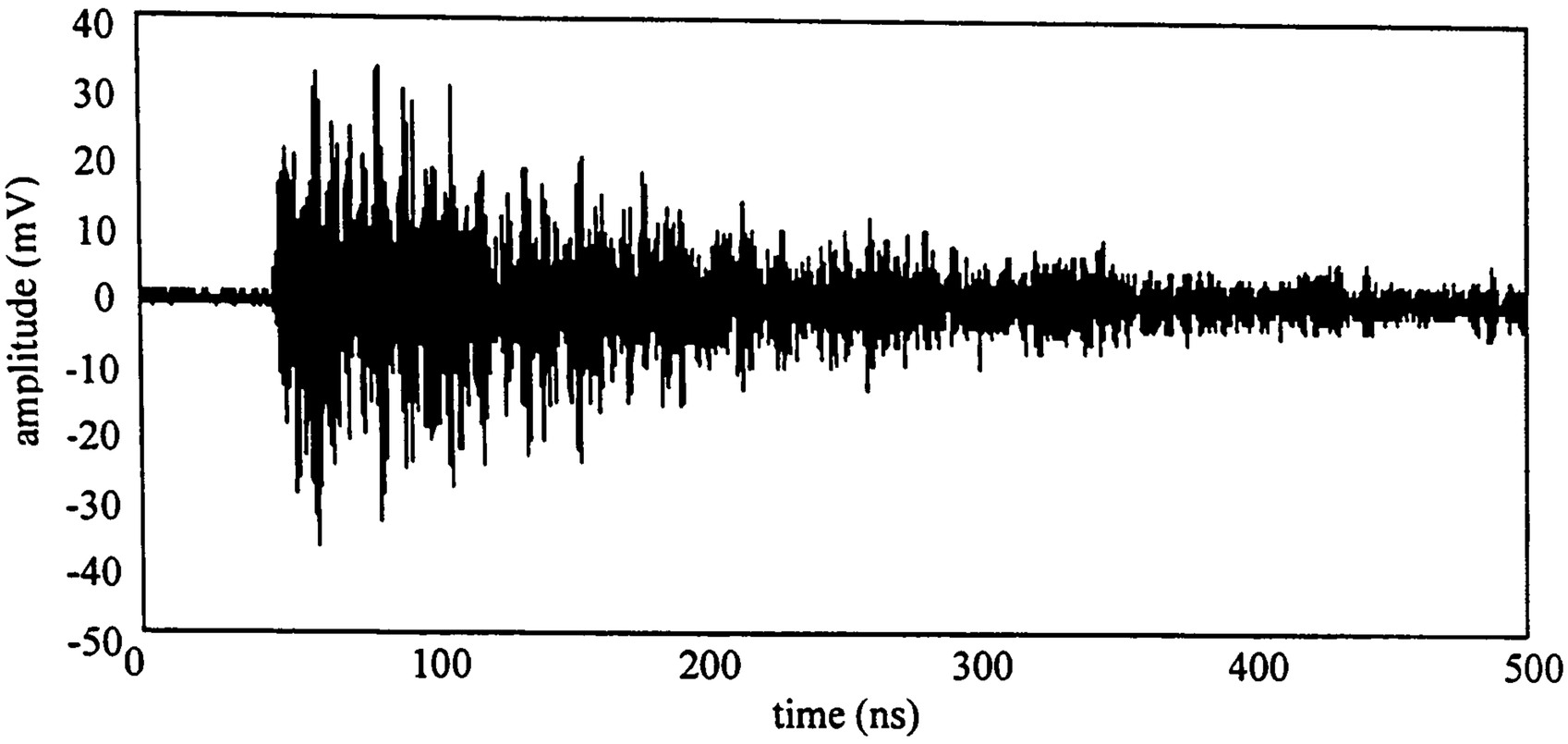

Figure 2.17 Example of a UHF signal measured using the D-dot sensor.

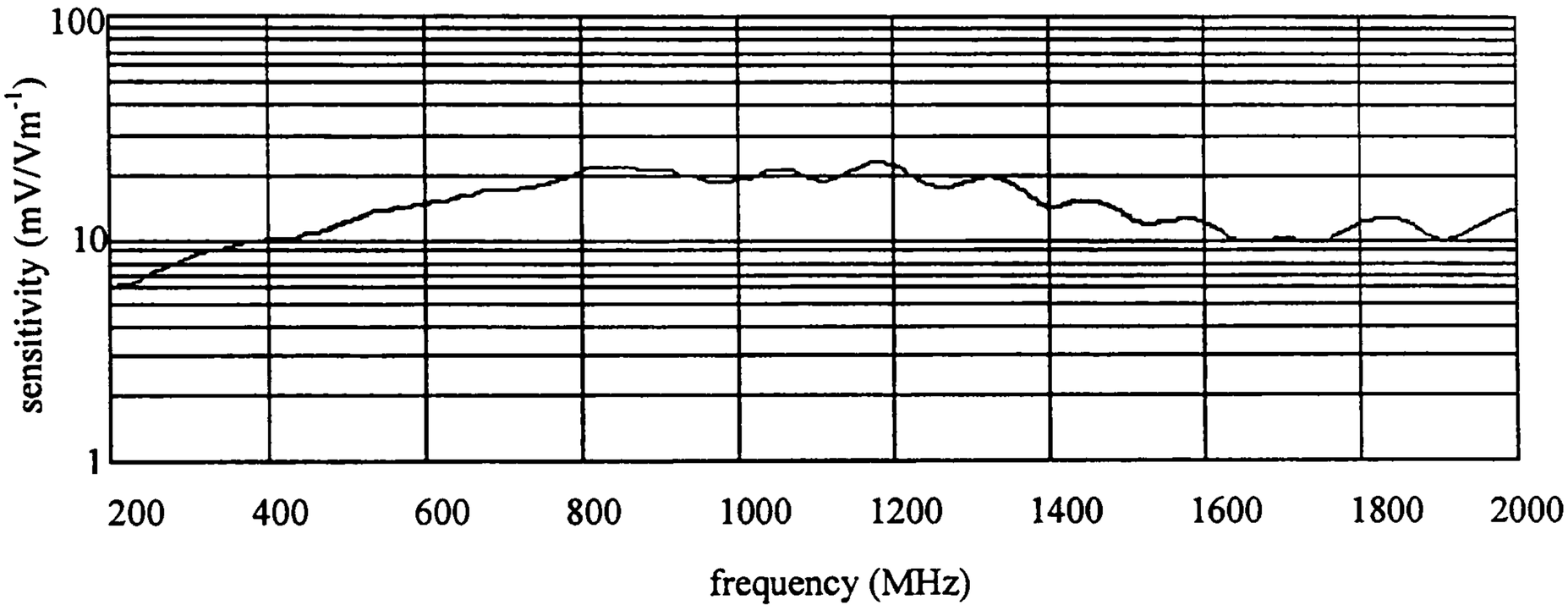

Figure 2.18 Measured frequency response of the D-dot sensor.

2.4.4 UHF pre-amplifier and attenuators

A set of attenuators covering the range 3 - 20 dB and UHF pre-amplifiers were used throughout this work. A vector network analyser was used to measure their frequency responses. Figure 2.19 shows that the frequency response of the attenuators is reasonably flat from 0 to 2500 MHz, and the gain of the UHF pre-amplifiers is at least 20 dB up to 2000 MHz. This finding confirms that these components are suitable for measuring UHF PD signals.

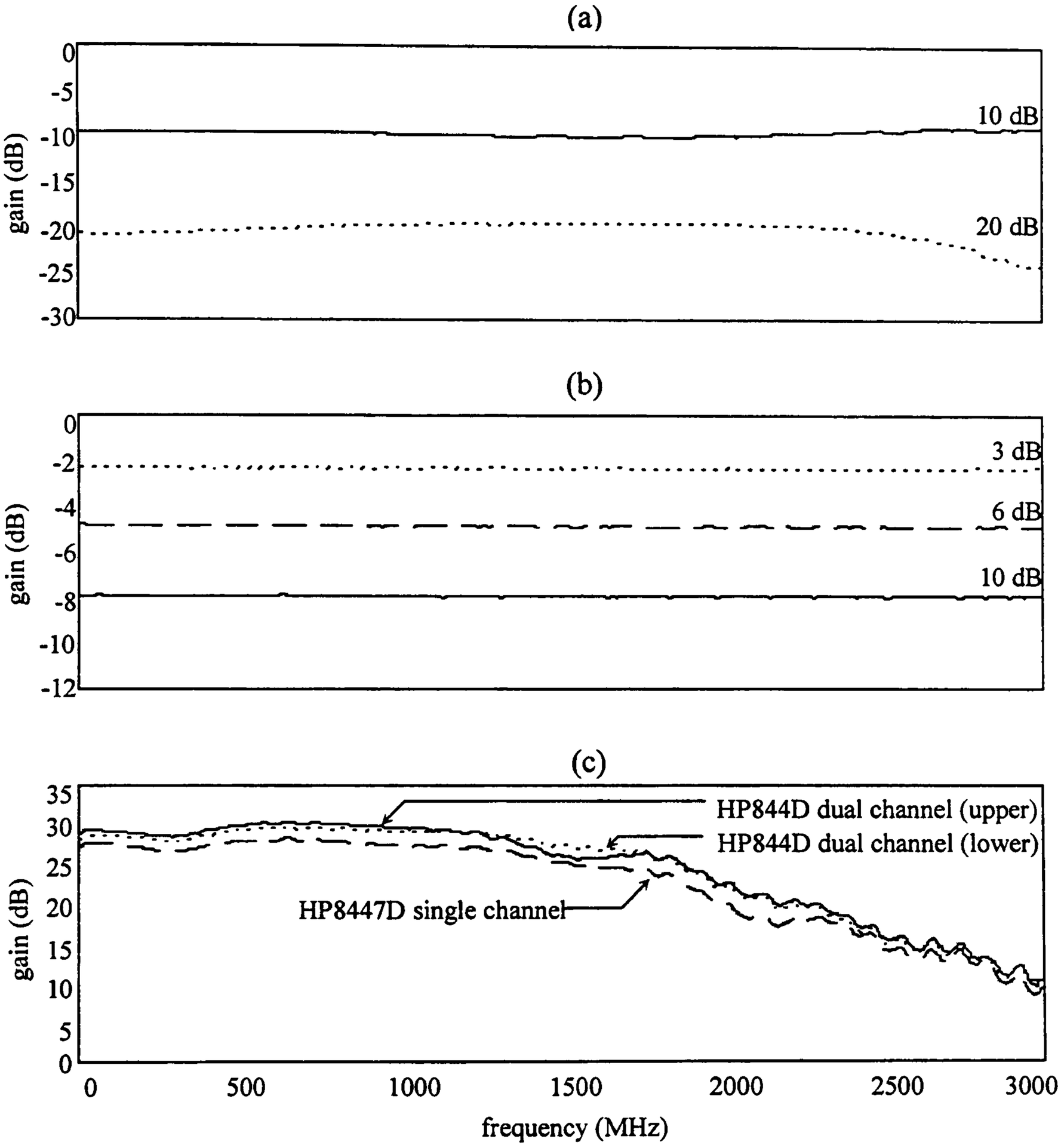

Figure 2.19 Frequency response of (a) BNC attenuators, (b) N type attenuators and (c) pre-amplifiers

2.4.5 Partial Discharge Monitor (PDM)

2.4.5.1 Overview

In the work of Chapter 6, a Partial Discharge Monitor (PDM) supplied by Diagnostic Monitoring Systems Ltd is used to record phase-resolved patterns for a range of PD sources. Since the PDM system was used extensively for recording PD data, it is useful to outline its operating principles. A schematic of the PDM circuitry is shown in Figure 2.20. A high-pass filter rejects frequencies below 500 MHz, with the envelope peak of the detected UHF signal subsequently being extracted and represented as a phase-resolved event.

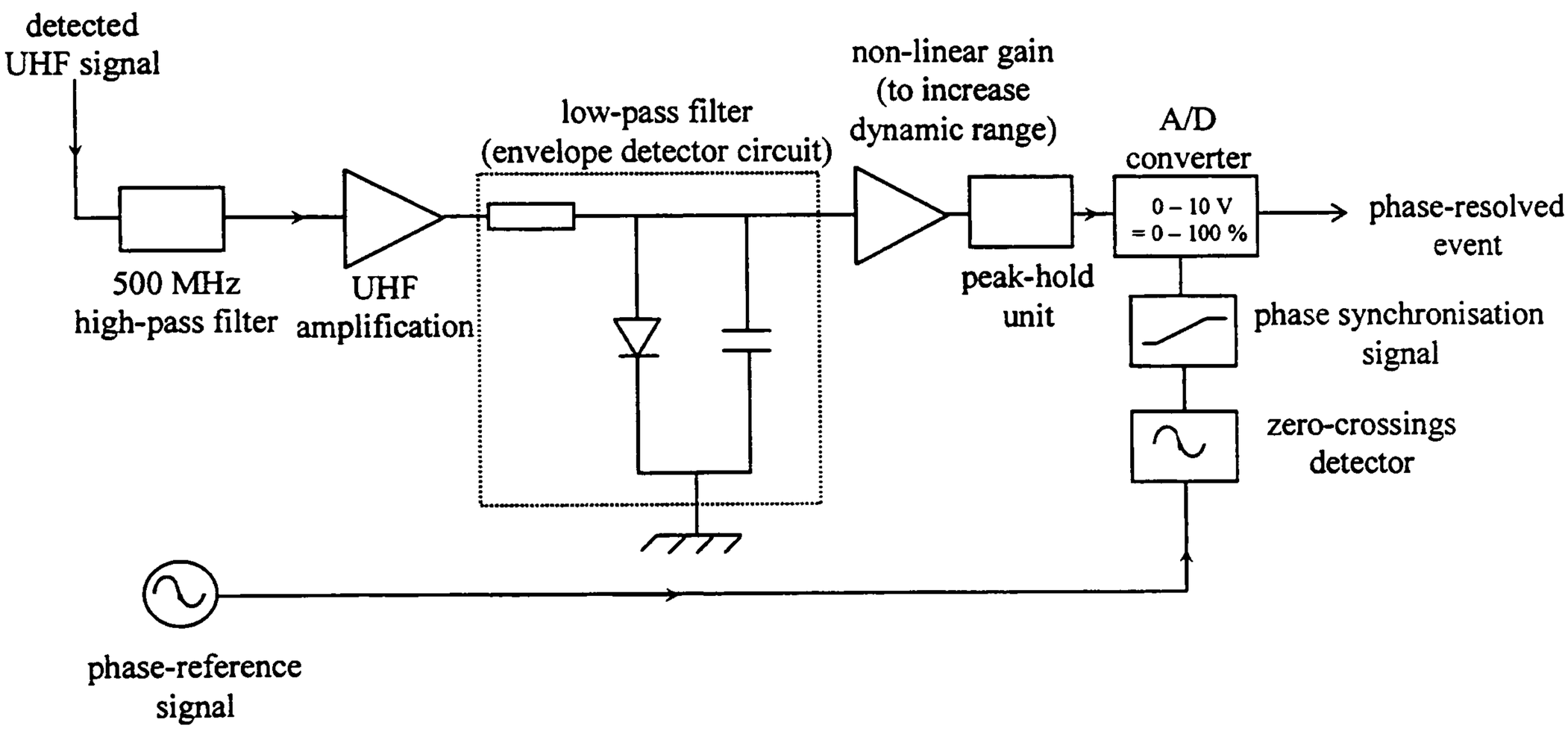

Figure 2.20 Schematic of PDM circuitry.

PD events are displayed as three-dimensional (*phase angle*, *pulse height* and *cycle number*) '*snapshots*'. The PDM resolves pulses into 64 phase windows, corresponding to a resolution of 5.6°. In each phase window, only the largest pulse is recorded. Measurements are performed for 50 sequential cycles and patterns can be saved as compressed data files [96].

2.4.5.2 Calibration of PDM

In this section, the relationship between the 'raw' UHF signal entering the PDM and its corresponding *pulse height* is investigated. The experimental arrangement used for this purpose is shown in Figure 2.21.

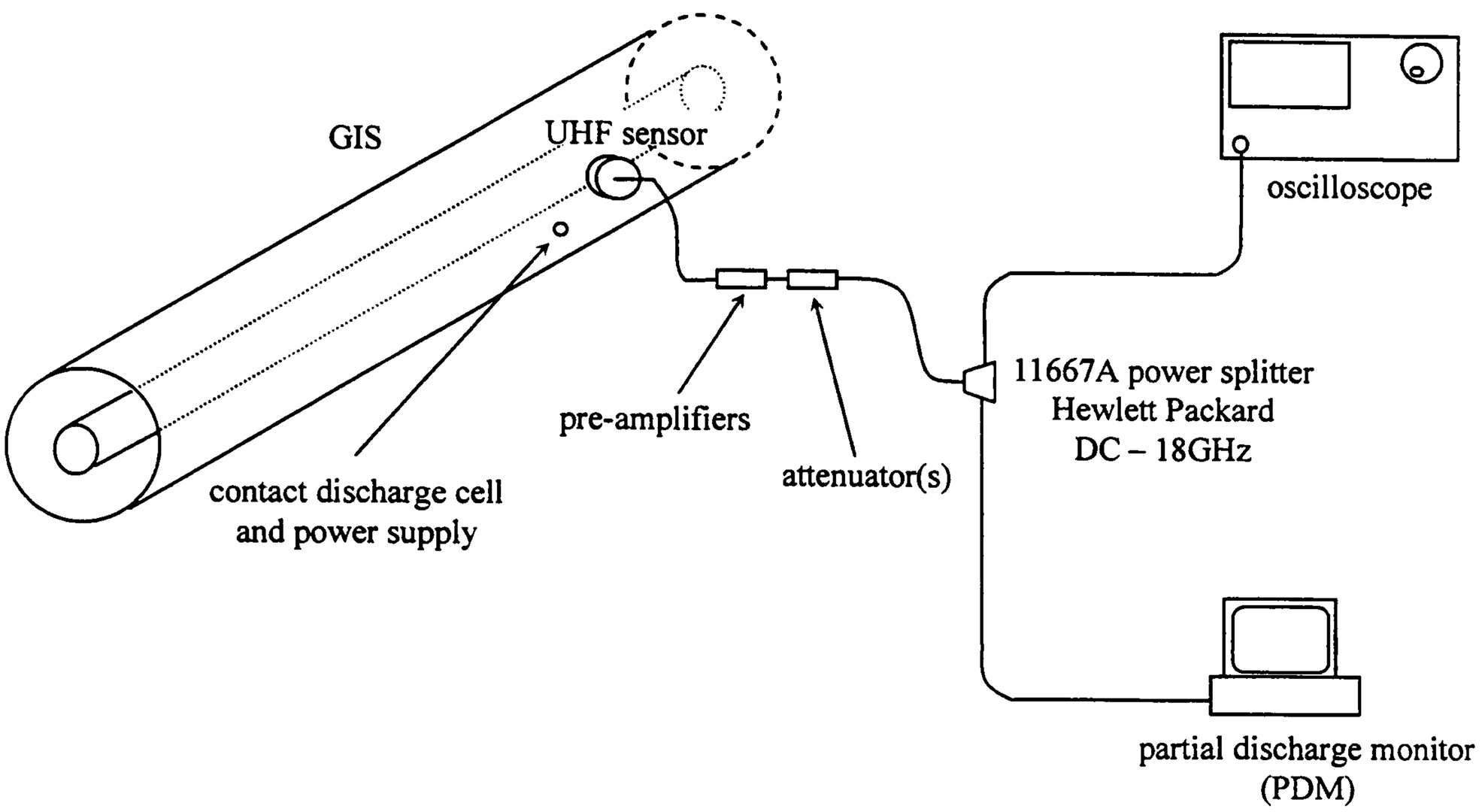

Figure 2.21 Experimental arrangement used to investigate the relationship between the detected UHF signal and *pulse height*.

A contact discharge cell [97] was positioned inside a GIS chamber; this provided a natural wave guiding structure for the UHF signals. The cell was then energised and this caused a single PD event and the excitation of a burst of UHF signal.

The UHF PD signal was detected using a UHF sensor that was mounted internally within the GIS. The UHF signal was subsequently amplified by 25 dB using the HP8447D pre-amplifier. This signal was attenuated prior to being divided equally using a 3dB 11667A Hewlett Packard power splitter, which ensures that identical UHF signals are supplied to the oscilloscope and the PDM.

Using this arrangement the relationship between the energy contained in the UHF signal measured using the oscilloscope (U), and the amplitude of the PD event (0-100%) displayed by the PDM (V_{PDM}) was investigated. UHF energy was calculated using:

$$U = \Delta t \sum_{n=0}^{N} \frac{V_n^2}{R_L} \qquad (2.6)$$

where R_L = 50 Ω, V_n is the voltage sampled using the oscilloscope, Δt is the time difference between successive samples and N is the number of samples in the record.

Attenuators covering the range 3 - 20 dB were used to vary the amplitude of the UHF signals that were detected allowing the relationship between U_{UHF} and V_{PDM} to be investigated over a wide range. The relationship between U_{UHF} and V_{PDM} is shown in Figure 2.22, revealing the nature of the non-linearity introduced by the PDM circuitry.

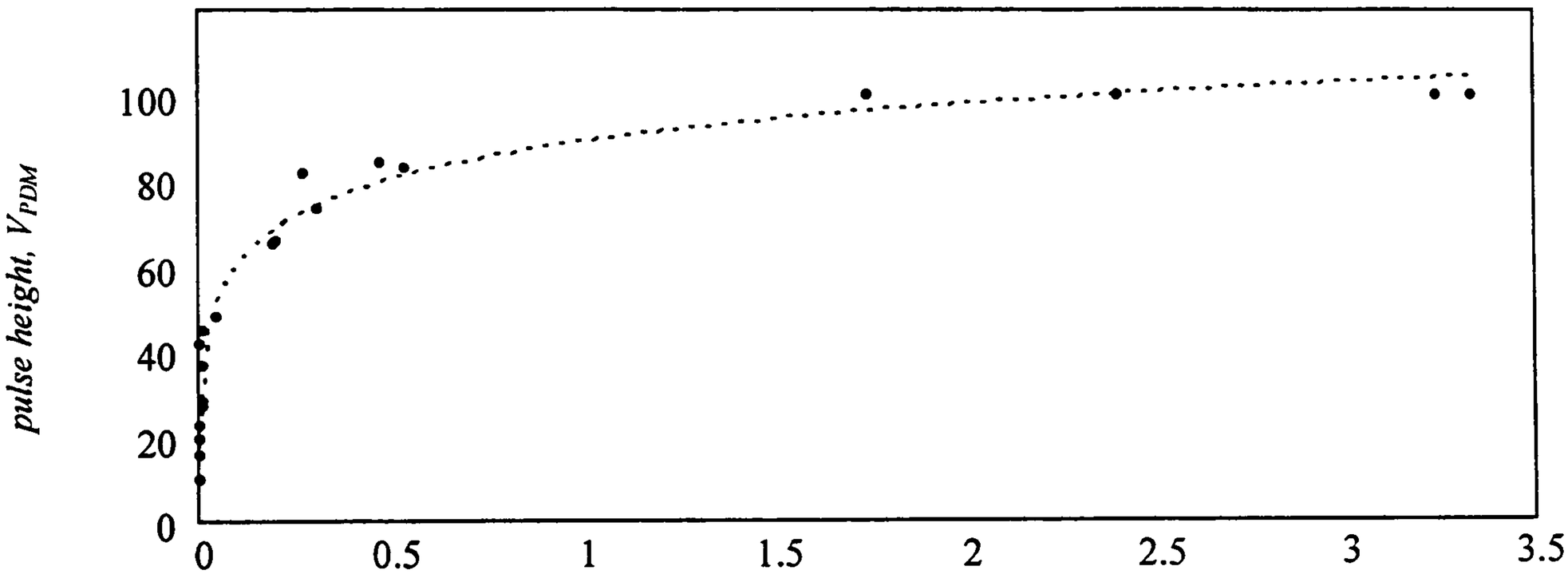

Figure 2.22 Relationship between UHF energy and the amplitude of pulses measured using the PDM.

This non-linearity is a feature of the PDM and allows defects of widely ranging PD levels to be represented on the same display. As will be described in Chapter 6, care must be taken in interpreting the amplitudes of pulses measured using the PDM for this reason.

2.4.5.3 Zero-crossing detector

An experiment was performed to confirm that the PDM triggered on the zero-crossing of the positive half cycle of the HV AC waveform. UHF signals from a HV corona source in air were measured in phase-resolved form using the PDM. These measurements were carried out at inception voltage. At inception voltage, PD events are restricted to the negative half cycle because electrons are readily available at the point-cathode.

Figure 2.23 shows PD pulses were restricted to the second half cycle, thus confirming that the PDM triggered on the first zero-crossing of the positive half cycle. This finding would be expected for a HV corona source in air, and confirms that the PDM triggered on the first zero-crossing of the positive half cycle [66,98].

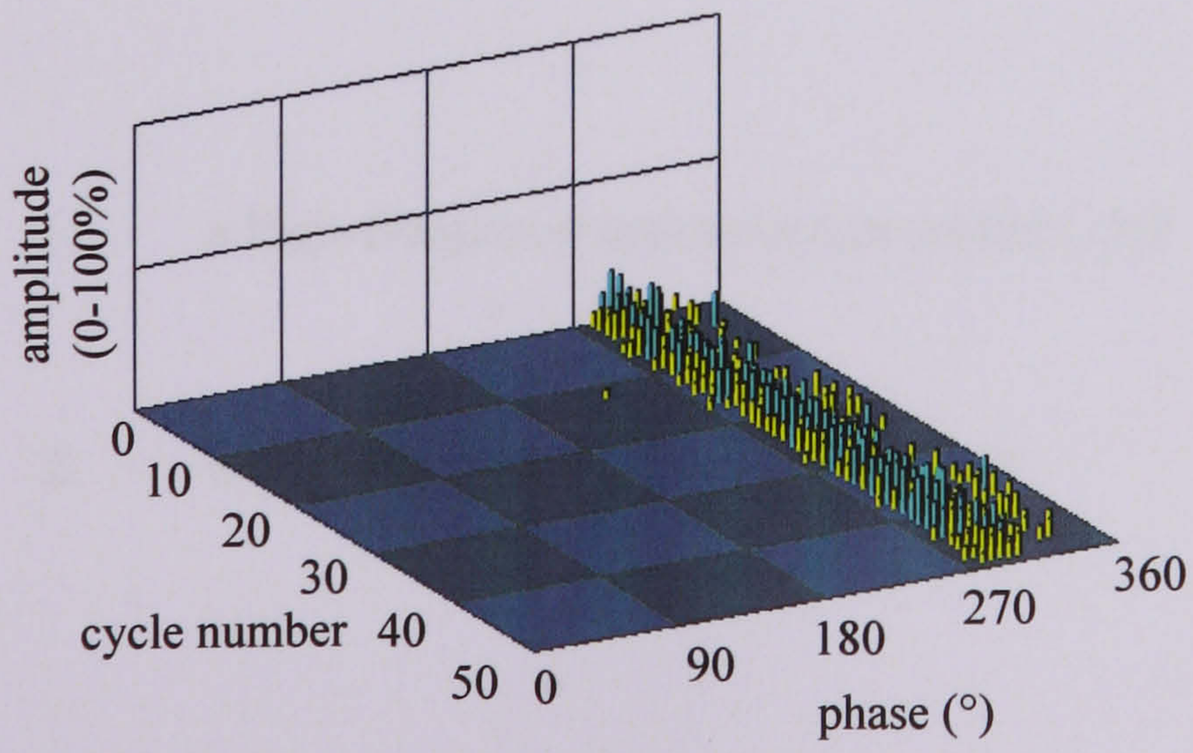

Figure 2.23 Phase-resolved pattern for a HV corona source in air at inception voltage.

3. MEASUREMENT OF PD CURRENT PULSES

3.1 Introduction

Liquid dielectrics are used in power transformers as they can be circulated to dissipate heat generated in the system. They provide good insulation and are more convenient than solids because they can fill a region to be insulated more easily [99]. However, despite of decades of research, the general understanding of electrical breakdown in liquid dielectrics is still relatively modest [100,101].

In this chapter, a brief overview of the physical processes that are involved when PD occurs in both gases and liquids is provided. Okubo et al [102,103] have shown that a PD current pulse conveys information relating to the PD process and so its accurate measurement is fundamental for the design of PD measuring systems [104,105]. In subsequent sections of this chapter, current pulses generated in oil are analysed to establish whether they are sufficiently short to cause the excitation of UHF signals.

The experiments described below involve PD generated in the insulating oil at the tip of a grounded protrusion. Current pulses are recorded using two measurement circuits:

1. a high-frequency measurement system, and

2. a high-frequency current transformer.

At inception voltages, current pulses are measured directly using a high-frequency measurement system and are found to lie on a sub-nanosecond timescale. At voltages well above inception, PD current pulses are measured using the high-frequency current transformer that was described in Section 2.4.1. The current pulses measured during the positive half cycle are found to lie on nanosecond timescales, whereas those measured during the negative half cycle are found to lie on a microsecond timescale. The comparably longer pulses measured during the negative half cycle are inspected, and the individual components of these pulses are shown to occur on nanosecond timescales. These experiments are of fundamental importance significance because UHF signals are only excited when discharges occur on timescales of around 1ns or less.

3.2 PD Processes in Gases and Liquids

For gaseous insulators, a good first-order model of breakdown has been established for almost a century, and is based on electron avalanches [23,106]. However, despite their widespread use, there remains a lack of understanding in the breakdown of liquid dielectrics [107,108]. This is because factors such as oil chemistry, fluid motion, particulate contamination, moisture content, temperature and space charges influence the breakdown process [87].

Although the general understanding of electrical breakdown in liquid dielectrics is still relatively modest processes such as: *field emission*, *electron attachment*, *collisional ionisation* and the existence of *streamer* and *leader* channels are similar in nature to those that have been found to exist in gaseous dielectrics [107, 108 and 109]. Therefore, an overview of the electrical breakdown characteristics of gases will be briefly considered.

3.2.1 PD in gases

Sulphur hexafluoride (SF_6) gas is commonly used for insulation in GIS, switchgear, power transformers and gas-insulated cables [109,110]. SF_6 is chosen for these applications as it is chemically stable, non toxic, has good heat transfer characteristics, a high dielectric strength and excellent arc-quenching properties [111].

The dielectric strength of SF_6, at atmospheric pressure, is three times that of air. At approximately 8 bar its dielectric strength is comparable to that of transformer oil.

The high dielectric strength of SF_6 is due to its property of *electron attachment* [109]. In this process, a free electron (e) moving in the applied electric field, which collides with a neutral molecule, may be attached to form a negative ion:

$$SF_6 + e = (SF_6)^- \qquad (3.1)$$

The free electron may be available due to cosmic radiation, natural radio-activity or field emission. The process of *electron attachment* competes with that of *collisional ionisation*. In the process of *collisional ionisation*, an electron with sufficient energy can remove an electron from a neutral molecule to create an additional free electron:

$$SF_6 + e = (SF_6)^+ + 2e \qquad (3.2)$$

Collisional ionisation is a cumulative process. If the electric field is sufficiently high, successive collisions can produce ever increasing numbers of free electrons and this may result in electrical breakdown of the gas. On the other hand, the heavy, slowly-moving negative ions which are formed by attachment are unable to accumulate the energy required to cause ionisation. Therefore, the *attachment process* effectively removes electrons and inhibits the formation of '*avalanches*' of electrons which might lead to breakdown.

The net rate of electron production in SF_6 depends on the gas pressure (p) and the applied field (E). The energy attained by charged particles moving in a gas varies linearly with both the applied field and the mean free path (λ) between collisions. If the temperature is constant, the energy varies directly with E/p.

The frequency of collisions made by a charged particle of a given energy increases with pressure. For an electron moving in a gas, the *probability of ionisation* for a single collision will be a function of E/p, while the *rate of ionisation* will be dependent on both pressure and E/p.

For a swarm of electrons moving in a gas under a uniform electric field, the *growth of ionisation rate* is defined by the number of ionising collisions per electron per cm travel in the gas. This parameter is termed the *ionisation coefficient* (α), that is

$$\alpha / p = fcn_1 (E/p) \qquad \text{(Eq 3.3)}$$

The removal of electrons from the swarm is determined by an *attachment coefficient* (η), and is defined as the number of attachments per electron per cm,

$$\eta / p = fcn_2 (E/p) \qquad \text{(Eq 3.4)}$$

The *net ionisation* is therefore dependent on the balance between ionisation and attachment. An important parameter describing the performance of SF_6 is the critical electric field ($E_{CRITICAL}$) at which, $\alpha = \eta$. For discharge phenomena to occur, it is necessary that $\alpha > \eta$, or $E > E_{CRITICAL}$ [109,110].

$$(\alpha - \eta) / p = fcn_1 (E/p) - fcn_1 (E/p) \qquad \text{(Eq 3.5)}$$

The development of an electron avalanche under uniform field conditions is shown in Figure 3.1. Most of the charge is contained in a very small region of approximately 10-100 μm diameter at the head of the avalanche. As will be described, the growth of this electron avalanche into a '*streamer*' depends on the balance between the ionisation and attachment processes.

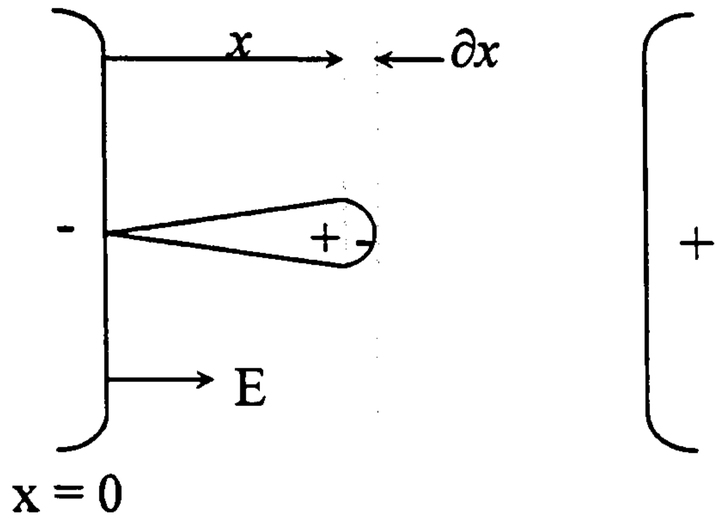

Figure 3.1 Development of an electron avalanche under uniform field conditions.

Figure 3.1 shows a swarm of electrons that have grown to contain $n(x)$ electrons at position x in the gap. By travelling a further incremental distance, ∂x, a new net charge will be generated as a result of ionising and attaching collisions with neutral molecules. This process can be represented by:

$$\partial n(x) = (\alpha - \eta)\, n(x)\, \partial x = \bar{\alpha}\, n(x)\, \partial x \qquad (3.6)$$

where $\bar{\alpha}$ is the *net ionisation coefficient*.

By integrating over the interval 0 to x the electronic charge contained in the avalanche tip can be evaluated:

$$\int_0^x \frac{\partial n(x)}{n(x)} = \int_0^x \bar{\alpha}\, \partial x \qquad (3.7)$$

hence:

$$n(x) = \exp\left\{\int_0^x \bar{\alpha}\, \partial x\right\} = \exp(\bar{\alpha} x) \qquad (3.8)$$

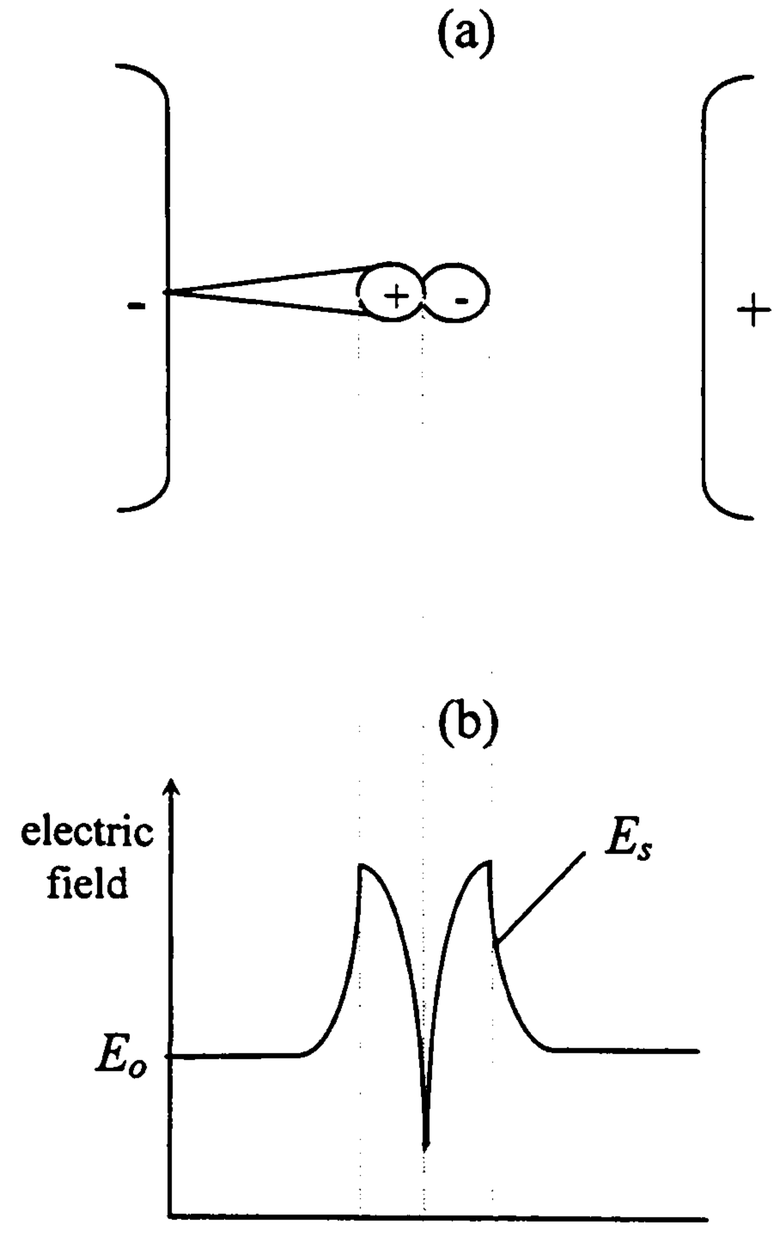

Figure 3.2 Electric field distortion due to a large electron avalanche.

Figure 3.2 shows the bipolar space charge distribution which can result from the ionisation process. This causes a distortion of the electric field (E) in the gap and ionisation activity ahead of and behind the avalanche tip is greatly enhanced. At a critical avalanche size, the space charge field (E_s) is high enough to generate rapidly moving ionisation channels called '*streamers*' which propagate towards both electrodes [109].

The propagation of cathode-directed streamers is dependent on electrons being released ahead of the streamer by photo-ionisation. On the hand, anode-directed streamers can propagate, without ionisation, when electrons are available from the streamer head. Typically, the time required for a streamer to travel 1 cm in SF_6 is approximately 10 ns [109]. At higher voltages, streamers can be replaced by highly conducting hot ionisation channels called '*leaders*' and flashover is very likely [69]. When electrons are accelerated and decelerated on a nanosecond timescale PD activity can be detected using the UHF technique. In subsequent sections of this thesis, the efficacy of using the UHF technique for the detection of discharge activity in insulating transformer oil is investigated.

3.2.2 PD in liquids

Optical measurements are often used to study the pre-breakdown phenomena in dielectric liquids [112,113,114]. These techniques are based on the principle that the refractive index of the region involving the discharge is different from that of the surrounding insulation [115]. When the sampling rate of an optical measuring system is sufficiently high, the temporal and spatial development of a PD can be studied [115,116,117]. Using optical measurements, several researchers have identified that electrical breakdown in a liquid consists of two separate phases. These are the '*bubble process*' and the '*electronic process*' [118,119].

The '*bubble process*' is best explained by considering a point-plane electrode system such as that shown in Figure 3.3. When the applied electric field is sufficiently high field emission occurs and electrons can escape from the tip of the point-cathode into the adjacent fluid [20,100]

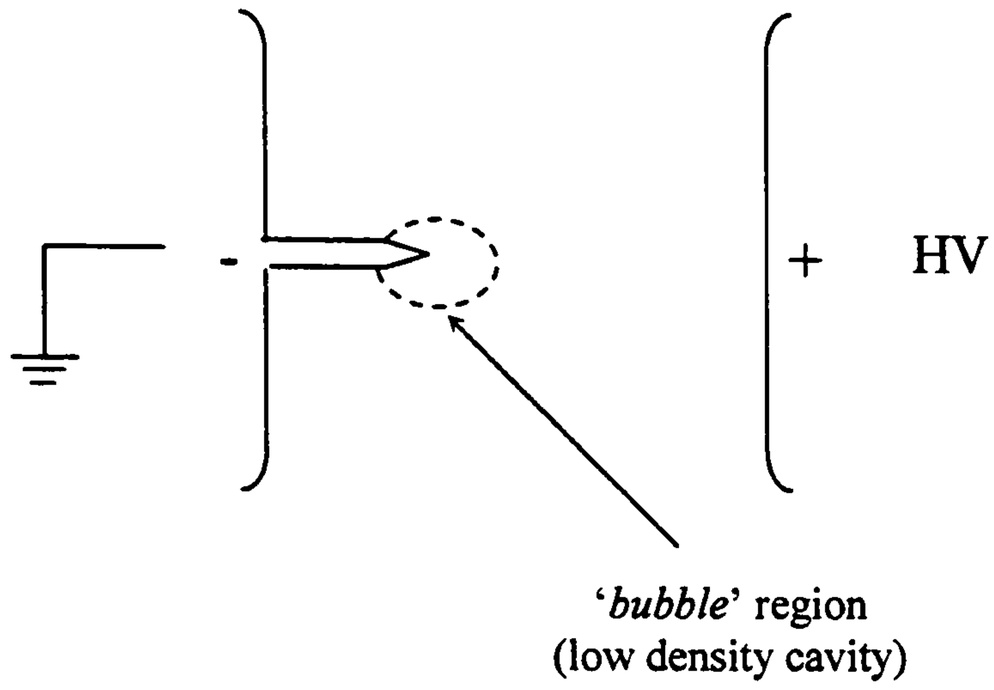

Figure 3.3 Formation of '*bubble*' in region of high electric field stress.

Optical experiments carried out by Watson et al [100 and 112] reported that a low-density cavity or '*bubble*' is formed in the region of high electric field stress. As more electrons escape from the protrusion into the cavity its volume will increase [20]. In the process of expanding, the cavity must do work against the ambient pressure and its size will be limited [120]. Watson et al [100,112], have reported an electro-hydrodynamic instability to occur at the surface of the cavity once it had reached a specific volume. Streamers were then observed to propagate from the surface of the cavity.

The propagation of streamers is termed as the '*electronic process*' [100,118]. It is generally accepted that streamers are gaseous filled channels, and their propagation is dependent on the direction of the geometrically defined electric field, the local electric field [114,115 and 116], the concentration of impurities [121], the conductivity and pressure of the streamer channel [118], and the accumulation of space charge at their tips [100,114 and 116].

Positive streamers, that is, those propagating from a point-anode, are generally described as being '*fast and filamentary*' [11,121]. On the other hand, negative streamers, that is, those propagating from a point-cathode and are described as being '*slow and bush-like*' [121,122]. Lesaint et al [123 and 124] have reported that the velocity of streamers in transformer oil, at inception voltage, is usually between 0.1 and 2.10^3 ms^{-1}. These experiments were carried out using impulse voltages, however observations relating to the propagation of streamers are of interest to this work.

It is generally accepted that positive streamers propagate by attracting negative charge from the liquid ahead of the streamer tip into the tip itself [121]. The propagation of positive streamers therefore relies on the presence of free electrons in the region surrounding its tip. Lundgaard et al [114,116] have suggested that streamer propagation is maintained by the evaporation of the liquid due to heating by electron avalanches. When electron avalanches occur at the tip of the streamer channel then the propagation of the streamer might be expected to be '*fast and filamentary*'. The length of a streamer is limited by the accumulation of space charge at its tip, or by a reduction in the externally applied electric field.

As already outlined, negative streamers are generally described as being '*slow and bush-like*'. This might be expected because electrons injected from the point-cathode into the oil will be subjected to a diverging electric field, and so negative streamers can break up and appear '*bush-like*'. Once these separate branches start to propagate, they have a tendency to shield each other. This regulates the electric field on each filament, and so limits the propagation velocity of negative streamers are limited [115,122].

3.2.3 PD current pulse shapes

Previous experiments involving SF_6 [125, 126] have shown that a PD current pulse can be simulated using

$$i(t) := i_e(t) + i_{ion}(t) \qquad (3.9)$$

$$i(t) := \frac{I_1}{T_1} t \cdot e^{\left(1 - \frac{t}{T_1}\right)} + I_2 \cdot e^{\frac{-t}{T_2}} \qquad (3.10)$$

where i_e and i_{ion} correspond to the electronic and ionic components of the current pulse respectively. The parameter t corresponds to time, and I and T define the peak current and risetime respectively.

Since the aim of this chapter is to establish whether the duration of PD current pulses in oil are sufficiently short to cause the excitation of UHF signals contributions from i_{ion} are neglected. This is because ionic components generally involve risetimes of some hundred nanoseconds and are lower in amplitude than the electronic components. Figure 3.4 shows three examples of simulated current pulses with risetimes of 0.035 ns, 1.0 ns and 1.7 ns and unity amplitude.

The total amount of charge q contained in each current pulse is

$$q = \int i(t)\, dt \qquad (3.11)$$

and its magnitude can be expressed in the frequency domain as

$$I(\omega) = \left| \frac{q}{(j + \omega)^2} \right| \qquad (3.12)$$

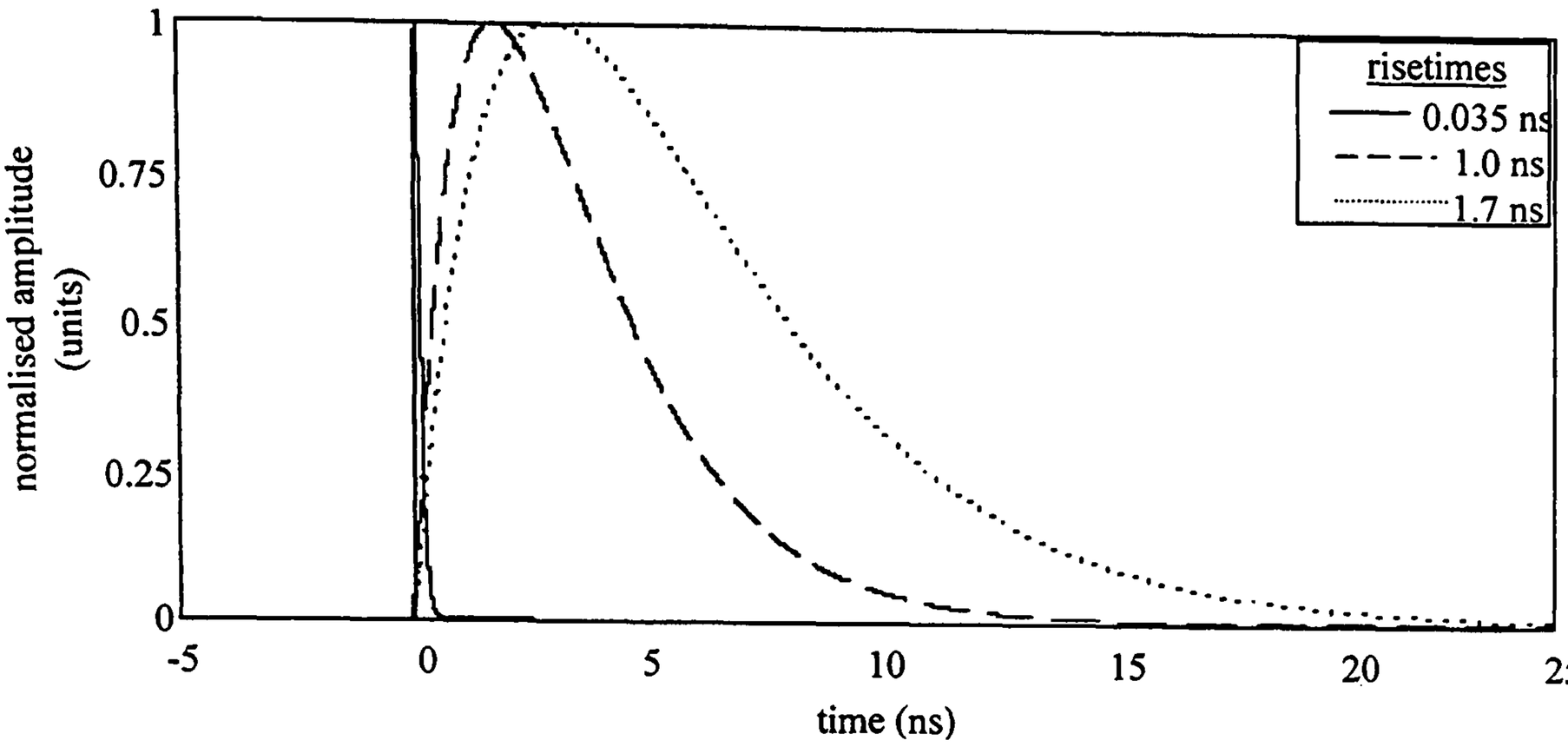

Figure 3.4 Simulated PD current pulses.

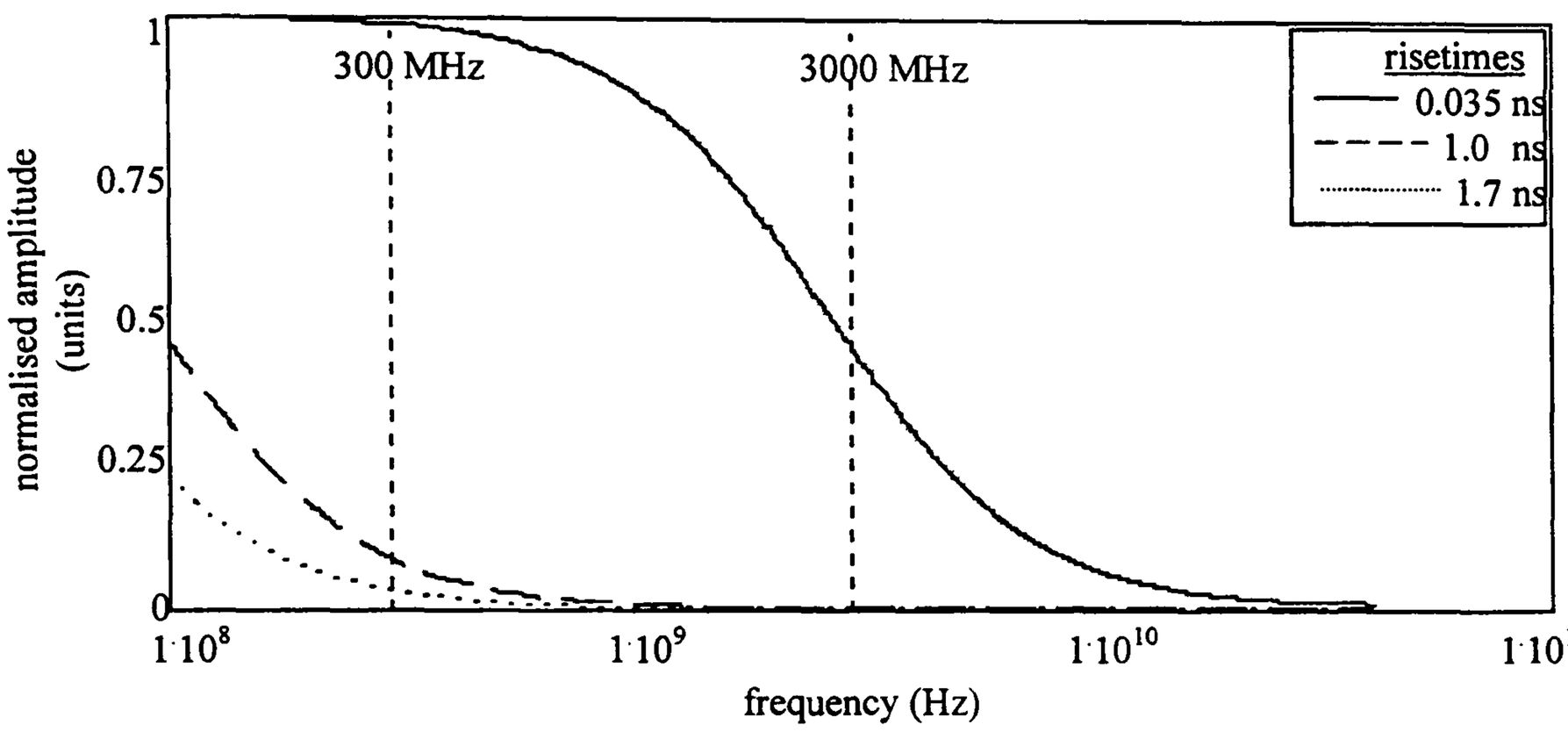

Figure 3.5 Frequency content of simulated current pulses.

Figure 3.5 shows the normalised spectral content of the simulated pulses, as determined numerically using a FFT. Clearly, the spectral content associated with a current pulse is inversely proportional to its duration [8]. Inspection of Figure 3.5 verifies that UHF signals are excited when PD current pulses occur with sub-nanosecond risetimes, that is, the curves relating to the pulses of 0.035 ns risetime is non-zero between 300-3000 MHz.

3.3 Current Pulse Measurement Systems

In Figure 3.6, the high frequency measurement systems that were used for measuring PD current pulses are shown. In both experiments, PD current pulse signals were attenuated by 20 dB to provide some protection for the measurement equipment.

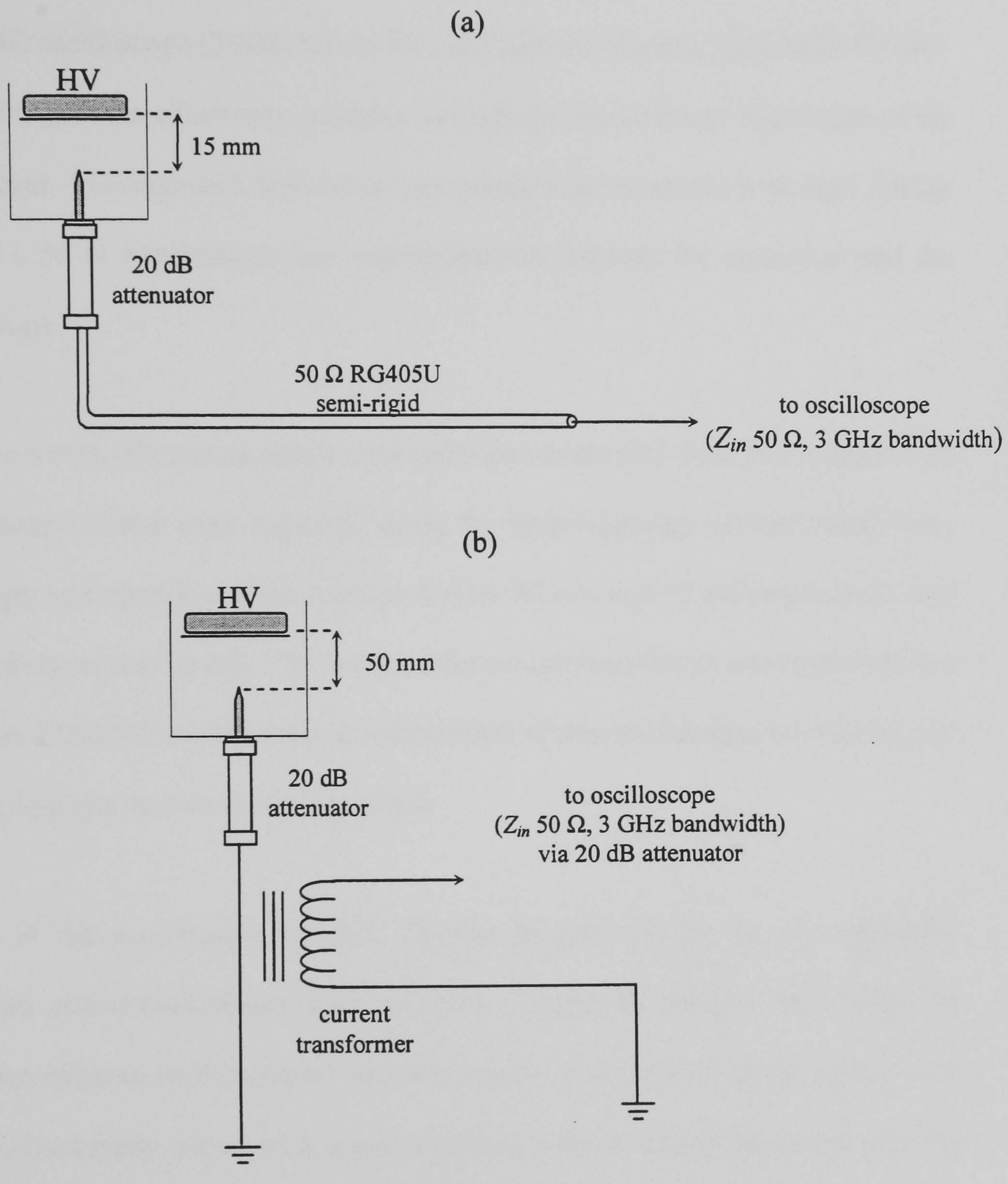

Figure 3.6 Measurement of PD current pulses using (a) the high-frequency measurement system and (b) the high-frequency current transformer.

For the electrode system shown in Figure 3.6(a), PD current pulses were measured at inception voltage using a high-frequency measurement system. The length and tip radius of the protrusion are 32 mm and 30 μm respectively and the gap distance was set at 15 mm. The electrode system was insulated using L10B oil, which is commonly used in power transformers in the UK. The protrusion was connected to a Tektronix TDS 694C oscilloscope (3 GHz bandwidth, 10 Gsamples/s) using 50 Ω RG405U low-loss cable, and was effectively grounded through the measurement impedance of the oscilloscope. This approach allowed current pulses to be measured with high fidelity because a 50 Ω transmission line was maintained between the attenuator and the oscilloscope.

In Figure 3.6(b), PD current pulses were generated in mineral oil at test voltages well above inception and were measured using the high-frequency current transformer. The length and tip radius of the protrusion were 50 mm and 35 μm respectively, and the gap distance was 50 mm. The output of the current transformer was connected to a Tektronix TDS694C oscilloscope. The bandwidth of this oscilloscope was 3 GHz, and the sampling rate was set at 10 Gsamples/s.

In both of the experiments outlined, PD was generated at the tip of a grounded protrusion and current pulses were recorded. During the positive half cycle, the protrusion behaved as the cathode and the polarity of measured current pulses were positive. Conversely, pulses with negative polarity were measured during the negative half cycle because electrons are attracted to the protrusion tip from the liquid dielectric [124]. The current pulse records that are discussed in this chapter are of interest because they will govern whether or not UHF signals are excited by partial discharges and give some insight into the temporal processes of PD in mineral oil.

3.4 Results and Discussion

3.4.1 Current pulses measured using the high-frequency measurement system

Figure 3.7 shows an example of a positive and a negative current pulse that were measured using the high-frequency measurement system [76]. The charge contained within the current pulse records shown was calculated to be 3.7 pC for the positive pulse, and –7.0 pC for the negative pulse.

The negative current pulse contained a greater amount of charge than the positive pulse, and this might be attributed to the presence of ionised regions within the oil in the region surrounding the point-anode. Under the influence of the high electric field, electrons can become detached from impurity molecules in the oil and can provide a source of electrons to the PD site. Under such conditions, PD current pulses measured at the point-anode might be expected to contain a greater amount of charge than those measured at the point-cathode. In the work of Chapter 4, PD current pulse shapes are discussed in greater detail.

Inspection of Figure 3.7 reveals that the risetime of the positive current pulse was approximately 0.1 ns, whereas the risetime of the negative current pulse was approximately 0.48 ns. These findings confirm that the UHF technique should be considered further for the detection of PD in oil.

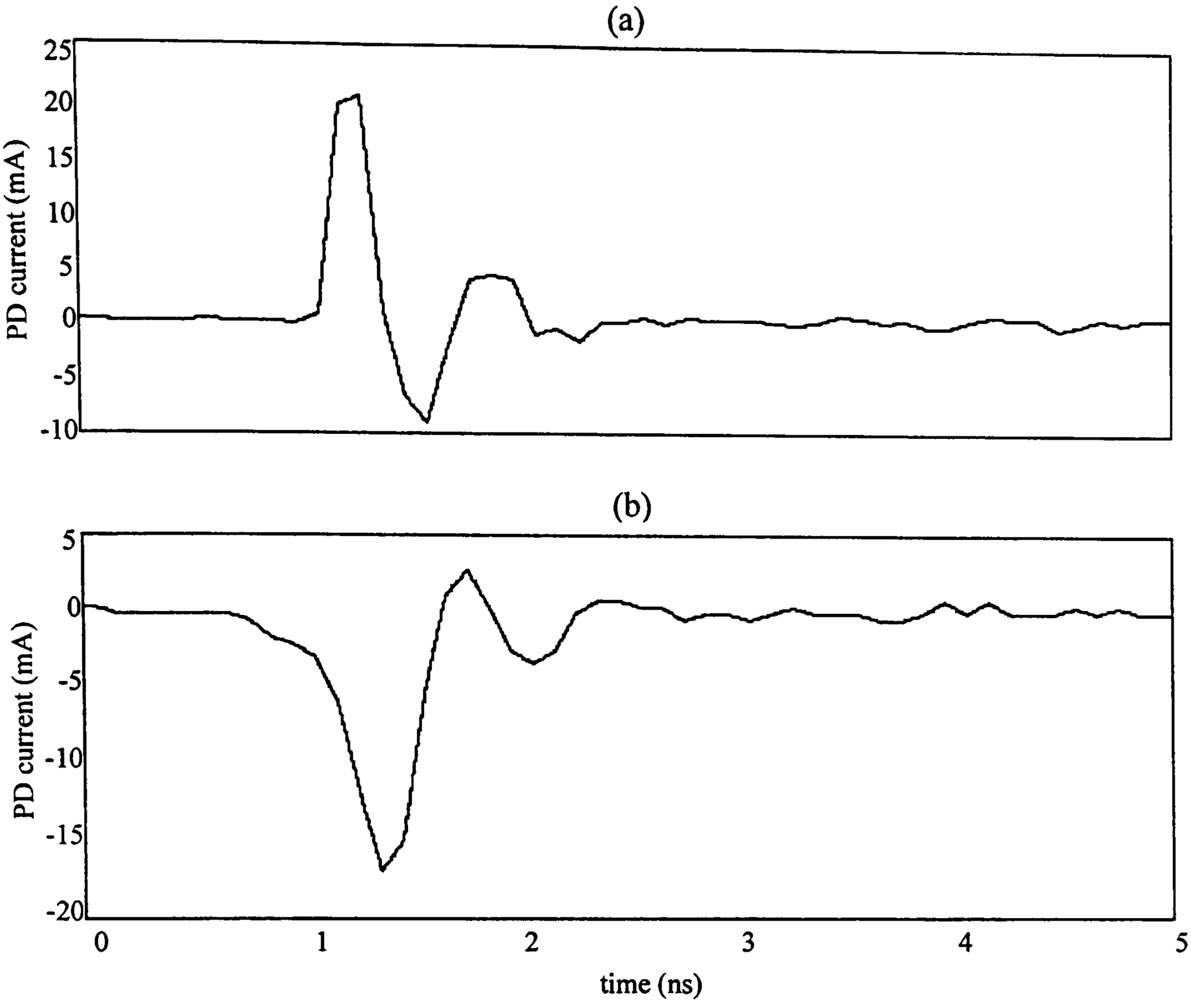

Figure 3.7 Examples of (a) positive and (b) negative PD current pulses measured using the high-frequency measurement system.

3.4.2 Current pulses measured using the high-frequency current transformer

Figure 3.8 shows an example of positive and negative current pulses that were measured using the high-frequency current transformer. These pulses were generated at test voltages well above inception. The positive current pulses occurred in separate bursts across a nanosecond timescale, whereas the negative current pulse consisted of shorter bursts that were superimposed on an underlying pulse of 10 μs duration.

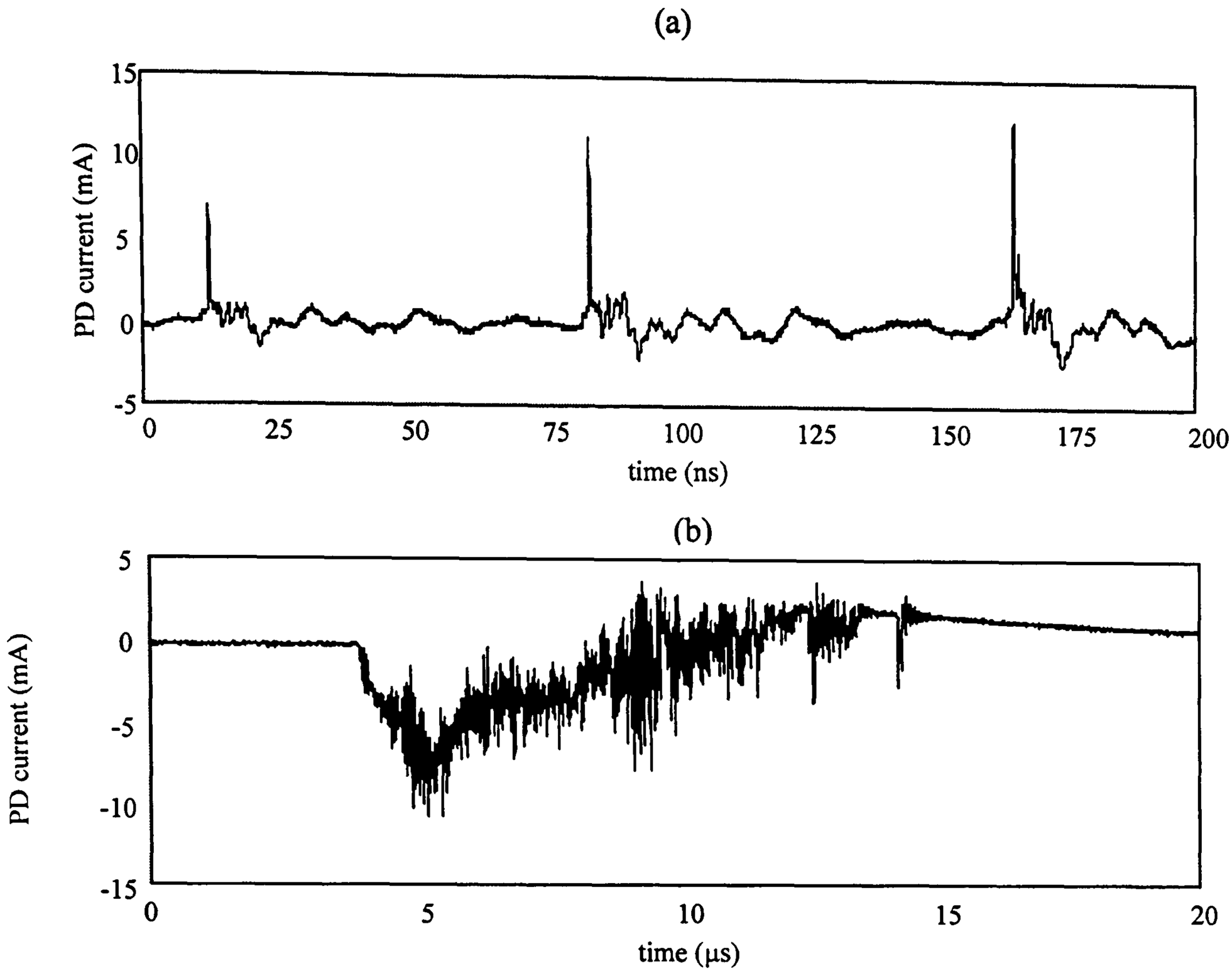

Figure 3.8 Examples of (a) positive and (b) negative triggering of PD current pulses using the high-frequency current transformer.

The positive current pulses shown in Figure 3.8(a) were measured when the protrusion was at a negative polarity with respect to the instantaneous voltage on the HV electrode. With reference to Section 3.2.3, these pulses might be representative of streamers that are '*slow and bush-like*'. On the other hand, the negative current pulses shown in Figure 3.8(b) were measured when the protrusion was at a positive potential. These pulses might be representative of streamers that are '*fast and filamentary*', and so shorter bursts of PD current might be expected to appear within the overall pulse.

Figure 3.9 shows an expanded view of some negative current pulses that were measured using the high-frequency current transformer. The corresponding UHF signal is also shown. Clearly, the current pulses occurred in bursts and the duration of each pulse was no more than a few nanoseconds [77]. These findings confirm that UHF signals can be excited during both half cycles, so the UHF technique should be considered further for PD monitoring.

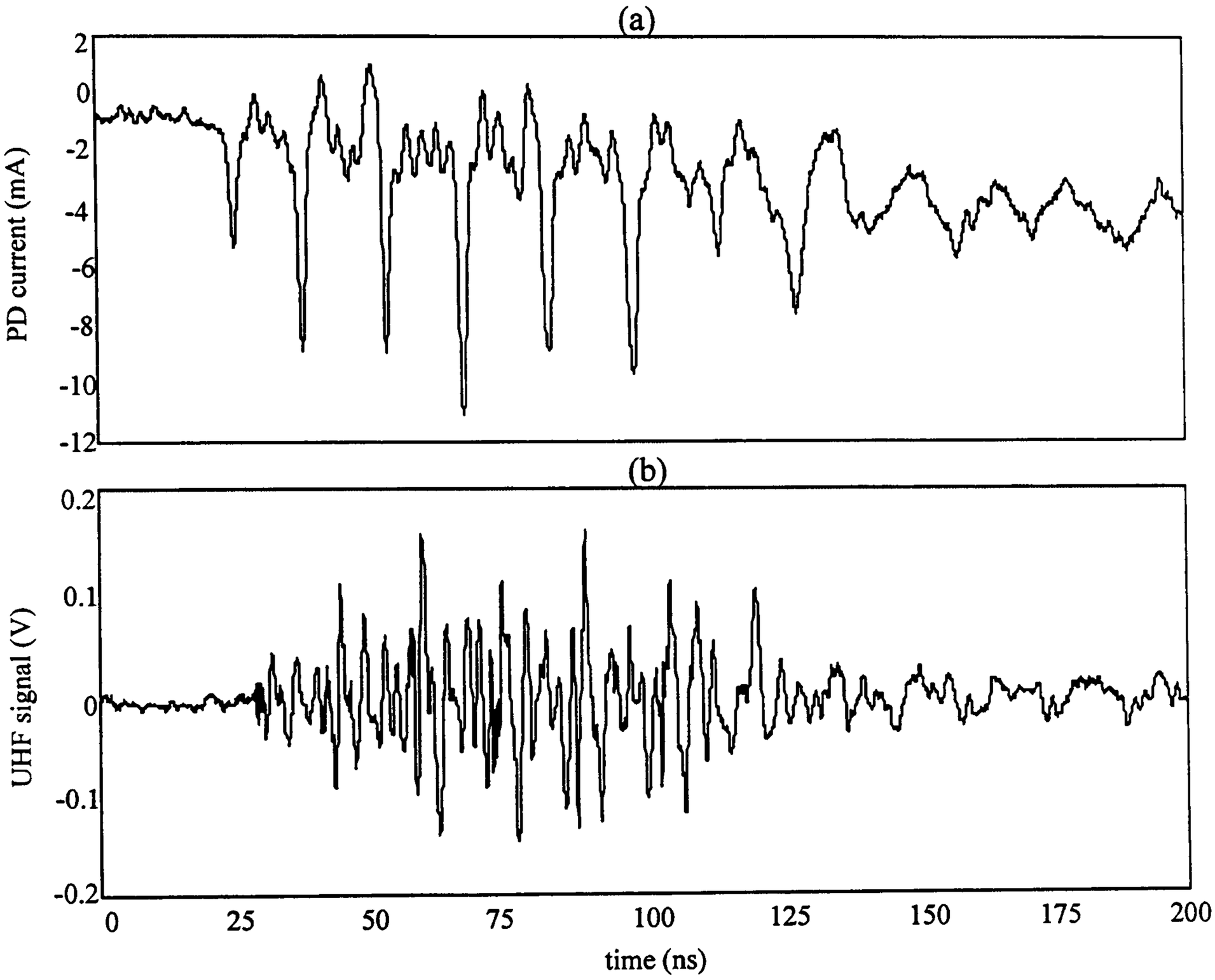

Figure 3.9 Expanded view of a (a) PD current pulse and (b) its corresponding UHF signal.

3.5 Conclusion

In this chapter, some of the physical processes that are associated with PD occurring in a liquid were reviewed. Experiments were carried out across a range of test voltages and PD was generated in the insulating oil surrounding the tip of a grounded protrusion. PD current pulses were recorded using detection circuits with different frequency responses and a variety of pulse shapes were recorded.

PD current pulses detected using the high-frequency measurement circuit were found to lie on sub-nanosecond timescales. At test voltages well above inception, the high-frequency current transformer was used to measure PD current pulses. The risetimes of the current pulses measured during the positive half cycle were found to lie on a sub-nanosecond duration. However, the negative current pulses consisted of shorter pulse bursts that were superimposed on an underlying pulse with a 10 μs duration. When these shorter pulse bursts were inspected they were found to lie on a sub-nanosecond timescale and cause the excitation of UHF signals. These measurements have shown that the risetimes of current pulses in oil can be sufficiently short to cause the excitation of UHF signals, at least under the highly divergent field conditions that exist at the protrusion tip.

It is suggested that further research should involve the simultaneous measurement of PD current pulses, UHF and optical emissions. In addition, chemical degradation of the oil might also be investigated. This would allow current pulse and UHF measurements to be better related to the PD mechanism.

4. COMPARISON OF CONVENTIONAL AND UHF MEASUREMENTS

4.1 Introduction

This chapter describes experiments in which PD is generated at the tip of a grounded protrusion and current pulse measurements are made simultaneously with both IEC 60270-based and UHF measurement systems. Since IEC 60270-based and UHF measurements systems operate on very different principles their responses to PD current pulses of known magnitude provides a useful basis for comparing the performance of both systems [78,79]. PD current pulses can be conveniently measured under laboratory conditions, but they cannot readily be measured on-site.

PD is generated in three different insulation media at the tip of the protrusion. The current pulses from PD generated in air, unused transformer oil and used transformer oil are measured using the high-frequency current transformer that was described in Section 2.4.1.

4.2 Experimental Procedure

4.2.1 Measurement of PD activity

PD activity was generated at the tip of a grounded protrusion as shown in Figure 4.1. The protrusion was created using a modified SMA monopole probe of length 14.5 mm and tip radius 125 μm. A pressboard barrier was positioned against the HV electrode to reduce the risk of breakdown, and the distance between the HV electrode and the protrusion was 3.5 mm. The type of unused transformer oil tested was BS148 Class 1–2512 [127]; this was chosen as it is commonly used by electrical utilities in the UK. The used transformer oil sample was taken from a ScottishPower transformer [128]. As can be seen from Figure 4.1, the test cell was positioned inside a chamber that provided a resonant cavity for UHF signals.

PD current pulse, IEC 60270-based and UHF measurements were simultaneously recorded using a LeCroy 960M-Wavepro oscilloscope (2 GHz bandwidth, 4 Gsamples/s per channel). The IEC 60270-based system was used to measure the *apparent charge* (q_a), and UHF PD signals were detected using a broadband electric field sensor. In order to isolate the oscilloscope, the high-frequency current transformer was used and its output attenuated by 20 dB.

The charge (q) associated with each PD current pulse, the peak of the corresponding IEC 60270-based waveform (V_{pk}) and the energy (U) associated with the measured UHF signal were found using numerical post-processing of the captured data.

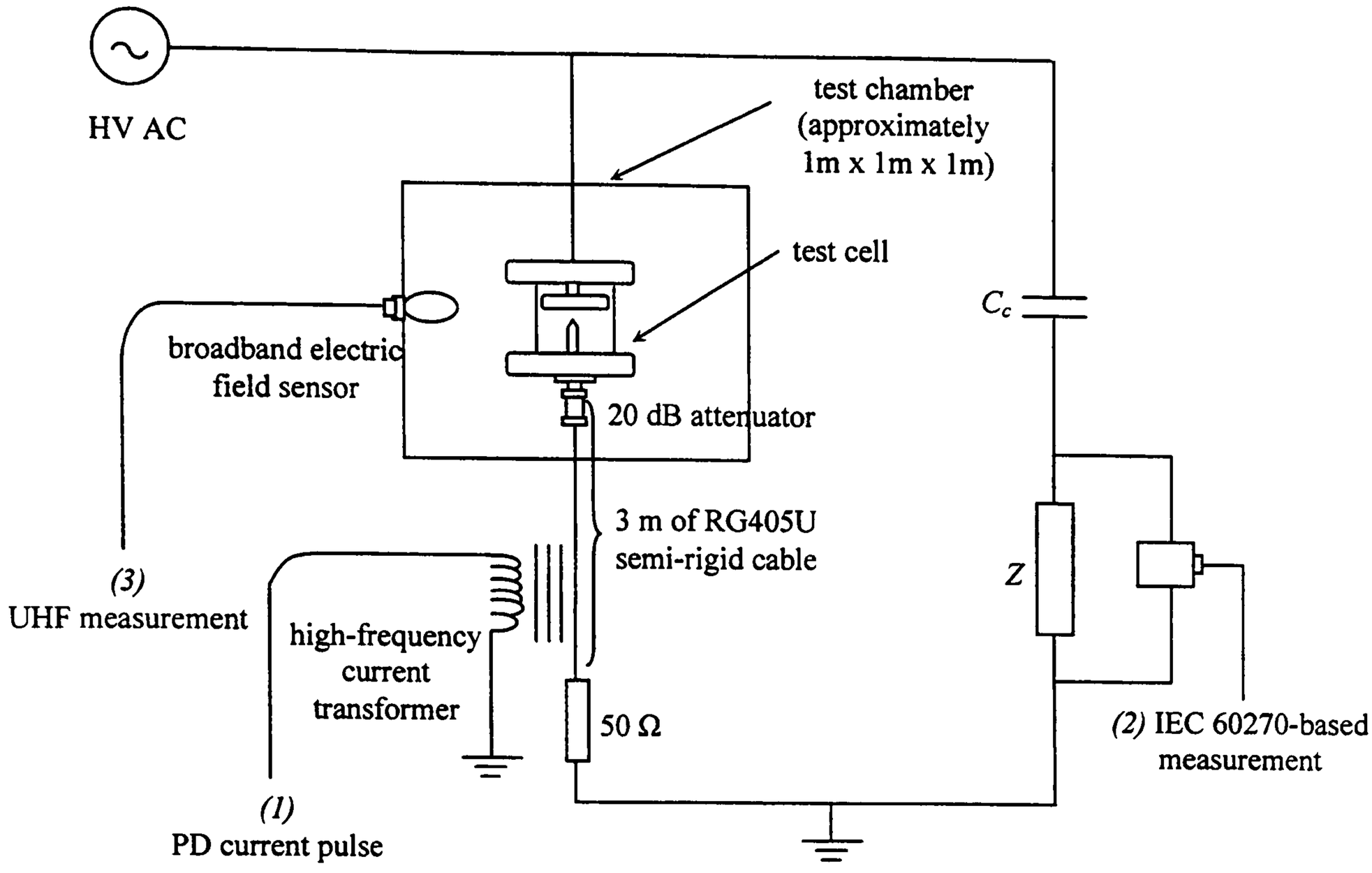

Figure 4.1 Arrangement for measuring PD activity, showing the three measured quantities:
(*1*) PD current pulse,
(*2*) IEC 60270-based and
(*3*) UHF measurement techniques.

In each experiment, the time-base of the oscilloscope was triggered on the PD current pulse signal. This allowed the polarity and amplitude threshold of the parameter most directly related to PD at the protrusion tip to be selected. The sampling rate of all measurements was 4 Gsamples/s. For each insulation medium, approximately 250 measurements were recorded using both positive and negative triggering. A PC was interfaced to the oscilloscope to allow measurements to be automatically saved as compressed data files. An example of simultaneous measurements of PD generated in unused transformer oil using the conducted current pulse method, IEC60270-based and UHF measurements are shown in Figure 4.2

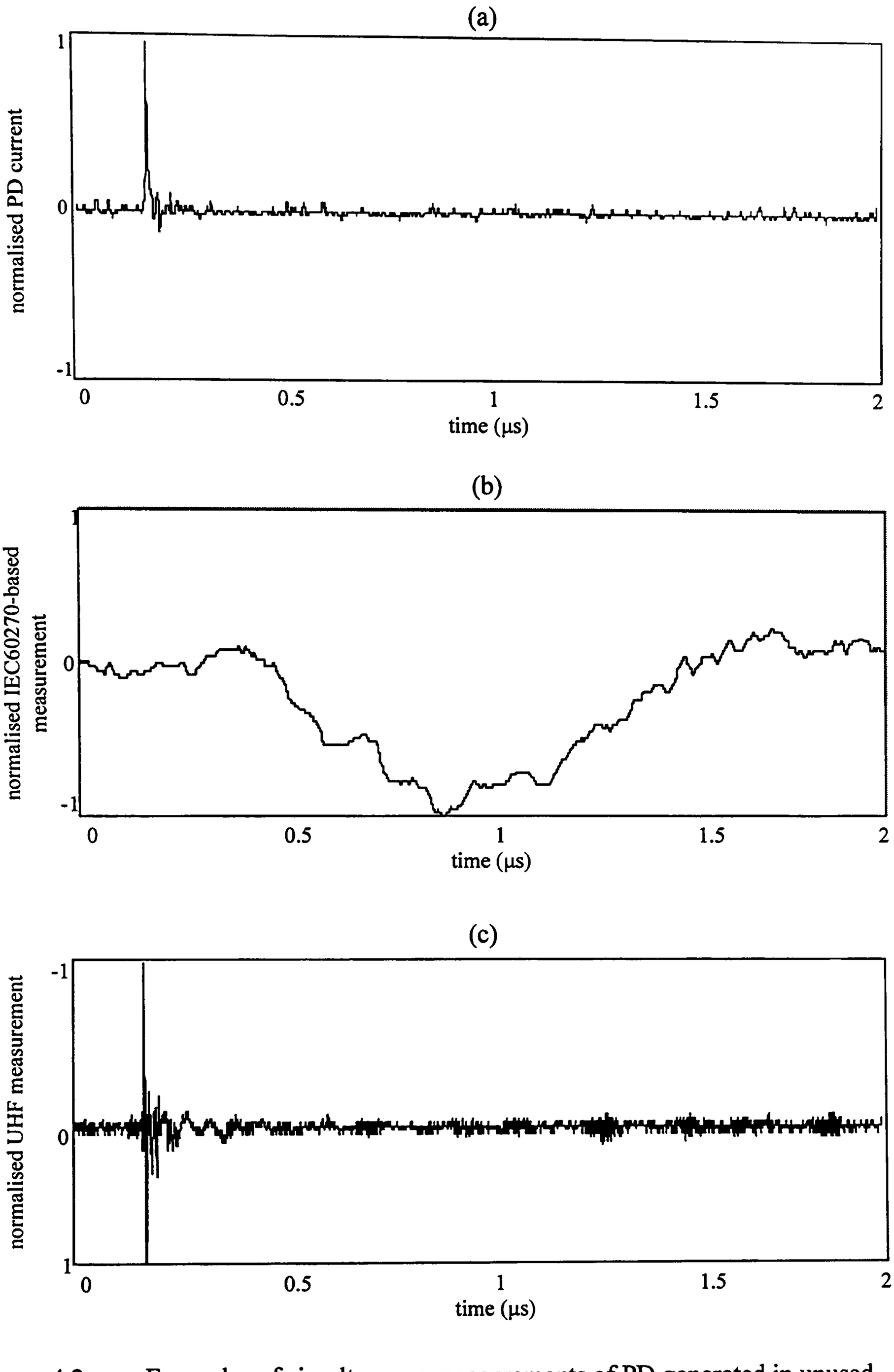

Figure 4.2 Examples of simultaneous measurements of PD generated in unused transformer oil using (a) PD current pulse, (b) IEC60270-based and (c) UHF systems.

4.2.2 Evaluation of PD current pulse shapes

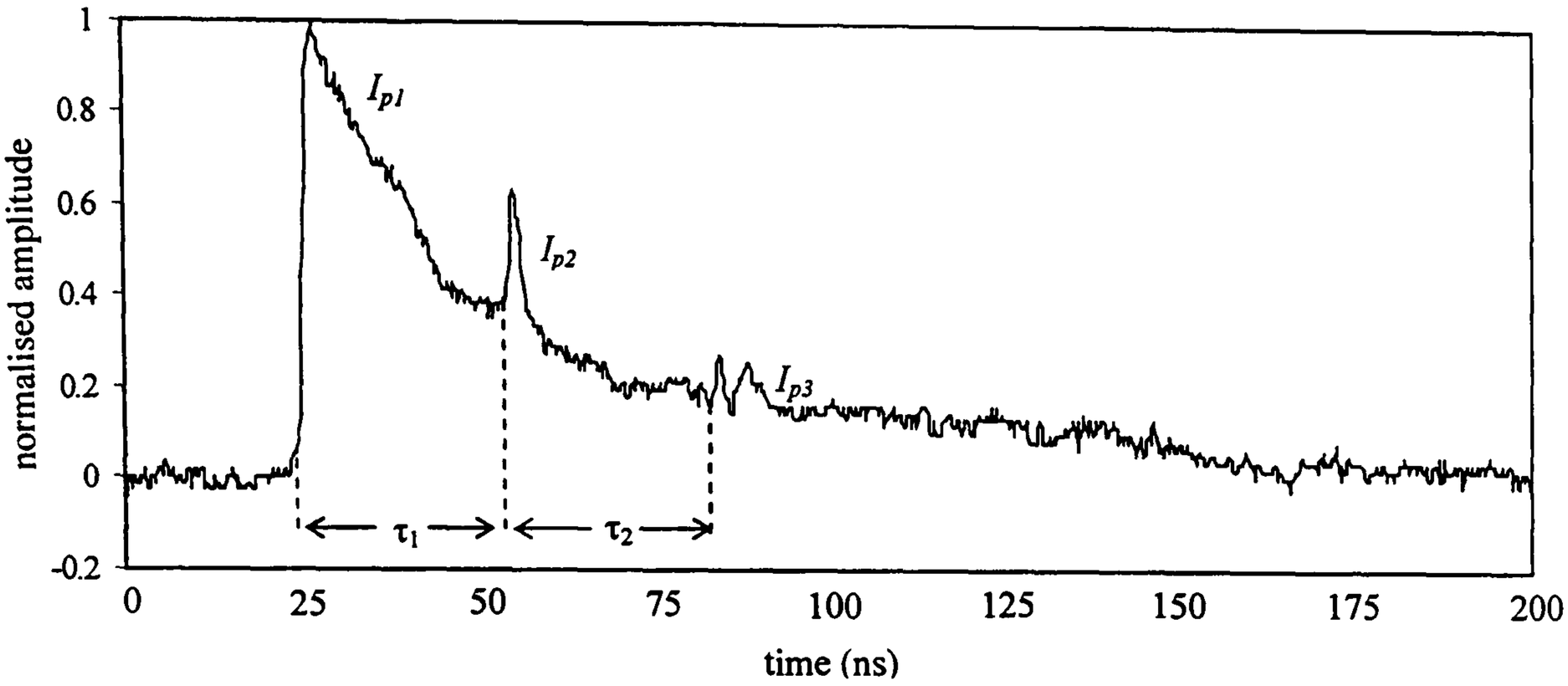

Figure 4.3 Example of a PD current pulse with reflections.

An example of a PD current pulse measured in air is shown in Figure 4.3. Inspection of this pulse shows that two smaller pulses I_{p2} and I_{p3} are superimposed on the falling edge of the main pulse I_{p1}. When the PD current pulse (I_{p1}) arrives at the 50 Ω resistor, part of it is reflected as it does not represent a perfect match at high frequencies. The reflected pulse then experiences a reflection when it reaches the open-circuit protrusion at the test cell. This pulse (I_{p2}) is again reflected at the 50 Ω resistor but part of this pulse will also be reflected. This reflected pulse (I_{p3}) will experience another reflection at the open-circuit protrusion at the test cell. This process continues until pulse reflections are small enough to be negligible.

The length of the RG405U cable between the protrusion and 50 Ω resistor is 3 m. Since the velocity of electrical signals in cables is $2x10^8$ ms^{-1}, then a time difference of 30 ns can be expected between pulses. As observed in Figure 4.2, the calculated value of τ agrees with the measured values. Although reflected pulses have an influence on the calculated values of q, this influence can be neglected as all pulses are scaled proportionally.

For each recorded current pulse, the peak current (I_p), risetime (t_r), pulse width (t_{pw}) at half-amplitude, falltime (t_f) and charge (q) were calculated automatically using software. The parameter q was calculated as the charge contained between 10% of I_p on the rising edge and 10% of I_p on the falling edge. This approach was chosen as it is consistent with the standard methods used to calculate the risetime and falltime of a signal.

In Figure 4.4, examples of PD current pulses measured in air, unused transformer oil and used transformer oil are shown. Single PD current pulses were measured in air and unused transformer oil and the response of the IEC 60270-based measurement system could be inspected on a timescale of 2 μs. For experiments involving used transformer oil, bursts of PD current pulses were measured and the response of the IEC 60270-based measurement system was inspected on a timescale of 20 μs. As will be described, the IEC 60270-based measurement system was unable to resolve individual bursts of PD current generated in used transformer oil because they occurred too close together. For all experiments, the calibration factor of the IEC 60270-based measurement system is 2.2 pC/mV.

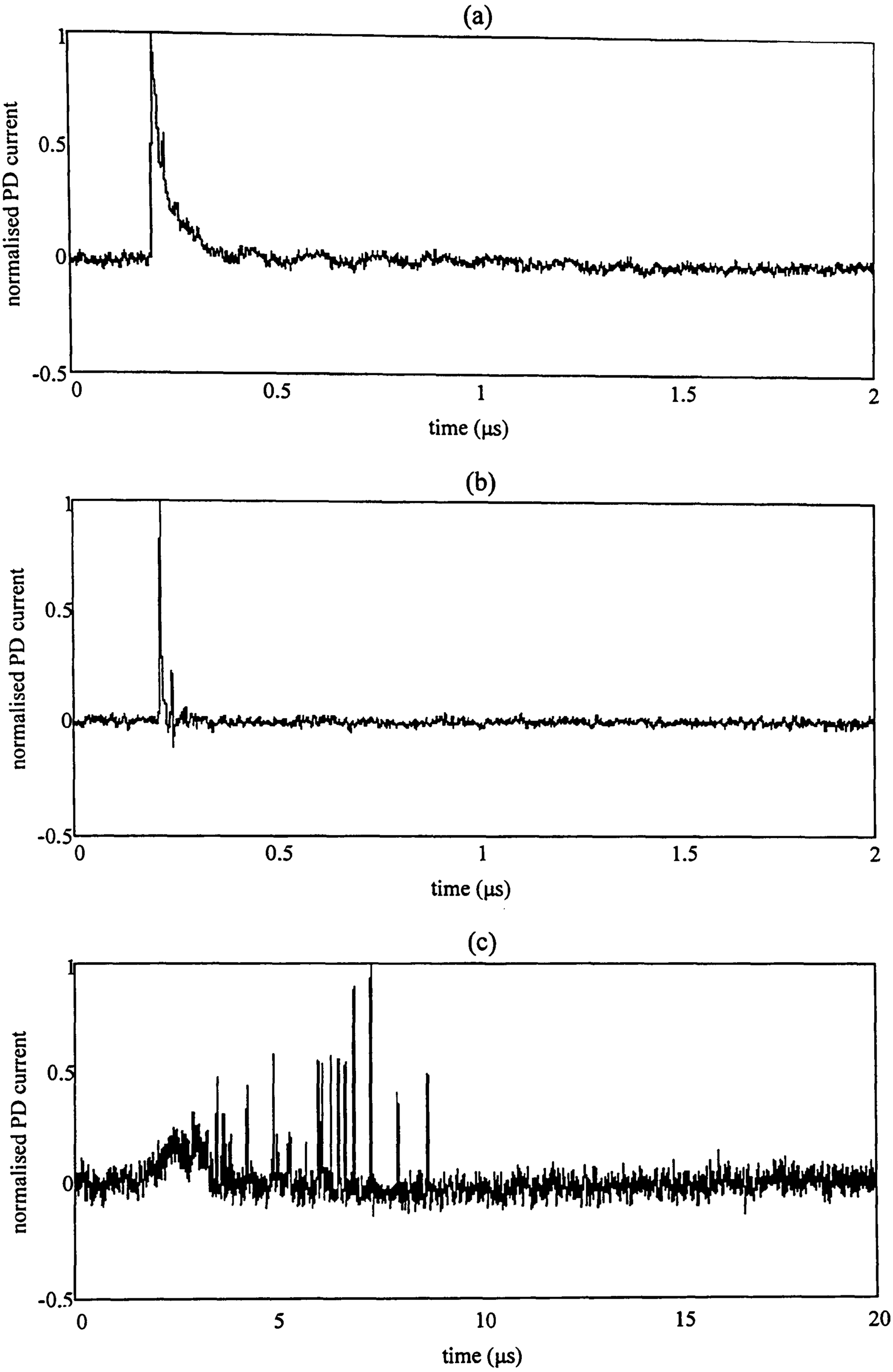

Figure 4.4 Examples of PD current pulses measured in (a) air, (b) unused transformer oil and (c) used transformer oil.

4.2.3 Correlation of measurements in air and in unused transformer oil

The remainder of this chapter is concerned with the correlation of PD current pulses with IEC 60270-based and UHF measurements. Since the IEC 60270-based measurement circuit could resolve single current pulses in air and unused transformer oil, the relationship between charge and the peak of the IEC 60270-based measurements was investigated by plotting q as a function of V_{pk}.

The acceleration and deceleration of charge at the PD site results in the excitation of an electric field. The UHF energy (U) detected at the output of a UHF sensor can be explained with reference to Figure 4.5.

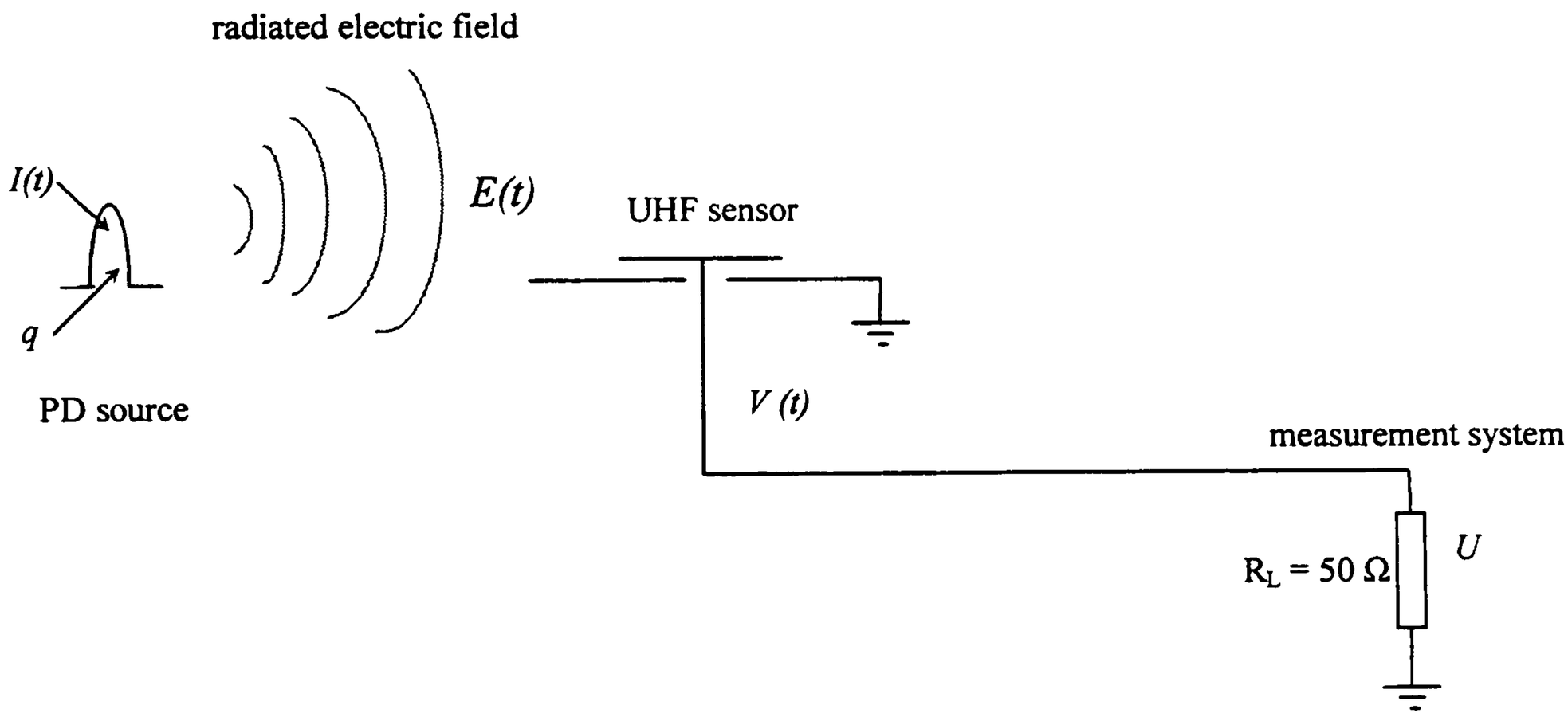

q	charge content of the PD pulse
$E(t)$	radiated electric field at UHF sensor
$V(t)$	UHF sensor output voltage
U	total energy delivered to measurement system

Figure 4.5 Relationship between PD current and instantaneous UHF sensor output.

For a single PD source in a fixed location the relationship between U and q can be predicted. By considering the output voltage from the sensor $V(t)$, the UHF electric field incident on the sensor $E(t)$ and the PD current $I(t)$, a linear relationship between $V(t)$ and q can be expected because:

1. The sensor is a passive linear device whose input quantity is $E(t)$ and output is $V(t)$, if $E(t)$ is scaled only in amplitude, $V(t)$ must scale proportionally.

2. $E(t)$ is the field radiated by $I(t)$. By similar reasoning, if $I(t)$ is scaled in amplitude, $E(t)$ will scale proportionally.

3. When $I(t)$ is scaled in amplitude, q will scale proportionally.

Under these well defined conditions, the amplitude of $V(t)$ will be proportional to q. This is a natural consequence of the passive, linear nature of all stages of the process. Since calculating U requires the squaring of V, searching for the expected linear relationship required that $\sqrt{U}$ be plotted against q.

The energy measured using the sensor is calculated using the procedures detailed in Section 2.4.5.2. In order to avoid problems associated with defining the start and the end of the UHF signal, the parameter U is calculated over the entire signal duration [81,129].

4.2.4 Correlation of measurements in used transformer oil

The IEC 60270-based measurement system was unable to resolve individual bursts of PD current because they occurred too close together. Consequently, the procedures used to correlate these measurements are more complex than those described for air and unused transformer oil.

As a first attempt at correlation, the total charge associated with every current pulse measured before the peak of the IEC 60270-based waveform was plotted against V_{pk}. This resulted in a very low amount of correlation because the IEC 60270-based measurement circuit was not fast enough to respond to separate current pulses. Better correlation was found between V_{pk} and the charge associated with the largest current pulse.

Since several PD current pulses were recorded during the response time of the IEC 60270-based measurement circuit, the UHF energy associated with the greatest current pulse was identified and U was plotted as a function of the peak of this pulse (I_p). Several UHF signals were inspected and 0.55 μs was found to be a reasonable approximation of their durations. For this calculation, the duration of each UHF signal was taken to be 0.55 μs.

4.3 Results and Discussion

Approximately 250 measurements were recorded using both positive and negative triggering. In Table 4.1, properties of measured PD current pulses and radiated UHF signals are shown. These parameters were calculated as being the mean value of measurements made during both the positive and the negative half cycle.

Table 4.1 – Properties of measured PD current pulses and radiated UHF signals.

Insulation medium and applied voltage	**Parameter – calculated as the mean value during the positive half cycle**						
	PD current pulse parameters					**IEC 60270-based**	**UHF**
	I_p (mA)	t_r (ns)	t_{pw} (ns)	t_f (ns)	q (nC)	V_{pk} (mV)	U (fJ)
Air 2.3 kV	33.0	1.63	16.60	77.50	0.97	-98.5	71.6
Unused transformer oil 13.3 kV	22.5	1.13	3.01	6.69	0.08	-18.6	65.5
Used transformer oil 14.7 kV	334.0	1.30	2.33	3.24	0.87	-358.0	12000
	Parameter – calculated as the mean value during the negative half cycle						
Air 2.3 kV	-49.0	4.99	14.20	44.00	-1.02	101.0	91.7
Unused transformer oil 13.3 kV	-6.72	2.04	4.77	10.20	-0.04	12.8	~0
Used transformer oil 14.7 kV	-218.0	2.21	2.68	3.78	-0.65	664.0	4030

4.3.1 Evaluation of measurements in air

4.3.1.1 Regularity of pulse shape

A linear correlation between I_p and q will indicate that the measured current pulses are scaled in terms of their amplitude, while a broad scatter would indicate pulse-shape variability. The regularity of pulse shapes was investigated by plotting the magnitude of I_p as a function of q

The regularity of current pulse shapes measured in air can be seen by examining Figure 4.6. Pulses measured during the positive half cycle revealed a stronger correlation between q and I_p than those measured during the negative half cycle.

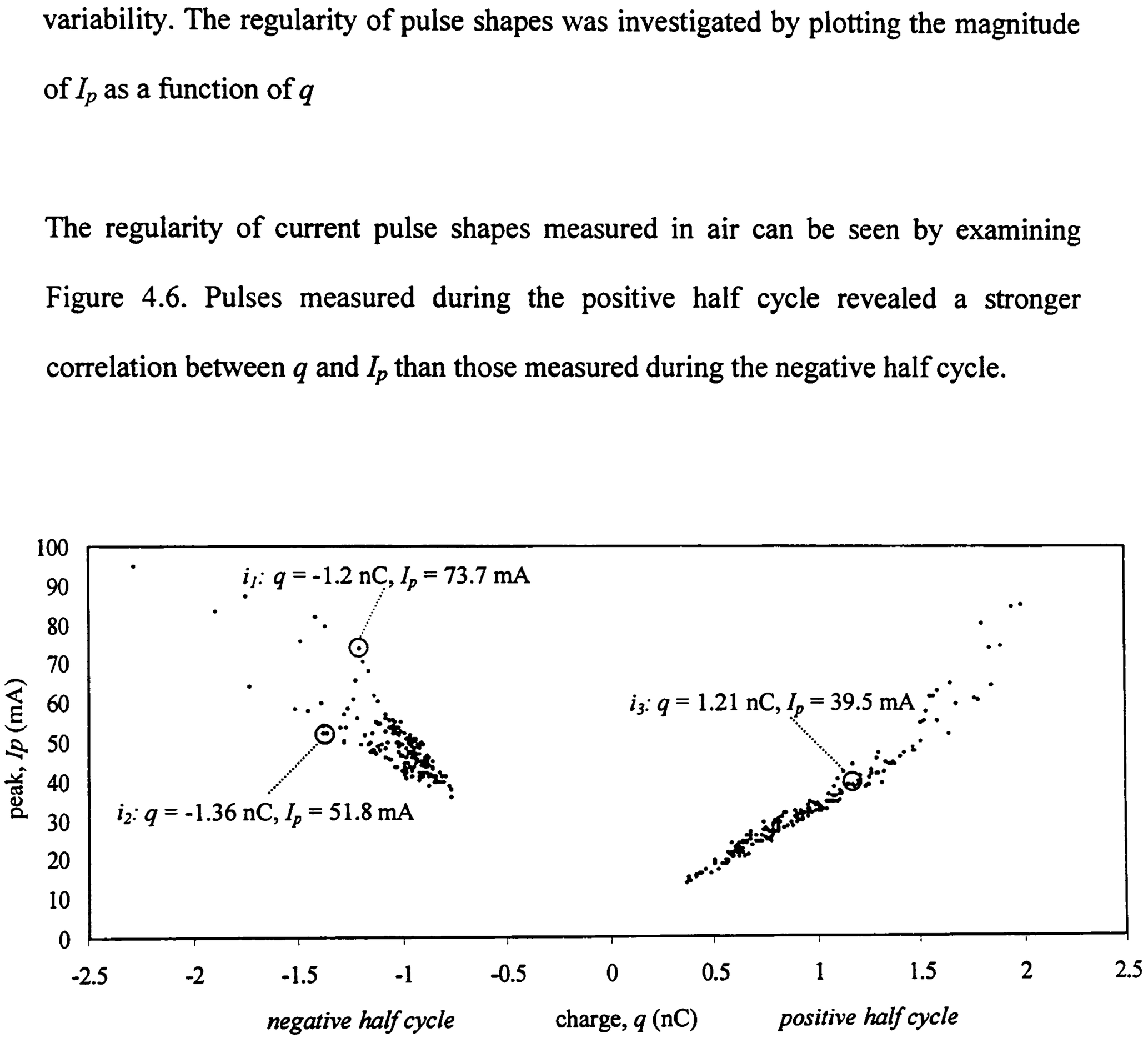

Figure 4.6 PD current pulses in air at 2.3 kV, showing correlation between q and I_p.

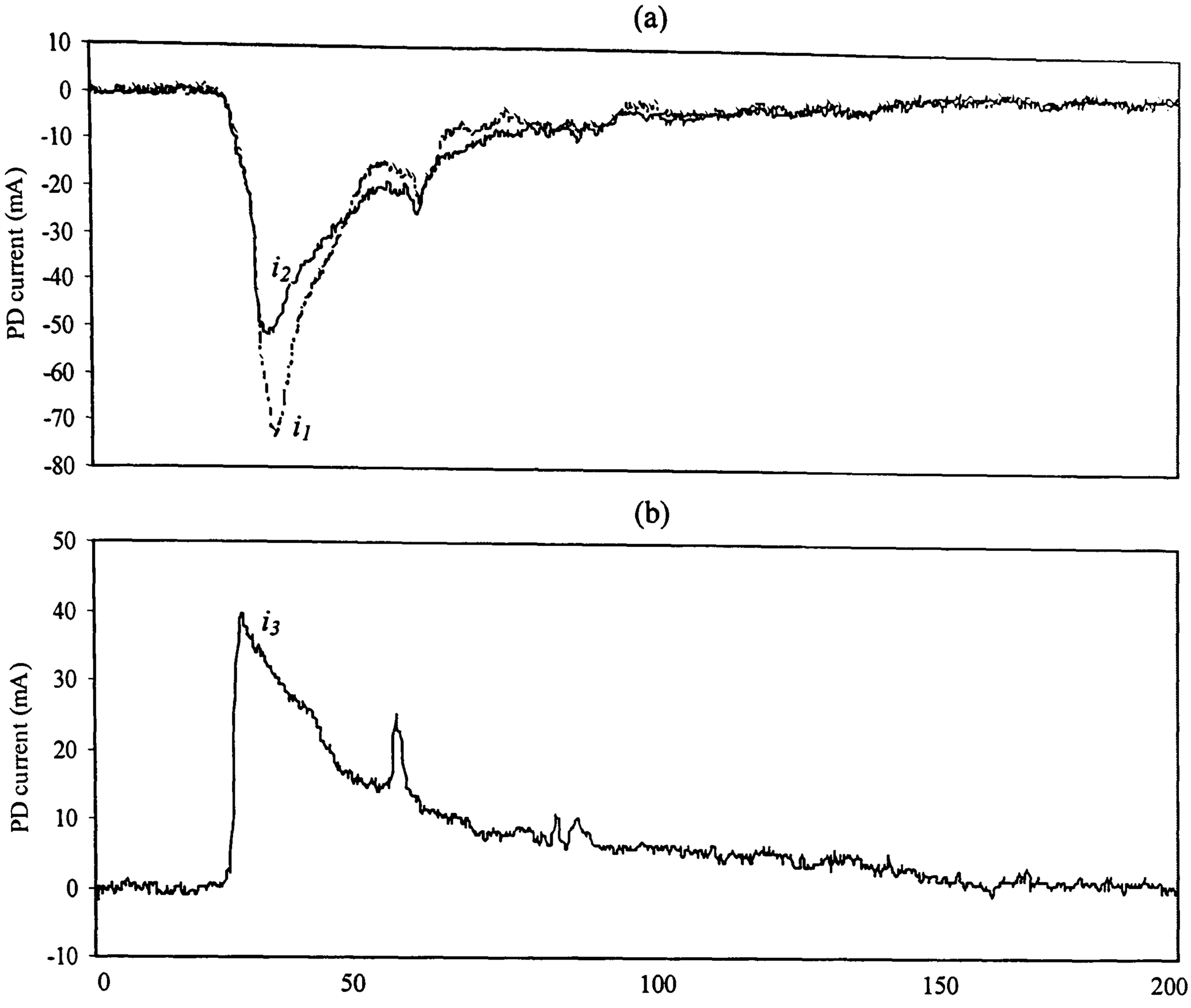

Figure 4.7 Expanded view of current pulses measured in air at 2.3 kV with (a) negative triggering and (b) positive triggering.

In Figure 4.7, current pulses for the highlighted data points of Figure 4.6 are shown. The charges associated with the negative pulses vary by a factor of 1.13, while their I_p values differ by a factor of 0.7. During the positive half cycle, electrons are supplied to the discharge site as a result of field emission and a consistent pulse shape results.

4.3.1.2 IEC 60270-based measurements

Figure 4.8 shows the relationship between q and V_{pk}. During both half cycles, q is closely proportional to V_{pk}. This confirms that measurements made using the IEC 60270-based system were less sensitive to variations in current pulse-shape, and that the system was behaving as designed for measuring PD current pulses in air.

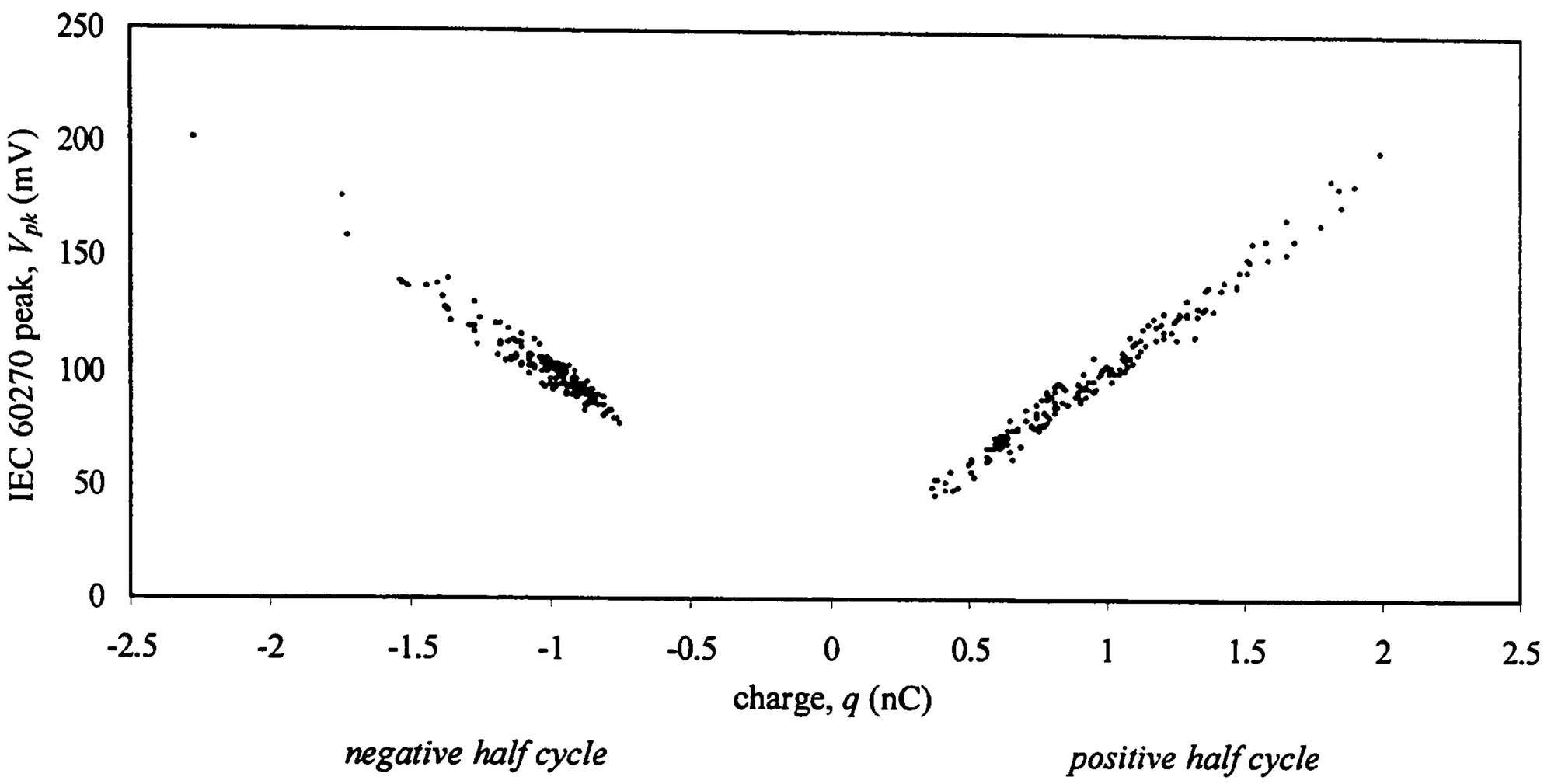

Figure 4.8 PD activity measured in air at 2.3 kV, showing correlation between q and V_{pk}.

4.3.1.3 UHF measurements

Figure 4.9 shows the relationship between UHF energy and charge. The correlation between $\sqrt{U}$ and q is closer during the positive half cycle than during the negative half cycle. This might be expected because current pulse shapes were found to be more repeatable during the positive half cycle. The current pulses shown in Figure 4.7 correspond to the data points that are highlighted in Figure 4.9.

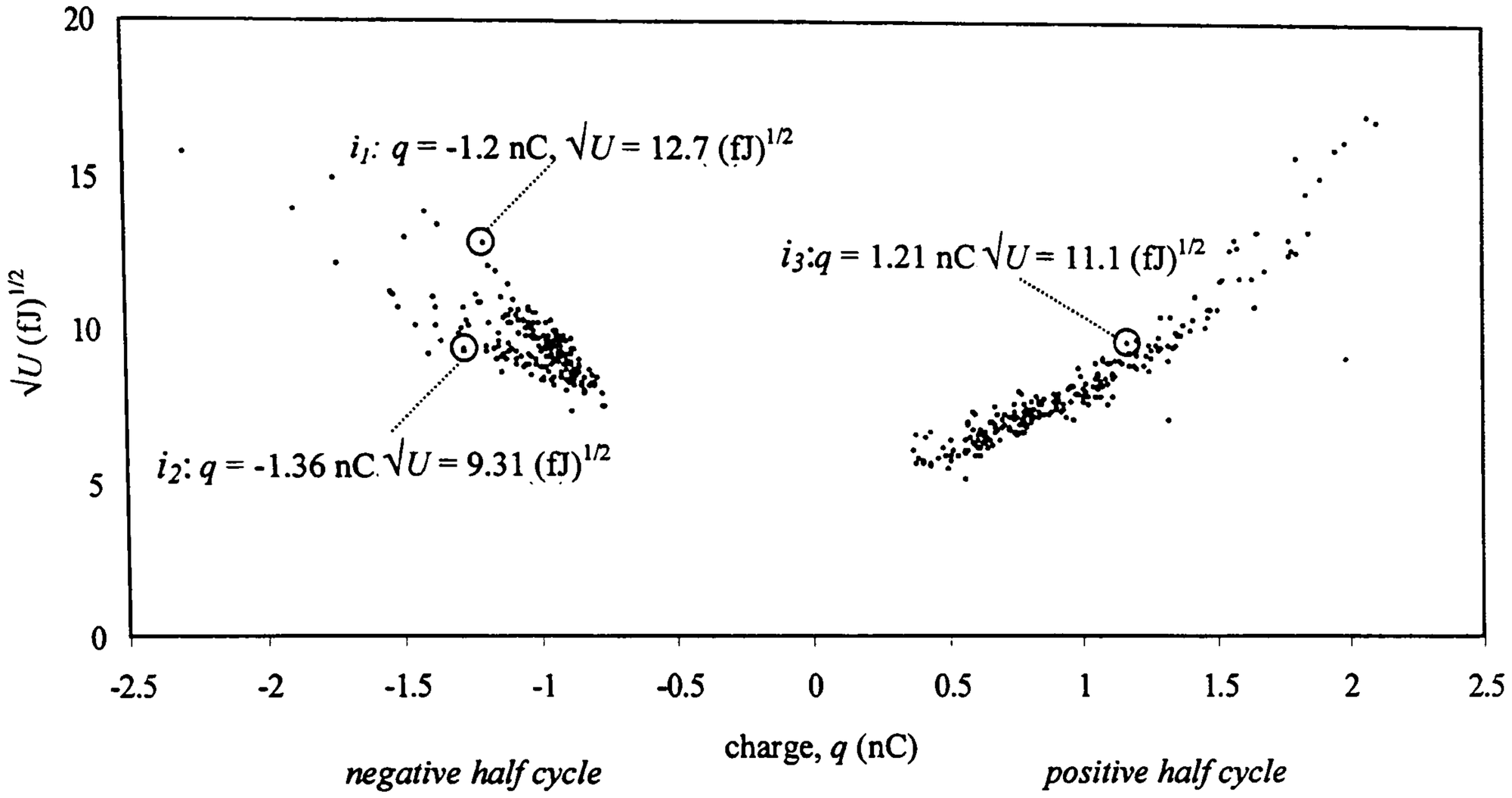

Figure 4.9 PD activity measured in air at 2.3 kV, showing correlation between q and $\sqrt{U}$.

While the charges associated with the two negative pulses only differ by a factor of 1.13, the corresponding values of $\sqrt{U}$ differ by a factor of 0.73. The correlation between $\sqrt{U}$ and q is more variable than the correlation between q and V_{pk}. This can be attributed to the fundamental difference between the IEC 60270-based and UHF measurement systems. In the IEC 60270-based system, PD current is integrated to obtain the *apparent charge* q_a. However, the UHF measurement system is primarily sensitive to the acceleration and deceleration of charge at the defect site [129]. Consequently, the UHF technique requires a different approach to the issue of calibration and this will provide interesting challenges for future research.

4.3.2 Evaluation of measurements in unused transformer oil

4.3.2.1 Regularity of pulse shape

Figure 4.10 shows the relationship between I_p and q obtained in unused transformer oil. The correlation between I_p and q is lower for experiments involving unused transformer oil than air. Therefore, pulse shapes in unused transformer oil are more variable than those in air.

In Figure 4.11, current pulses for the highlighted data points of Figure 4.10 are shown. An inspection of the negative current pulses reveals two distinct pulse shapes, with the charge contained in i_1 being transferred over a comparably shorter time. The q values of these pulses vary only by a factor of 1.05 but their I_p values vary by a factor of 2.

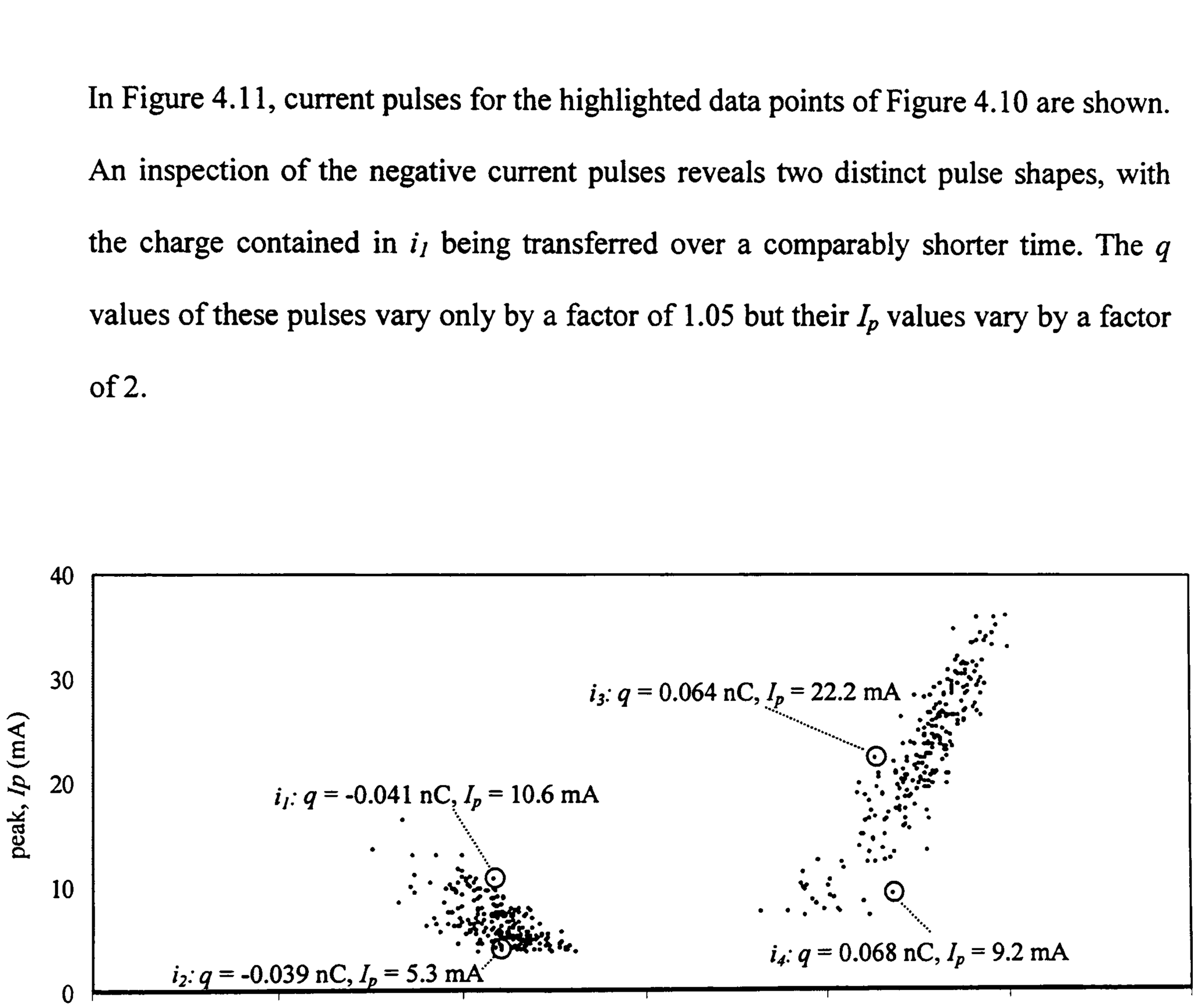

Figure 4.10 PD current pulses in unused transformer oil at 13.3 kV, showing correlation between q and I_p.

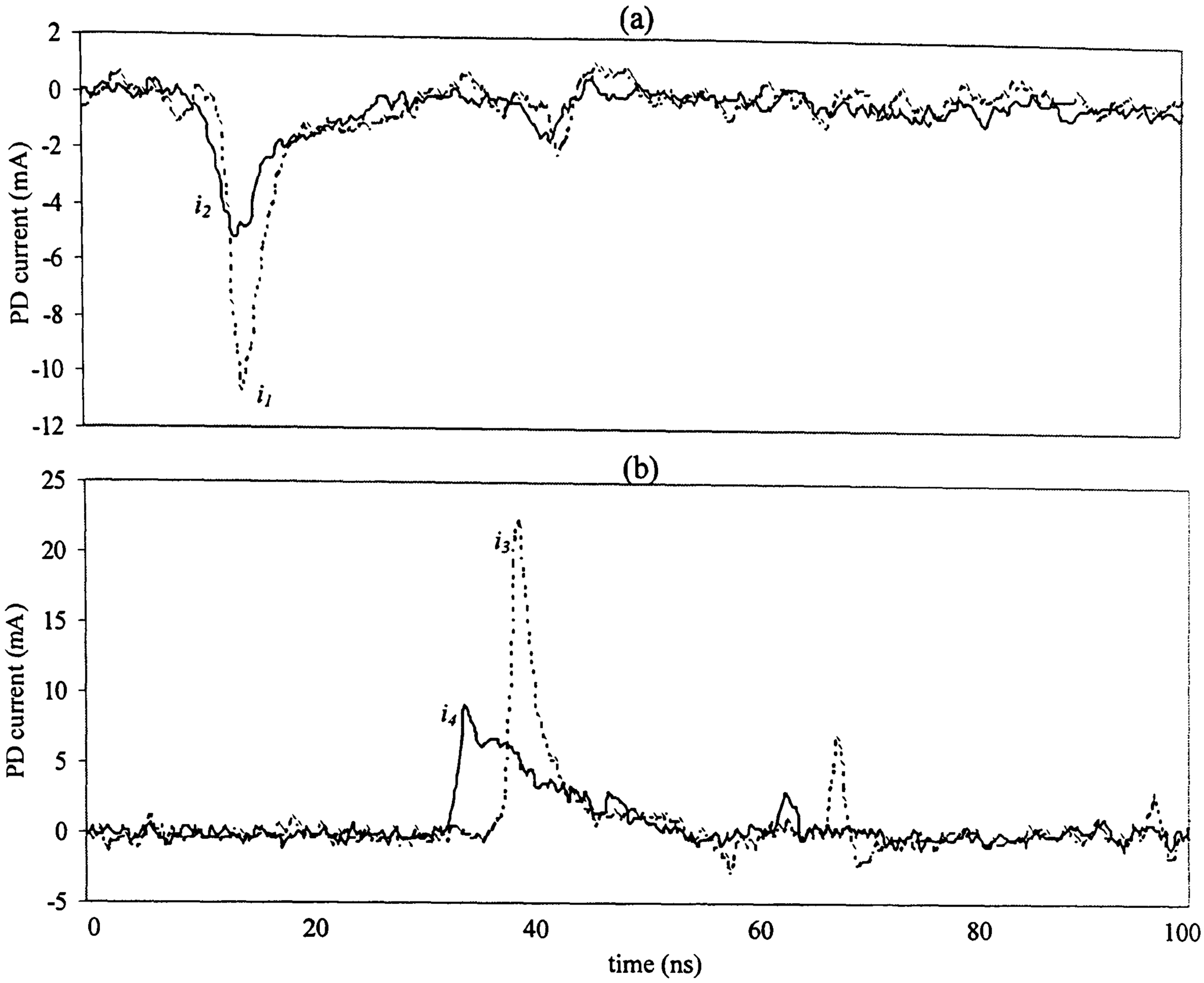

Figure 4.11 Expanded view of current pulses measured in unused transformer oil at 13.3 kV with (a) negative and (b) positive triggering.

In the case of the positive current pulses, two distinct pulse shapes are also observed. The q of these pulses values vary only by a factor of 1.06 but their I_p values vary by a factor of 0.41. As shown in Table 4.1, a greater charge (q) is associated with the current pulses that were measured in unused transformer oil during the positive half cycle. This might be expected because electrons can readily be supplied from the point-cathode to the discharge site as a result of field emission.

In comparison to experiments in air, PD current pulse shapes in unused transformer oil were found to be much more variable. Because of the complexity of the processes involved, the general understanding of electric breakdown in liquid dielectrics is still relatively modest [100,101]. Discharge processes in liquids are often complicated by the presence of impurities such as dissolved gases, moisture and particulate matter [115,116, and 130]. Previous experiments by Nelson et al [87] have reported that both conducting and non-conducting particles have a tendency to drift into a region of high electric field stress, such as at the tip of a metallic protrusion. The difference in permittivity of impurities, micro-bubbles and the liquid will lead to a variation in the local electric field at the tip. As successive PD events occur, the impurity content in the region will change because of variations in dissolved gas concentrations, moisture and particulate matter. As already outlined in Section 3.2.3, this will influence the propagation of streamers [115], and so greater pulse shape variability might be expected for experiments involving unused transformer oil.

4.3.2.2 IEC 60270-based measurements

The relationship between q and V_{pk} is shown in Figure 4.12. The correlation between these parameters is lower than in the case of experiments in air. As can be seen from Table 4.1, the charge (q) associated with pulses measured in unused transformer oil was significantly lower than for those measured in air. The charge associated with pulses measured in air was 0.97 nC and -1.02 nC during the positive and negative half cycles respectfully. In the case of pulses measured in unused transformer oil, the charge associated with pulses was 0.08 nC and -0.04 nC during the positive and negative half cycles respectfully. It is suggested that the IEC 60270-based measurement system did not have sufficient sensitivity to detect the relatively smaller PDs that were generated in unused transformer oil and so a low correlation was found.

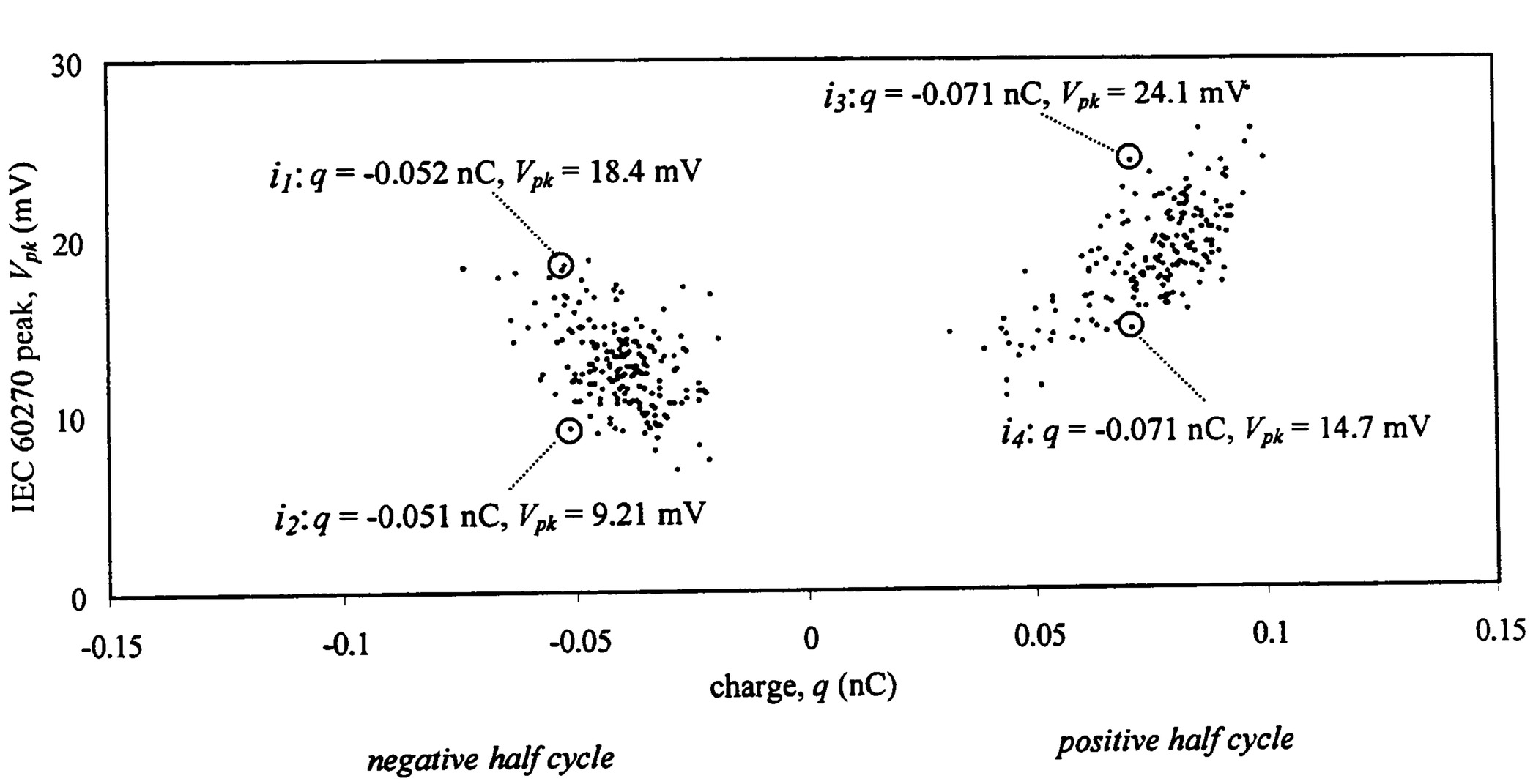

Figure 4.12 PD activity measured in unused transformer oil at 13.3 kV, showing correlation between q and V_{pk}.

4.3.2.3 UHF measurements

The relationship between UHF energy and charge is shown in Figure 4.13, no UHF energy was measured during the negative half cycle. As indicated in Table 4.1, the risetimes (t_r), pulse widths (t_{pw}) and falltimes (t_f) of negative current pulses were greater and the charge (q) associated with them was lower than for those measured during the positive current half cycle. It is suggested that the rate of change of PD current pulses measured during the negative half cycle was so low that no UHF energy was measured.

Although the UHF signals were measured for PD generated during the positive half cycle, the correlation between $\sqrt{U}$ and q was lower than for experiments in air. This lower correlation would be expected given the comparably greater amount of pulse-shape variability that was found for experiments in unused transformer oil.

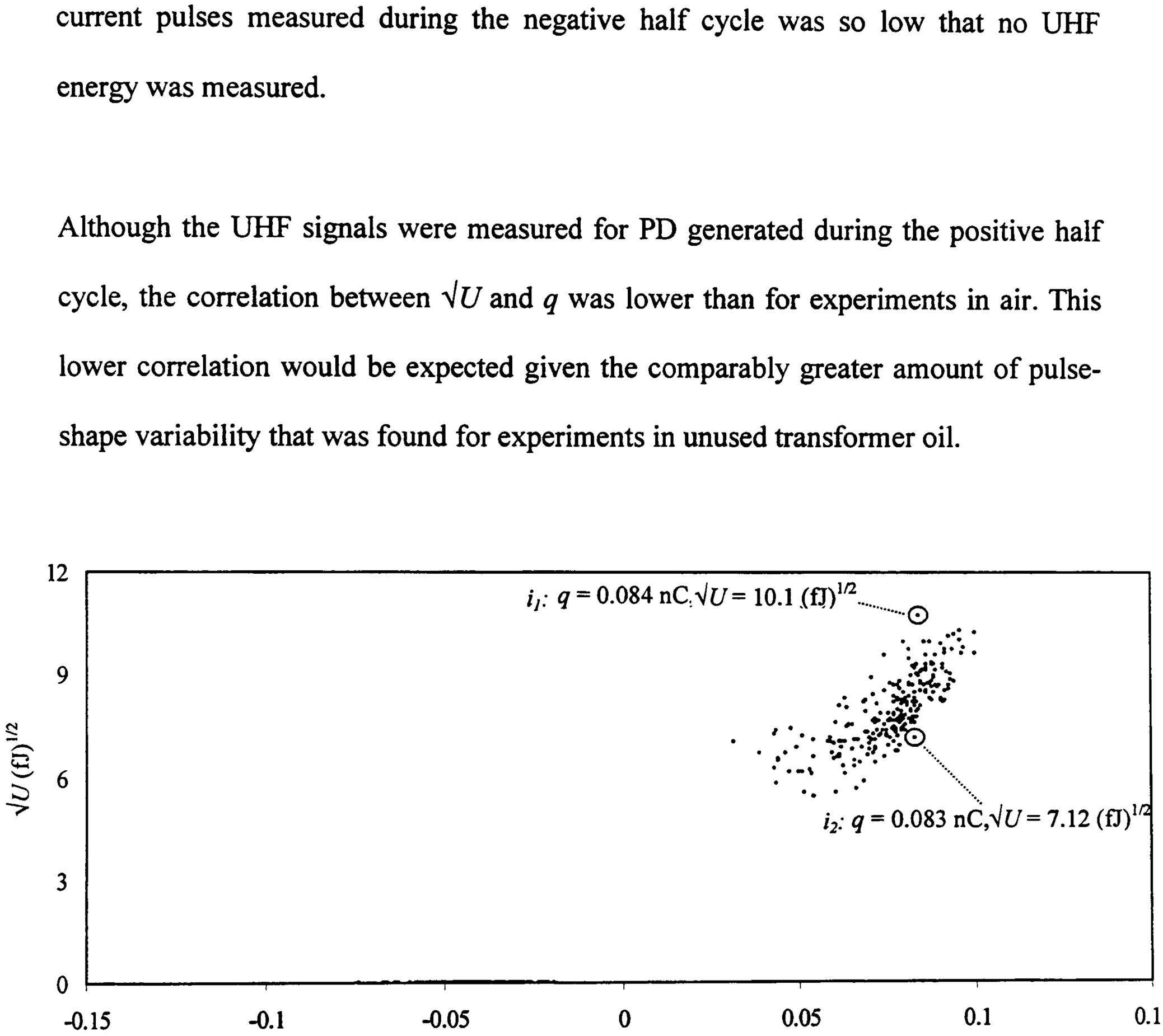

Figure 4.13 PD activity measured in unused transformer oil at 13.3 kV, showing correlation between q and $\sqrt{U}$.

4.3.3 Evaluation of measurements in used transformer oil

4.3.3.1 Regularity of pulse shape

The irregularity of current pulses shapes in used transformer oil is evident from the correlation in Figure 4.14. The low correlation between I_p and q is accounted for in terms of the variability of shape from pulse to pulse, which is greater than for air and unused transformer oil.

Figure 4.15 shows both the positive and negative current pulses that correspond to the data points highlighted on Figure 4.14. Inspection of these current pulses reveals that two distinct current pulse shapes, single peak and double peak, were recorded. Both of the negative pulses shown have similar q values, but their I_p values vary by a factor of 2.3, and both positive pulses also have similar q values but their I_p values vary by a factor of 2.2. Since only single peak pulse shapes were measured in air and unused transformer oil, this result is evidence that the PD process in used transformer oil is significantly different.

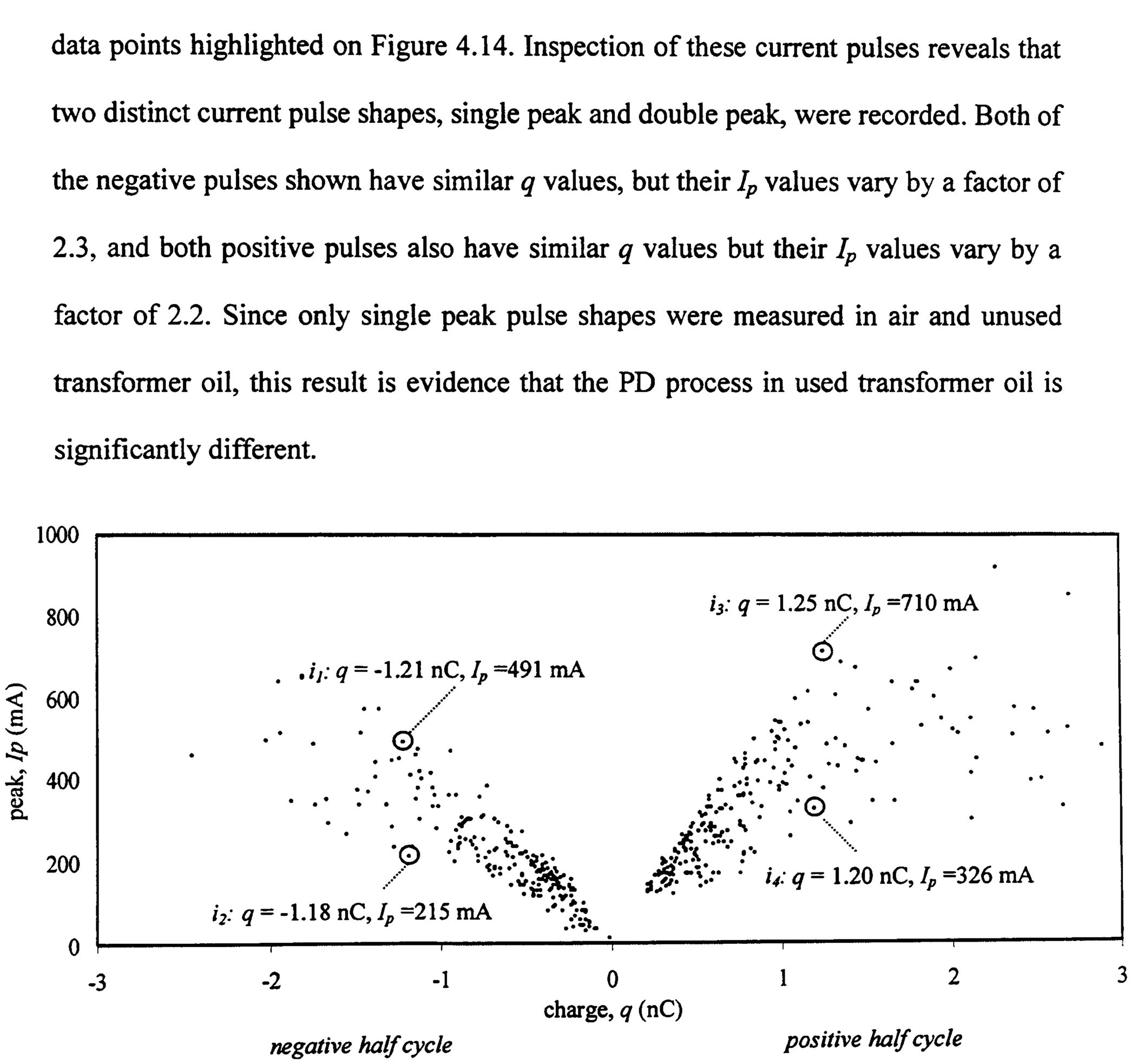

Figure 4.14 PD current pulses in used transformer oil at 14.7 kV, showing correlation between I_p and q.

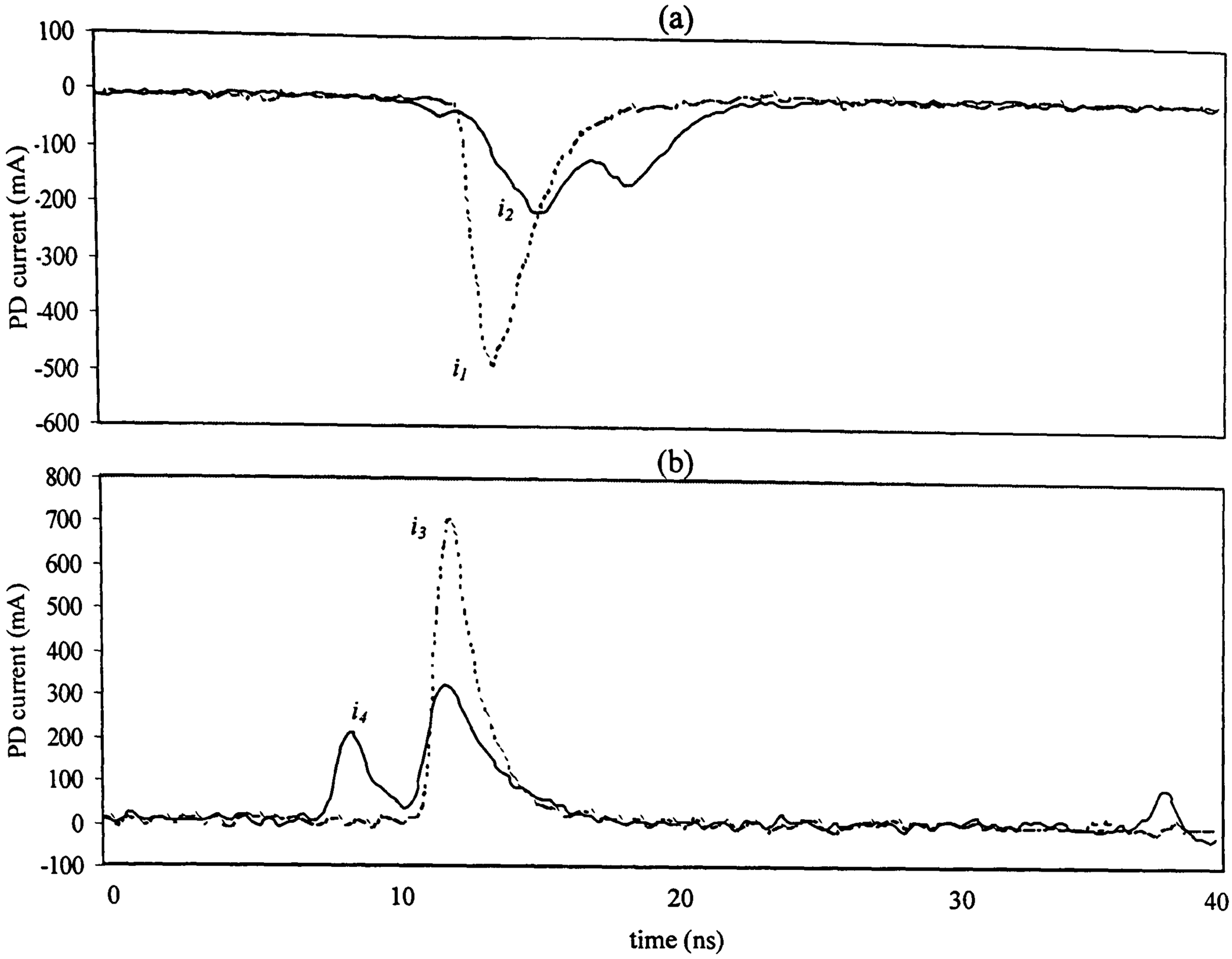

Figure 4.15 Expanded view of current pulses measured in used transformer oil at 14.7 kV with (a) negative triggering and (b) positive triggering.

The double pulse of Figure 4.15(a) was measured when the protrusion was behaving as the point-anode. It is suggested that the risetime of the first pulse of i_2 corresponds to electrons being accelerated from negative ions towards the point-anode. These electrons will experience a converging electric field as they travel towards the point-anode but their mobility will be limited. The falltime of the first pulse of i_2 relates to an accumulation of space charge, that is, it is representative of the deceleration of electrons [103]. However, this space charge is superseded by another burst of electrons that travel towards the point-anode. This is evident as the risetime of the second pulse of i_2. Following this the PD event is terminated.

On the other hand, the double pulse of Figure 4.15(b) was measured when the protrusion was behaving as the point-cathode. It is suggested that the risetime of the

first pulse of i_4 corresponds to electrons being accelerated from the point-cathode into the oil. However, these electrons will loose kinetic energy as they travel into the oil medium under the influence of a diverging electric field [20]. Therefore, they might attach to oil molecules or impurities and form a cloud of space charge. The falltime of the first pulse of i_4 is evidence of this process. Inspection of the current pulse record shows that this space charge is superseded by another burst of electrons that travel from the point-cathode. The risetime of the second pulse of i_4 is evidence of this process. The falltime of the second pulse of i_4 is evidence of another accumulation of space charge in the oil gap. Following this, the PD terminates.

In comparison to experiments involving unused transformer oil, the greater irregularity of current pulses in used transformer oil was noticeable. This might be attributed to a higher concentration of impurities in the used transformer oil sample. The local electric field at the tip of the protrusion will be significantly modified as a result of impurities, and this might result in greater irregularity of pulse shapes. Experiments by Krins et al [10, 12 and 13] have also reported that a greater impurity content is generally associated with used transformer oil and this often leads to the variability of experimental results.

4.3.3.2 IEC 60270-based measurements

The relationship between V_{pk} and q is shown in Figure 4.16. The data points highlighted during both half cycles have similar charge values, but their V_{pk} values vary by a factor of 1.44 during the negative half cycle, and a factor of 2.86 during the positive half cycle. On the whole, the correlation between q and V_{pk} is lower than in the case of experiments in air and unused transformer oil. This lower correlation might be expected because bursts of PD current were detected for experiments in used transformer oil.

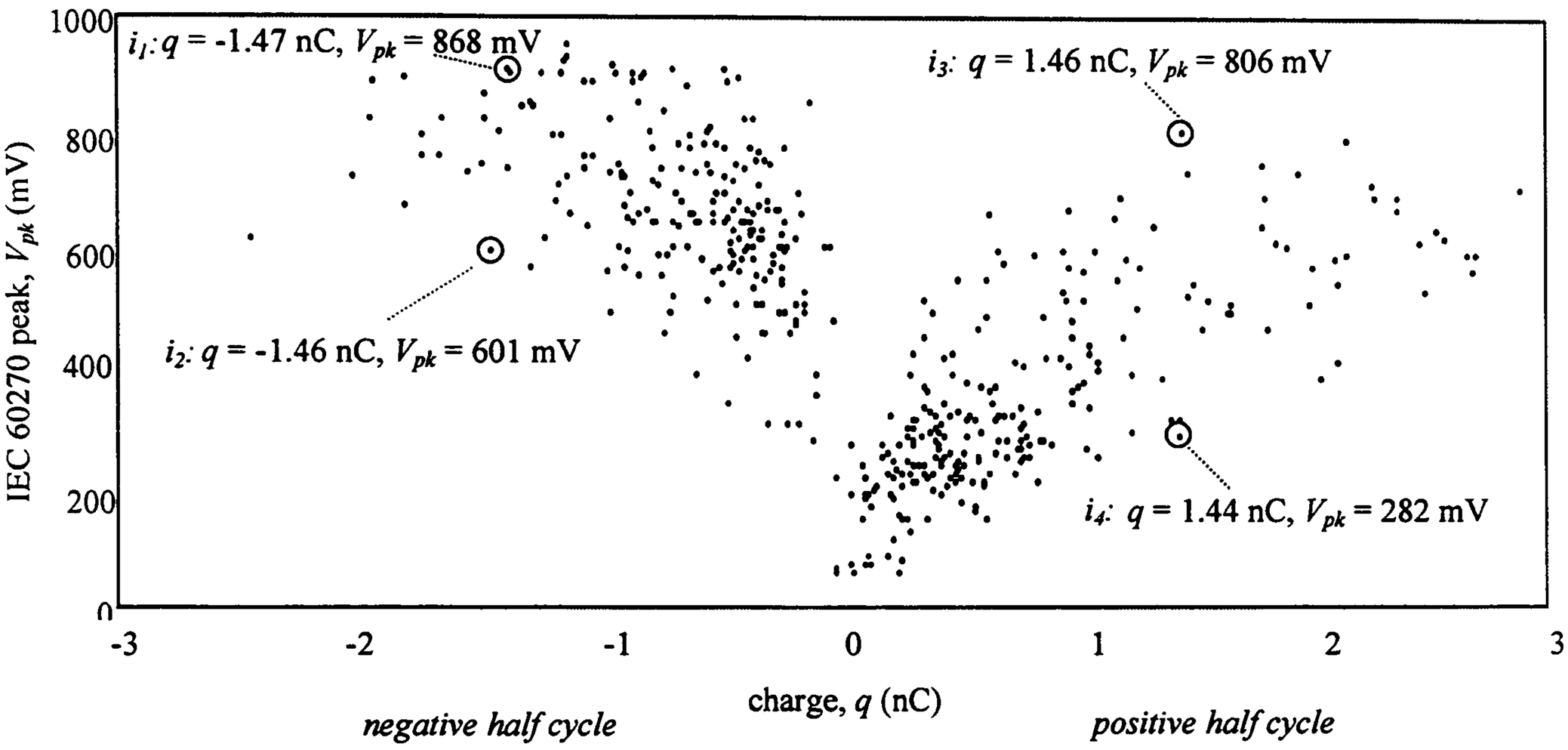

Figure 4.16 PD activity measured in used transformer oil at 14.7 kV, showing correlation between q and V_{pk}.

Furthermore, the lower amount of correlation might be attributed to the different operating principles of the PD current pulse and IEC 60270-based measurement systems. As already outlined, q corresponds to the charge contained in PD current pulses that were measured at the tip of the protrusion using the high-frequency current transformer. However, V_{pk} corresponds to IEC 60270-based measurements which

record the *apparent charge* by means of a coupling capacitor connected directly to the HV electrode [78,79]. The IEC 60270-based measurement technique responds to displacement of charge anywhere in the volume between the electrodes. Therefore, PD occurring at the pressboard barrier, or within the main oil bulk might also be detected using the IEC 60270-based measurement system. Consequently, a low correlation might be expected between q and V_{pk} for experiments in used transformer oil because PD is likely to occur simultaneously at several sites within the test cell.

Experimental observations showed that the pressboard barrier was degraded with extensive testing. As outlined in Section 1.2, streaming electrification at pressboard barriers is a known cause of transformer failure [14,15], and this process is likely to be accelerated by a higher concentration of impurities in the surrounding liquid. The impurities might also promote PD in the oil bulk as a result of complex interactions between charges trapped within tiny water droplets or gas bubbles [80].

4.3.3.3 UHF measurements

The relationship between UHF energy and charge is shown in Figure 4.17. As might be expected, the correlation between these parameters is much lower than in the case of experiments involving air and unused transformer oil. The data points highlighted during the negative half cycle have similar q values but their $\sqrt{U}$ values vary by a factor of 2.8, and those highlighted during the positive half cycle also have similar q values but their $\sqrt{U}$ values vary by a factor of 1.27.

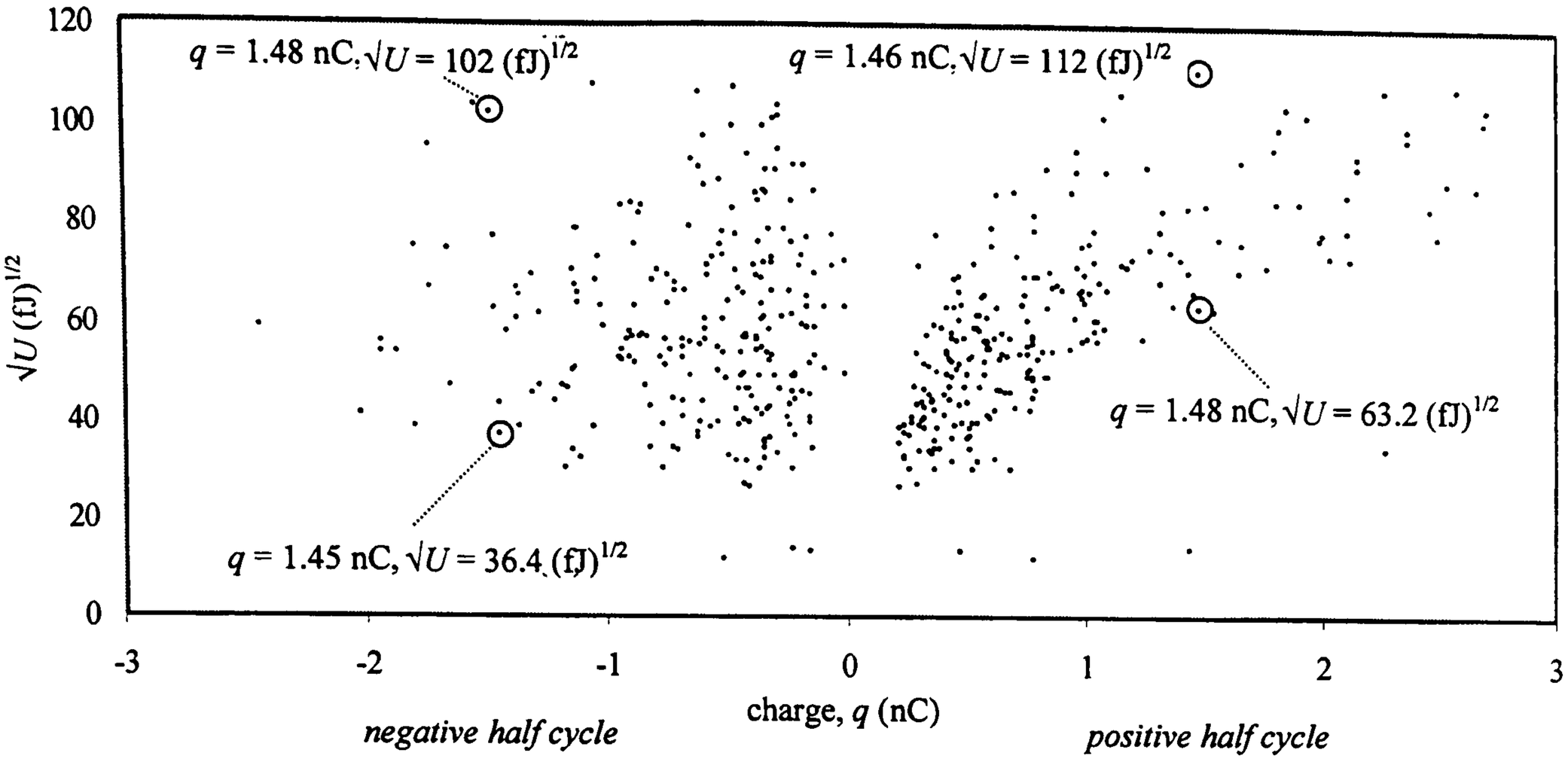

Figure 4.17 PD activity measured in used transformer oil at 14.7 kV, showing correlation between $\sqrt{U}$ and q.

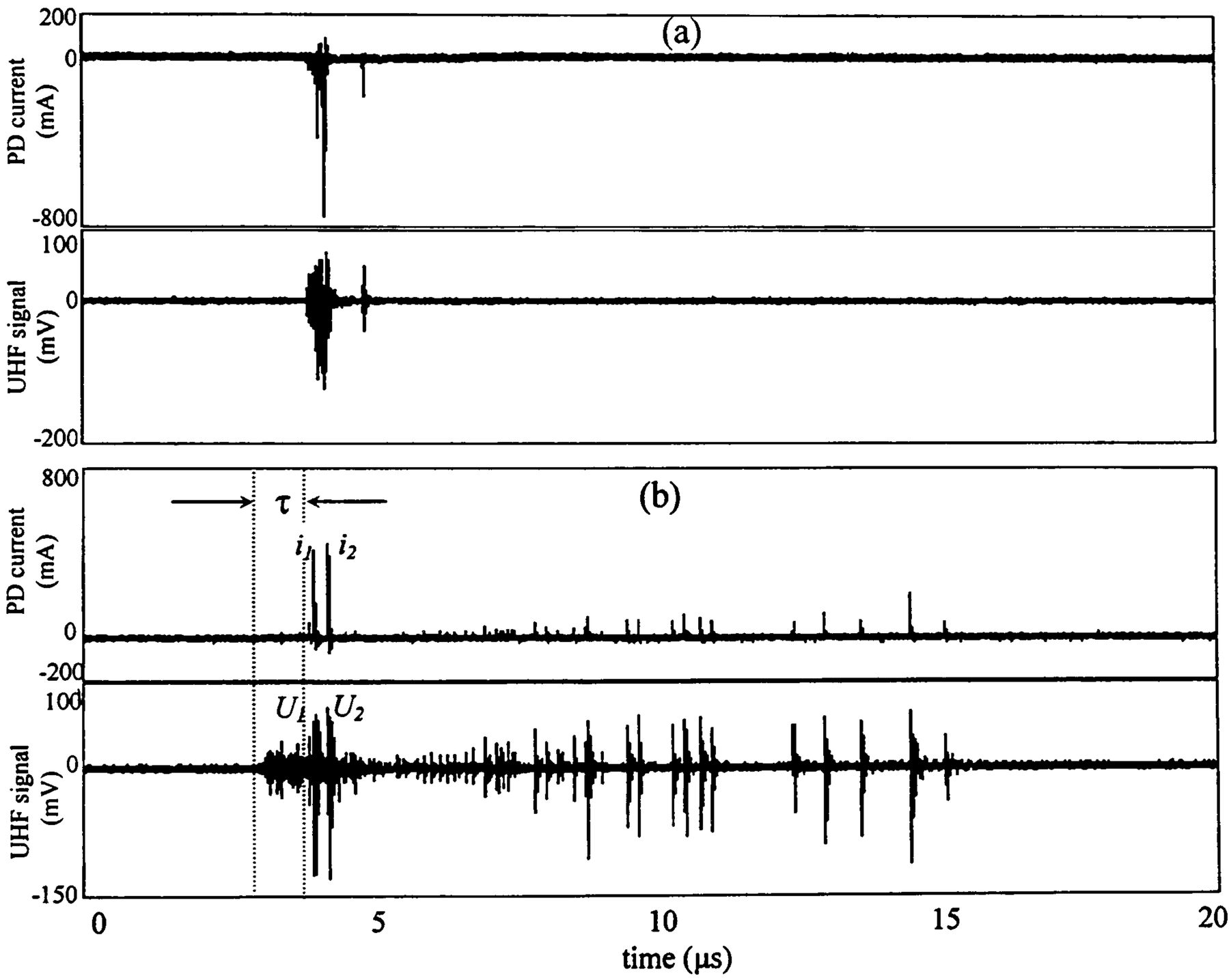

Figure 4.18 Examples of current pulses and corresponding UHF measurements in used transformer oil at 14.7 kV during (a) the negative half cycle and (b) the positive half cycle.

Figure 4.18 shows an example of PD current pulses measured during both half cycles, together with the corresponding UHF measurements. These plots demonstrate that individual PD current pulses in used transformer oil were detected using the UHF measurement system. Again, a greater number of pulses were observed during the positive half cycle.

The low correlation between $\sqrt{U}$ and q will now be discussed. Inspection of Figure 4.18(b) reveals that UHF signals were measured in the region $\tau \sim$ 3-4 μs. However, no PD current pulses were recorded during this time. This might correspond to PD that was generated in the liquid bulk or at the pressboard barrier, but not at the tip of the protrusion. Both IEC 60270-based and UHF measurement systems can respond to signals that are excited from PD occurring within the liquid bulk or at the pressboard barrier, but recorded current pulses are only representative of PD occurring at the tip of the protrusion. Consequently, a low correlation between q and $\sqrt{U}$ might be expected.

In Figure 4.18(b), current pulse i_2 occurred before the UHF signal corresponding to i_1 decayed to the background noise level. Inspection of the plot reveals that the UHF signals of U_1 and U_2 were found to overlap. This phenomenon has previously been discussed by Wanninger [125] for experiments involving SF_6, and can also help explain the lack of correlation between the parameters $\sqrt{U}$ and q.

4.3.4 IEC 60270-based and UHF measurements

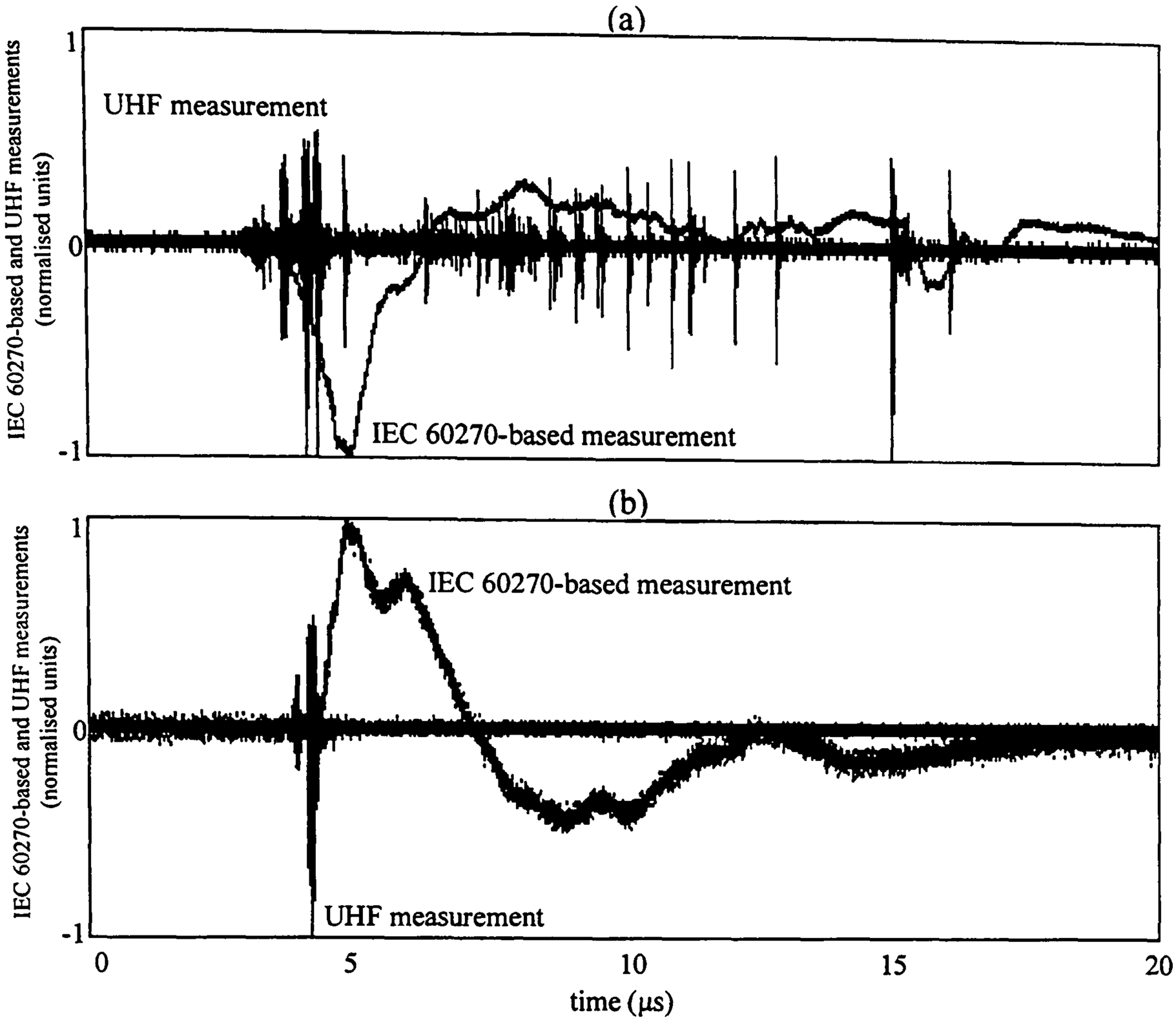

Figure 4.19 Example of IEC 60270-based and UHF measurements during (a) the positive half cycle and (b) the negative half cycle.

Figure 4.19 shows an example of IEC 60270-based and UHF measurements that were measured during both half cycles. Again, these records show that pulses occurred more frequently during the positive half cycle.

This work has shown that several PDs can occur in oil on a microsecond timescale and cause the excitation of separate bursts of UHF signal. However, the IEC 60270-based system can only respond to PDs on a microsecond timescale. Previous work by Debruyne and Lesaint [124] has also reported that several PDs can occur on a

nanosecond timescale, and so conventional measurement systems often strongly underestimate the number of PDs in oil.

As already described in Section 4.1, conducted PD current pulses cannot be measured directly on-site. However, both IEC 60270-based and UHF measurement systems can be used for the detection of PD in operational power transformers [21, 84 and 85]. Inspection of Figure 4.19(a) shows that the tail of the IEC 60270-based waveform was modified by the PDs that occurred in the region 6-20 μs. In this figure, both IEC 60270-based and UHF measurements have been normalised. Interpretation of the shape of the IEC 60270-based waveform would have been more difficult if the UHF signal had not also been measured. At present, UHF and IEC 60270-based measurements are not simultaneously recorded during on-site tests as common practice. It is suggested that this technique should be considered further for PD monitoring of power transformers. This might assist with the interpretation of measurements carried out on-site, and might provide a better indication of discharge severity for risk assessment purposes. Clearly, further research is required to investigate this approach.

4.4 Conclusion

A wide-band measurement system has been used to measure PD current pulses in air, unused transformer oil and used transformer oil. Current pulses were recorded and correlated with measurements made using IEC 60270-based and UHF measurement systems. Pulses in air were quite regular, whereas those in used transformer oil had a much more variable pulse shape.

For experiments in air, a close correlation was found between charge and IEC 60270-based measurements. In addition, a clear relationship was found between charge and UHF energy. These findings demonstrate that both the IEC 60270-based and UHF techniques were suitable for measuring PD generated in air. These measurements were correlated on a pulse-by-pulse basis.

For experiments in unused transformer oil, the correlation between charge and IEC 60270-based measurements was found to be lower than for air. A low correlation was also found between charge and UHF energy during the positive half cycle. However, no UHF energy was measured during the negative half cycle because the rate of change of measured PD current pulses were too low when the protrusion was behaving as the point anode.

For each of the experiments outlined, the lowest amount of correlation was found in used transformer oil. This arises because measured current pulses were only representative of PD occurring in the oil surrounding the tip of the protrusion, but both IEC 60270-based and UHF measurement systems were influenced by PD in the

oil surrounding the tip of the protrusion, PD in the liquid bulk and PD occurring at the pressboard barrier.

This work has demonstrated that several PD current pulses can be measured on a nanosecond timescale, but the IEC 60270-based measurement circuit described was only able to respond to PD on a microsecond timescale. For this reason, IEC 60270-based measurements commonly underestimate the number of PDs in transformer oil. It was suggested that the interpretation of PD activity might be improved by simultaneously recording IEC 60270-based and UHF measurements. It is anticipated that this approach will assist with the interpretation of measurements carried out on-site, and will provide a better indication of discharge severity in terms of pC.

5. STUDIES OF TRANSFORMER INSUALTION DEFECTS

5.1 Introduction

The results reported in Chapters 3 and 4 demonstrate that PD current pulses measured at an oil-insulated grounded electrode protrusion can excite UHF signals [76,79 and 82]. This chapter reports PD measurements for a variety of insulation defects. The types of defect considered are:

- Protrusion
- Bad contact
- Free metallic particle
- Moisture contamination

Conducted PD current pulses are measured at the grounded electrode for the protrusion, the bad contact and the free particle. These current pulses are measured at operating voltages greater than inception using a high-frequency current transformer and the corresponding UHF signals are detected using a pair of broadband electric field sensors. Signals are recorded using a Tektronix 694C (3 GHz bandwidth, 10 GS/s) oscilloscope. The relationship between measured current pulses and the radiated UHF signal energy is investigated.

Previous work involving '*discharge mapping*' has demonstrated how UHF signals measured from several PD sources could be separated according to their point of origin [85]. As well as time-of-flight information, the technique used energy ratios at

sensor pairs to distinguish between different PD sources. In this investigation, PD activity is generated at a fixed location using each of the aforementioned defect sources. The ratio of energies measured using two sensors is shown to exhibit characteristics dependent on the discharge process.

The spectral content of UHF signals measured during each polarity of half cycle is computed to establish whether it can be used for the interpretation of discharge behaviour. Finally, UHF signals are measured for PD activity involving moisture contamination.

5.2 Experimental Procedures

5.2.1 PD sources

Figure 5.1 shows the electrode arrangements used to represent a metallic protrusion, a bad contact, a free metallic particle and moisture contamination. In the configuration of Figure 5.1(a), a brass protrusion (length = 21 mm, tip radius ~ 35 μm) was mounted on the earthed electrode and the gap distance was set to 22 mm. The bad contact was created using a piece of aluminium foil placed between the pressboard barrier and the earthed electrode as shown in Figure 5.1(b). These two open electrode arrangements were simulated using the test rig that was described in Section 2.2. The test configuration was then immersed in a 50-litre oil bath for testing.

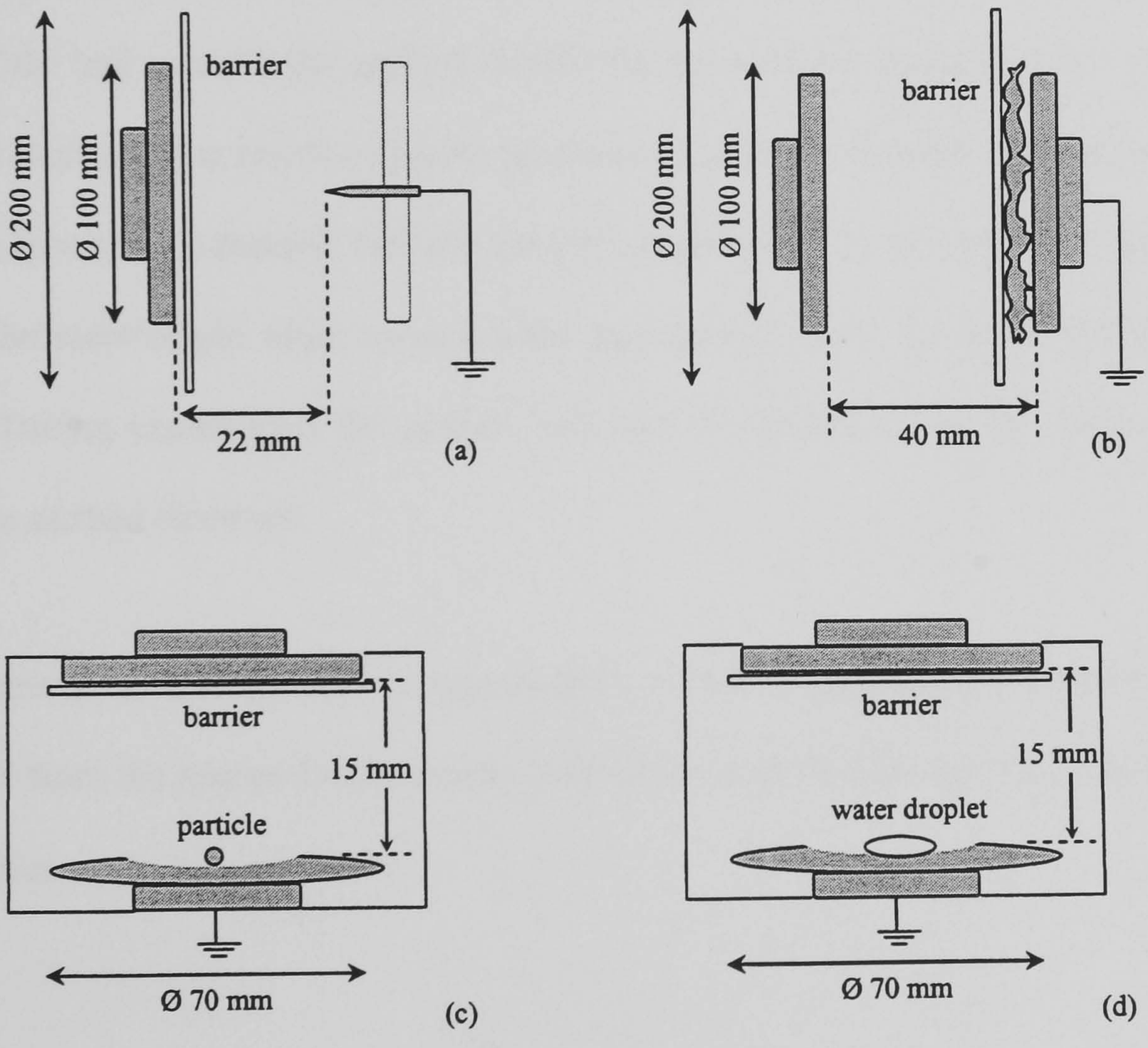

Figure 5.1 PD test configurations used to simulate (a) a protrusion, (b) a bad contact (c) a free particle and (d) moisture contamination.

The enclosed test cell configuration of Section 2.2 was used for the free metallic particle and moisture contamination, which require vertical mounting. The particle (diameter = 2.5 mm, stainless steel) or the water droplet (2 ml) was placed on the concave dished earthed electrode prior to filling the test cell with insulating oil. The configurations that were used to contain the free particle and the water droplet are shown in Figures 5.1(c) and (d). The oil used for all experiments was reclaimed light grade transformer oil (L10B).

The protrusion, the bad contact and the free particle were located at the earthed electrode to allow PD current pulses at the defect site to be measured. When the applied voltage was sufficiently high PD activity was generated at each defect. In the case of the bad contact, the applied electric field caused the metallic foil to vibrate, with its motion being restricted by the pressboard barrier. This action resulted in a bad contact between the metallic foil and the earthed electrode. In the case of the particle, when the electrostatic force exceeded the gravitational force the particle started to move. During experiments the particle was seen to lift and fall at the centre of the concave earthed electrode.

Experiments involving water contamination revealed that smaller droplets were stripped from the source droplet and a cloud of moisture rapidly developed within the oil medium.

5.2.2 Measurement system

The entire measuring system for current pulses and UHF signals is shown in Figure 5.2. The current transformer described in Section 2.4.1 was used to measure current pulses flowing at the protrusion, the bad contact and the free particle. To protect the oscilloscope, the output of the current transformer was attenuated by 20 dB, and no measurements were carried out when intense arcing was present at the defect.

Electromagnetic signals radiated from the PD source were detected using two broadband UHF electric field sensors mounted on a large metal test chamber. For each experiment, the distances of $Sensor_1$ and $Sensor_2$ from the PD source were approximately 0.75 m and 2.00 m respectively. The frequency response of the type of sensor selected was described in Section 2.4.3. In this investigation, UHF signals were amplified by 26 dB prior to being recorded.

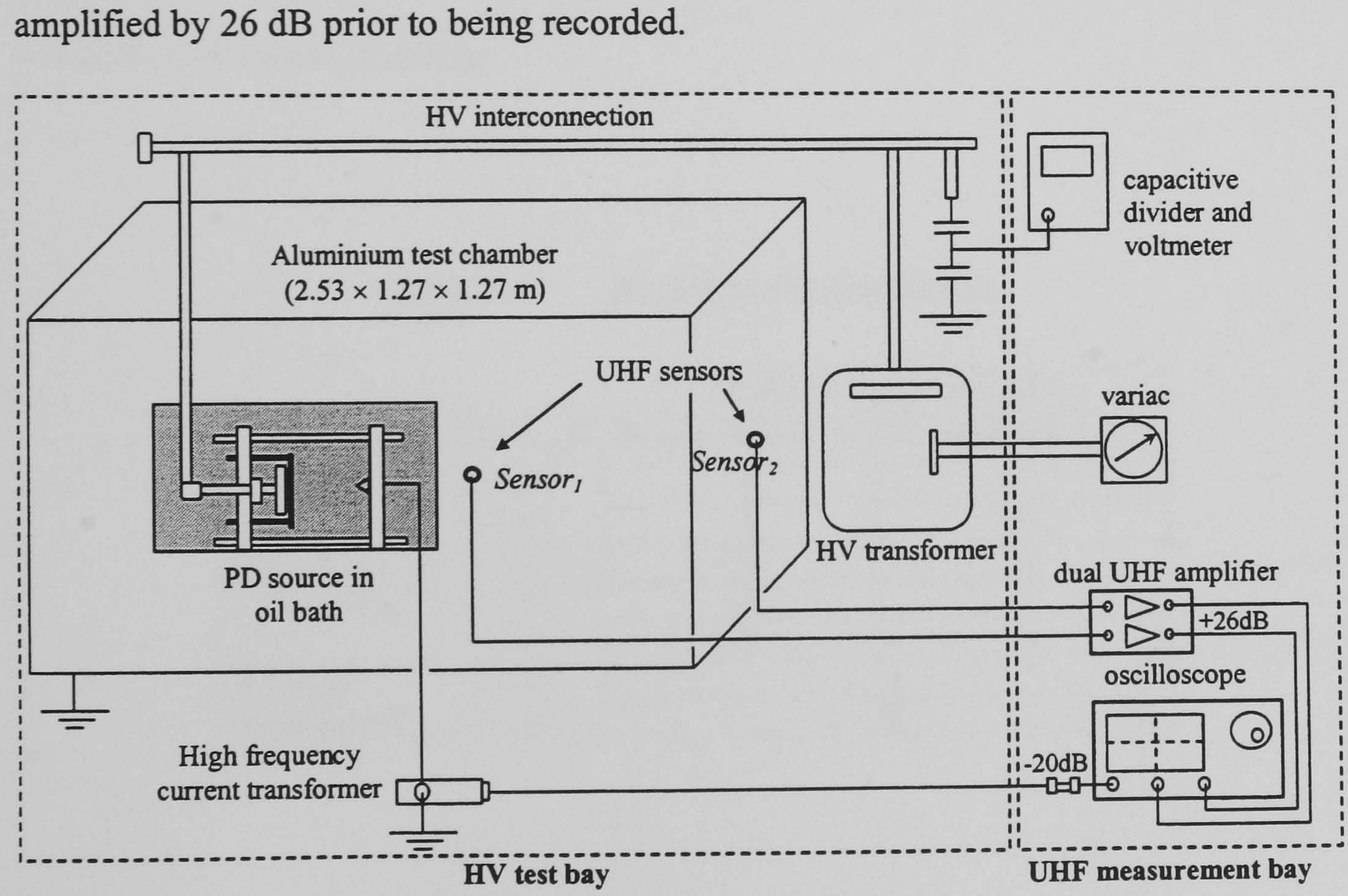

Figure 5.2 Experimental arrangement used to energise PD sources and perform simultaneous measurement of conducted current pulses and UHF signals radiated inside the test chamber.

5.2.3 Experimental method

A variac and the 230V to 40kV step-up transformer (Section 2.3.2) were used to energise each test configuration. Current pulses and radiated UHF signals were captured simultaneously. The oscilloscope time-base was triggered using the current pulse, so that even PD events that do not excite UHF signal can be recorded. The sampling rate of the oscilloscope was set at 10 GS/s, and all measurements were captured in a 200 ns window.

For each PD source, the experimental procedures are detailed in Table 5.1. In the case of moisture contamination, PD current pulses were not recorded because the onset of arcing was unpredictable and so the polarity of the power cycle is unknown. For safety reasons, fewer measurements were made at the higher operating voltage because of the onset of arcing.

Table 5.1 Experimental procedures.

Defect and applied voltage		Number of pulses recorded	
		Positive half cycle	Negative half cycle
Protrusion	19.4 kV	75	-
	23.3 kV	75	60
Bad contact	19.4 kV	75	75
Free particle	13.6 kV	75	75
	23.3 kV	75	75
Moisture contamination	1.5 kV	75	
	2.7 kV	50	

5.2.4 Data processing

The conducted current pulse waveforms that are presented should not be considered as exact representations of the pulse at the PD site. Pulse shapes will be modified because of

1. the relatively large area of the earth electrode in relation to the pulse wavefront,
2. distortion due to propagation along the unshielded earth lead, and
3. reflections of the pulse on the earth lead, which make it appear to have an oscillatory nature.

For each recorded current pulse, the peak current (I_p) and the total charge (q) were calculated. The total charge was calculated by integrating the current in the first lobe of the measured pulse. Regularity of pulse shape was investigated by plotting I_p as a function of q. As outlined in Section 4.3.1.1, a linear relationship between I_p and q would indicate that measured current pulses are simply scaled in terms of their amplitude while a broad scatter would indicate pulse shape variability [81].

The UHF energy (U) associated with a PD event was calculated using the method outlined in Section 2.4.5.2. In this chapter, the parameter $\sqrt{U}$ was calculated over the 200 ns signal duration, and the relationship between q and $\sqrt{U}$ was investigated to determine how the UHF signal relates to the charge transferred at the discharge site.

The spectral content of UHF signals measured during each polarity of half cycle was computed using the FFT to establish whether it could be used for the interpretation of discharge behaviour. In general, the spectral variation between successive measurements was very small. Mean spectral coefficients were calculated for all signals recorded under each polarity of the AC supply and the data was then normalised. This data is analysed in graphical form to determine whether it can be used to assist with the classification of defect type [131].

The ratio of the energies measured using each UHF sensor was calculated ($U_{Sensor2}$ / $U_{Sensor1}$) for discharges during both the positive and negative half cycles. This energy ratio, which is independent of the magnitude of measured PD events, was then normalised relative to the mean energy ratio (R). Measurements above and below the mean energy ratio were counted and grouped in bands of 10% either side of the mean. The organisation of measurements in this form allowed a distribution of measured energy ratios to be determined so that variability can be related to discharge behaviour. An energy ratio plot with a concentration of measurements at the distribution centre implies that the position and orientation of current pulses was well defined because the radiation pattern must be consistent. Conversely, a distribution with a scatter of measurements could indicate that the positions and/or orientations of current pulses were not well defined.

5.3 Results and Discussion

5.3.1 Pulse shape observations

Figure 5.3 shows typical examples of current pulses for measurements involving the protrusion, the free particle and the bad contact. The shortest (10%-90%) risetimes were measured for the protrusion, typically 0.9 ns during the positive half cycle and 2 ns during the negative half cycle. The risetime measured with the free particle was 2.5 ns during the positive half cycle and 2.7 ns during the negative half cycle. For the bad contact, the risetimes were 10 ns and 17 ns during the positive and the negative half cycles respectively.

To some extent, the risetimes associated with current pulses measured for a particular defect are influenced by the geometry of the test arrangement. For example, PD at the protrusion tip has the simplest path to earth, unimpeded by the earth plate which is common to both the bad contact and free particle (Figure 5.1). Although the charge calculated from the measured pulses will not necessarily equal the charge content of the PD, it provides a value that is proportional to PD occurring at the discharge site.

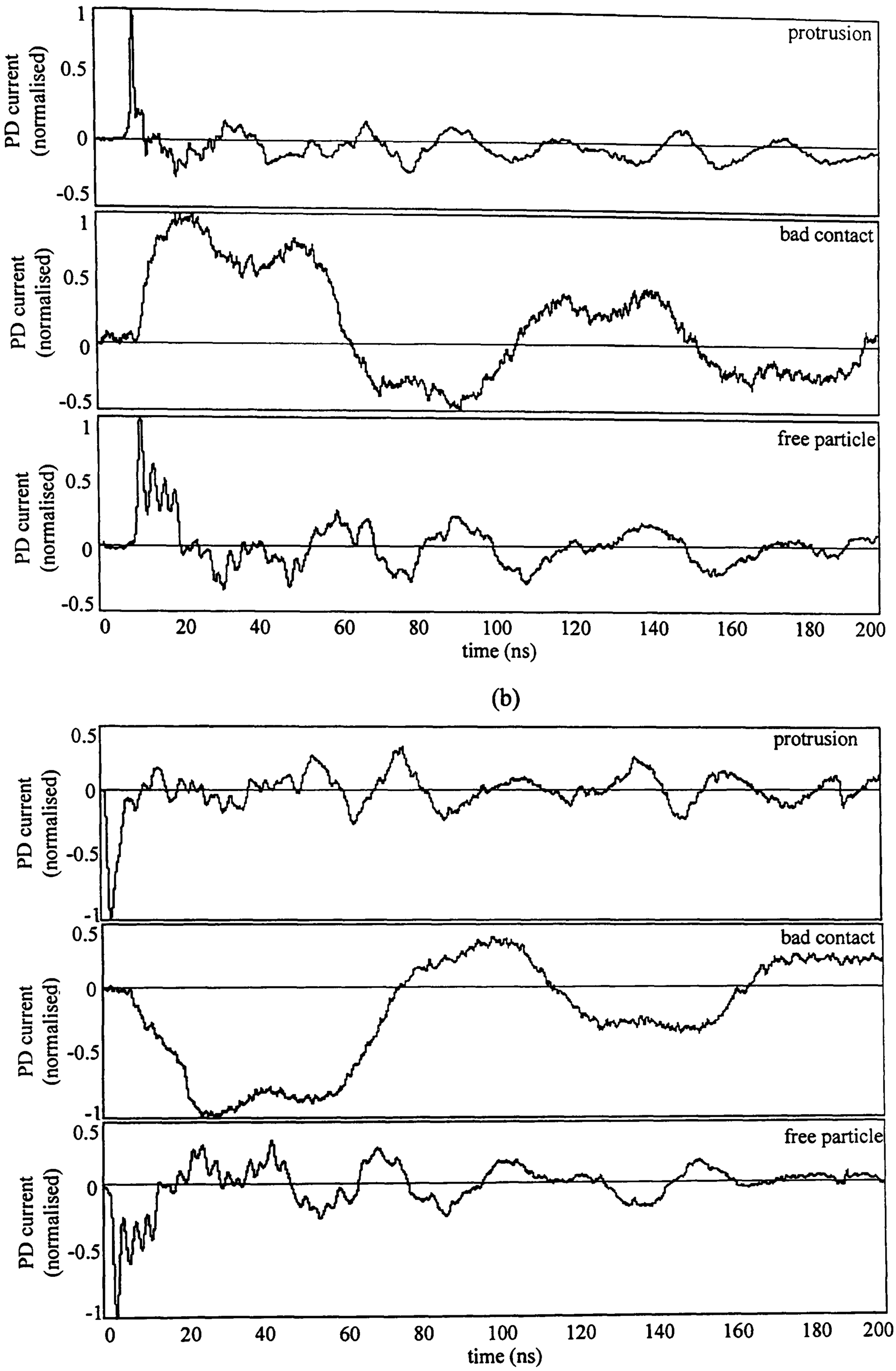

Figure 5.3 Examples of PD current pulses measured at the protrusion bad contact and free particle during (a) the positive half cycle and (b) the negative half cycle.

Properties of measured PD current pulses and radiated UHF signals are outlined for each defect in Table 5.2. In the case of the protrusion, PD current pulses were detected during both half cycles when the applied voltage was increased from 19.4 kV to 23.3 kV. When the applied voltage was 23.3 kV, the mean value of I_p/q was 1.4 mA/pC during the positive half cycle and 0.46 mA/pC during the negative half cycle (Table 5.2). These findings indicate that the shape of pulses measured at the protrusion was dependent on the instantaneous field polarity.

The relationship between I_p and q for the protrusion is shown in Figure 5.4 (a). The plot shows that pulse shapes were dependent on both polarity and magnitude of the applied voltage. At the lower applied voltage (19.4 kV) pulses were only detected during the positive half cycle. Current pulses with a lower value of I_p/q were measured towards the end of the experiment, evident as a row of points to the right of the main group. Figure 5.5 (a) shows an example of a current pulse belonging to each group. The pulse with the lower I_p/q ratio is longer and contains a greater amount of charge relative to the peak current.

Table 5.2 **Properties of measured PD current pulses and radiated UHF signals.**

Defect and applied voltage		Parameter – calculated as the mean value for each half cycle					
		Positive half cycle			Negative half cycle		
		I_p (mA)	q (pC)	U_{SI} (fJ)	I_p (mA)	q (pC)	U_{SI} (fJ)
Protrusion	19.4 kV	13.7	10.4	93.8	-	-	-
	23.3 kV	49.3	36.7	847.2	-17.1	-37.0	25.6
Bad contact	19.4 kV	8.2	208.0	0.32	-14.8	-510.0	0.71
Free particle	13.6 kV	28.4	125.0	38.1	-26.1	-110.0	37.6
	23.3 kV	34.1	148.0	63.7	-32.5	-140.0	52.2

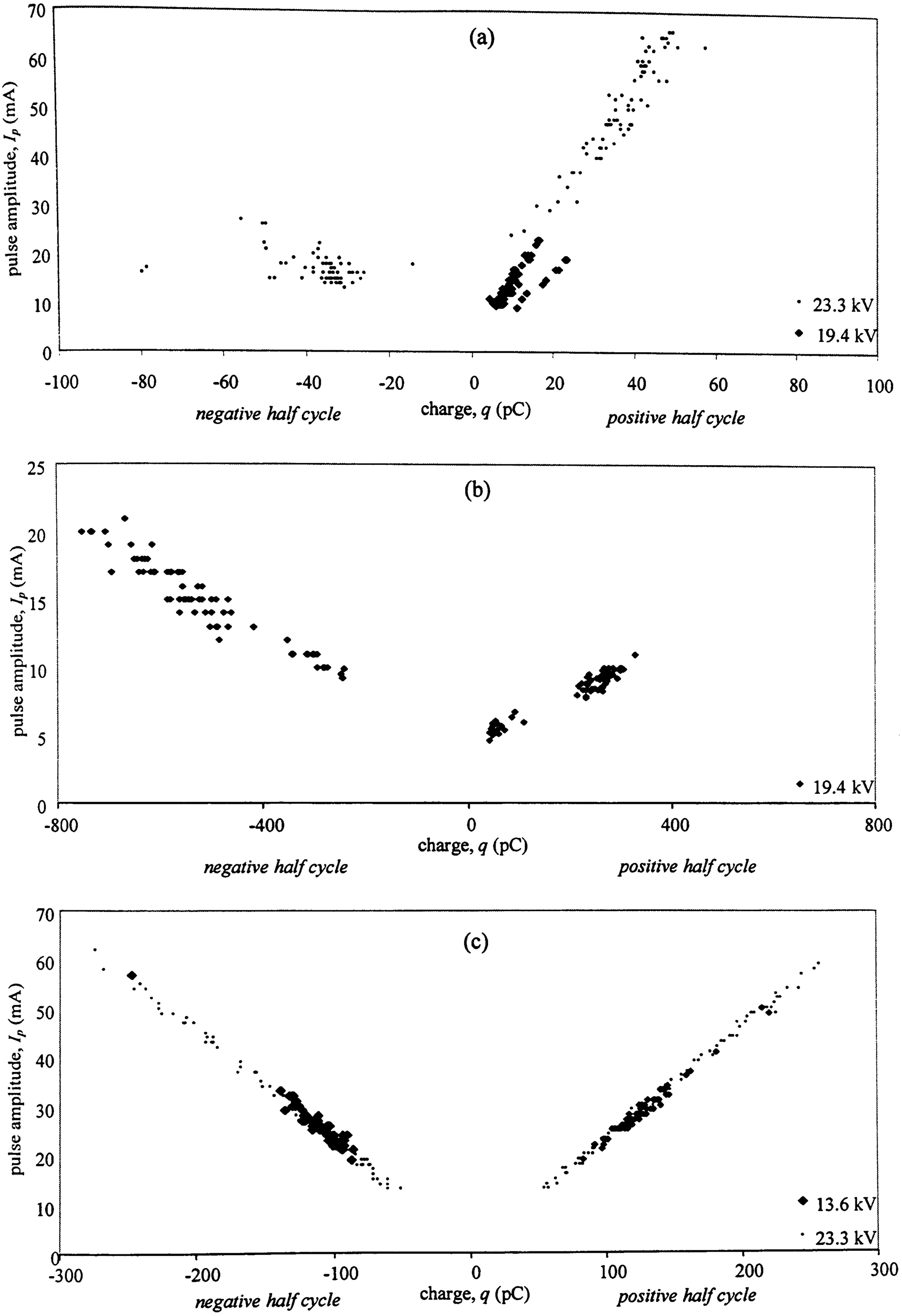

Figure 5.4 Correlation between q and I_p for the (a) protrusion, (b) bad contact and (c) free particle.

At 23.3 kV, the correlation between I_p and q is lower during the negative half cycle and so pulses are more variable in shape during the negative half cycle. This is consistent with the findings for the air-insulated protrusion of Section 4.3.1.1. As already described, greater pulse-shape repeatability might be expected during the positive half cycle because the protrusion behaves as the cathode.

Figure 5.4(a) contains two outlying points at about –80 pC, measured during the negative half cycle. These were acquired towards the end of the experiment just before PD activity ceased of its own accord. Figure 5.5(b) compares one of these pulses with a typical pulse from the main group; it can be seen that the outlier is a double pulse. This suggests that the PD mechanism changed towards the end of the experiment.

In Figure 5.4(b), measurements involving the bad contact revealed a reasonable correlation between I_p and q during the negative half cycle. As indicated in Table 5.2, the mean charge measured during both half cycles was greater than in the case of the protrusion. Measurements made during the positive half cycle form the two clusters evident in Figure 5.4(b). These clusters have different I_p/q ratios, 0.10 mA/pC and 0.03 mA/pC. Figure 5.5(c) shows representative current pulses from each cluster. These clusters are probably indicative of two different discharge sites, which would be likely given the structure of the test object.

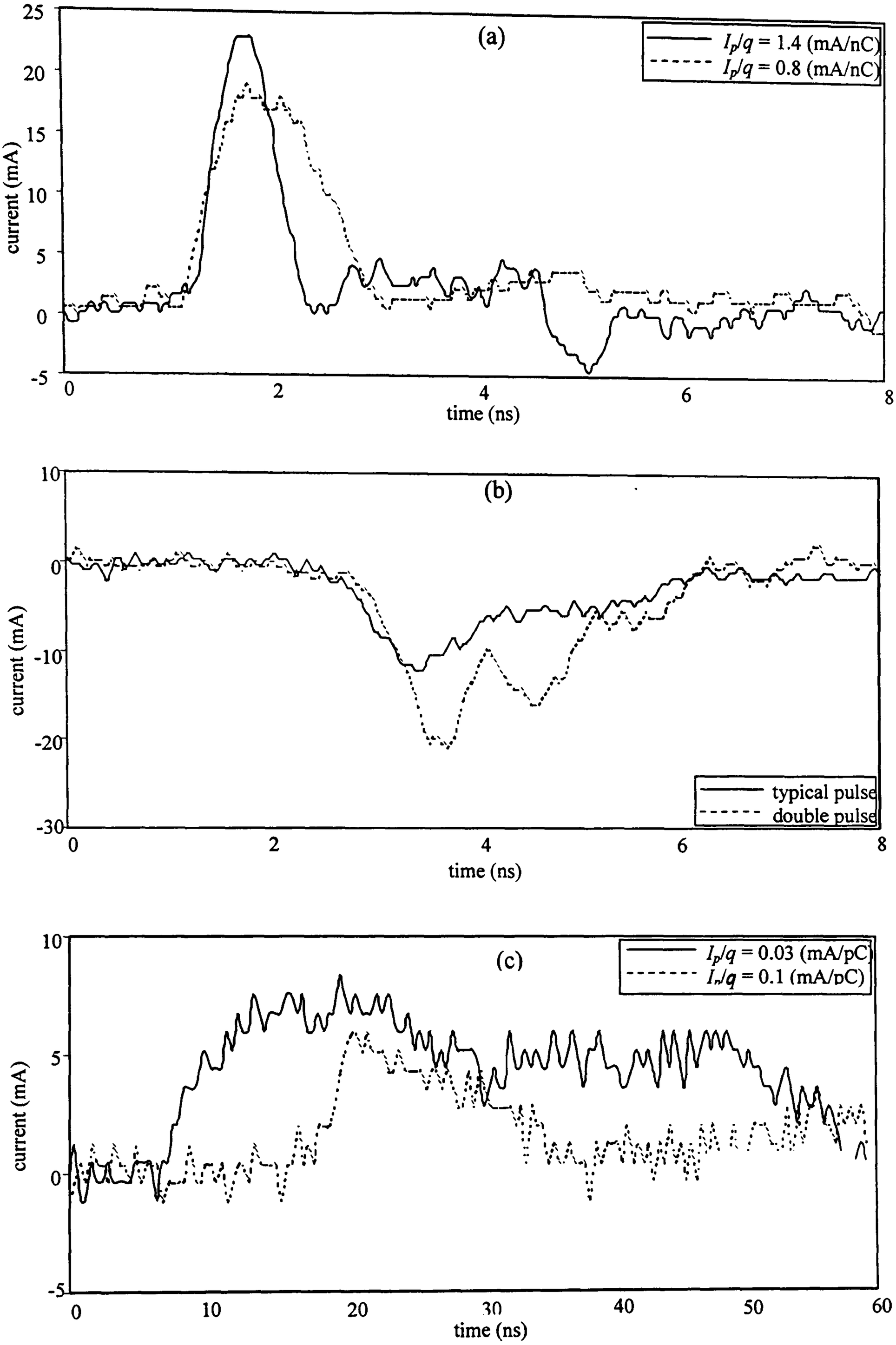

Figure 5.5 Illustrating pulse shape variability: (a) protrusion (positive half cycle), (b) protrusion (negative half cycle) and (c) bad contact (positive half cycle).

Results for the free particle revealed the strongest correlation between I_p and q as can be seen in Figure 5.4(c). This plot indicates that the pulse shape was virtually independent of the magnitude of the applied voltage because similar I_p/q ratios were observed at both 13.6 kV and 23.3 kV. The plot also shows that the pulse shape was virtually independent of the polarity of the applied voltage because the magnitude of the I_p/q ratios were similar during both half cycles. As indicated in Table 5.2, the mean charge (q) associated with the free particle was greater than the mean charge (q) associated with the protrusion during each half cycle.

As mentioned in Section 5.2.1, the particle lifted from the grounded electrode when the electrostatic force exceeded the gravitational force [81]. The charge acquired by the particle was dependent on factors such as its size and the applied voltage. Similarly, the subsequent motion of the particle was dependent on factors such as its mass, the viscosity of the liquid dielectric, and the applied voltage [132,133].

When the particle began to fall towards the grounded electrode this caused the electric field between the particle and the grounded electrode to increase. When the gap distance between the particle and the grounded electrode was small relative to the diameter of the particle then the field in this region can be considered uniform. The surfaces of both the particle and the electrode were smooth, and so there was minimal local field enhancement at either surface. Under such conditions, it is difficult to liberate a free electron.

However, at a sufficiently short gap, ionisation is likely and a micro-spark might be generated in the region between the grounded electrode and the particle. If the gap is very small when it breaks down, and electrons are supplied by one or other of the metallic surfaces, it is possible that the oil will have little effect on the pulse shape. The ready supply of electrons from a metal surface could have resulted in the consistent pulse shape that was observed.

5.3.2 Relationship between current pulses and UHF energy

Since the amplitude of radiated UHF signals is dependent on the acceleration and deceleration of electrons at the defect site, the shape of each PD current pulse plays a critical role in determining the amount of UHF energy radiated [129]. In this section, the relationship between charge and measured UHF energy is investigated.

For experiments involving the grounded protrusion, at the lower test voltage PD was detected only during the positive half cycle. At the higher test voltage, PD was detected during both half cycles and was polarity dependent. Figure 5.6(a) shows that measurements involving the protrusion indicate a stronger correlation between $\sqrt{U}$ and q during the positive half cycle then during the negative half. Therefore, pulse-shapes were more regular when the protrusion was behaving as the point cathode. Table 5.2 shows that while the amounts of charge transferred during each half cycle at the higher operating voltage were comparable, the mean UHF energy measured during the positive half cycle was more than 30 times greater than the mean UHF energy measured during the negative half cycle. A greater amount of UHF energy was measured during the positive half cycle when the applied voltage was increased, that is, 93.8 fJ was measured at 19.4 kV whereas 847.2 fJ was measured at 23.3 kV. Since the current pulses measured during the positive half cycles had shorter risetimes then they can be expected to cause the excitation of a greater amount of UHF energy (Figure 5.5(a) and (b)).

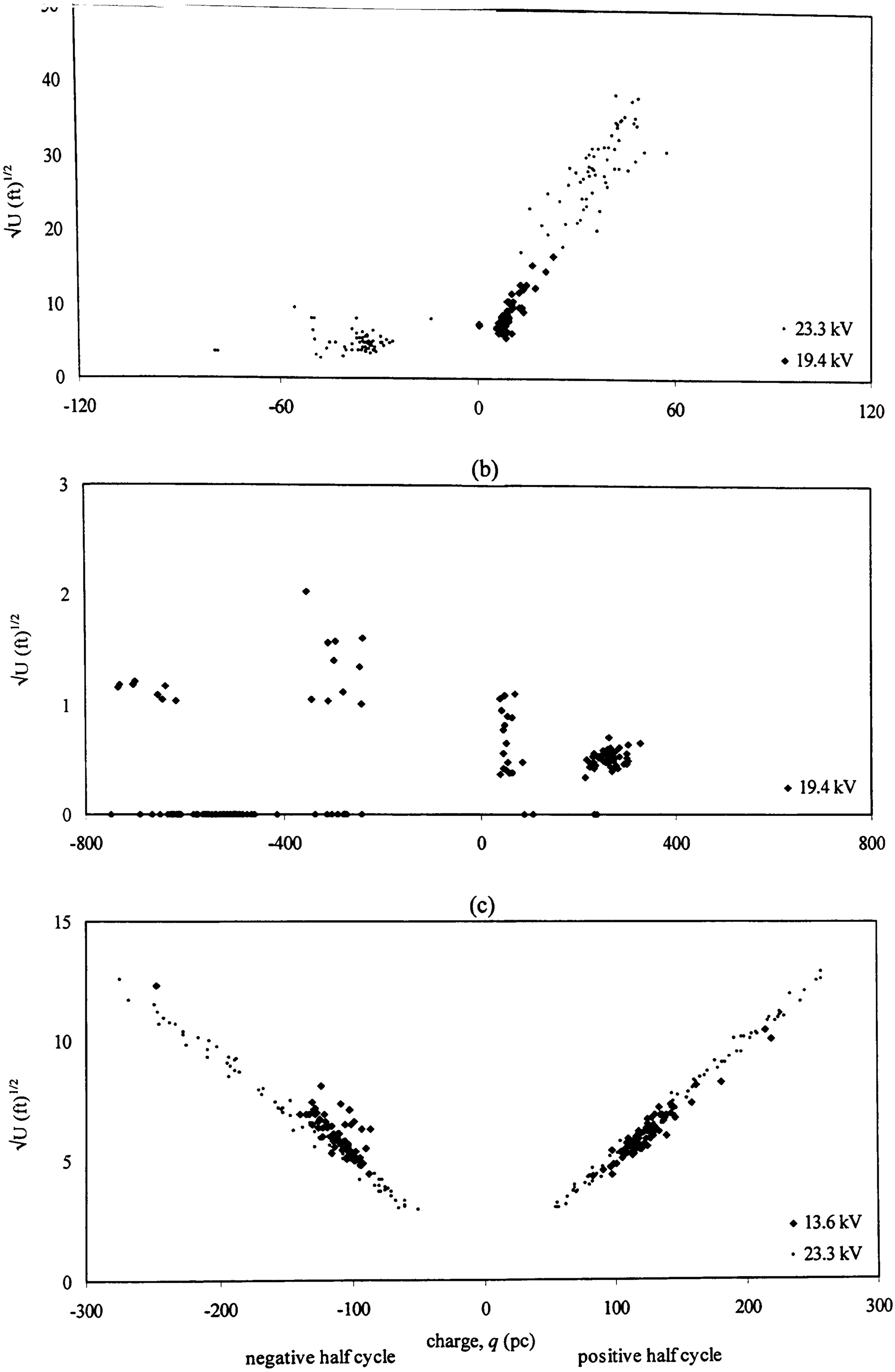

Figure 5.6 Correlation between q and $\sqrt{U}$ for
(a) protrusion, (b) bad contact and (c) free particle.

Figure 5.6(b) reveals no correlation between $\sqrt{U}$ and q for the bad contact. As shown in Figure 5.3, the duration of current pulses measured at the bad contact clearly appeared to have the longest ristimes and so the levels of UHF energy measured were small. In some instances no UHF signal was detected. An examination of pulses shapes did not reveal any obvious variation between pulses where small amounts of UHF energy was measured and pulses where no UHF was measured. This can be attributed to the fact that the electrode system is rather large, causing considerable band limiting of the current pulse measurement.

Results for the free particle possessed a linear relationship between $\sqrt{U}$ and q as can be seen in Figure 5.6 (c), which is to be expected when the pulse shape is very consistent [81,129]. This correlation became stronger when the applied voltage was increased from 13.6 kV to 23.3 kV. Greater correlation might be expected at the higher test voltage because of an improved signal-to-noise ratio, that is, larger values of $\sqrt{U}$ and q were measured at 23.3 kV (Table 5.2).

5.3.3 Spectral content and energy ratios

The spectral content and UHF energy ratios at the two sensors were analysed as described in Section 5.2.4. Since results for different operating voltages were similar for each defect type only those experiments carried out at the higher test voltages are presented.

Figure 5.7(a) shows the frequency content of UHF signals excited by the protrusion. Data is presented in such a way that if there was no difference between the frequency content recorded under each polarity, the plot would appear as a mirror image from left to right. However, in the case of the protrusion higher frequencies were more strongly excited during the positive half cycle. This is a natural consequence of the shorter risetimes of current pulses measured during the positive half cycle. The asymmetry of the physical process is evident in the asymmetry of the spectral plot.

Figure 5.7(b) is a histogram based on data for the ratio of UHF signal energy detected at $Sensor_1$ and $Sensor_2$ for the protrusion. If the ratio had been constant from pulse to pulse, then a single vertical bar of amplitude 100% would have been centred on the mean ratio values $\overline{R_n}$ and $\overline{R_p}$ during the negative and positive half cycles respectively. Values of the mean energy ratios are not given since they are dependent on the senor positions and have no absolute significance. This investigation is only concerned with the variability.

For the protrusion, UHF signals recorded during the negative half cycle exhibit a more variable energy ratio than those in the positive half cycle, which have a large peak centred on $\overline{R_p}$. This finding might be expected because the shapes of current pulses were found to be more variable during the negative half cycle, that is, when the protrusion was behaving as the anode.

In the case of the bad contact, Figure 5.8(a) shows that comparatively low frequencies within the UHF band were excited and the spectrum was similar for each polarity. The excitation of lower frequencies can be attributed to the longer current pulse risetime relative to measurements involving the protrusion and the free particle. Figure 5.8(b) demonstrates that the energy ratio distribution measured during both half cycles was quite variable, being broader than in the case of the protrusion and the free particle. This suggests a significant variation in the position and orientation of PD current pulses at the bad contact, which would be expected since it is likely that several discharges were active on the metallic foil.

Figure 5.9 shows that, for PD generated with a free metallic particle, the spectral content and energy ratios measured during both half cycles were similar. These findings suggest that the PD mechanism was independent of power cycle polarity.

In the water contaminated oil investigation, PD was generated at 1.5 kV and then the experiment was repeated at 2.7 kV. The mean UHF signal energies detected at 1.5 kV and 2.7 kV were 0.07fJ and 0.043 fJ respectively. As shown in Table 5.2, these values are much lower than for any of the other PD sources. Figure 5.10 shows the frequency content of UHF signals recorded during the experiments involving moisture

contamination. PD was found to excite a narrower band of UHF frequencies as the test voltage was increased. Figure 5.11 shows the energy ratio distribution, which is quite variable. This is due to the unpredictable nature of the PD source and the fact that PD activity takes place at a number of sites within the cell as the water droplet disperses.

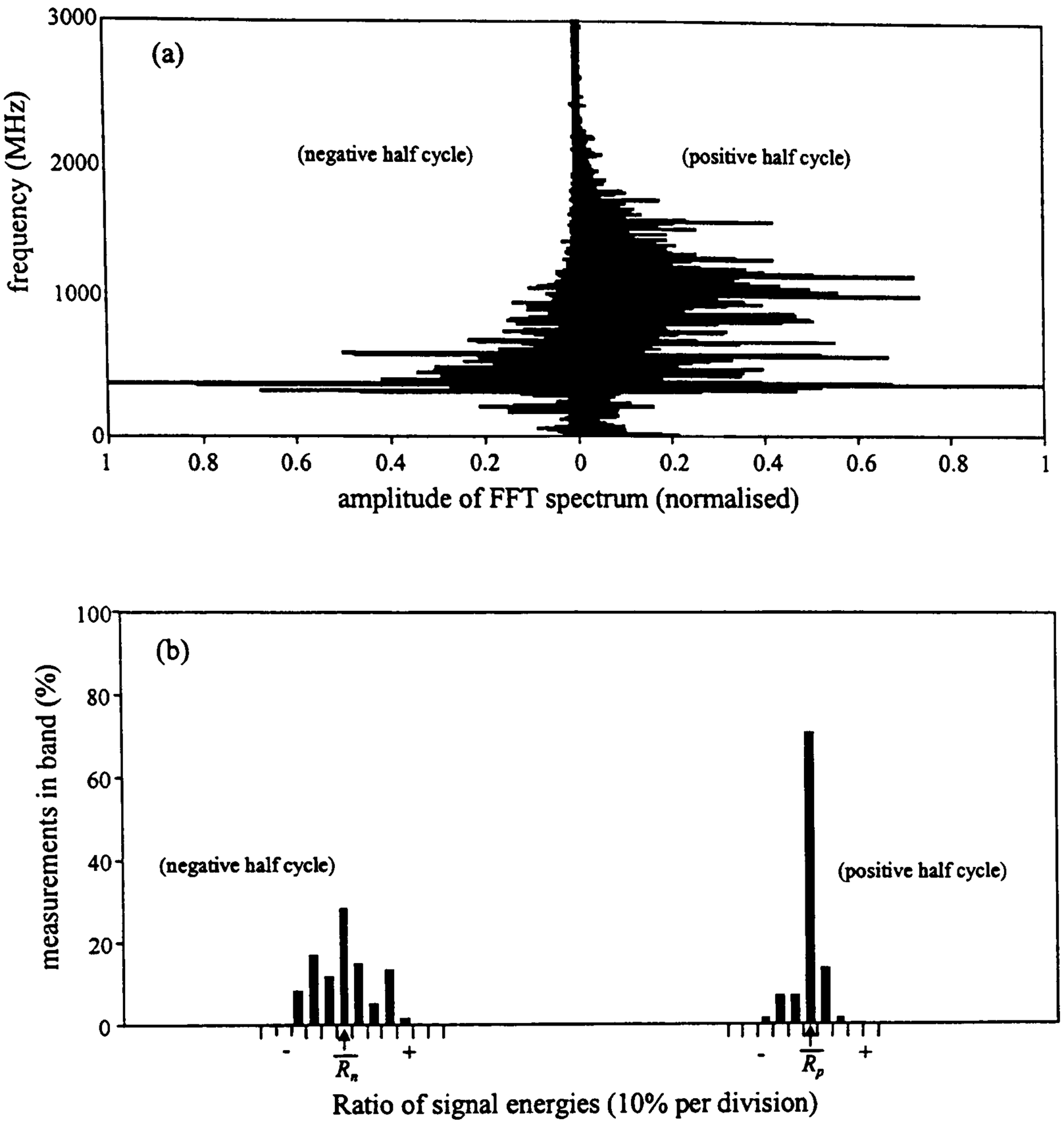

Figure 5.7 Results for the protrusion at 23.3 kV, comparing properties of the UHF signals recorded during each half cycle. (a) Distribution of spectral energy, and (b) Distribution of UHF energy ratio (U_{S2} /U_{S1}) around the mean ratios $\overline{R_n}$ and $\overline{R_p}$.

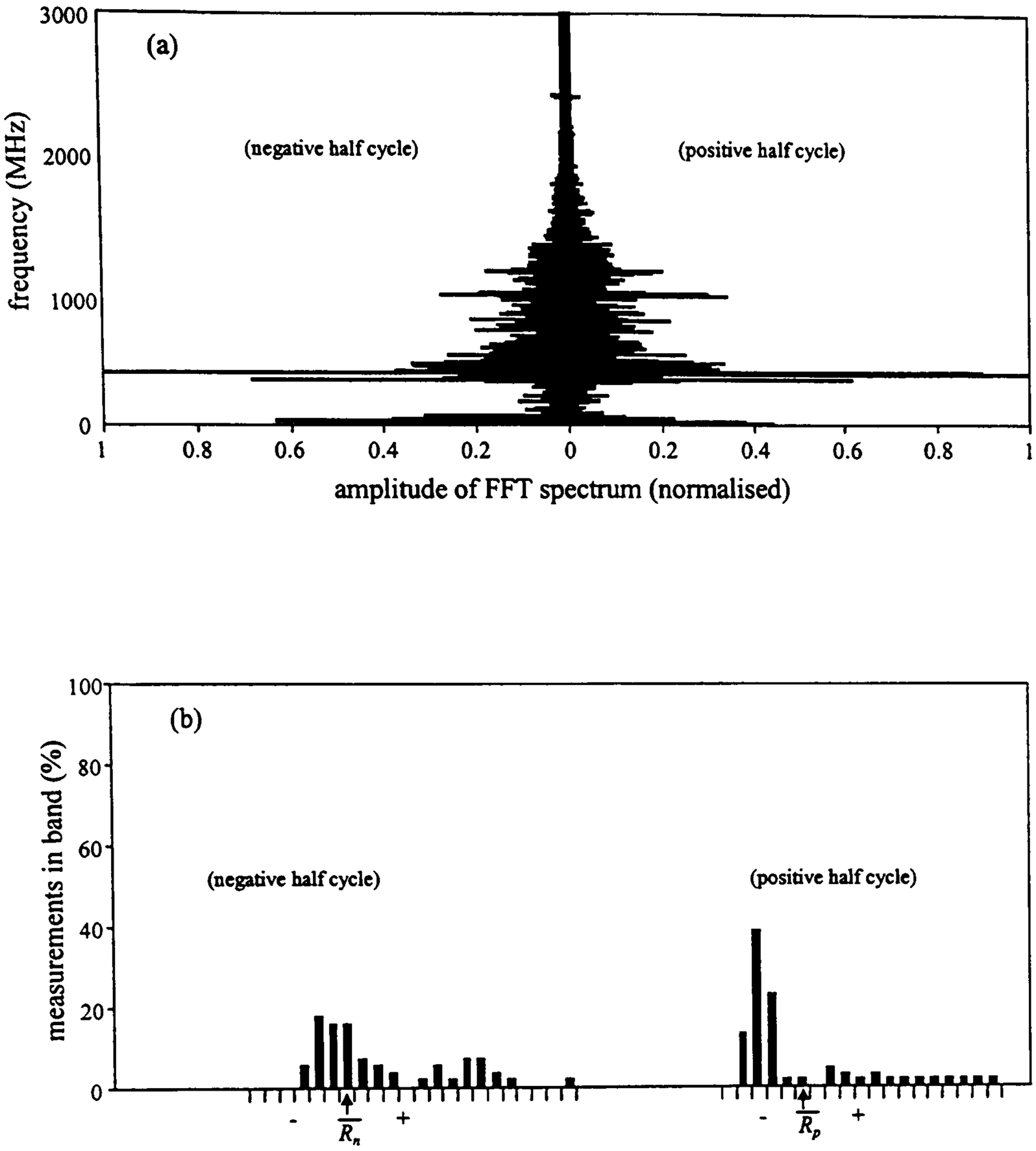

Figure 5.8 Bad contact at 19.4 kV. (a) Distribution of spectral energy, and (b) Distribution of UHF energy ratio (U_{S2} /U_{S1}) around the mean ratios $\overline{R_n}$ and $\overline{R_p}$.

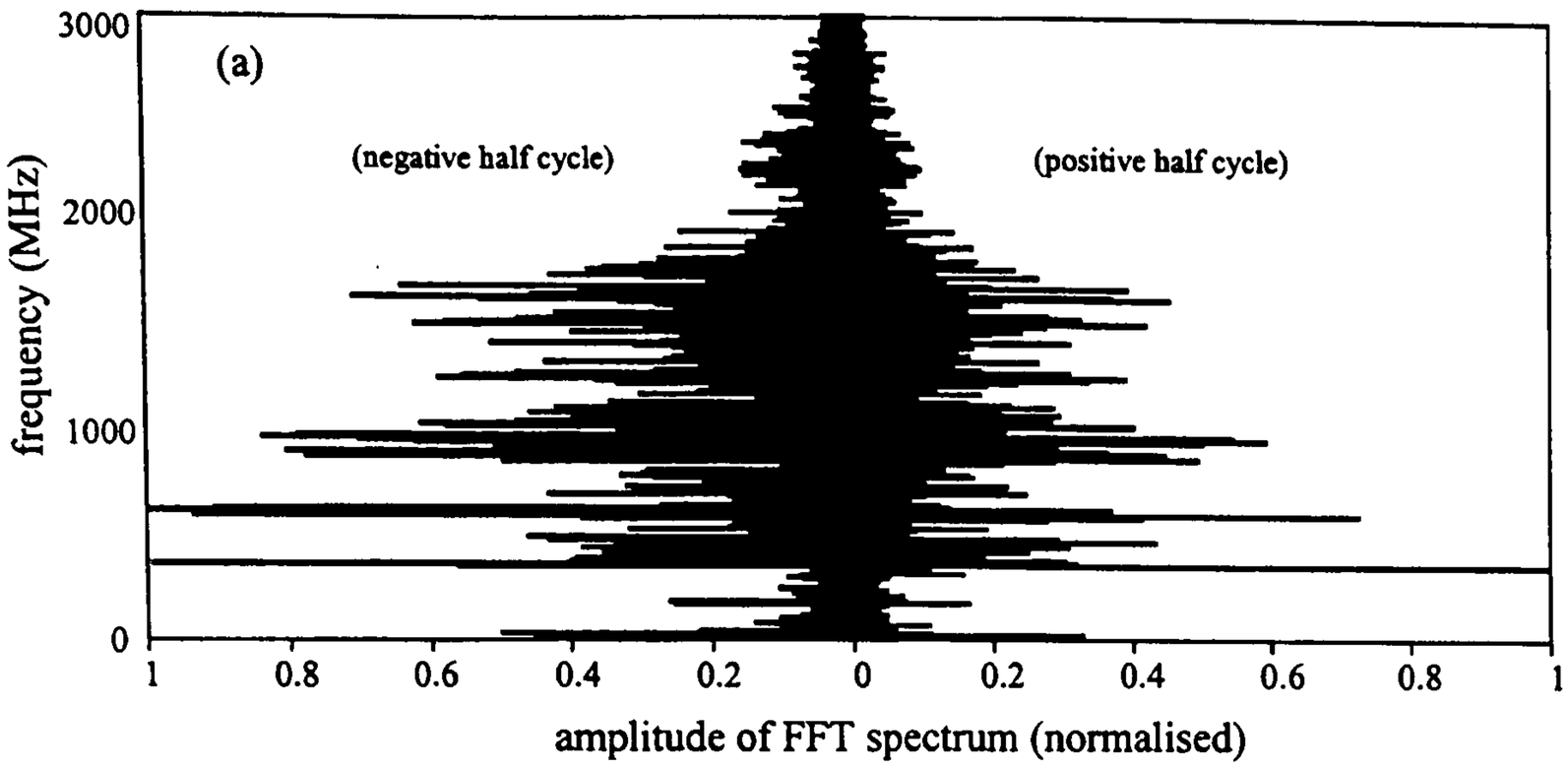

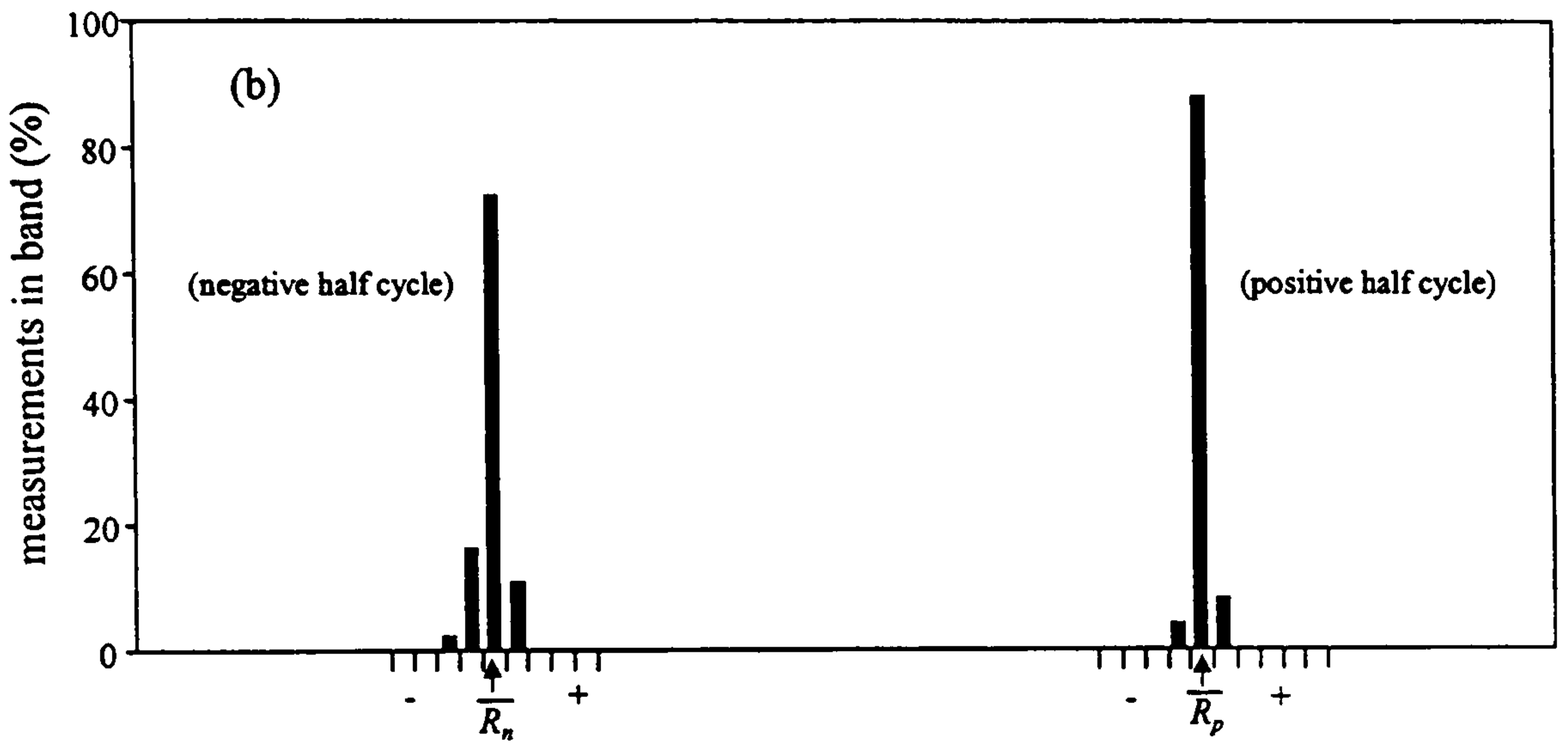

Figure 5.9 Free particle at 23.3 kV. (a) Distribution of spectral energy, and (b) Distribution of UHF energy ratio (U_{S2} /U_{S1}) around the mean ratios $\overline{R_n}$ and $\overline{R_p}$.

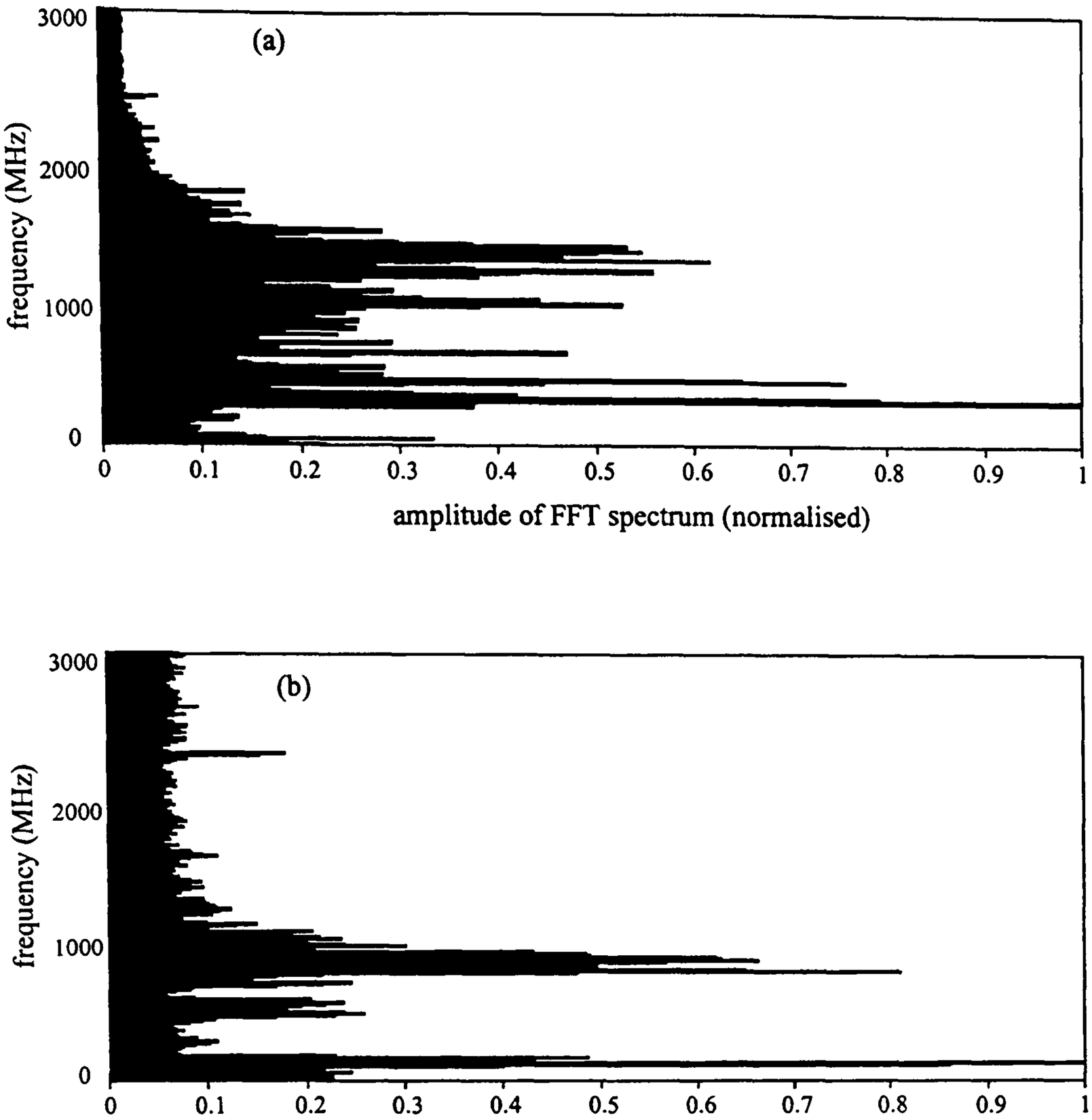

Figure 5.10 Spectral content of UHF signals generated by PD in moisture contaminated oil at different applied voltages (a) 1.5 kV, and (b) 2.7 kV.

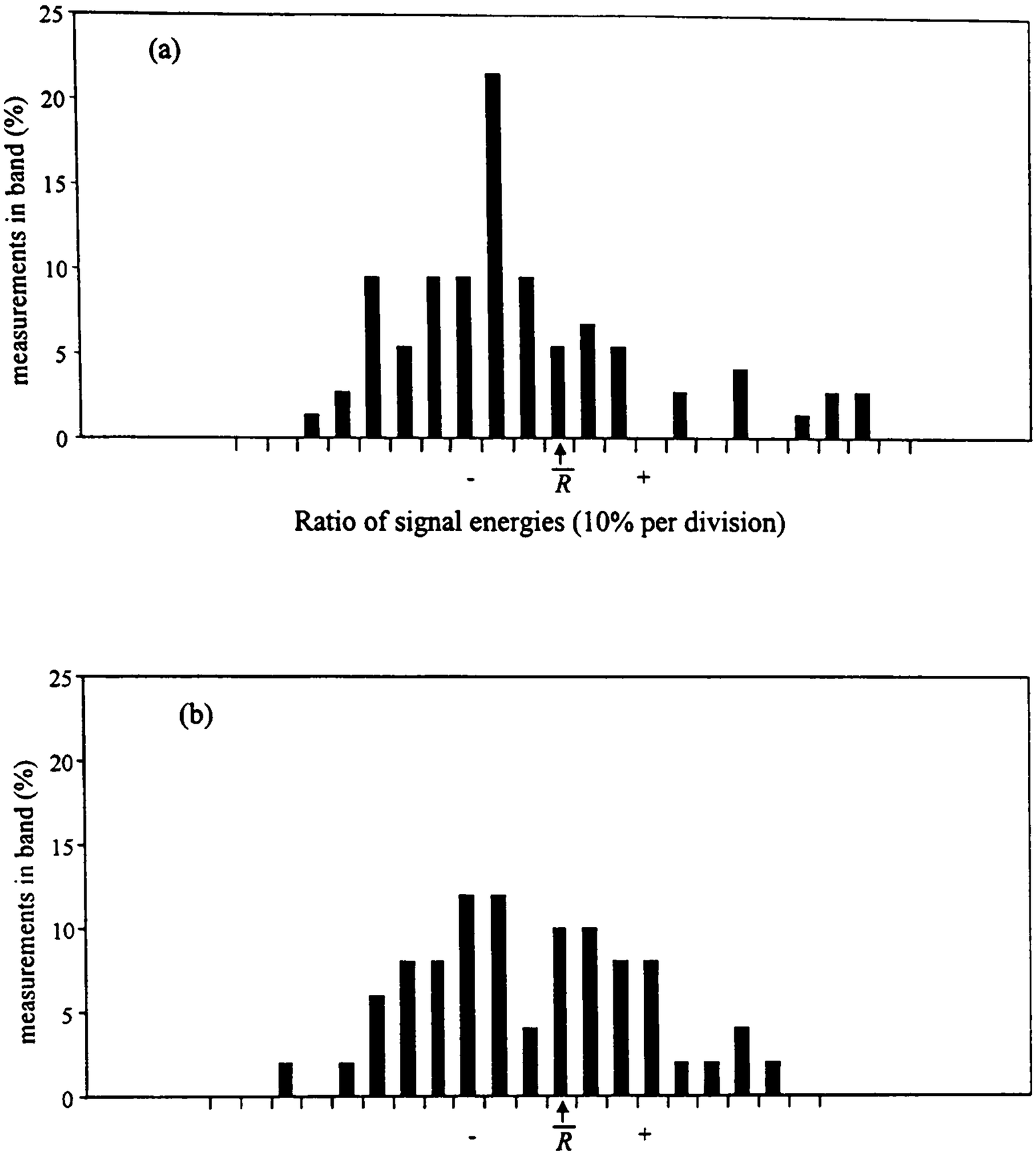

Figure 5.11 Distribution of UHF signal energy ratios around the mean value $\overline{R}$ for PD in moisture contaminated oil at different applied voltages. (a) 1.5 kV, and (b) 2.7 kV.

5.4 Conclusion

Measurements of PD current pulses indicate that the protrusion and the bad contact exhibit the greatest amount of pulse-shape variability. For the protrusion, the variability was most evident in the difference between the positive and negative pulses because of the different physical processes of the discharge mechanism. In the case of the bad contact, the presence of several PD sites was the most probable cause of the observed variations.

PD generated at the protrusion excited the most energy; however, this is probably because the protrusion is an efficient radiating structure (monopole) for high frequency electromagnetic energy. On the other hand, the bad contact radiated less energy despite larger amounts of charge being transferred during pulses. This is attributed to the longer current pulses and rather poor radiating structure of the discharge site. Experiments involving the free metallic particle illustrated very well the proportionality between radiated UHF energy and the square root of the charge transferred during a PD pulse that occurs when pulse shape and orientation are consistent from pulse to pulse.

In this chapter, two new ways of analysing UHF signals have been presented. These are the spectral content and the ratio of energies methods. Both compare discharge activity during the positive and negative half cycles of the power frequency in a way that could allow different sources to be distinguished. By plotting the spectral energy during both half cycles differences in discharge mechanisms can be identified. Similarly, the ratio of energies method can be used to assess variability in the pattern of radiation from the PD source.

The advantage of the two new methods is that they use only normalised data derived from the UHF signals. Therefore, these methods could be applied to the 'black box' situation which is more likely to be encountered in measurements carried out on operational power transformers. It is anticipated these methods will complement existing techniques, such as phase-resolved measurements for PD diagnostics.

6. PHASE-RESOLVED PARTIAL DISCHARGE MEASUREMENTS

6.1 Introduction

The results and discussion of Chapters 3, 4 and 5 have established that the UHF measurement technique can be used to detect PD generated in transformer insulating oil. This chapter describes and discusses PD that is generated at a variety of insulation defects that would cause concern in an operational power transformer. The types of defect considered are:

- HV electrode protrusion in air
- HV electrode protrusion in oil
- Surface discharges
- Bad contact
- Floating component
- Suspended particle
- Free metallic particle
- Arcing sources

For each defect type, radiated UHF PD signals are recorded as phase-resolved events using the PDM that was outlined in Section 2.4.5. By performing experiments over a range of test voltages, information can be obtained on whether the PD activity is changing in character or severity.

Phase-resolved measurements are analysed in ways that provide evidence of the physical differences between the insulation defects. This work has resulted in a reference database that could be valuable for comparison with field measurements. The data gathered from this investigation has been used by others to develop an expert system for the automatic classification of defect type [134,135], which will be discussed briefly at the end of the end of this chapter.

6.2 Experimental Procedure

6.2.1 PD test apparatus and test cell

The experimental arrangement used for measuring UHF PD signals is shown in Figure 6.1. The electromagnetic signals radiated from the PD sources were detected using the broadband UHF electric field sensor that was described in Section 2.4.3. These signals were amplified or attenuated prior to being measured in phase-resolved form using the PDM. In this chapter, UHF PD signals were recorded using the PDM described in Section 2.4.5. For each experiment, the type of oil used was reclaimed light grade transformer oil (L10B).

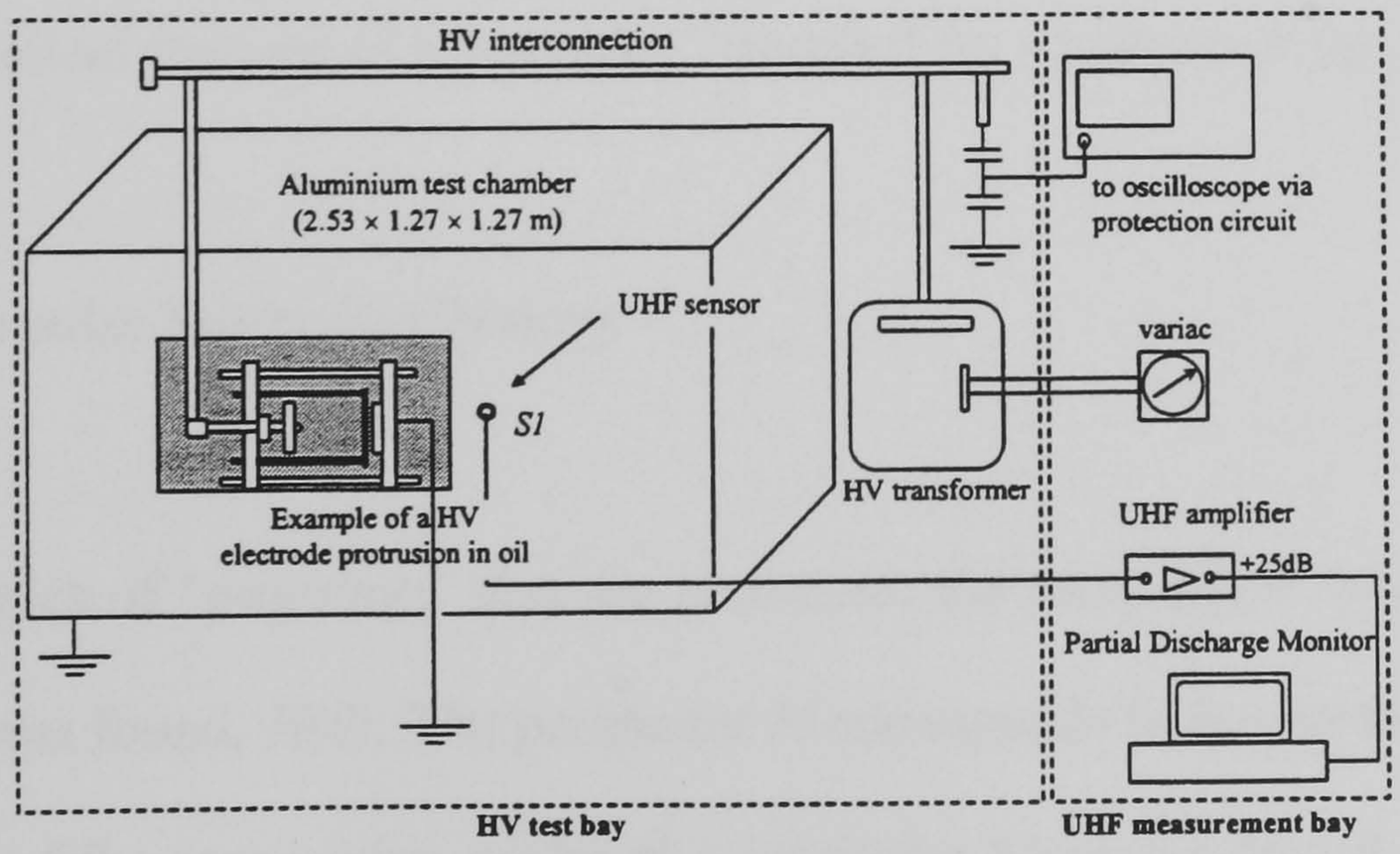

Figure 6.1 Experimental arrangement used to energise PD sources and measure UHF PD signals in phase resolved form

6.2.2 Evaluation of measurements

6.2.2.1 Three-dimensional PD plots

The PDM was used to record '*snapshots*', that is, PD data in the three-dimensional form of *phase angle*, *pulse height* and *cycle number*. The salient features of a '*snapshot*' are shown in Figure 6.2.

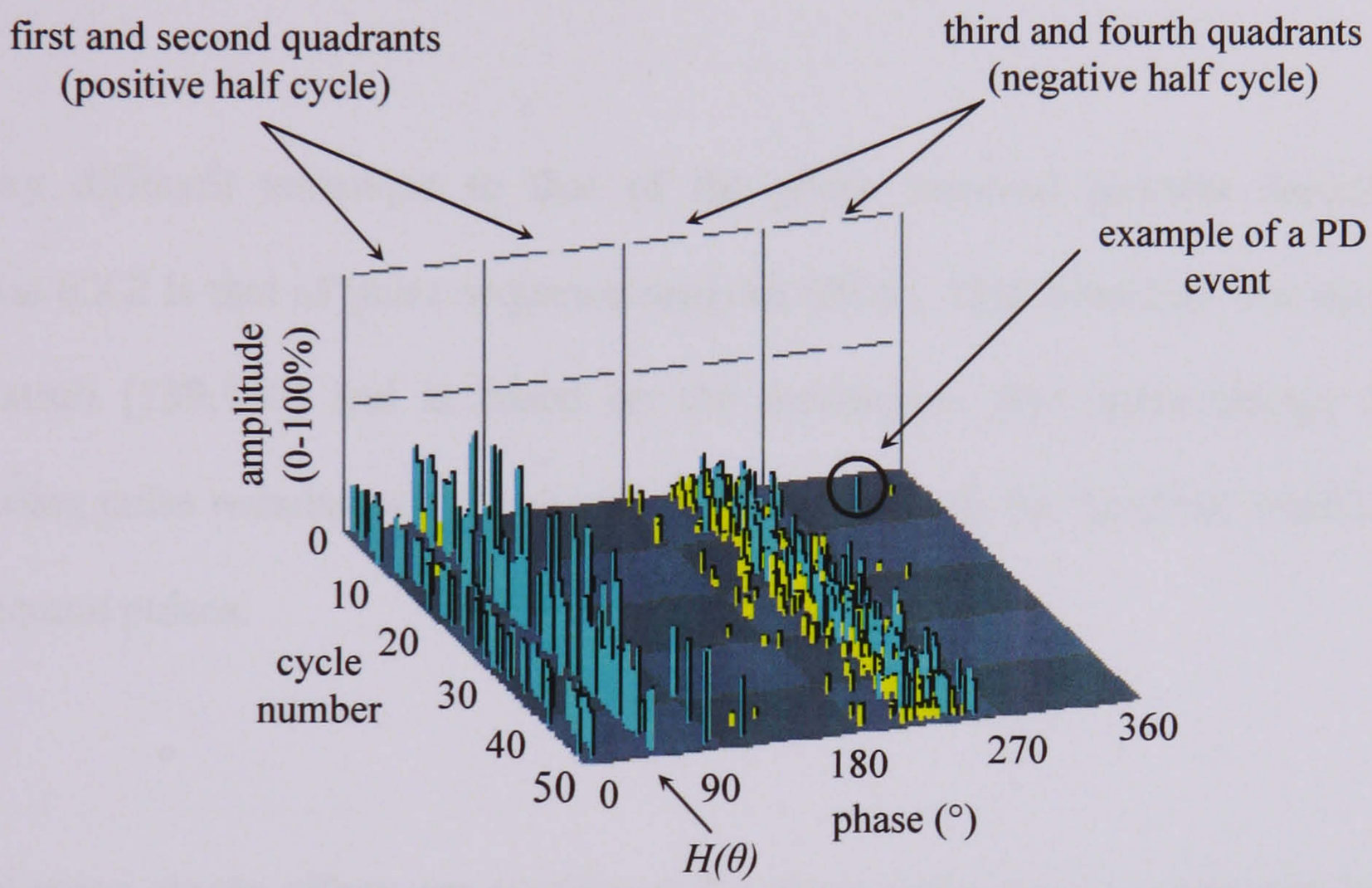

Figure 6.2 Salient features of a '*snapshot*' recorded for a bad contact at 1.8 kV.

6.2.2.2 Mean pulse height distributions

From the examples of '*snapshots*' that are presented, the *mean pulse height* at each phase position was found, $H(\theta)$. The parameter H corresponds to the mean amplitude of PD events on fifty consecutive cycles at a particular phase window θ. The PDM resolved pulses into 64 phase windows on each power cycle. This corresponds to a phase resolution of $\Delta\theta = 5.6°$.

Each '*snapshot*' consisted of fifty cycles of power frequency, that is, one second's worth of PD data at 50 Hz. At each phase position, the amplitudes of all PD pulses occurring on each power cycle were summed and then divided by fifty. This approach was used to find $H(\theta)$ for each '*snapshot*' and is based on a technique pioneered by Kreuger [136, 137, 138] that been shown to provide a means for interpreting PD activity generated in SF_6 when recorded using a conventional measurement system.

6.2.2.3 Study of successive PD pulses

A very different technique to that of the phase resolved patterns described in Section 6.2.2 is that of pulse sequence analysis (PSA). This technique was pioneered by Patsch [139,140] and is based on the assumption that space charge from a preceding pulse remains near the discharge site and affects the 'ignition' conditions of subsequent pulses.

When space charge effects are significant the phase angle cannot necessarily be taken as a representative parameter for the local electric field that determines the PD process, and so conventional phase-resolved measurements can be misleading. However, PSA is a promising technique as it is not based on the absolute value of the phase angle but the local electric field and its change, which is a function of both the time between pulses (Δt) and the difference in applied voltage (ΔV) between successive PD pulses.

The basic principle of the PSA technique pioneered by Patsch [139, 140] is explained with reference to Figure 6.3. The PD pulses presented are shown for illustration purposes only and do not relate specifically to any of the experiments carried out in this chapter.

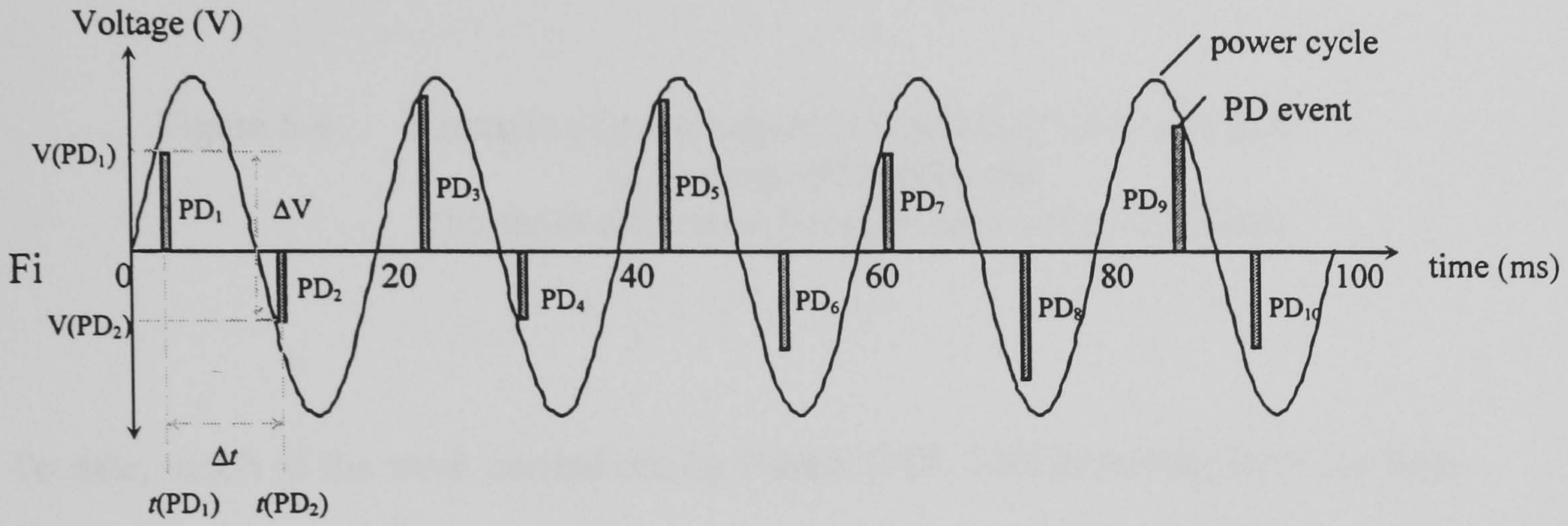

$$\Delta V_{2\text{-}1} = V(PD_2) - V(PD_1) \qquad \Delta t_{2\text{-}1} = t(PD_2) - t(PD_1)$$

Figure 6.3 Overview of the pulse sequence analysis (PSA) technique.

From Figure 6.3, the time difference between the first two PD pulses is denoted as $\Delta t_{2\text{-}1}$ and the difference in applied voltage between these pulses is denoted as $\Delta V_{2\text{-}1}$. A matrix consisting of all Δt and ΔV values is formed and accumulated with the number of successive PD pulses possessing a particular difference in time and voltage. As shown in Figure 6.4, this data can be plotted in graphical form to assist with interpretation. Again, these distributions do not specifically relate to any of the experiments carried out in this chapter.

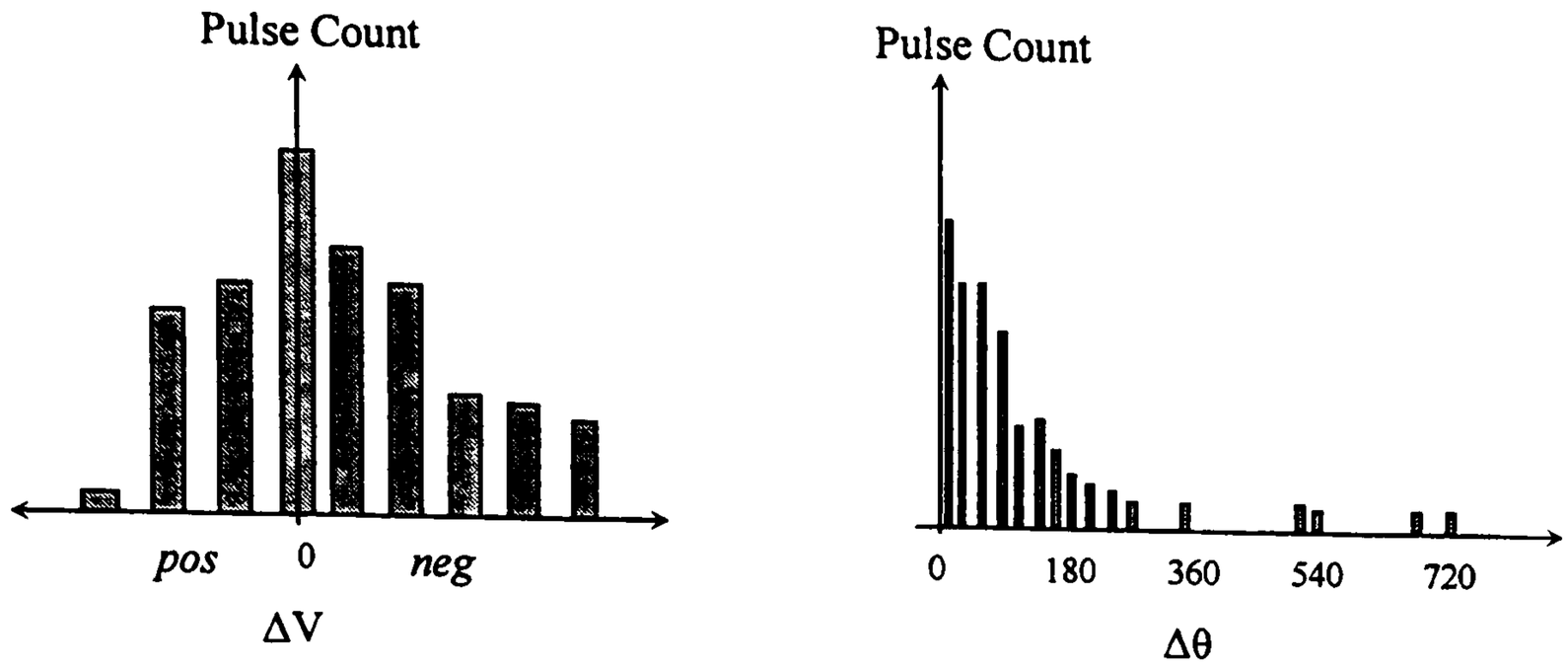

Figure 6.4 Example of pulse sequence analysis (PSA) technique,
(a) voltage difference and
(b) phase difference between successive PD pulses.

To date, much of the work carried out by Patsch [139, 140] involving PSA has been associated with electrical trees in polyethylene. For experiments involving polyethylene, the PSA technique was shown to be particularly useful in interpreting PD behaviour. This was because PD was highly affected by the space charge generated at the discharge site and so few PD pulses were measured per cycle. However, it is expected that using PSA to interpret PD generated in insulating liquids will be more difficult. This is because pulse repetitions in oil are high and suitable acquisition technology is expensive.

The PSA method relies on an acquisition technique that resolves individual pulses and can provide PD pulse data from several consecutive pulses. As already outlined, the phase resolution of the PDM is $\Delta\theta = 5.6^{\circ}$, that is 0.3125 ms, and the PDM only records the largest pulse in each window (Section 2.4.5). However, as shown in Chapter 4 (Figure 4.18) several PD pulses can be generated in oil on a timescale of

20 μs (0.02 ms). Clearly, the PDM would not have sufficient resolution to detect all of the PD pulses that were generated on the 20 μs timescale.

In the work of this chapter, PD was generated at a range of electrode configurations but it is unlikely that the PDM had sufficient resolution to detect all of the PD pulses that were generated. As a result, the technique of PSA that was pioneered by Patsch [139, 140] cannot be applied directly to the experimental data. Instead, a simplified version of the technique was developed to assist with interpreting the phase-resolved data. This simplified technique was inherently limited by the low sampling rate of the PDM. However, it is anticipated that the study of successive PD pulses in oil will become more powerful when suitable acquisition technology is available.

As will be described, this technique involved calculating the difference in phase angle ($\Delta\theta$) between successive PD pulses, and is explained with reference to Figure 6.5. PD pulses that occurred during the positive and negative half cycles of the '*snapshot*' were separated as shown in Figure 6.5 (a). The plan view of these plots is shown in Figure 6.5(b) where the difference in phase angle ($\Delta\theta$) between successive PD events is more clear.

PD pulses occurring on adjacent half cycles were then concatenated and the difference in phase angle ($\Delta\theta$) between successive PD pulses was found. Figure 6.5(c) shows an example of successive PD pulses that have a difference in phase angle corresponding to $\Delta\theta \sim 146°$. Inspection of the plot shows that these pulses occurred on adjacent half cycles. The first pulse was detected at extinction voltage on the first half cycle, whereas the second pulse was detected at inception voltage on the following half

cycle. PD pulses that occurred on consecutive phase positions, that is, $\Delta\theta = 5.6°$, are termed as being '*adjacent pulses*'.

A matrix consisting of $\Delta\theta$ values in the range 0° to 360° was formed. This matrix was populated by accumulating the number of successive PD pulses possessing a difference in phase angle of $\Delta\theta$. For each experiment, the difference in phase angle for PD occurring on both half cycles will be presented. Since $\Delta\theta$ values between successive PD events were generally less than two half cycles the upper limit of the $\Delta\theta$ axis was set to 360°. The *pulse count* axis was scaled as appropriate for each simulated defect.

Since the relationship between the energy contained in the '*raw*' UHF signal and the PD pulse measured using the PDM was non-linear (Section 2.4.5.2) the difference in amplitude between successive PD pulses was not investigated.

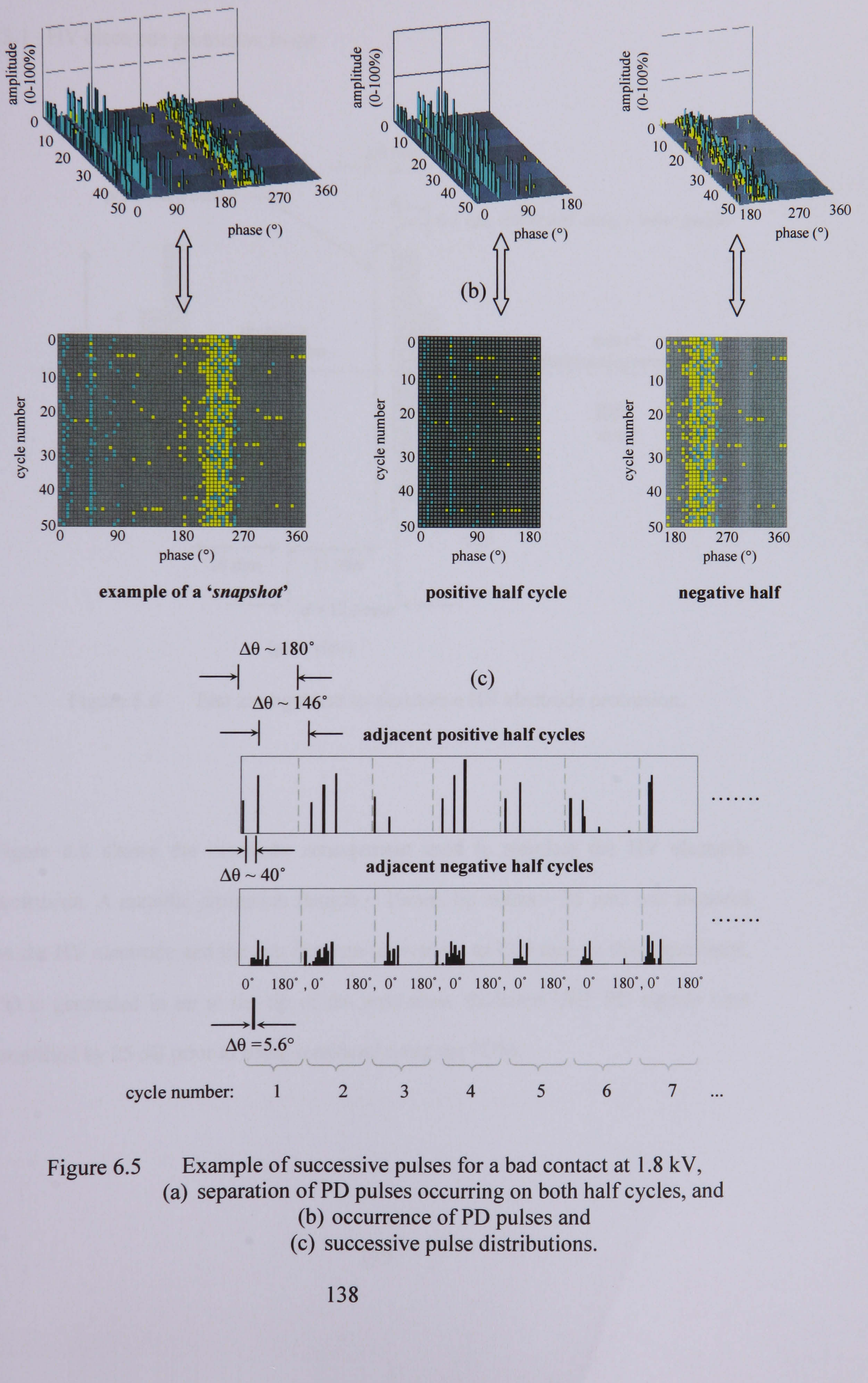

Figure 6.5 Example of successive pulses for a bad contact at 1.8 kV,
(a) separation of PD pulses occurring on both half cycles, and
(b) occurrence of PD pulses and
(c) successive pulse distributions.

6.3 Results and Discussion

6.3.1 HV electrode protrusion in air

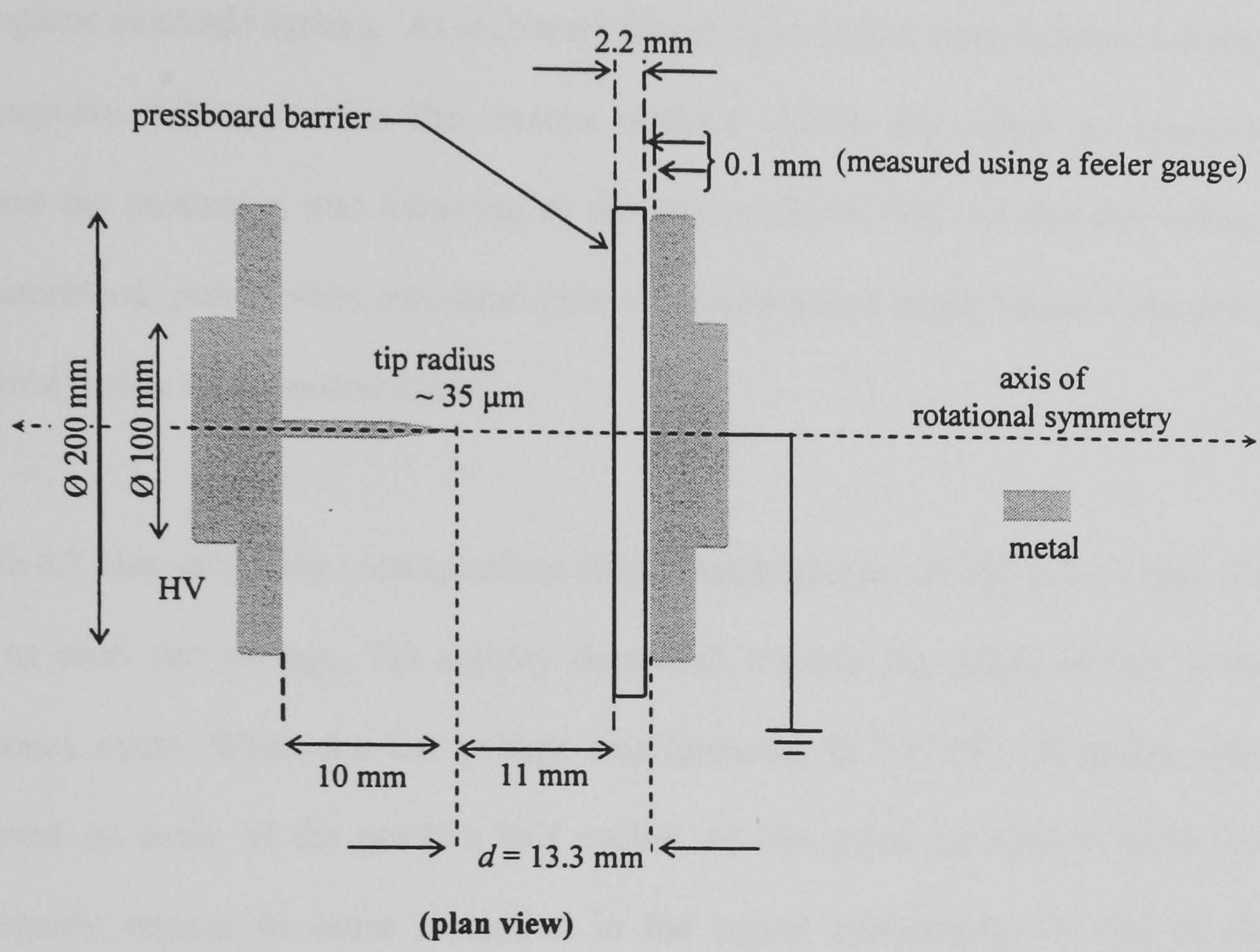

Figure 6.6 Test arrangement to simulate a HV electrode protrusion.

Figure 6.6 shows the electrode arrangement used to simulate the HV electrode protrusion. A metallic protrusion (length = 10mm, tip radius ~ 35 µm) was mounted on the HV electrode and the gap distance (d) was set to 13.3 mm. In this experiment, PD is generated in air at the tip of the protrusion. Radiated UHF PD signals were amplified by 25 dB prior to being measured using the PDM.

Figure 6.7 shows examples of phase-resolved patterns measured for the air-insulated HV electrode protrusion at 1.8 kV, 2.5 kV and 3.3 kV. The asymmetry of PD activity in the positive and negative half cycles can be attributed to the asymmetry of the point-plane electrode system. At each test voltage, more pulses were measured during the negative half cycle. For the reasons outlined earlier, this might be expected because the protrusion was behaving as the point-cathode [98]. As the test voltage was increased, pulses were measured over a broader phase angle because inception occurred earlier on the power cycle.

Figure 6.7 also shows the corresponding $H(\theta)$ distributions at 1.8 kV, 2.5 kV and 3.3 kV. At each test voltage, PD activity decreased towards the peaks of the power frequency cycle. When the test voltage was increased to 2.5 kV, PD pulses were observed on some of the positive half cycles. At this point the electric field was sufficiently intense to cause ionisation in the region surrounding the tip of the protrusion. At 3.3 kV, PD occurred on every positive half cycle. The development of the PD pattern in this way shows that the UHF signals do relate to the severity of the PD.

Figure 6.8 shows the corresponding successive pulse distributions at the three test voltages. In all cases, the majority of PD events measured during the negative half cycle were found to occur on adjacent phase positions. As the test voltage was increased, a greater number of pulses were found to occur on adjacent phase positions. This is an indication that PD activity was more severe at the higher test voltages. The composition of air is mainly nitrogen, oxygen and carbon dioxide.

Nitrogen does not form negative ions, and oxygen and carbon dioxide are considered as weakly attaching gases [106]. As a result, the influence of space charge will be negligible and so pulses might be expected to occur continuously until extinction voltage. Once inception voltage had been exceeded, PD pulses, in general, were measured continuously until extinction voltage.

At each test voltage, a small group of PD pulses is also evident in the region $90^\circ \sim \Delta\theta \sim 180^\circ$ during the negative half cycle. These concentrations are representative of successive PD events that occurred on adjacent half cycles. As the test voltage was increased, the centres of these concentrations were observed to shift to the left of the plot. This occurred because inception occurred at an earlier phase position and extinction occurred at a later phase position when the test voltage was increased.

As already outlined, relatively fewer PD pulses were measured during the positive half cycle. This is because the protrusion was behaving as the point anode.

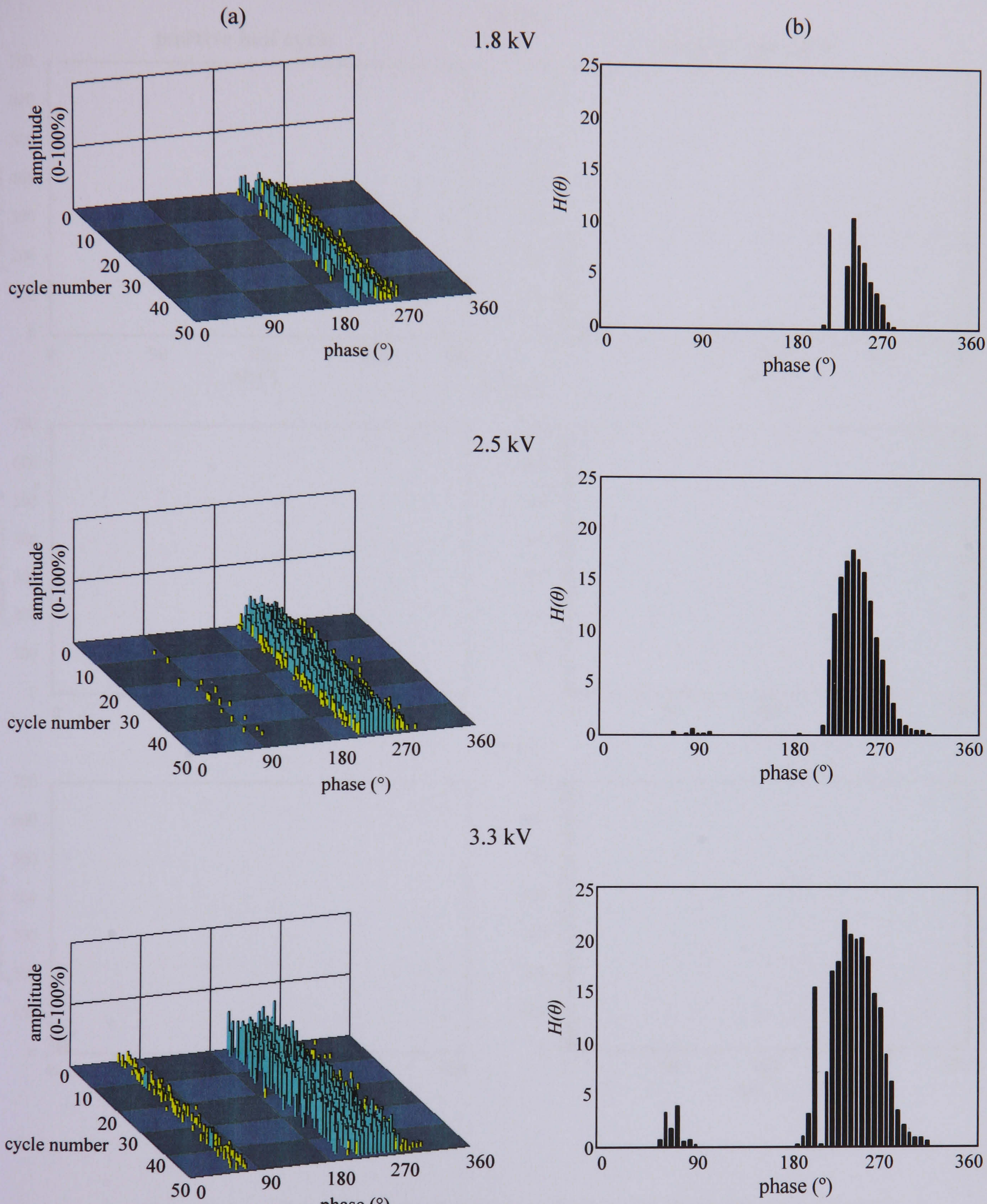

Figure 6.7 HV electrode protrusions in air at 1.8 kV, 2.5 kV and 3.3 kV, (a) examples of '*snapshots*' and (b) corresponding *H(θ)* distributions.

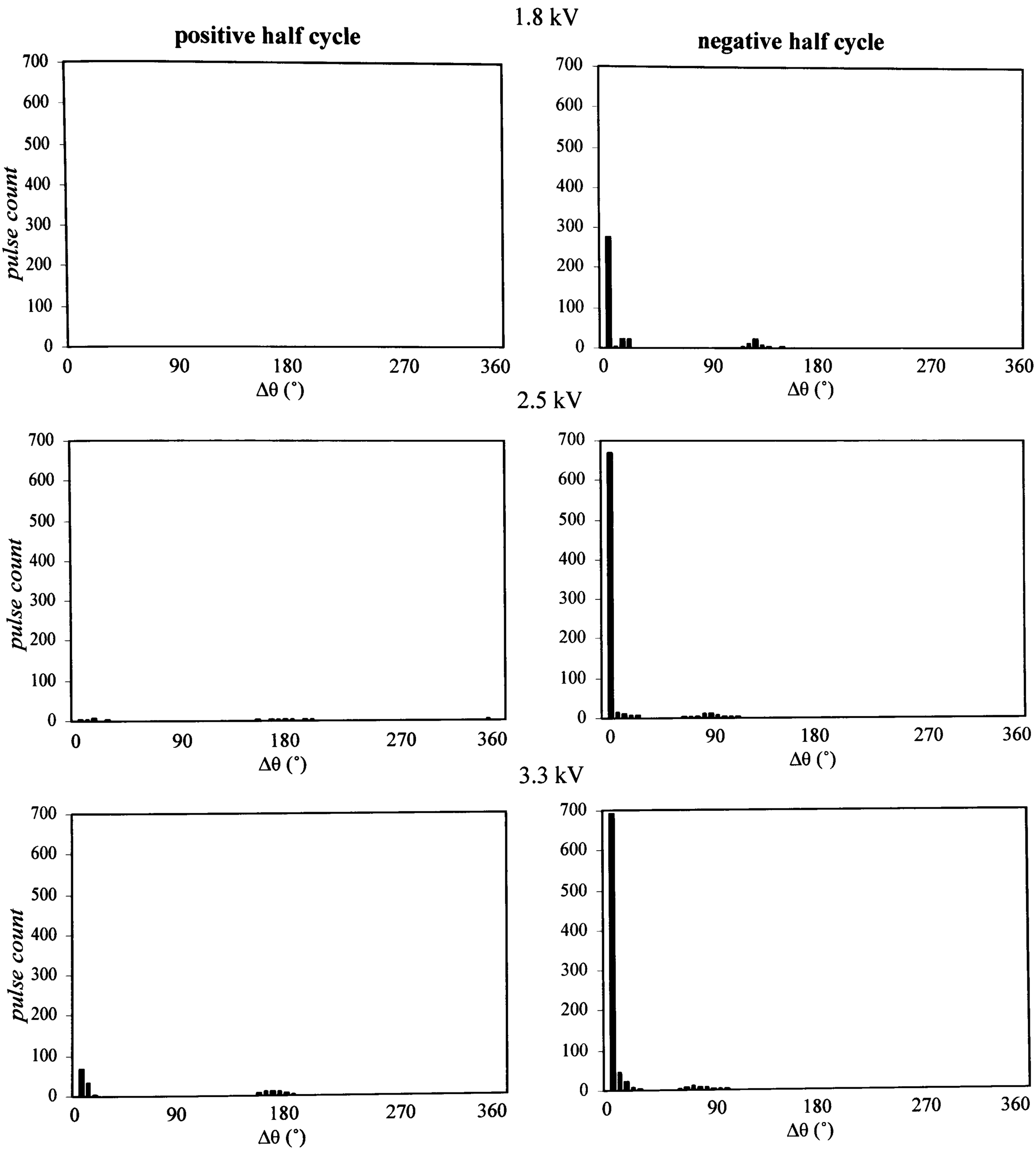

Figure 6.6 Pulse-sequence distributions for the HV electrode protrusion in air at 1.8 kV, 2.5 kV and 3.3 kV.

6.3.2 HV electrode protrusion in oil

The electrode system shown in Figure 6.6 was placed in an oil bath and used to simulate the oil-insulated HV electrode protrusion. Again, radiated UHF PD signals were amplified by 25 dB prior to being measured using the PDM. PD inception voltages were higher because of the greater dielectric strength of oil.

Figure 6.9 shows examples of phase-resolved patterns measured for this defect at 18.0 kV, 28.2 kV and 35.9 kV. Pulses occurred more frequently and were generally greater in amplitude when the test voltage was increased from 18.0 kV to 28.2 kV. At 28.2 kV and above, pulses were measured over a broader phase angle because inception occurred earlier on the power cycle.

The magnitude and number of PD events was greater during the positive half cycle, that is, when the protrusion was behaving as the anode. Previous experiments by Raja et al [141], have also reported greater amounts of UHF energy for PD occurring in oil insulation surrounding a point-anode. As outlined in Section 3.4.2, the duration of current pulses measured at the point-anode can be longer than those measured at a point-cathode. However, inspection of the longer current pulses revealed that they actually consisted of shorter components of PD current. These components occurred on a nanosecond timescale, and caused the excitation of UHF signals. For this reason, greater levels of UHF energy might be expected during the positive half cycle.

In Chapter 3, it was suggested that these shorter components of current were representative of streamers. This might be because of PD occurring in a gaseous channel within a liquid dielectric. Since positive streamers are generally recognised as being '*fast and filamentary*' [11,115], then large amounts of UHF energy could be expected to be measured during the positive half cycle. On the other hand, negative streamers (emanating from a point-cathode) are often described as being '*slow and bush-like*' [11,115]. As negative streamers branch out into the diverging electric field, and their mobility is reduced due to an accumulation of space charge at their tips then a lower amount of UHF energy might be expected during the negative half cycle.

Figure 6.9 also shows the corresponding $H(\theta)$ distributions. These plots show PD pulses centred on the peaks of the power cycle. This might be due to the protrusion tip becoming eroded with extensive testing. These plots also show that the number of pulses and their amplitudes were significantly greater during positive half cycle. Different amounts of PD activity might be expected during both half cycles given the asymmetry of the electrode system.

At 18.0 kV, PD events were not measured on every cycle. This behaviour can be explained in terms of the injection of space charge into the liquid dielectric as successive PD events occur when the applied field is increasing. Once the voltage peaks are approached and dV/dt reduces, the existing space charge around the tip of the protrusion suppresses the local field and PD activity diminishes [103, 140, 141].

As the test voltage was increased from 28.2 kV to 35.9 kV, $H(\theta)$ was found to decrease. If the protrusion tip became more eroded at the higher test voltage, due to extensive testing, then the electric field at the tip of the protrusion would have been less divergent and so lower magnitudes of UHF PD signals might be expected at the higher test voltage. Alternatively, the PD generated at the tip of the protrusion might have changed in character, for example, to a 'glow-type' discharge which might not have resulted in the excitation of UHF signals.

Figure 6.10 shows the corresponding successive pulse distributions at 18.0 kV, 28.2 kV and 35.9 kV. At 18.0 kV, a broad variation is noted in terms of the difference in phase angle between successive PD events. This variation is noted for PD events occurring on both half cycles. At 28.2 kV and 35.9 kV, the majority of PD events measured during the positive half cycle were found to occur at successive phase positions. A concentration of activity is also noted in the region $\Delta\theta \sim 90°$, which is representative of successive pulses that occurred on adjacent half cycles. At 28.2 kV and 35.9 kV, a broad variation is evident in terms of the difference in phase angles for PD pulses occurring on the negative half cycle.

During the negative half cycle, electrons can readily be supplied from the tip of the metallic protrusion to the oil bulk. These electrons might attach to oil molecules or impurities and form negative ions. This negative space charge will superimpose the geometrically defined electric field, and the local electric field at the PD site will be reduced. Therefore, PD activity will be suppressed and a broad variation might be expected in terms of the difference in phase angle between PD pulses measured during the negative half cycle.

The difference in phase angle between successive PD events is more variable for PD generated in oil than air. This difference has been attributed to the accumulation of space charge in the oil but not in the air. Van Brunt et al [142] has suggested that space charge can result in a '*memory propagation*' that influences PD behaviour. Whenever a PD event occurs, it can leave an '*imprint*' in the region surrounding the PD. This can modify the conditions in the discharge gap for times that may be comparable to or significantly longer than the mean time between PD pulses.

There are two categories of '*memory effect*' that can influence the PD process. The first category is concerned with processes, such as space charge accumulation, from which the discharge site can recover. The second category, is concerned with processes that result in permanent damage of the region surrounding the discharge, such as, the deposition of permanent surface charge or chemical degradation [143,144]. Moreover, '*memory propagation*' can make the interpretation of phase-resolved PD measurements difficult.

In this discussion, PD was generated at the tip of an oil-insulated protrusion mounted on the HV electrode. A grounded protrusion, under the same experimental conditions, would possess identical phase-resolved patterns but shifted in phase by 180° due to the polarity reversal of the applied AC field.

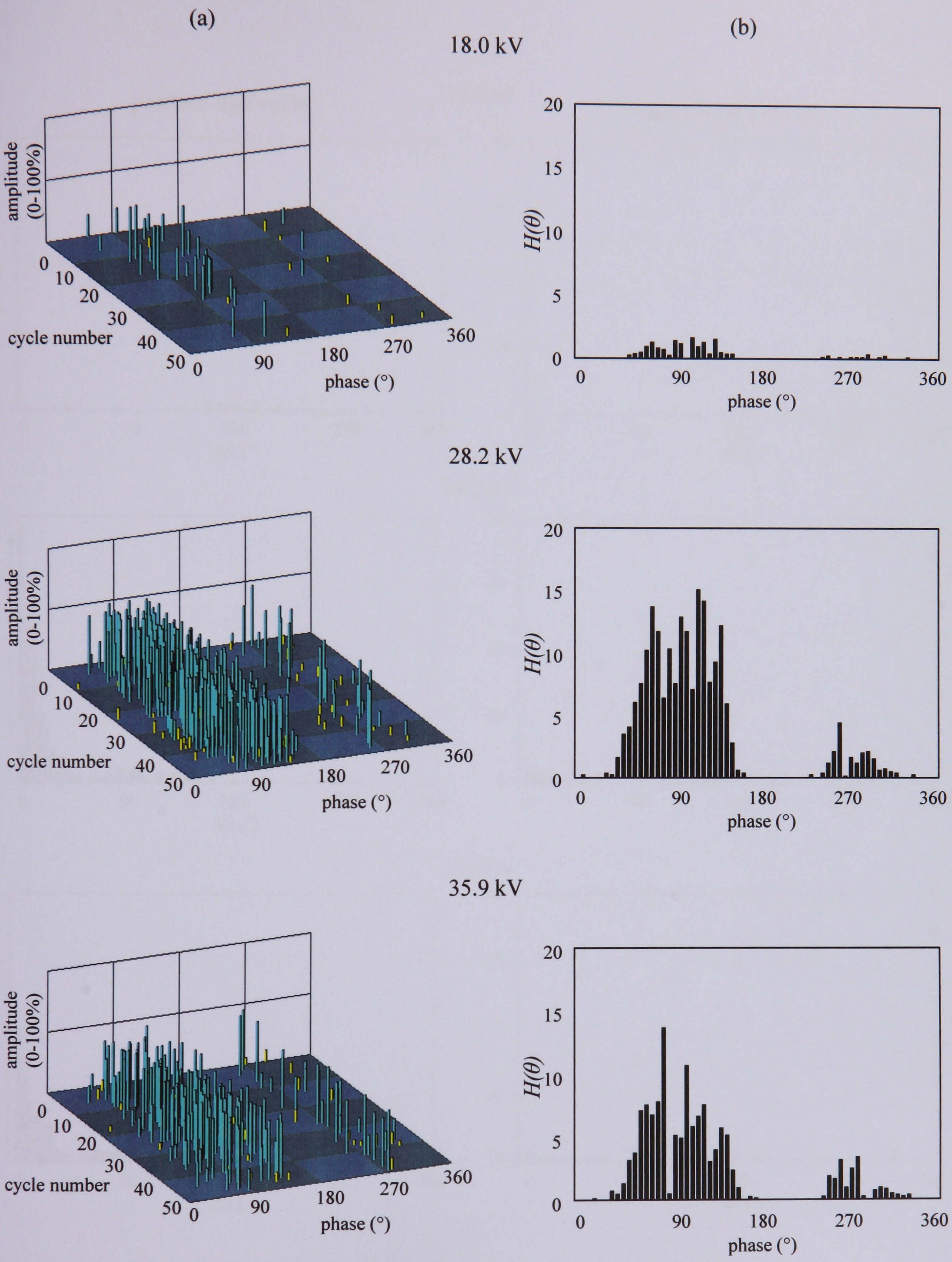

Figure 6.9 HV electrode protrusions in oil at 18.0 kV, 28.2 kV and 35.9 kV, (a) examples of '*snapshots*' and (b) corresponding $H(\theta)$ distributions.

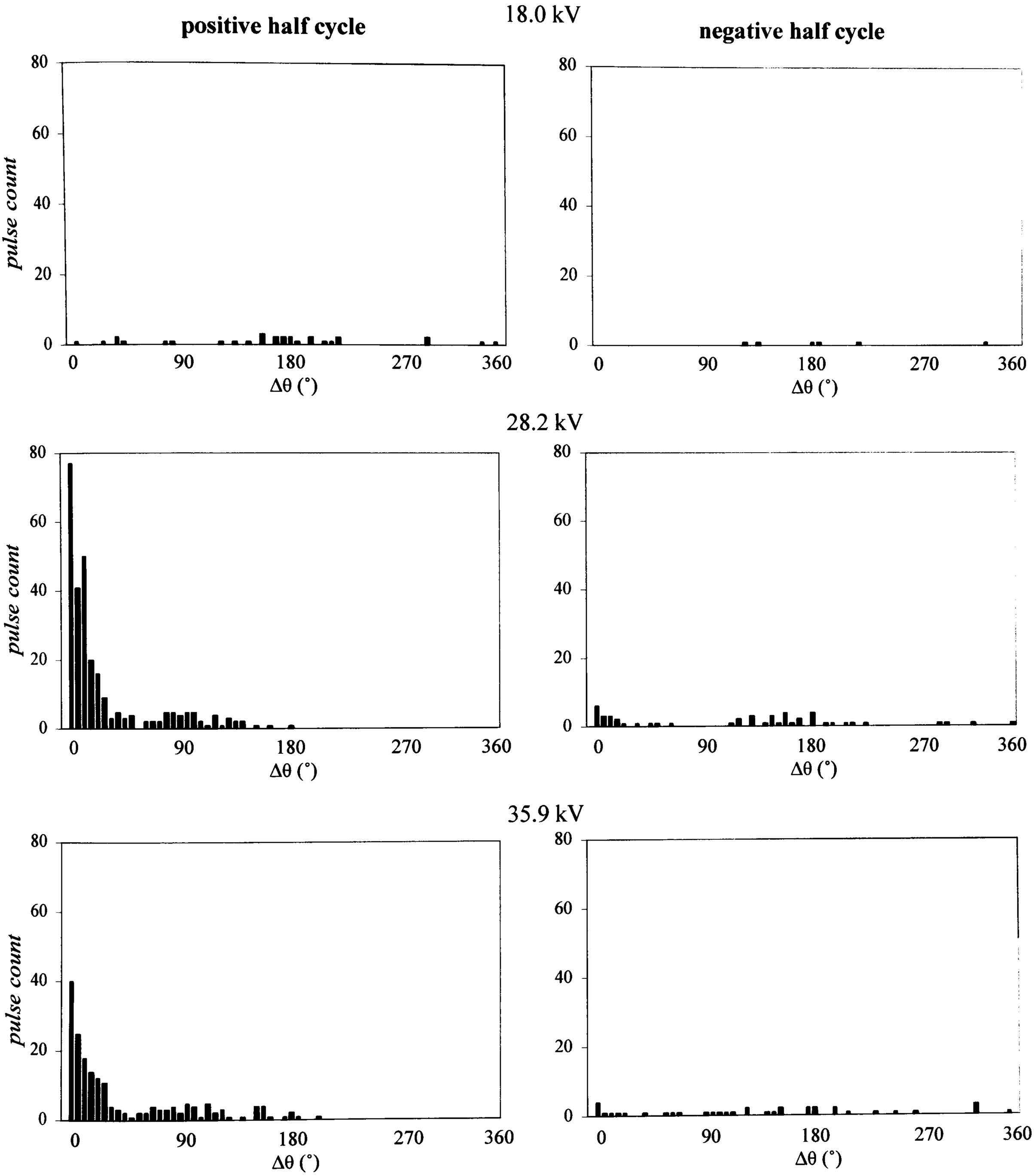

Figure 6.10 Pulse-sequence distributions for the HV electrode protrusions in oil at 18.0 kV, 28.2 kV and 35.9 kV.

6.3.3 Surface discharges

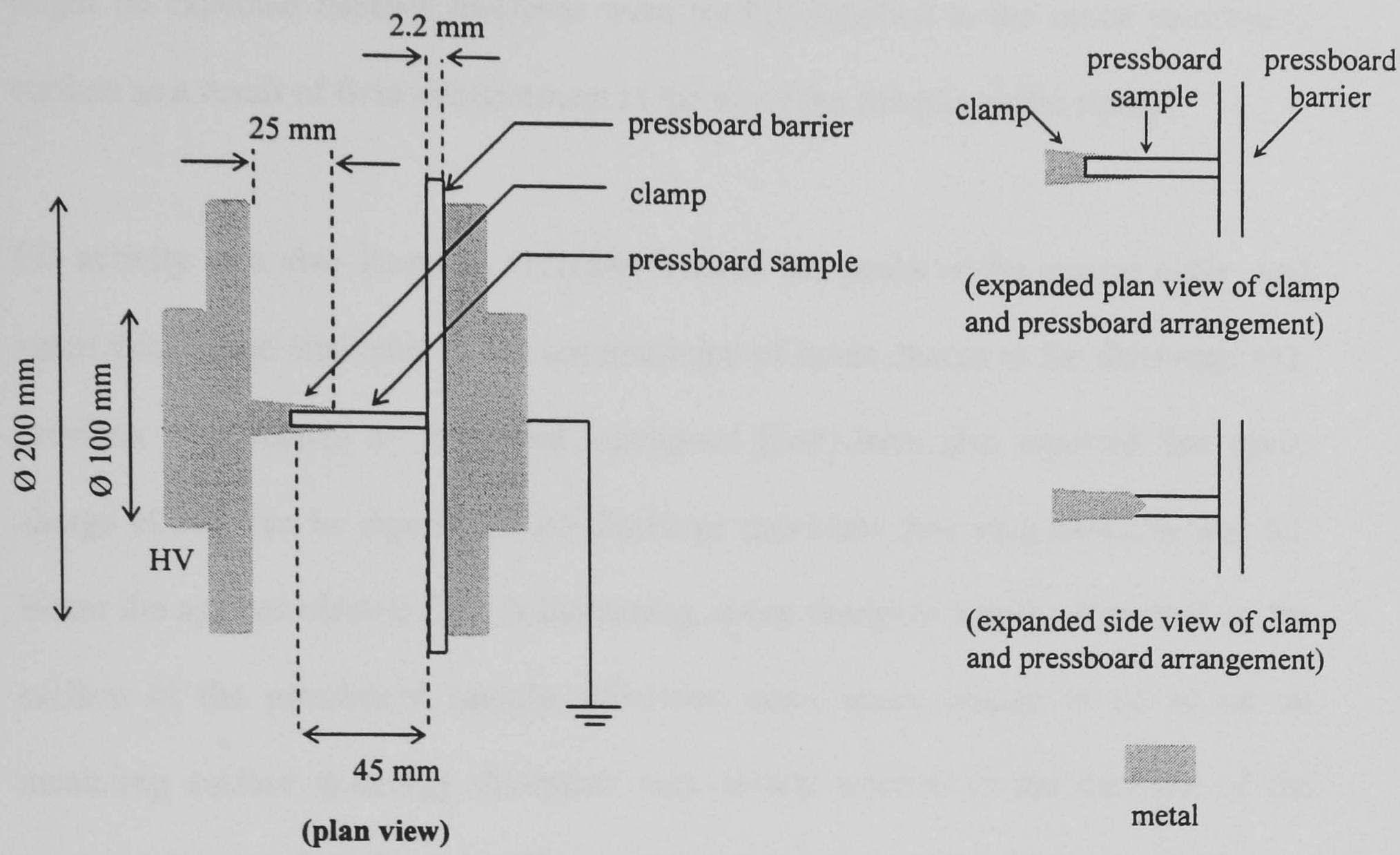

Figure 6.11 Test arrangement used to generate surface discharges

Figure 6.11 shows the electrode arrangement that was used to generate surface discharges on a moist pressboard surface. As described in Section 1.2, moisture contamination can cause concern in a power transformer. In order to ensure that PD could be generated at the pressboard sample it was soaked in water for 24 hours prior to being tested. In this experiment, 7.96 kV was applied to the HV electrode and radiated UHF PD signals were amplified by 25 dB prior to being measured using the PDM.

Figure 6.12 shows an example of a phase-resolved '*snapshot*' pattern for the surface discharge experiment; the corresponding $H(\theta)$ plot is also shown. On the whole, the phase-resolved patterns revealed very similar characteristics to experiments carried out by Berg and Lundgaard [144,145] which involved the simulation of a wedge type discharge in transformer insulating oil. Figure 6.12 shows that a greater number and

amplitude of PD pulses were measured during the negative half cycle. This finding might be expected because electrons were readily supplied to the moist pressboard surface as a result of field enhancement at the tip of the sharp metallic clamp.

PD activity was also found to decrease towards the peaks of the power cycle, and again this can be attributed to the accumulation of space charge at the discharge site. Previous experiments by Berg and Lundgaard [144] have also reported that space charge effects can be significant for discharge processes involving cellulose and oil. When the applied electric field is increasing, space charge is readily deposited on the surface of the pressboard sample. However, since space charge in oil or on an insulating surface generally dissipates very slowly relative to the duration of the power cycle, then its influence will be evident in the phase-resolved pattern [146].

Figure 6.12 shows that PD was detected at the zero-crossing positions. Space charge can have the effect of decreasing the local electric field at the peaks of the power cycle, but can also create enough residual electric field at the zero-crossing positions to maintain PD activity. On completion of the experiment, visual inspection revealed evidence of tracking on the pressboard sample, confirming that PD was generated on the surface of the pressboard sample.

Figure 6.13 shows the successive pulse distributions for PD generated on the pressboard surface. During both half cycles, the majority of PD events were found to occur at successive phase positions. This might be expected for PD that is generated on a moist pressboard surface because electrons can readily be supplied from ionised water molecules.

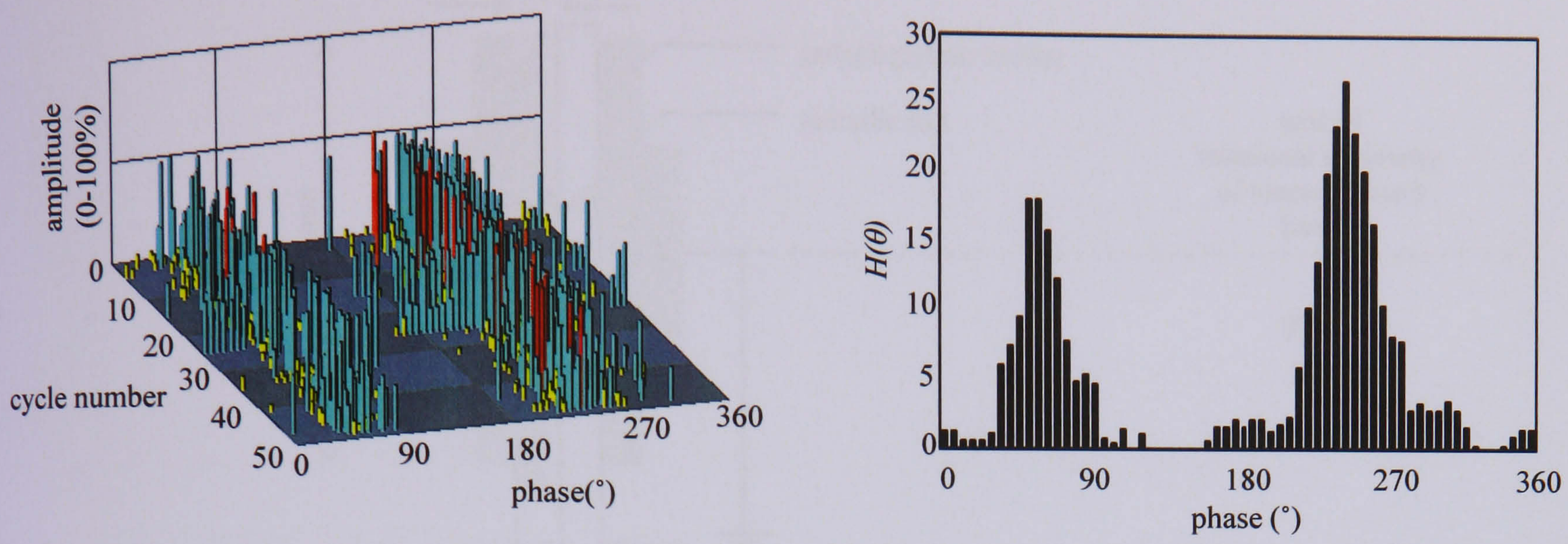

Figure 6.12 Surface discharges at 7.96 kV - (a) examples of '*snapshots*' and (b) corresponding $H_{qn}(\theta)$ distributions.

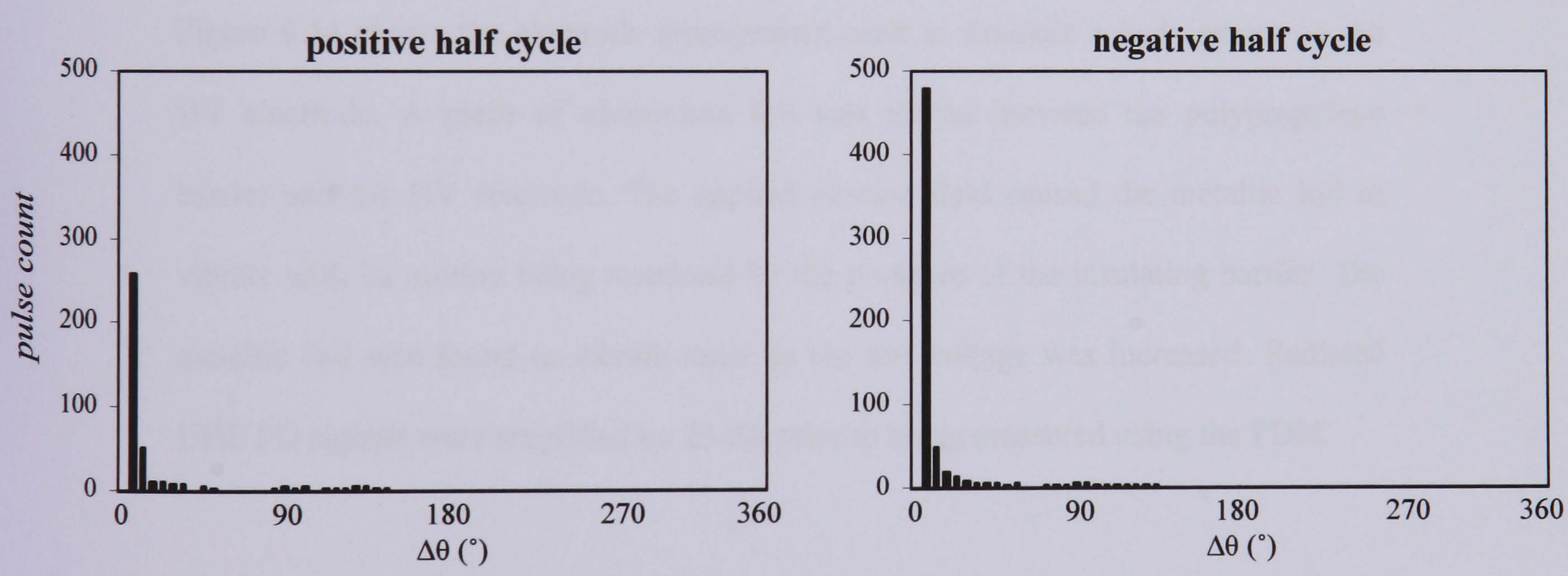

Figure 6.13 Successive pulse distributions for the surface discharges at 7.96 kV.

6.3.4 Bad contact

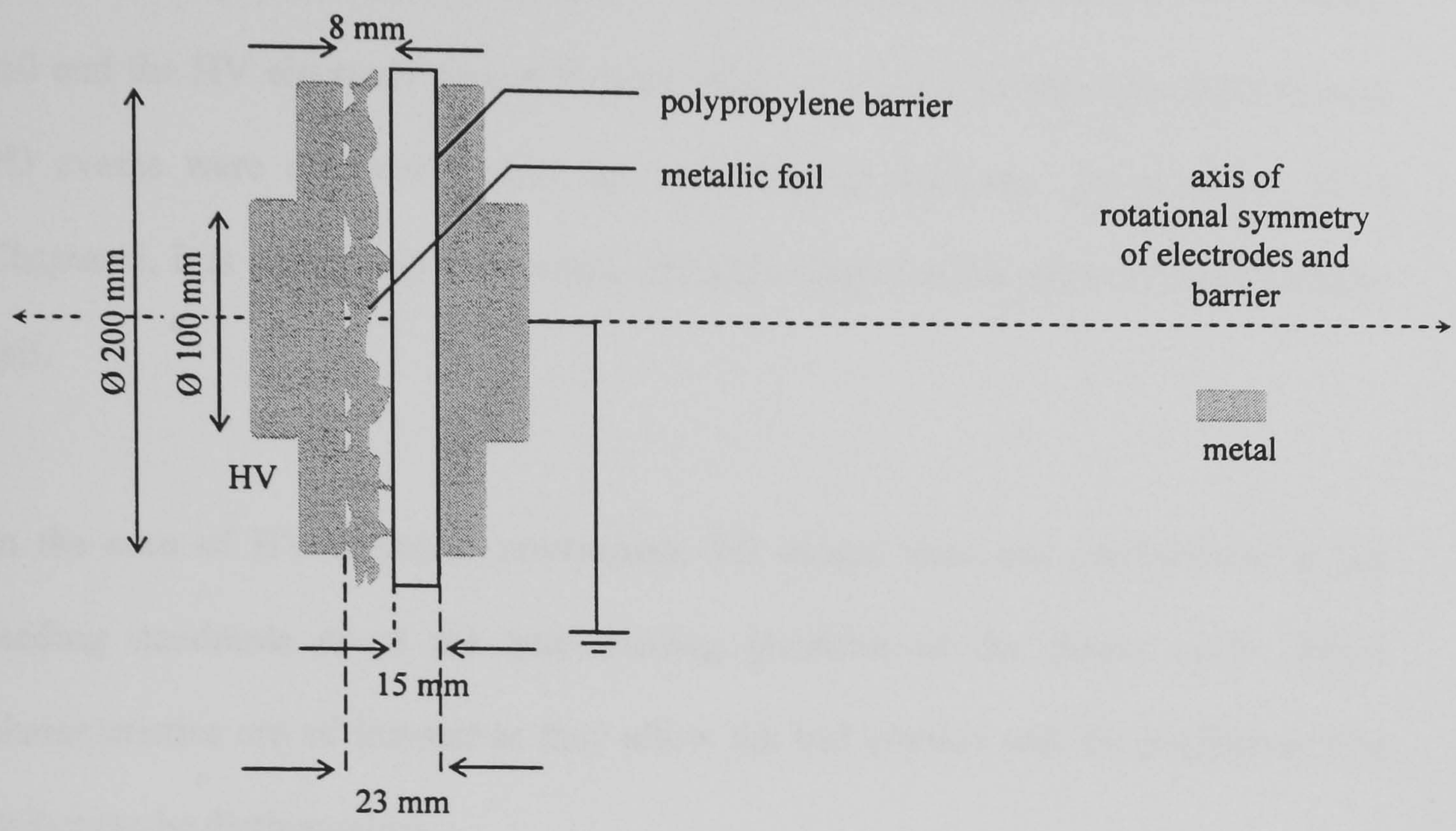

Figure 6.14 Test arrangement used to simulate a bad contact.

Figure 6.14 shows the electrode arrangement used to simulate a bad contact on the HV electrode. A piece of aluminium foil was placed between the polypropylene barrier and the HV electrode. The applied electric field caused the metallic foil to vibrate with its motion being restricted by the presence of the insulating barrier. The metallic foil was found to vibrate more as the test voltage was increased. Radiated UHF PD signals were amplified by 25 dB prior to being measured using the PDM.

Figure 6.15 shows examples of phase-resolved patterns measured for the bad contact at 1.8 kV, 2.0 kV and 2.3 kV. At each test voltage, PD pulses were generally concentrated in the first and third quadrants of the power cycle, that is, where the power cycle has changed polarity from the previous quadrant. PD pulses were also detected at the zero-crossing positions of the power cycle. This characteristic would

be anticipated for a defect that is electrically floating because the Aluminium foil can acquire a charge from the HV electrode. When the electric field between the metallic foil and the HV electrode was sufficiently high to cause a localised breakdown then PD events were detected around the zero-crossing positions. As described in m Chapter 5, it is very likely that several PD sites existed at the surface of the metallic foil.

In the case of HV electrode protrusions, PD events were not concentrated in the leading quadrants or at the zero-crossing positions of the power cycle. These characteristics are of interest as they allow the bad contact and the protrusion type defects to be distinguished.

Figure 6.15 also shows the corresponding $H(\theta)$ distributions at each test voltage. These distributions reveal that PD activity decreased towards the peaks of the power cycle, and again this can be explained in terms of the injection of space charge into the liquid dielectric as successive PD events occur when the applied field was increasing [82]. The asymmetry of PD activity in the positive and negative half cycles can be attributed to geometry of the electrode system.

Figure 6.16 shows the successive pulse distributions for the bad contact at 1.8 kV, 2.0 kV and 2.3. kV. At 1.8 kV, a difference in phase angle of $\Delta\theta \sim 45°$ is noted for the majority of PD pulses that were measured during the positive half cycle. This is also evident from the '*snapshot*' of Figure 6.15(a). It is suggested that PD events caused the injection of a considerable amount of charge so that subsequent PD events were only measured when there was a significant change in the value of the externally

applied electric field. During the negative half cycle, the majority of PD events were found to occur on adjacent phase positions. This might be expected because electrons can readily supplied from the defect site(s) as a result of field enhancement.

At 2.0 kV and 2.3 kV, the majority of PD events measured during the positive half cycle were found to occur on successive phase positions. Experimental observations report that the connection between the metallic foil and the HV electrode was poorer at the higher test voltages. It is likely that several PD sites existed at the surface of the metallic foil and this caused UHF PD signals to be superimposed on the phase resolved measurements. Under such conditions, the interpretation of phase-resolved patterns can become complex.

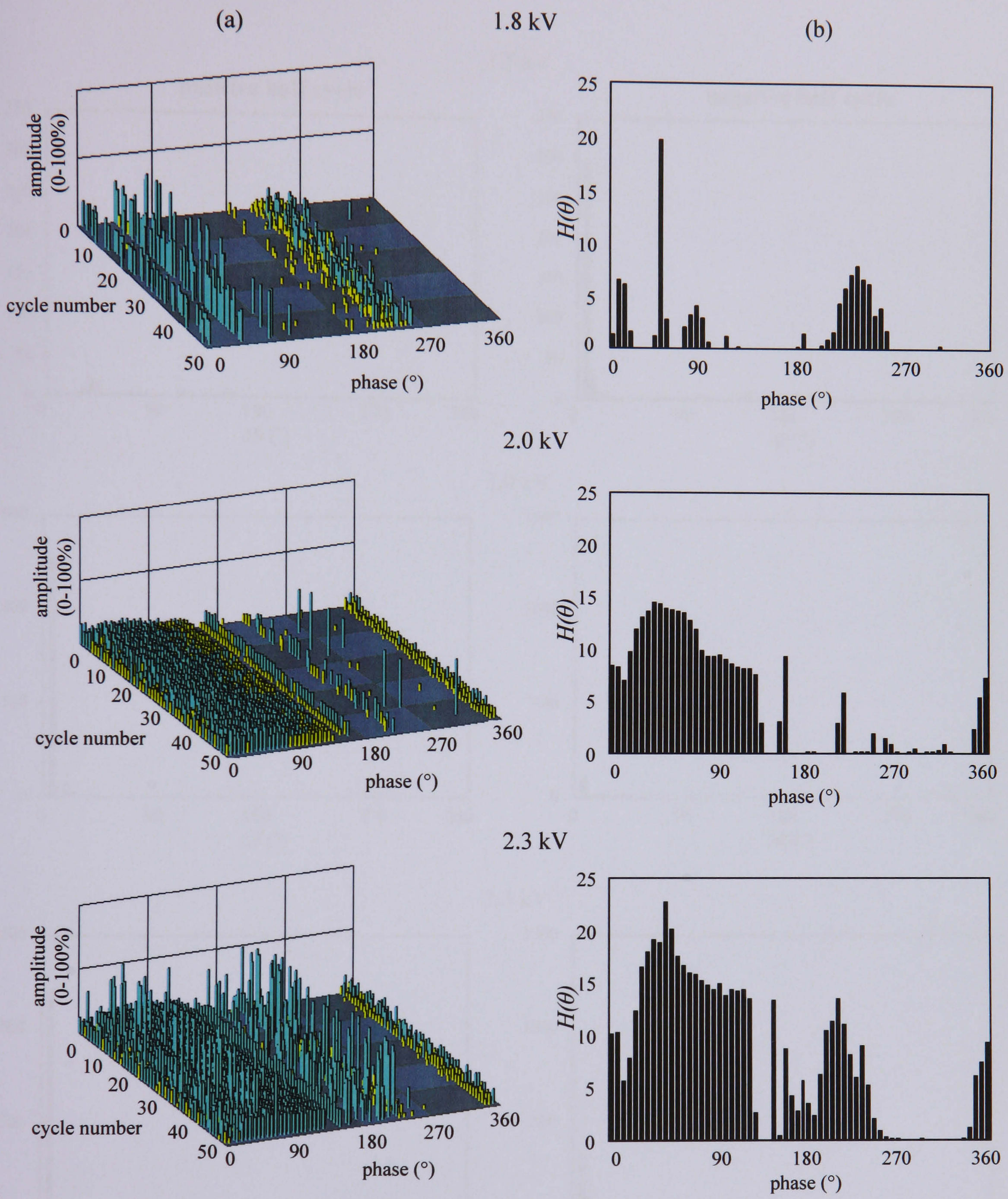

Figure 6.15 Bad contact at 1.8 kV, 2.0 kV and 2.3 kV,
(a) examples of '*snapshots*' and (b) corresponding *H(θ)* distributions.

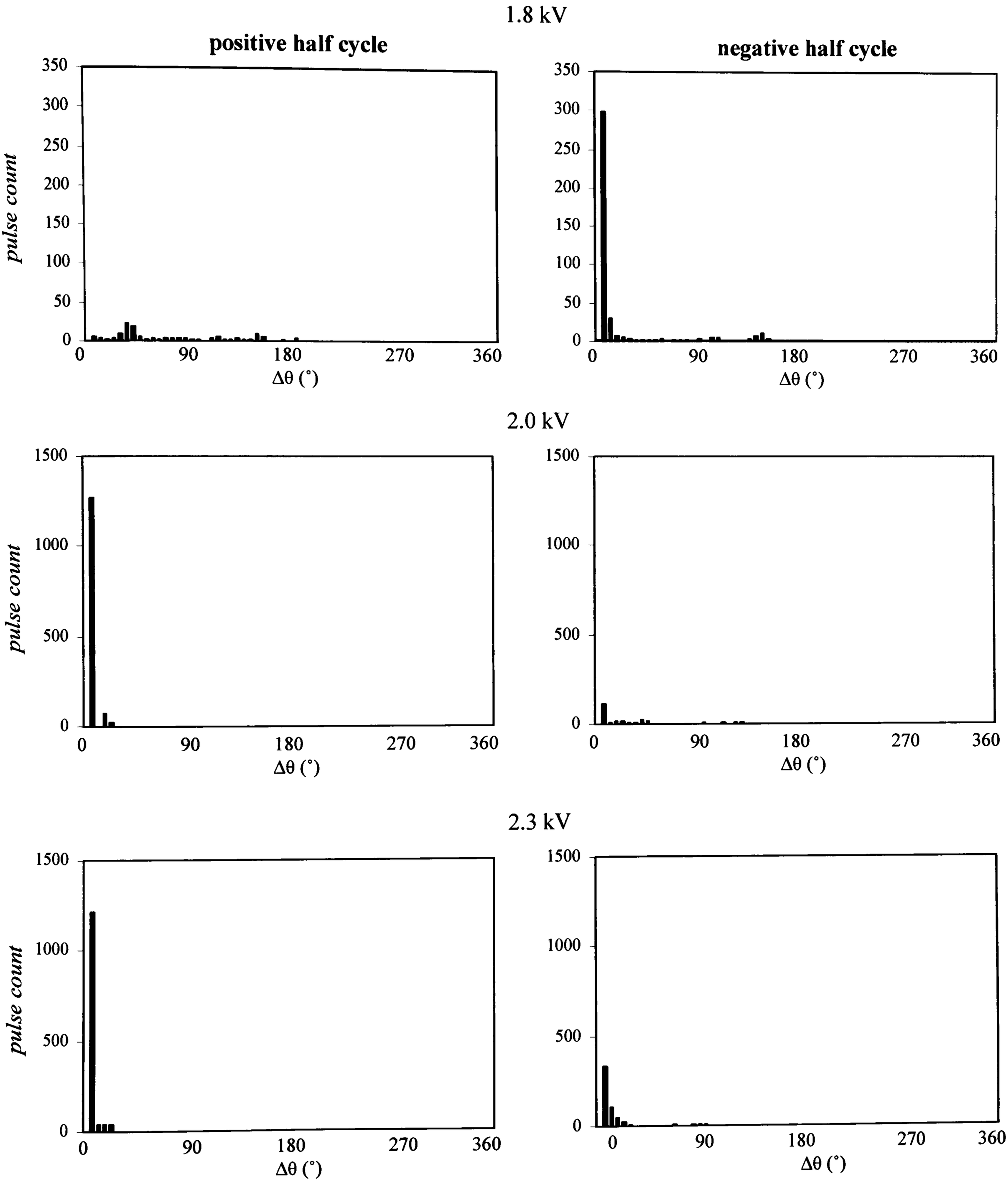

Figure 6.16 Successive pulse distributions for the bad contacts at 1.8 kV, 2.0 kV and 2.3 kV.

6.3.5 Floating component

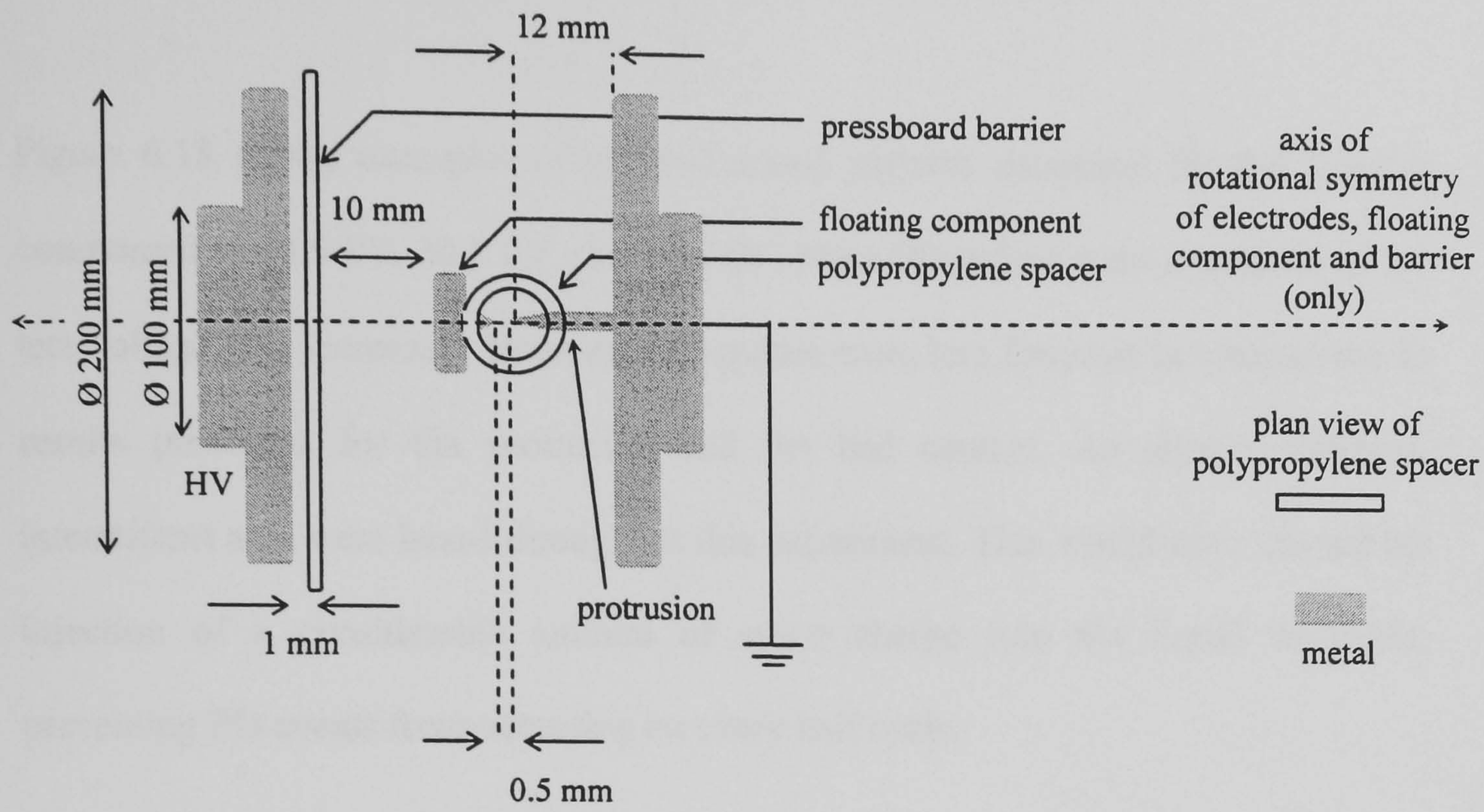

Figure 6.17 Test arrangement used to simulate a floating component.

Figure 6.17 shows the electrode arrangement used to simulate the floating component type defect. The floating component was suspended between the HV electrode and an earthed electrode protrusion using a polypropylene spacer. The floating component consisted of a flat metallic electrode (to provide capacitive coupling with the HV electrode) and a protrusion. The length and tip radius of the earthed electrode protrusion were 12 mm and ~ 35 μm respectively. The length and tip radius of the suspended protrusion were 8 mm and ~ 35 μm respectively. The distance between the suspended protrusion and the earthed electrode protrusion was set to 0.5 mm.

During testing, intermittent arcs were heard during the experiment and the amplitude of measured PD events was high. UHF signals were therefore attenuated prior to being measured using the PDM. At 20.5 kV, radiated UHF PD signals were

attenuated by 20 dB. At 30.8 kV and 34.3 kV, they were attenuated by 60 dB. Care must be taken when comparing measurements at each test voltage.

Figure 6.18 shows examples of phase-resolved patterns measured for the floating component at 20.5 kV, 30.8 kV and 34.3 kV. More PD pulses were measured as the test voltage was increased. However, PD pulses were less frequent in comparison to results presented for the protrusion and the bad contact. As already outlined, intermittent arcs were heard throughout this experiment. This would have caused the injection of a considerable amount of space charge into the liquid dielectric, preventing PD events from occurring on every half cycle.

The $H(\theta)$ distributions of Figure 6.18 show that PD events were generally measured during the leading quadrants of both half cycles. At 30.8 kV and 34.3 kV, both distributions reveal a reasonable amount of 180° symmetry, implying that the discharge mechanism was not dependent on the orientation of the electric field. This suggests that due to capacitive coupling between the floating component and the HV electrode the system behaved like a point-point gap. This characteristic reflects the symmetrical nature of the electrode system and allows the floating component to be classified from the other defects that have previously been described.

At 30.8 kV and 34.3 kV, PD was detected around the zero-crossing positions. This characteristic would be anticipated for a defect that is electrically floating and arises because the floating component can acquire charge so that the field in the gap is not dependent solely on the instantaneous applied voltage.

As shown in Figure 6.17, the distance of the polypropylene spacer from the tip of the floating component and the protrusion is very small. When the electric field in this region is high it is likely that discharges might also be generated at the surface of the insulating spacer. Inspection of the phase resolved patterns shown in Figure 6.16 shows that PD pulses were detected prior to the peaks of the power cycle and at the zero-crossing positions. It is interesting to note that these characteristics are similar to those relating to the surface discharge experiment (Section 6.3.3) and so it is likely that discharges were generated at the surface of the polypropylene spacer.

Figure 6.18 shows the successive pulse distributions for the floating component at various test voltages. At 20.5 kV and 30.8 kV, a large variation is noted in terms of the difference in phase angle between PD pulses that were measured during both half cycles. At 20.5 kV, the difference in phase angle between all pulses measured during the positive half cycle was greater than 360˚. Therefore, no PD pulses are shown on the pulse-sequence analysis plot. These findings might be attributed to the injection of space charge into the liquid dielectric when arcing occurs.

At 34.3 kV, a smaller variation is noted in terms of the difference in phase angle between PD pulses occurring on both half cycles. This might be because there is a limit to the space charge created by a PD and when the voltage is increased the effect of the external field becomes more predominant.

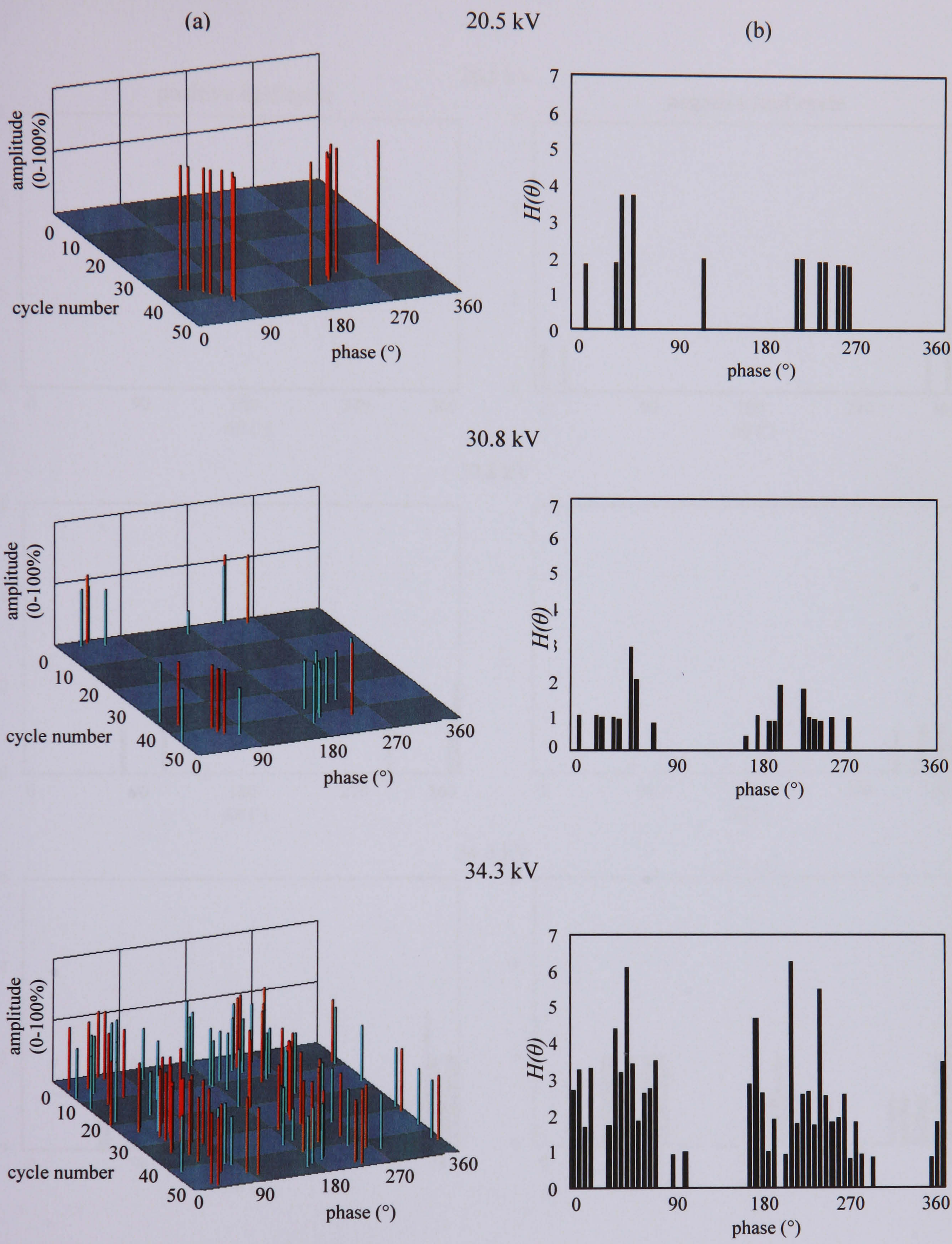

Figure 6.18 Floating component at 20.5 kV, 30.8 kV and 34.3 kV (a) examples of '*snapshots*' and (b) corresponding *H(θ)* distributions.

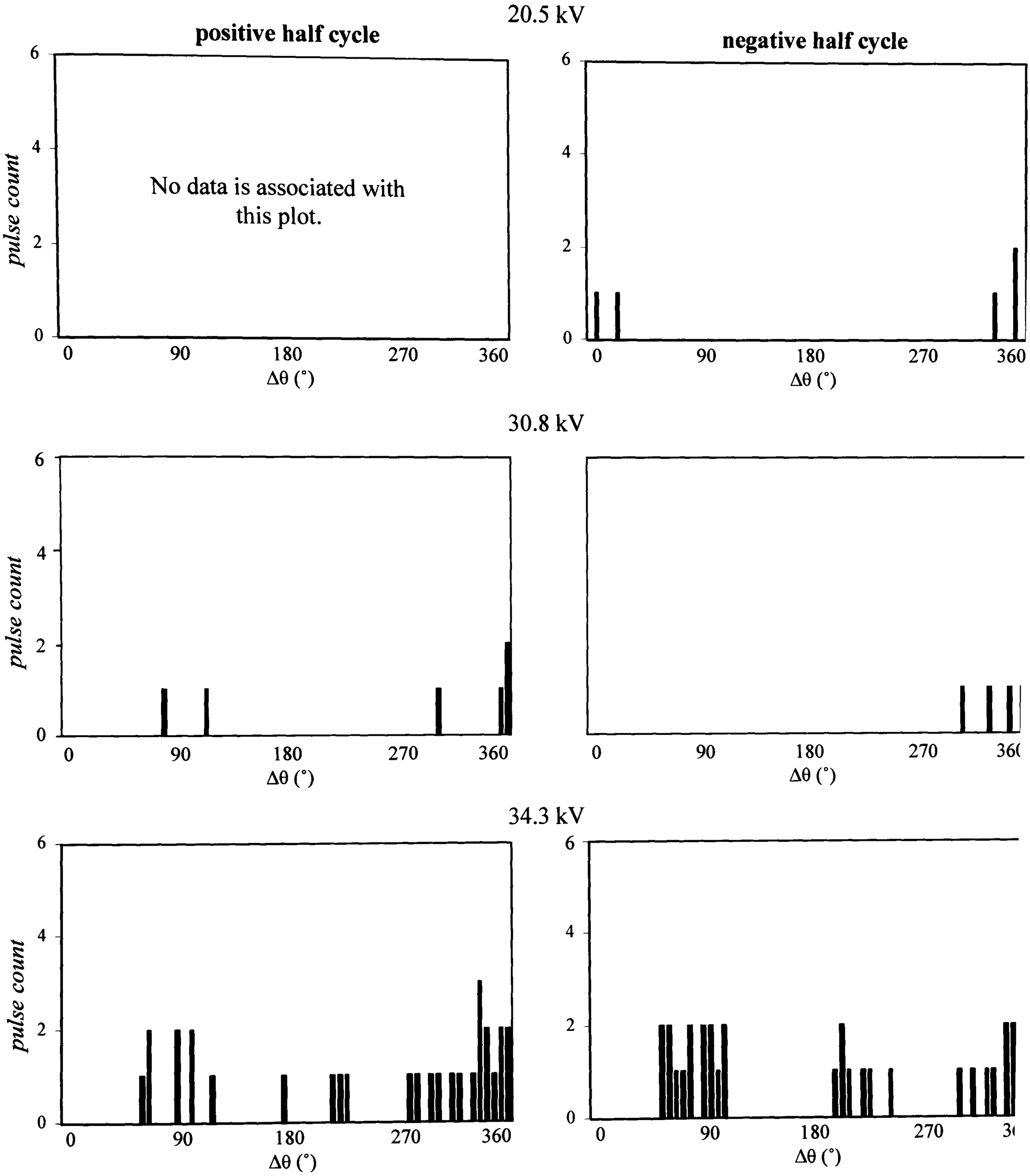

Figure 6.19 Successive pulse distributions for the floating component at 20.5 kV, 30.8 kV and 34.3 kV.

6.3.6 Suspended particle

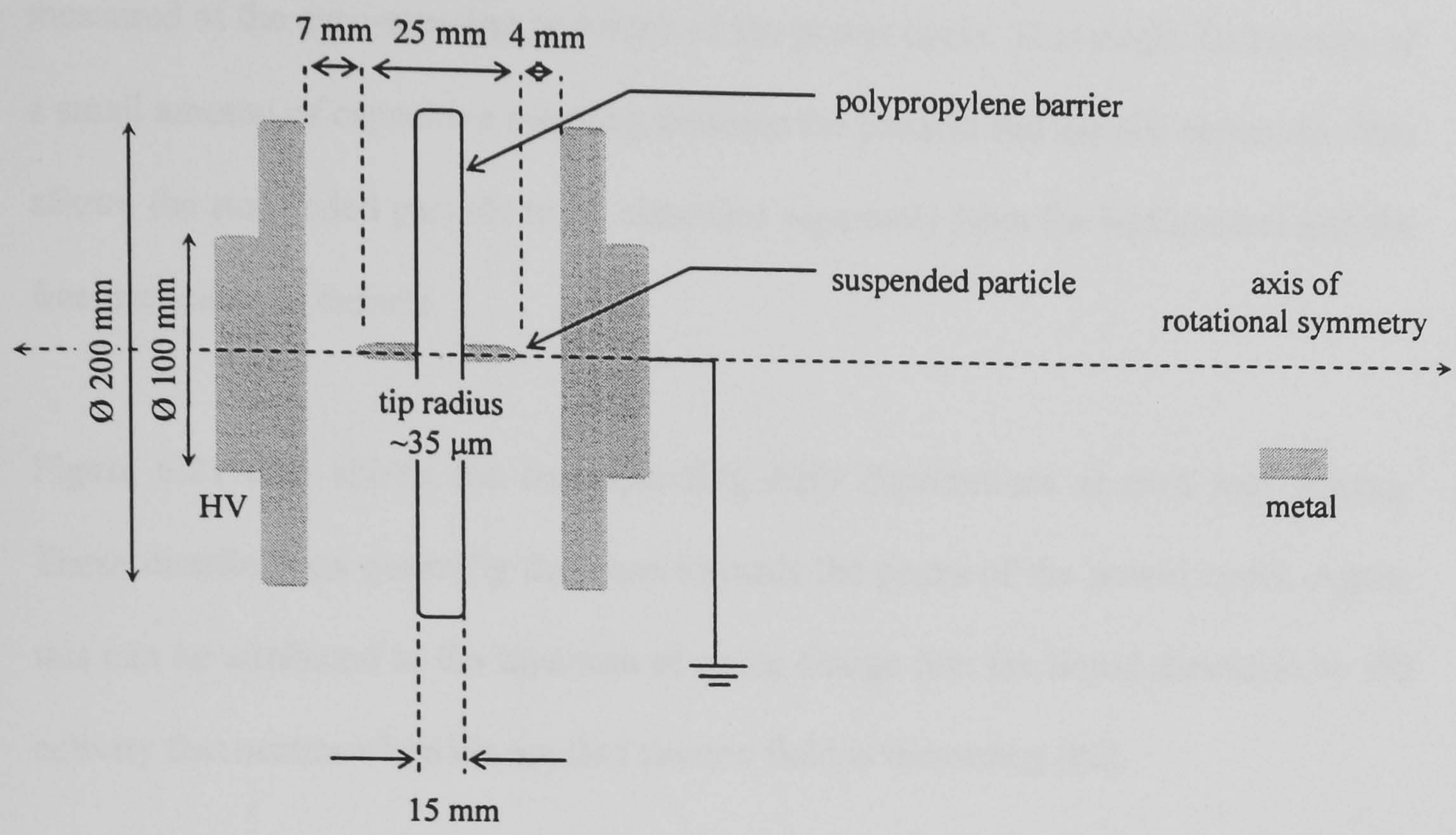

Figure 6.20 Test arrangement used to simulate a suspended particle.

Figure 6.20 shows the electrode arrangement termed a 'suspended particle' defect. A brass rod of diameter 3 mm was suspended between the HV and earthed electrodes using a polypropylene barrier, the length of the rod was 35 mm and the radii of the tips were ~ 35 µm. At 13.2 kV and 15.9 kV, radiated UHF PD signals were amplified by 25 dB prior to being measured using the PDM. At 18.1 kV, radiated UHF PD signals were attenuated by 20 dB as their amplitudes were much greater. As a result, care must be taken when comparing measurements at each voltage.

Figure 6.21 shows some examples of phase-resolved patterns at different voltages. The distributions reveal a reasonable 180° separation between pulses measured during both half cycles. This characteristic reflects the symmetrical nature of the electrode system and allows the suspended particle to be differentiated from the HV electrode protrusions.

Although the suspended particle is at a floating potential, very little PD activity was measured at the zero-crossing positions of the power cycle. This might be because of a small amount of capacitive coupling between the particle and the HV electrode. This allows the suspended particle to be classified separately from the bad contact and the free particle type defects.

Figure 6.21 also shows the corresponding $H(\theta)$ distributions at each test voltage. These distributions generally decrease towards the peaks of the power cycle. Again, this can be attributed to the injection of space charge into the liquid dielectric by PD activity that occurs when the applied electric field is increasing [82].

Figure 6.22 shows the successive pulse distributions. At 13.2 kV, the distributions show a much higher incidence of pulses on successive phase positions than at the higher test voltages. The similar pulse-sequence distributions during both half cycles might be expected because of the symmetrical nature of the defect.

At 15.9 kV, a broad variation can be seen in the difference in phase angle between successive PD pulses occurring on both half cycles. It is suggested this was caused by space charge trapped in the region surrounding the tips of the suspended particle. At 18.1 kV, a broad variation can also be observed in the phase angle between successive PD events occurring on both half cycles. This finding can be attributed to the larger PD pulses that appear, superimposed on the more regular pattern of PD activity.

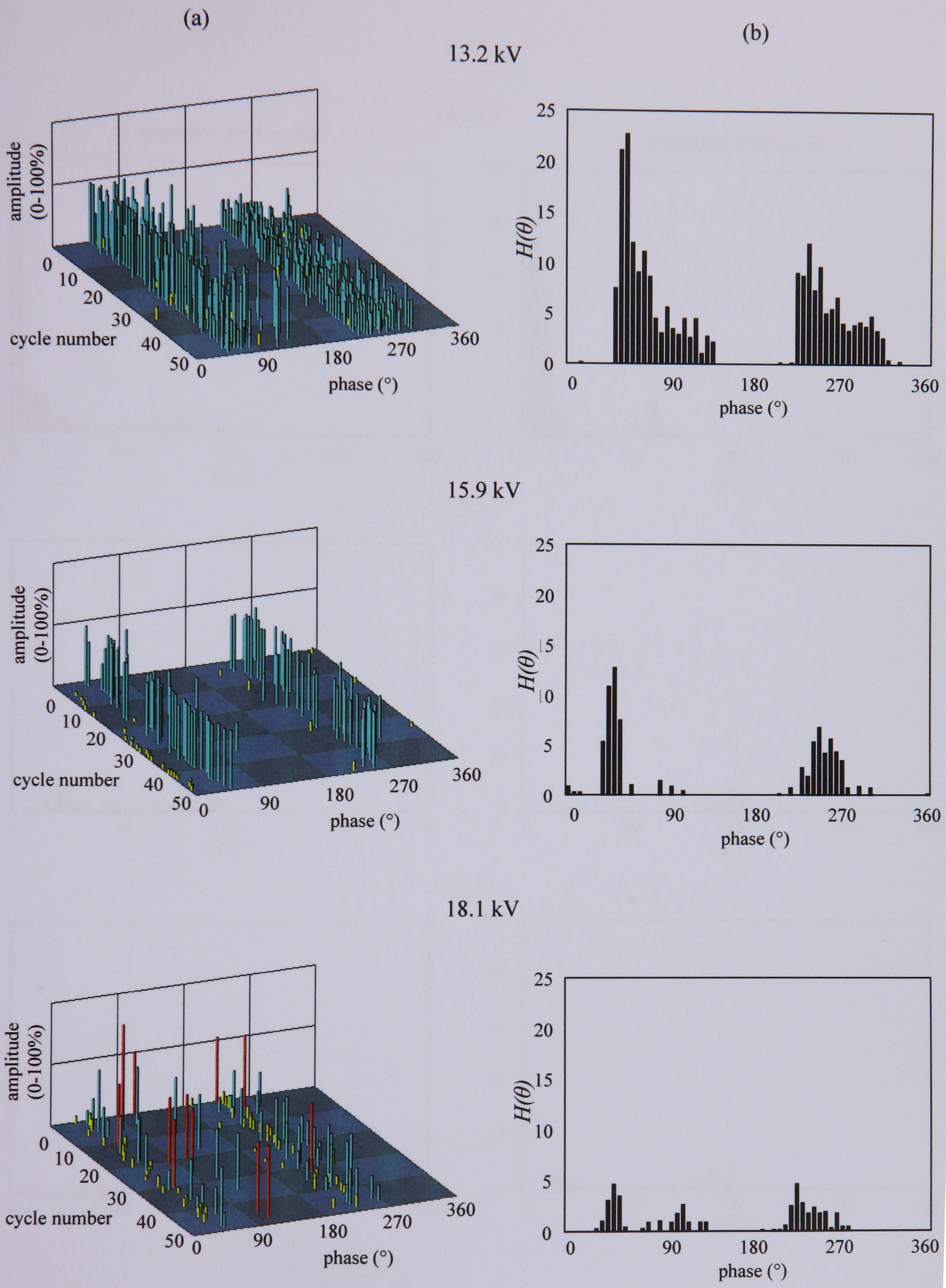

Figure 6.21 Suspended particle at 13.2 kV, 15.9 kV and 18.1 kV
(a) examples of '*snapshots*' and (b) corresponding $H_{qn}(\theta)$ distributions.

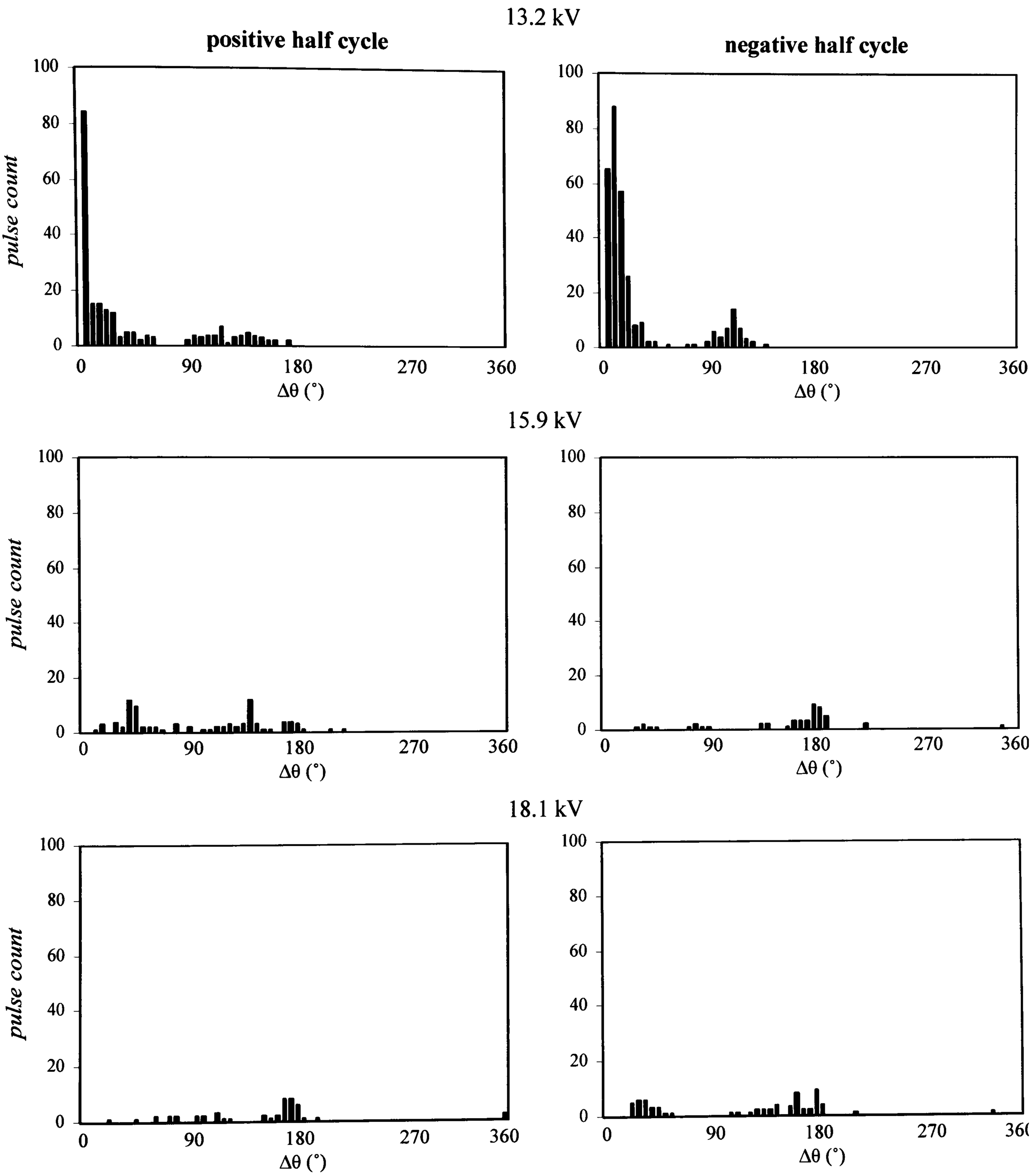

Figure 6.22 Successive pulse distributions for the suspended particles at 13.2 kV, 15.9 kV and 18.1 kV

6.3.7 Free metallic particle

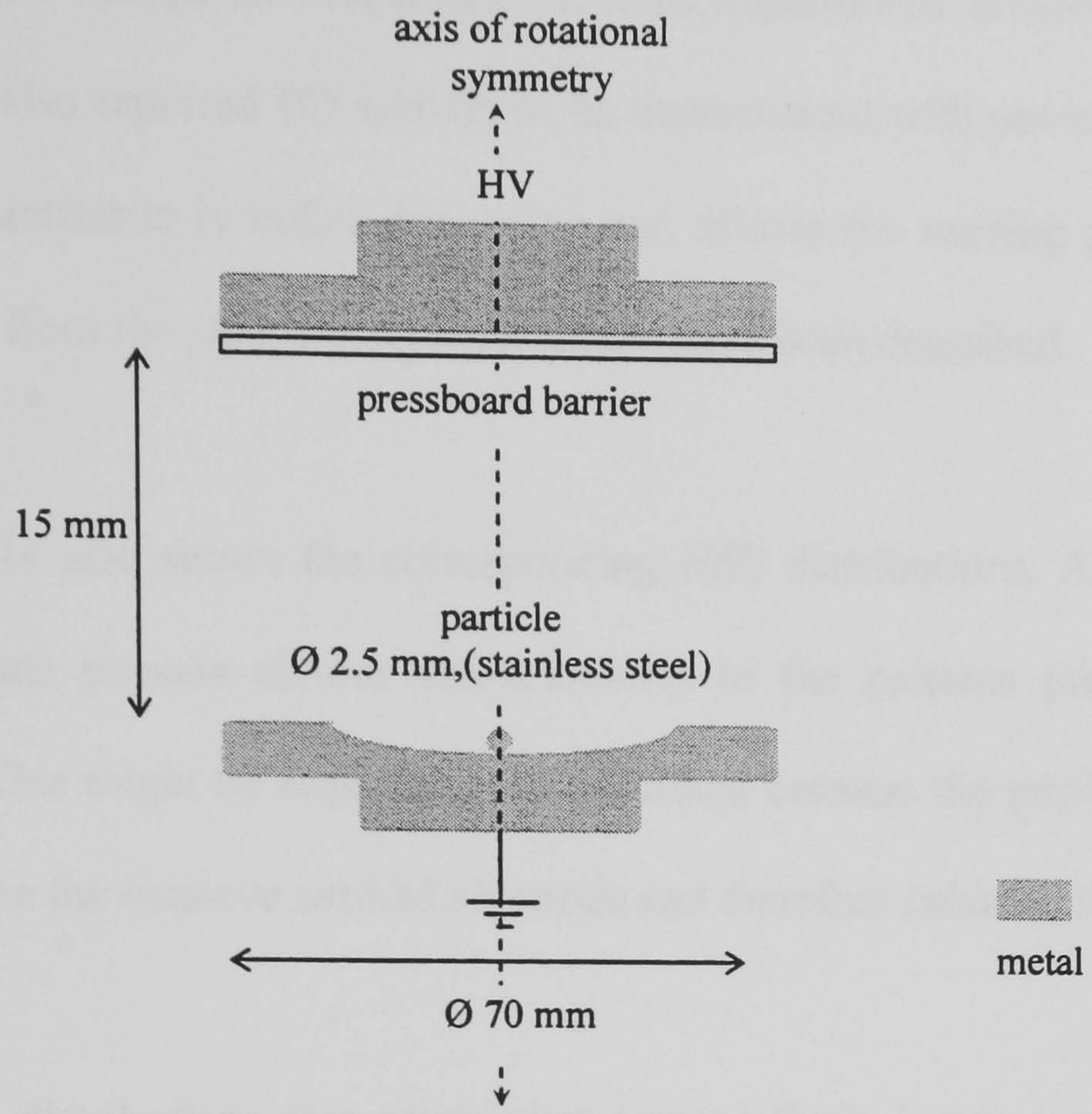

Figure 6.23 Test arrangement used to simulate a free particle.

Figure 6.23 shows the electrode arrangement used to support a free particle defect. A stainless steel particle of 2.5 mm diameter was placed on the concave earthed electrode prior to filling the test cell with oil. When the electrostatic force exceeded the gravitational force the particle started to move. At 25.2 kV, the particle was observed to '*shuffle*' on the earthed electrode. At 33.4 kV and 35.9 kV, the particle was observed to lift and fall at the centre of the concave earthed electrode. UHF PD signals were amplified by 25 dB prior to being measured using the PDM.

Figure 6.24 shows examples of phase-resolved patterns measured for the free particle. These plots reveal that PD activity changed in character when the test voltage was increased above 25.2 kV. At 25.2 kV, when the particle was observed to '*shuffle*', PD events were well correlated with the power cycle.

At 33.4 kV and 35.9 kV, the particle was observed to lift and fall and PD events were uncorrelated with power frequency. Previous experiments involving a free particle in SF_6 have also reported PD activity to be uncorrelated with power frequency [18,70]. This characteristic is rather distinctive and allows the moving particle to be easily classified from the other defect sources that have been described.

Figure 6.24 also shows the corresponding *H(θ)* distributions. At 25.2 kV, the *H(θ)* distributions possess similar characteristics to the patterns presented for the bad contact. This might be expected at this voltage because the particle was observed to '*shuffle*' on the concave earthed electrode and therefore behaved as a bad contact.

The *H(θ)* distributions also reveal that comparatively lower amounts of PD activity were detected at the higher test voltages. This arises because PD pulses were generated less regularly, and this is an example of where *H(θ)* distributions must be interpreted with care. Previous experiments involving particles in SF_6 have shown that longer periods between pulses can indicate that the particle is in flight for a longer time and may reach a location where breakdown might occur [70].

Figure 6.25 shows the successive pulse distributions. These plots show that the PD changed in character as the test voltage was increased above 25.2 kV. At 25.2 kV, similar pulse distributions were found during both half cycles and the majority of PD pulses were found to occur on successive phase positions during both half cycles. In addition, PD pulses are also noted in the region $90^\circ < \Delta\theta < 180^\circ$. These are representative of successive PD pulses that occurred on adjacent half cycles.

The broad scatter in phase difference between successive PD events at the higher test voltages should be noted. This might be expected because the 'random' motion of the free metallic particle resulted in PD pulses not being correlated with the power cycle. Again, this feature is rather distinctive and allows the moving particle to be easily classified.

25.2 kV

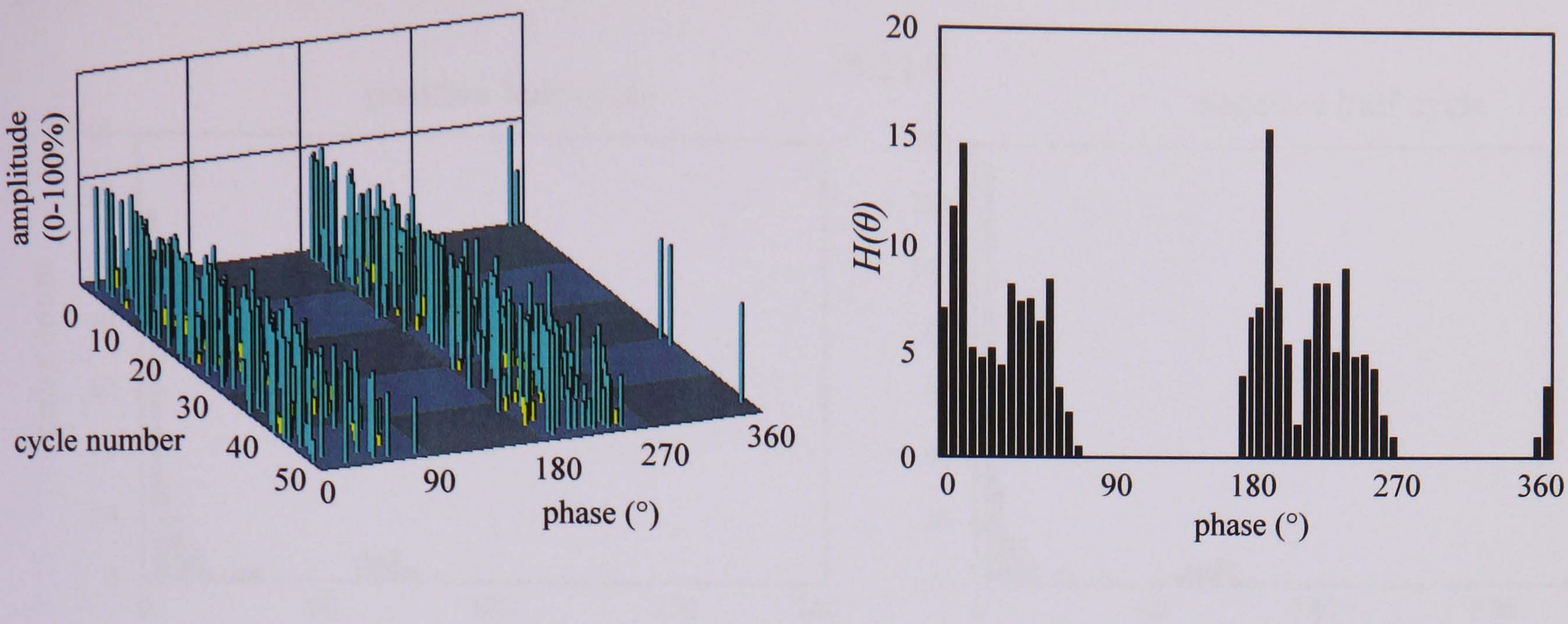

33.4 kV

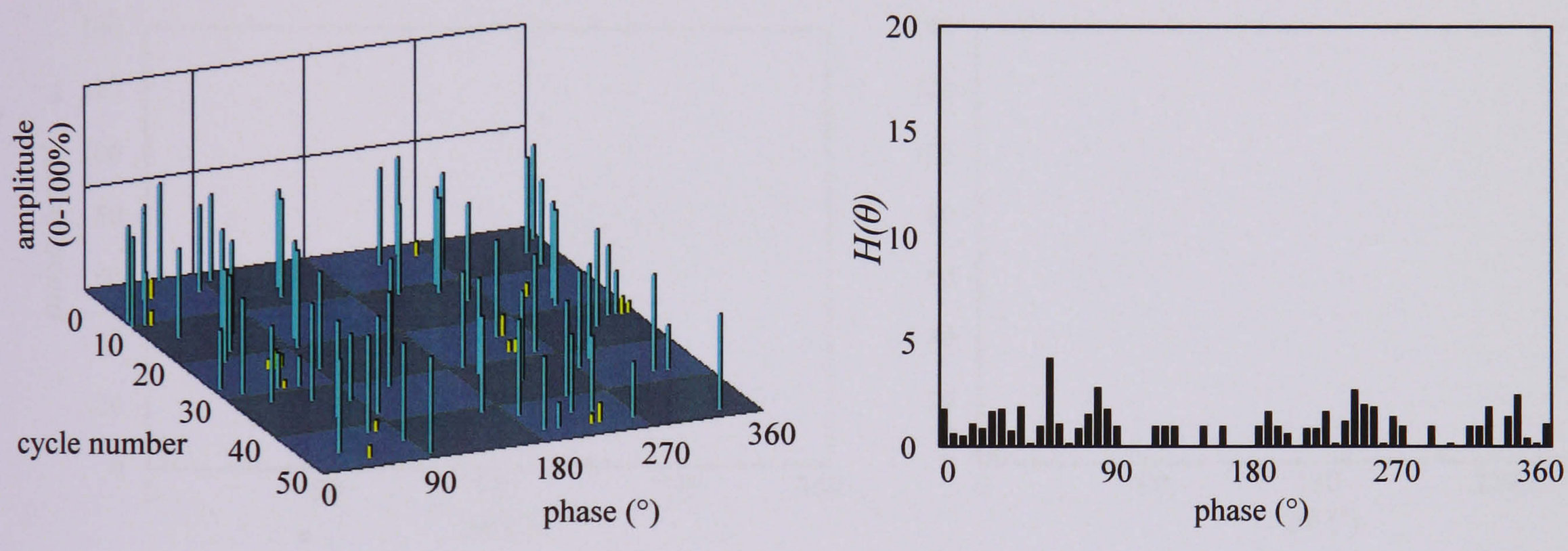

35.9 kV

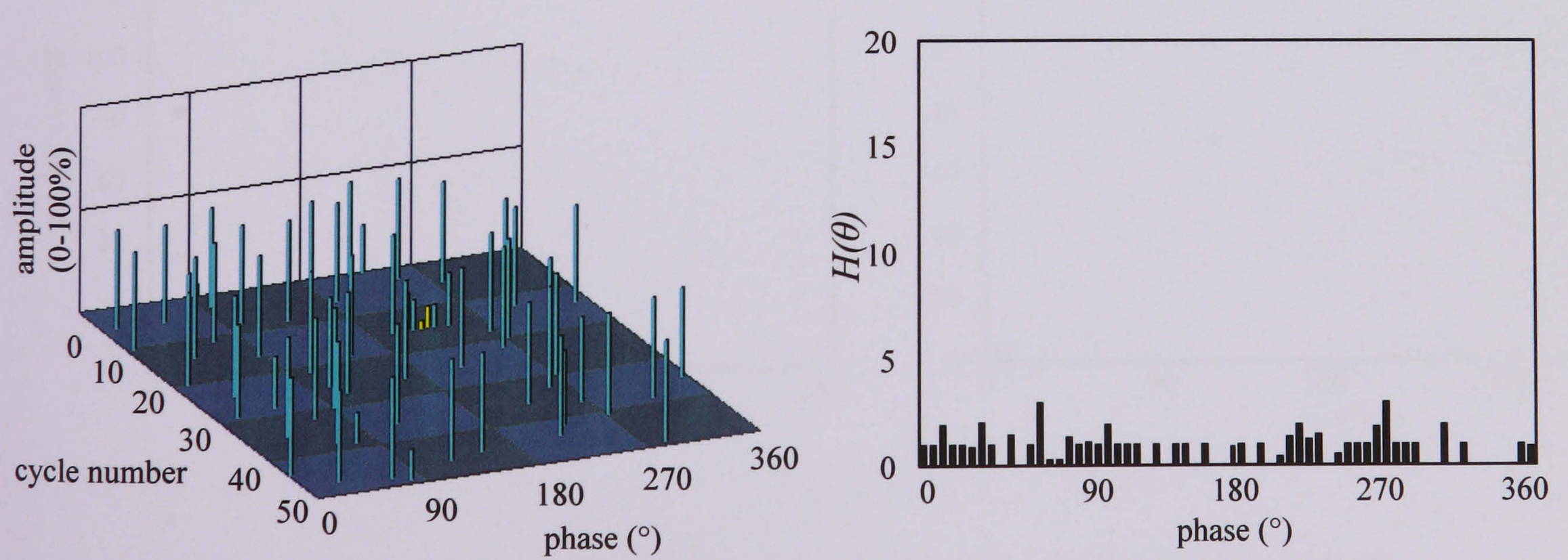

Figure 6.24 Free particle at 25.2 kV, 33.4 kV and 35.9 kV (a) examples of '*snapshots*' and (b) corresponding *H(θ)* distributions.

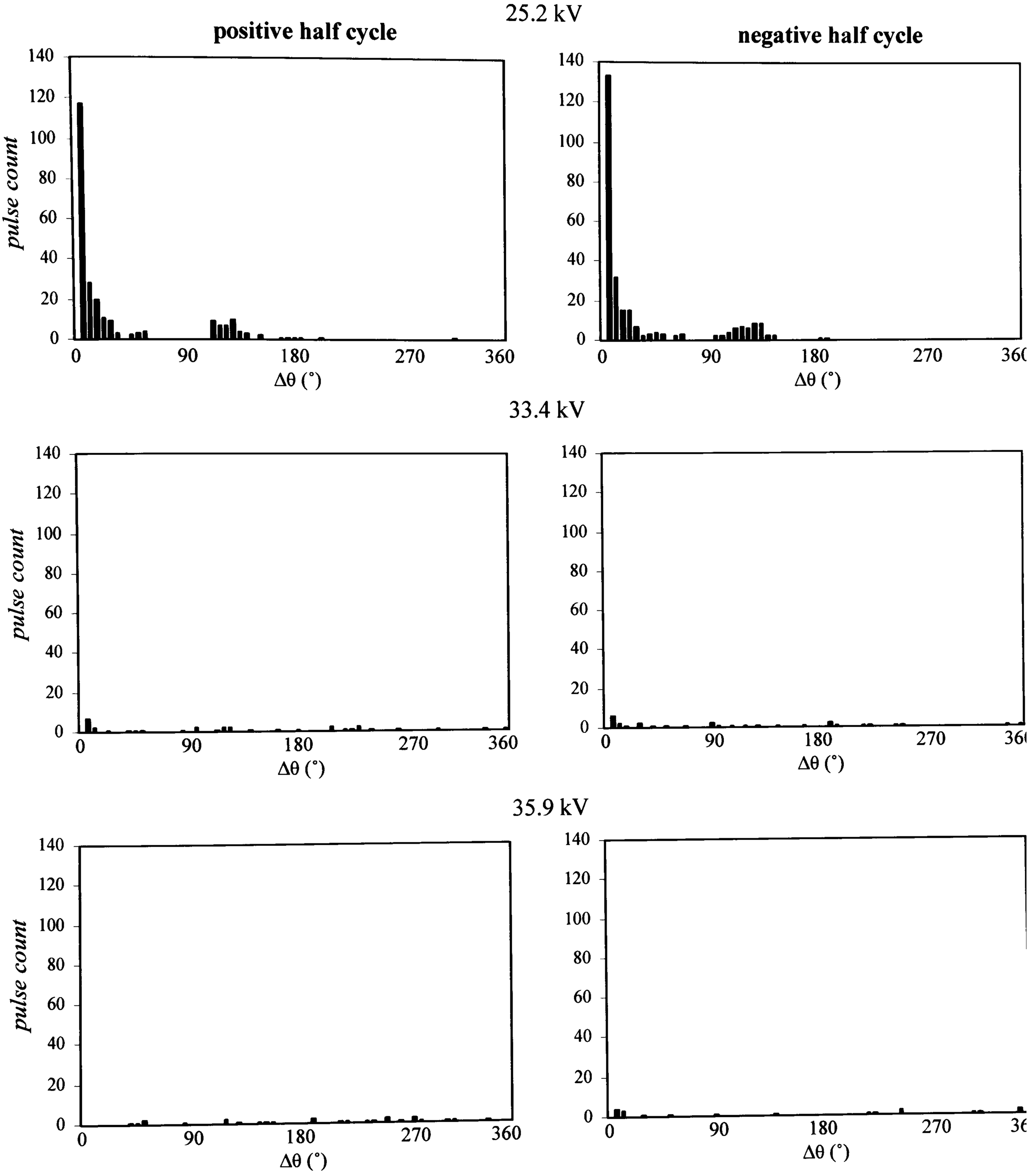

Figure 6.25 Successive pulse distributions for the free particles at 25.2 kV, 33.4 kV and 35.9 kV.

6.3.8 Arcing

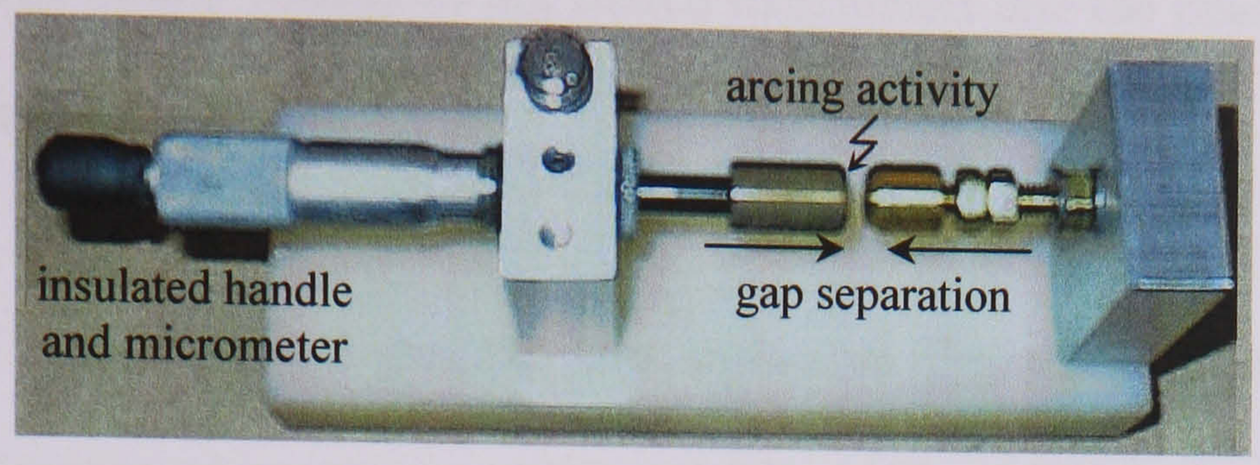

Figure 6.26 Test apparatus for simulating arcing across a current-carrying gap.

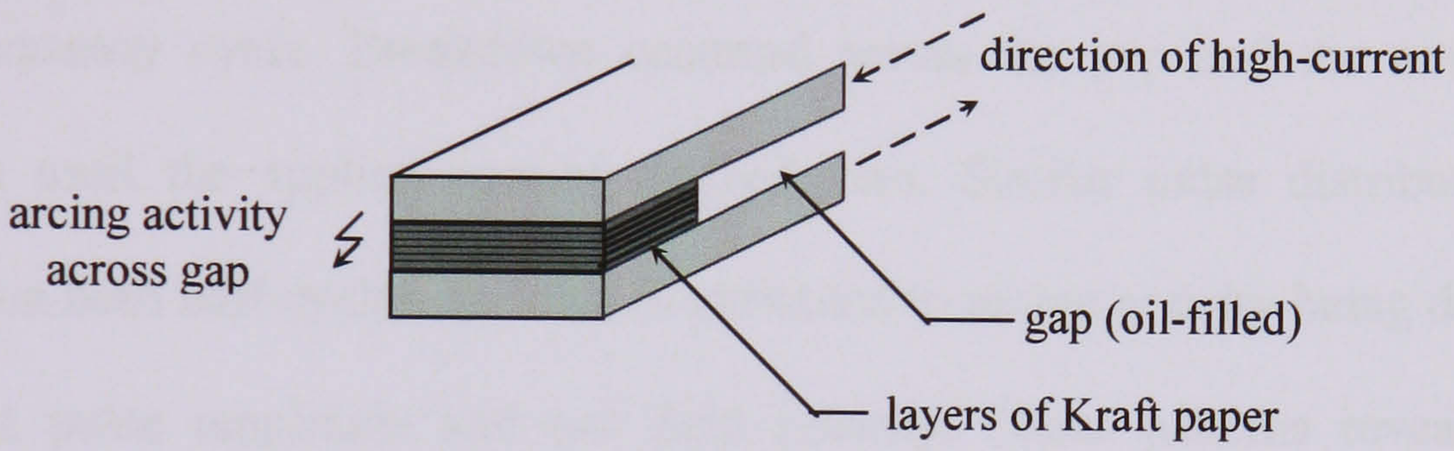

Figure 6.27 Electrode configuration for simulating arcing activity between two adjacent turns on a winding.

Figure 6.26 shows the test apparatus that was used to simulate high-current arcing activity such as that which might take place between two tap changer contacts. The brass electrodes were initially placed in contact and a current of 60 A was passed through them. The gap was then slowly increased until an arc was generated in the oil between both electrodes.

The experimental arrangement used to simulate arcing between two adjacent turns on a winding is shown in Figure 6.27. Initially, both copper strips were placed together and a current of 400 A was passed through them. An arc was generated in the oil when a small gap was created between the copper strips.

In both experimental arrangements, a transformer capable of delivering a high current (Claude & Lyons) was used. This current was measured using a Fluke current transformer. The output voltage of the source transformer and the phase reference of the PDM were synchronized.

Examples of phase-resolved patterns are shown in Figures 6.28 and 6.29. The amplitudes of measured events were high and this can be attributed to the intense arcs that were generated. Inspection of the $H(\theta)$ distributions reveals that PD events were principally measured during the lagging quadrants, that is, following the peaks of the power cycle. These plots demonstrate that inception occurred at the peaks of the power frequency cycle. Breakdown occurred across the gap and the arc did not extinguish until the applied current reached zero. Similar pulse distributions are observed on both half cycles, and this is attributed to arcing activity being dependent on current pulse amplitude and not field polarity. These patterns reveal similar characteristics to those relating to a faulty joint in a GIS [98].

Figure 6.30 and Figure 6.31 show the successive pulse distributions for both of the arcing sources that have been outlined. Similar distributions were found for each defect source and pulse-sequence distributions were also similar during both half cycles. This is because arcing activity was dependent on current amplitude and not on field polarity. Furthermore, the symmetry of the electrode system meant that the arcing mechanism was independent of polarity. For each of the plots shown, the majority of pulses were measured on successive phase positions from inception of the arcing until its extinction.

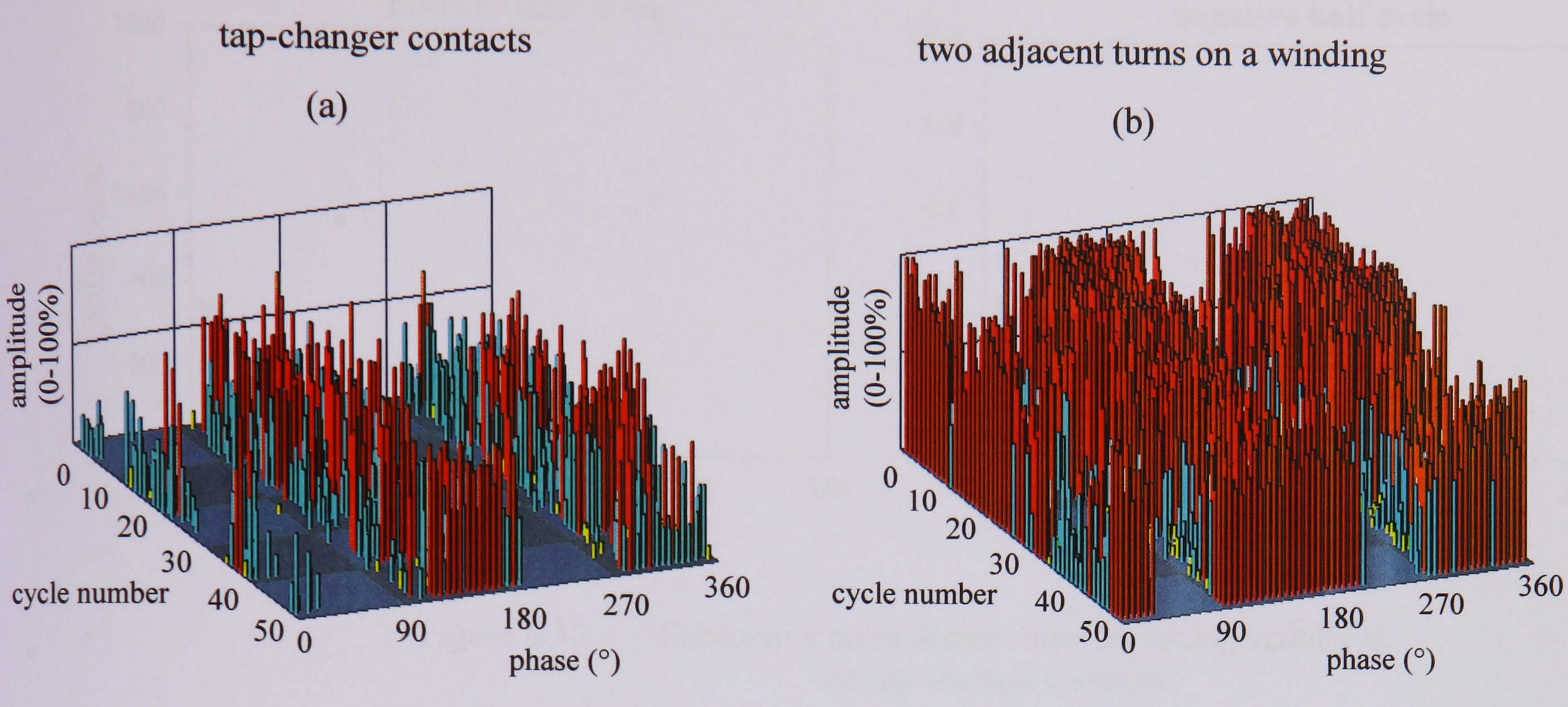

Figure 6.28 Phase-resolved patterns corresponding to arcing at
(a) tap changer contacts and
(b) two adjacent turns on a winding.

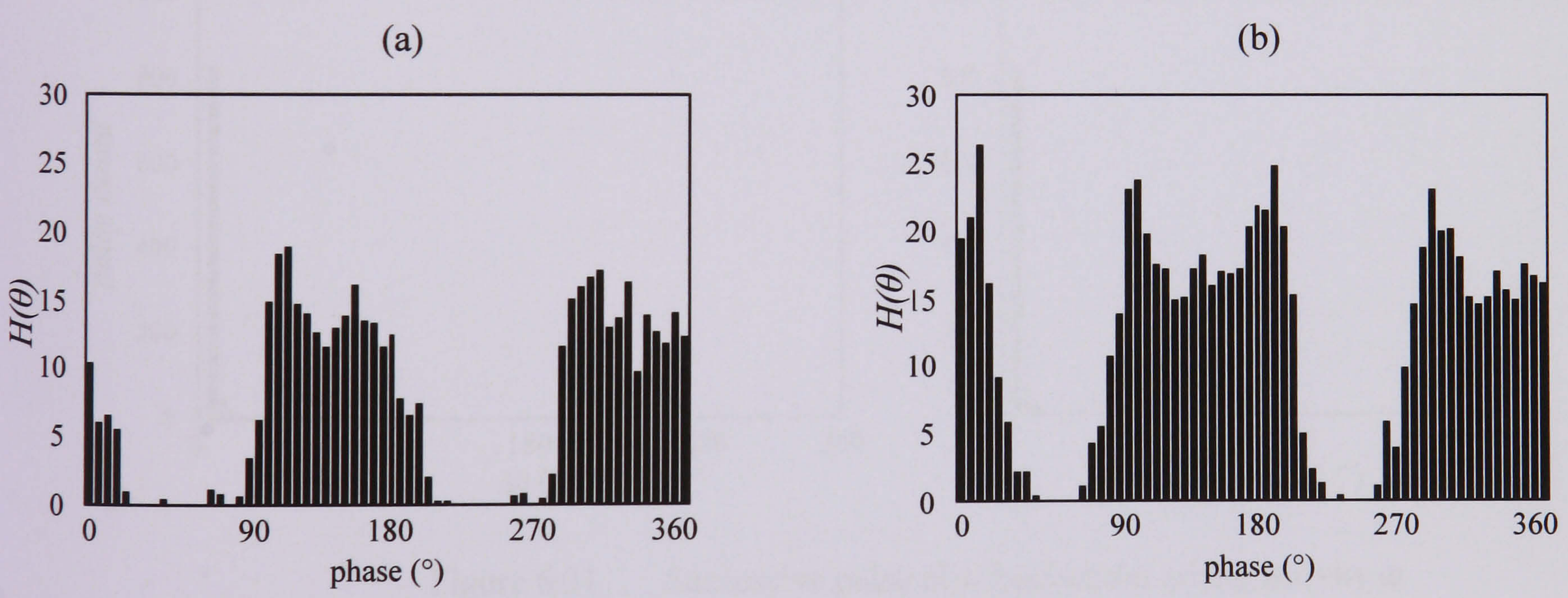

Figure 6.29 *H(θ)* distributions corresponding to arcing at
(a) tap changer contacts and
(b) two adjacent turns on a winding.

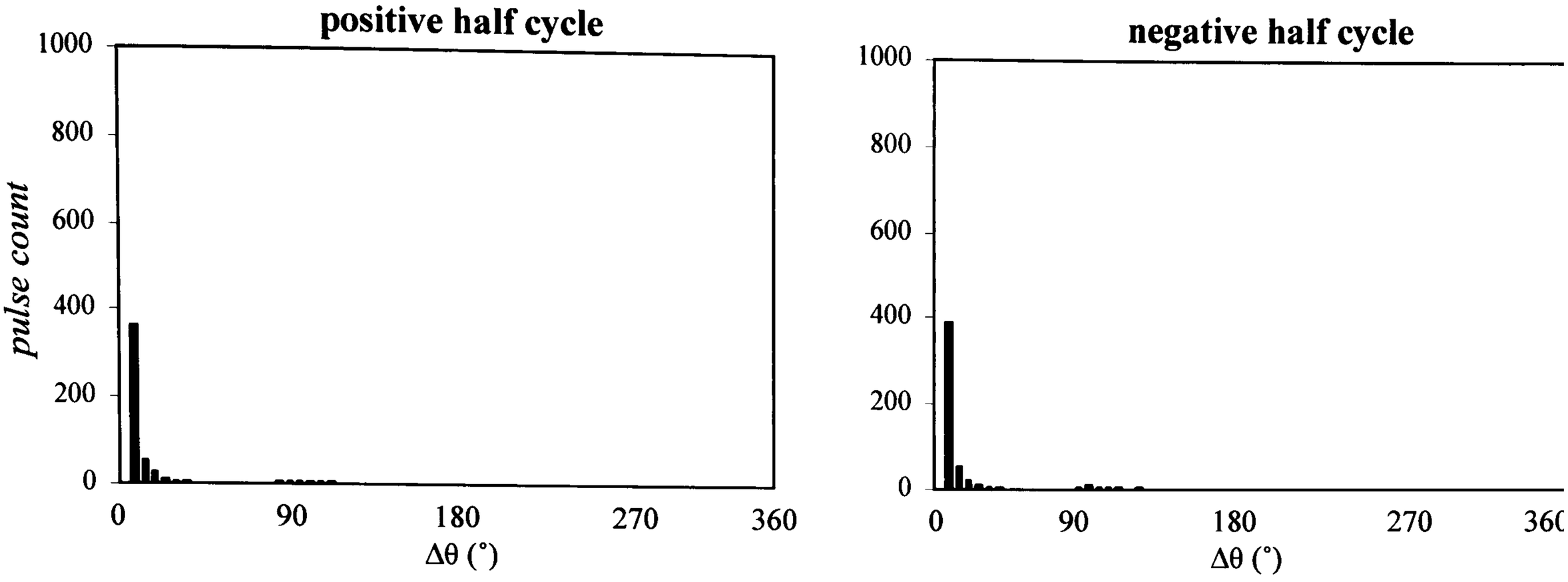

Figure 6.30 Successive pulse distributions for arcing activity at the tap changer contacts.

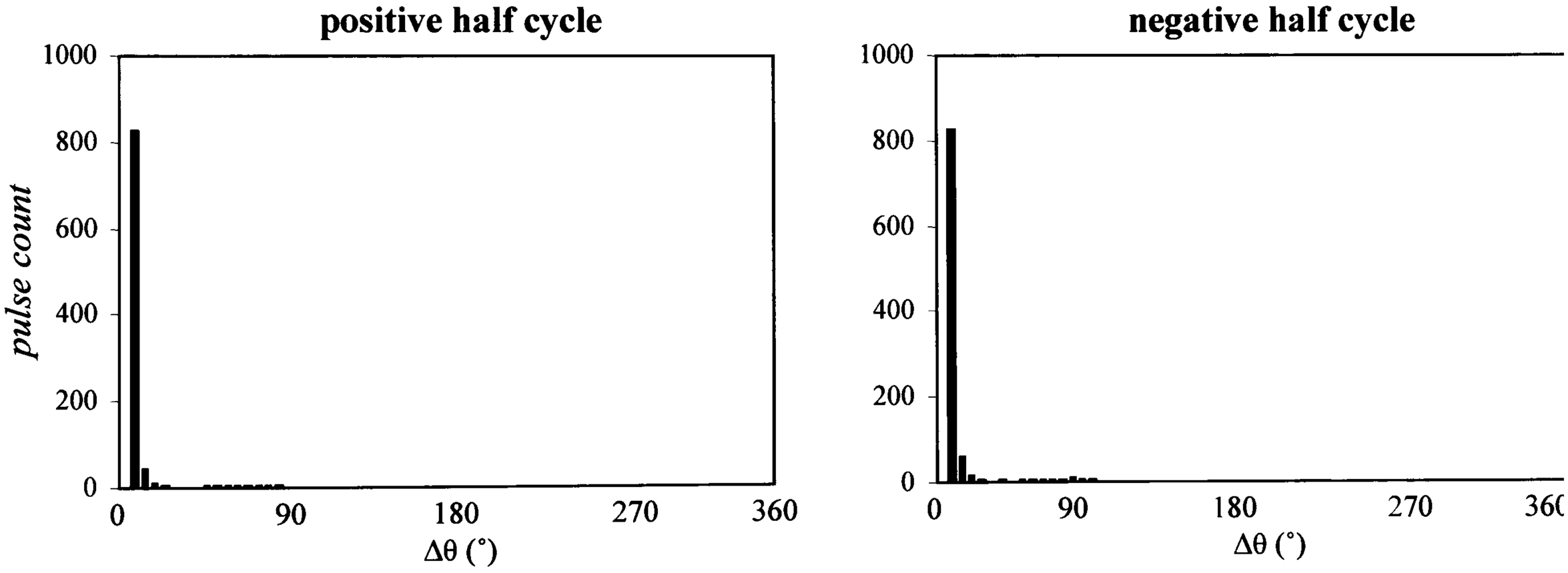

Figure 6.31 Successive pulse distributions for arcing activity at two adjacent turns on a winding.

6.3.9 Summary of the characteristics of UHF PD patterns for different defects

In Table 7.1, the principal features associated with each defect are outlined.

Table 7.1 Summary of defect characteristics.

Defect	Characteristics
HV protrusion in air	A greater magnitude and number of PD pulses were measured on the negative half cycle than the positive half cycle. The magnitude of PD pulses decreased towards the peaks of the power cycle.
HV protrusion in oil	A greater magnitude and number of PD pulses were measured on the positive half cycle than on the negative half cycle. PD pulses were concentrated around the peaks of the power cycle.
Surface discharges	The magnitude of PD pulses were found to decrease towards the peaks of the power cycle. PD pulses were detected at the zero crossing positions of the power cycle.
Bad contact	PD pulses were detected at the zero crossing positions of the power cycle. The magnitude of PD pulses decreased towards the peaks the power cycle.
Floating component	PD pulses were concentrated in the first and third quadrants of the power cycle. In general, PD pulses measured on both half cycles were observed to be symmetrical. PD pulses generally did not occur on successive phase positions. PD pulses were detected at the zero crossing positions of the power cycle.
Suspended particle	The magnitude of PD pulses decreased towards the peaks the power cycle. Very little amounts of PD were detected at the zero-crossing positions of the power cycle.
Free metallic particle	At inception voltage, PD activity was correlated with the power cycle and decreased towards the peaks of the power cycle. In general, the pattern was similar to those found for the bad contact. At voltages greater than inception, PD pulses were uncorrelated with the power cycle.
Arcing sources	PD pulses were concentrated in the second and fourth quadrants of the power cycle. PD pulses were detected at the zero-crossing positions of the power cycle. PD pulses measured on both half cycles were observed to be symmetrical.

6.3.10 Computer-aided discharge diagnosis

Since PD monitoring systems can create a large amount of phase-resolved data the techniques pioneered by Kreuger and his co-workers [136, 137 and 138] are often used to assist with the interpretation of PD activity. Kreuger recorded PD activity from a range of defect sources using a conventional detection circuit. Measurements were recorded in a phase-resolved form and statistical features were extracted and used to train intelligent software systems to recognise particular defect types. This approach has been found to be very successful for interpreting UHF PD signals in GIS [18].

Based on this success, statistical features were extracted from the measurements described in this chapter [134, 135]. In general, 100 '*snapshots*' were acquired at each test voltage and statistical parameters were extracted from the corresponding $H(\theta)$ distribution. These parameters were used by co-workers at the University of Strathclyde to train intelligent software systems. However, it was found that classification using C5.0 Rule Induction, Back Propagation Neural Networks and K-means clustering was sometimes inconclusive. This can be accounted for by the following reasons.

Firstly, the approach pioneered by Kreuger [136, 137 and 138] was based on a fundamentally different experimental technique. In general, this involved generating PD in SF_6 gas and using conventional IEC60270-based detection circuits. As already described in this work, interpreting the results from PD generated in oil is more complex than interpreting PD generated in a gas.

Secondly, statistical features are purely descriptive parameters and are not necessarily related to the physics of the discharge process [147]. As already described '*memory propagation*' can strongly influence PD behaviour [142,143]. Under such conditions, the phase angle is not necessarily representative of the local electric field at the PD site. Consequently, statistical feature extraction can lead to misleading results [148].

Thirdly, the PDM used in this work introduces a non-linear relationship between the '*raw*' UHF energy and *pulse height*, as described in Section 2.4.5.2. It is suggested that future work might involve recording '*raw*' UHF energy in a phase-resolved form.

As already described in Chapter 4, UHF energy might be used to provide an indication of PD severity in terms of pC. In addition, the work of Chapter 5 showed that the spectral content and ratio of energies measured using two sensors exhibit characteristics dependent on the discharge process. Therefore, it is proposed that further analysis of this nature might assist with the interpretation of PD generated in operational power transformers.

6.4 Conclusion

In this chapter, it is has been demonstrated that UHF signals radiated from a range of PD sources can be analysed in ways that provide evidence of physical differences in the nature of each insulation defect. A range of PD sources that are known to cause concern in operational power transformers were investigated. UHF PD signals were recorded in a phase-resolved form. These patterns and their corresponding successive pulse distributions were analysed. Experiments were carried out over a range of test voltages to determine how the PD activity changed in character or severity.

Statistical parameters were extracted from $H(\theta)$ distributions and were used by co-workers at the University of Strathclyde to train intelligent software systems. At present, work is underway to develop an expert system for the automatic classification of defect type. It is proposed that this system will be based on the physical observations of Table 7.1

The work of this chapter has allowed a comprehensive reference database to be created. As will be described in Chapter 7, this database is useful for comparing with the results of field trials.

7. FIELD MEASUREMENTS: POWER TRANSFORMER MONITORING USING THE UHF TECHNIQUE

7.1 Introduction

This chapter describes and discusses field tests that were carried out on a ScottishPower transformer that was known to be discharging. The transformer investigated was a three-phase, 1000 MVA, 400 kV/ 275 kV autotransformer (SGT4 at Neilston substation). It was manufactured by Hackbridge Hewittic in 1972 (S/N 218184). This unit was chosen for investigation as it was producing abnormally high amounts of dissolved gas prior to being taken out of service [149].

UHF sensors were retrofitted to the transformer [72], and used to detect discharge activity during site tests. The transformer was energised through its tertiary winding using a mobile generator and a step-up transformer. When the unit was operated at 60 Hz and at voltages exceeding 115 % of its normal operating level, discharge activity was detected using the UHF technique [84,85].

The detection system was found to be immune to the external corona present on the bushing terminals. Radiated UHF signals were measured in both the time domain and as phase-resolved events. Analysis of time-of-flight data allowed two separate sources of discharge activity to be identified. Their phase-resolved patterns are analysed in the light of Chapter 6.

7.2 UHF Measurement System

7.2.1 Installation of UHF sensors

Figure 7.1 Example of a UHF sensor fitted on top of the transformer tank.

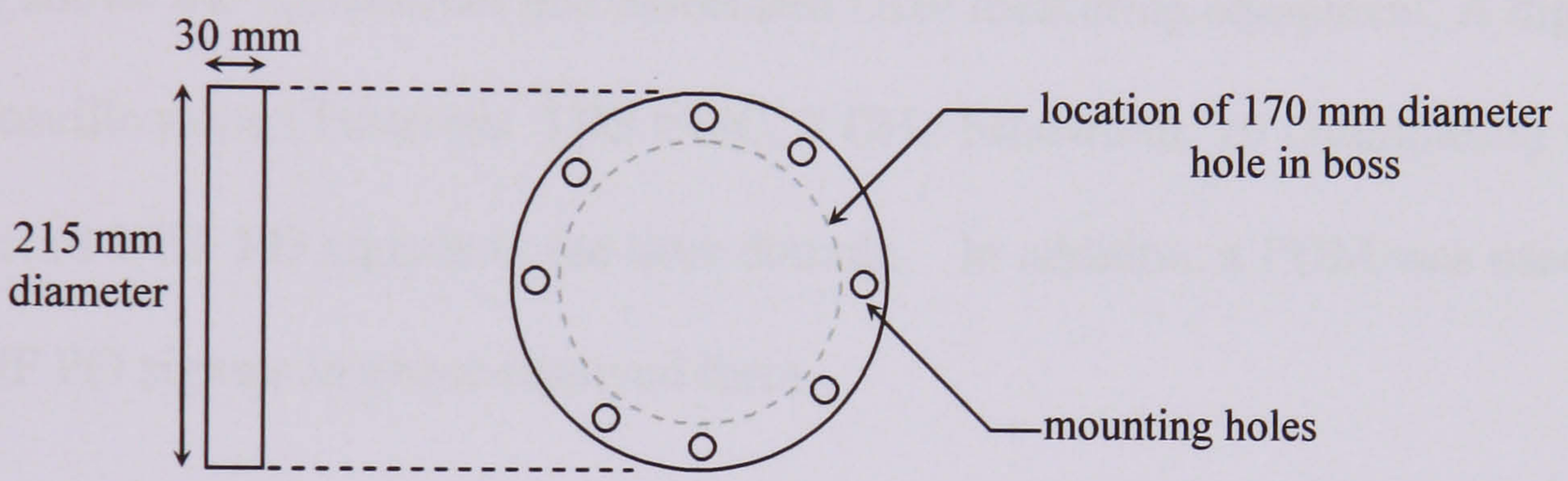

Figure 7.2 Dielectric window made from Nylon 66.

An example of a UHF sensor that was retrofitted to the transformer is shown in Figure 7.1. The sensor was coupled to the transformer tank through a dielectric window. This allowed the oil seal to be maintained and provided an aperture for UHF signals to pass. In Figure 7.2, the dimensions of the dielectric window are shown [72]. The mounting positions of both sensors ($Sensor_1$ and $Sensor_2$) are shown in Figure 7.3.

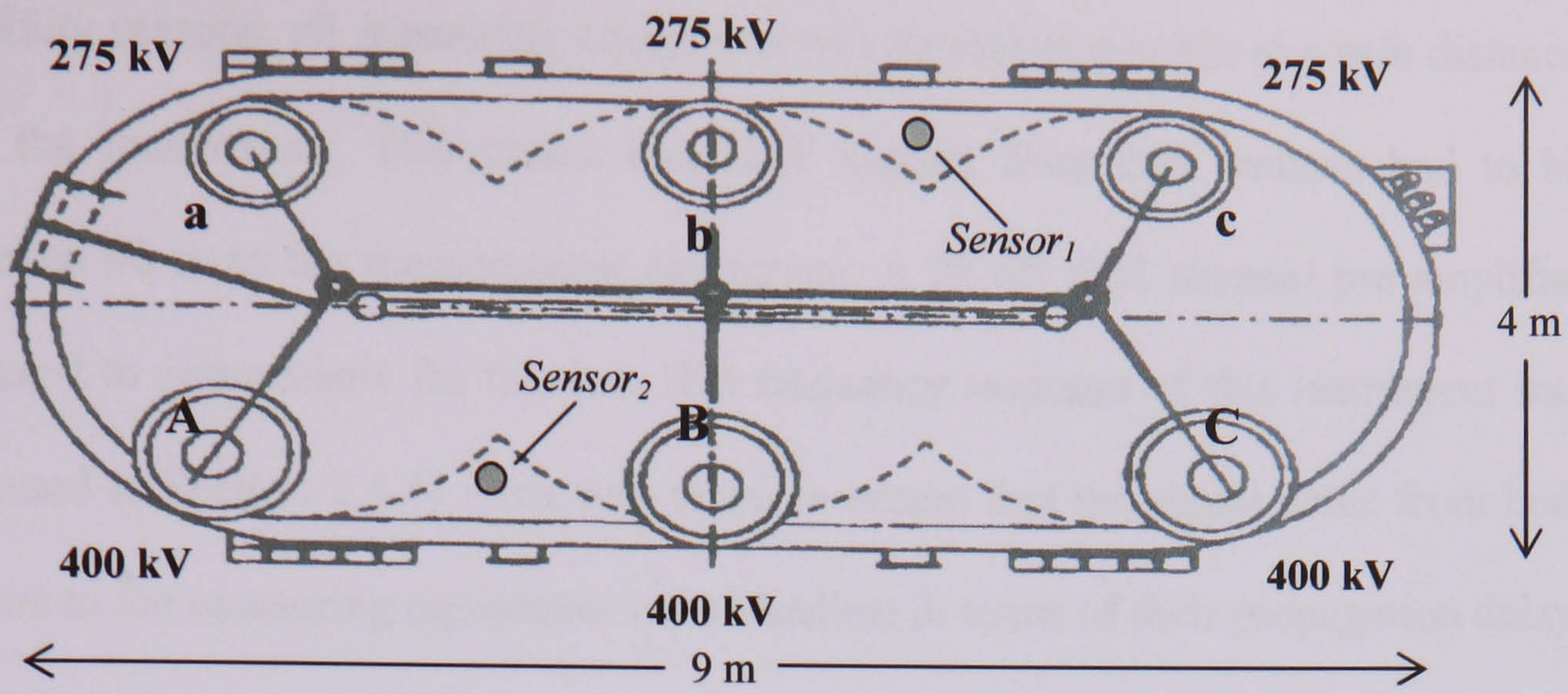

Figure 7.3 Plan view of the 400 kV / 275 kV transformer showing the UHF sensor locations.

Figure 7.4 shows the transformer and associated UHF measuring equipment. A digital sampling oscilloscope (Tektronix TDS 694C, 3 GHz bandwidth, 10 Gsamples/s) was used to record UHF PD signals in the time domain. In addition, a PDM was used to record UHF PD signals in phase-resolved form.

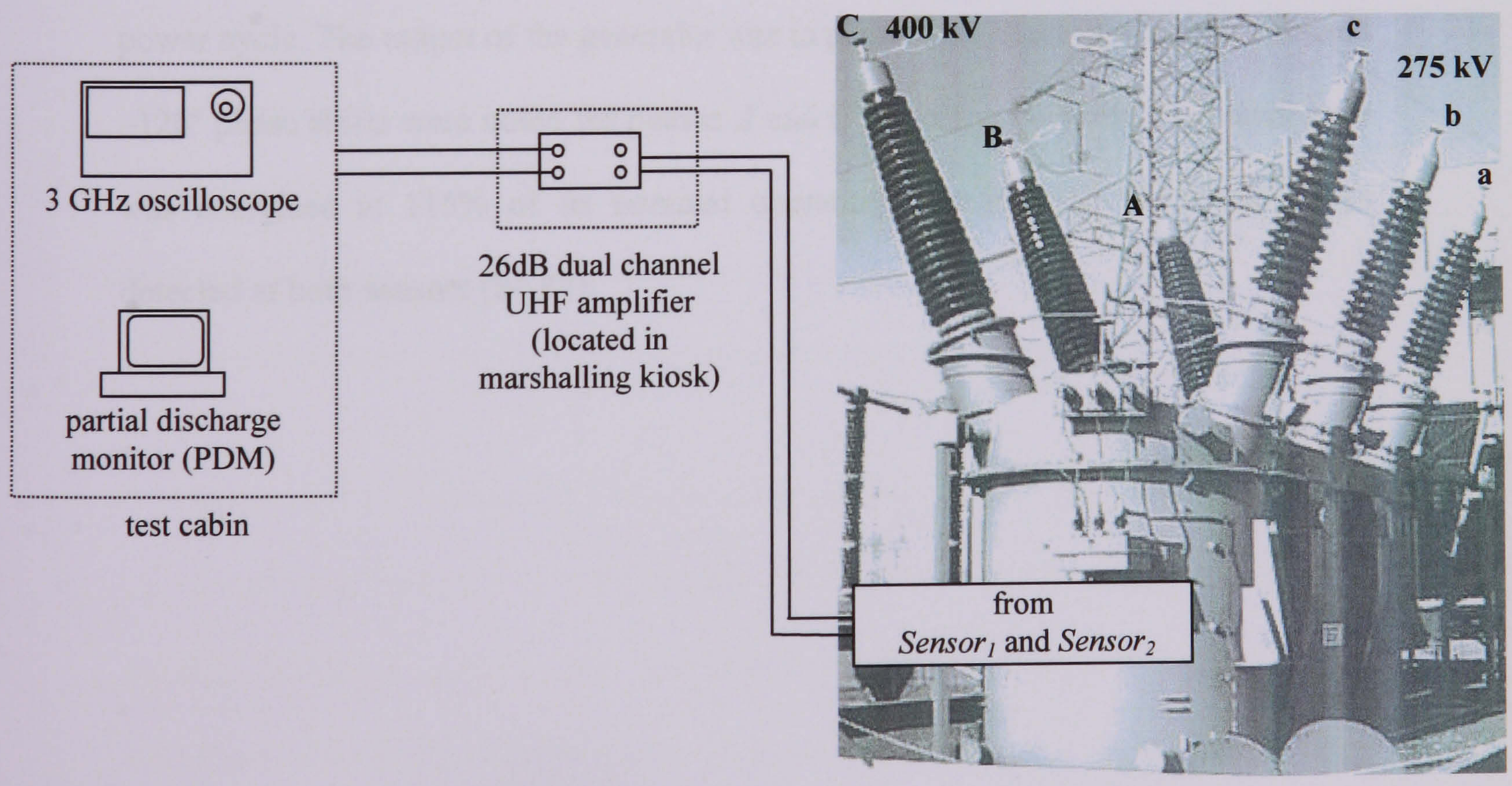

Figure 7.4 400 kV/275 kV, 3-phase transformer and associated UHF measurement equipment.

For safety reasons, all measuring equipment was located in a cabin at a safe distance from the transformer. This meant that UHF signals from both sensors had to be conveyed 46 m to the measurement equipment. A 26 dB dual channel pre-amplifier was used to compensate for this loss (the frequency response of this instrument was presented in Section 2.4.4). Care was taken to ensure that the signal paths from both sensors to the measuring equipment were identical in terms of their propagation delay, gain and frequency response.

7.2.2 Measurement procedure

During testing, all three windings of the transformer were energised simultaneously through its tertiary winding using a mobile generator and a step-up transformer. An AC reference waveform (0 - 300 V) was connected from the generator to a trigger module. This provided a phase reference signal for synchronising the PDM to the power cycle. The output of the generator was in phase with phase *B*, whereas 120° and –120° phase shifts were noted for phases *A* and *C* respectively. When the transformer was energised at 115% of its nominal operating voltage UHF PD signals were detected at both sensors [84,85].

7.3 Results and Discussion

7.3.1 Time domain measurements

The oscilloscope was used to acquire several pairs of UHF signals and the difference between arrival times of signal pairs was used to identify the number of active PD sources. The difference in arrival times was calculated as $\Delta t = t_{Sensor2} - t_{Sensor1}$. The parameters $t_{Sensor1}$ and $t_{Sensor2}$ correspond to the start time of the UHF signal measured at $Sensor_1$ and $Sensor_2$ respectfully.

An example of two consecutive PD events that were measured using the oscilloscope are shown in Figure 7.5. The difference in arrival times of these signals is Δt = 7.5 ns, and this indicates that the active discharge source is closer to $Sensor_1$. In addition, the amplitudes of the UHF signals measured at $Sensor_1$ are larger and so the PD source must have been closer to $Sensor_1$.

Following a number of acquisitions, two distinct but repeatable time differences became apparent, suggesting the presence of two active discharge sources. The important characteristics of these measurements are outlined in Table 7.1. These measurements were immune to external corona on the bushings because only two distinct PD sources were identified, whereas corona was present on all six bushings.

It is interesting to note that UHF PD signals lasted for approximately 100 ns, therefore signals arriving towards the end of this period will have travelled around 20 m through the oil and cellulose and experienced multiple reflections. This indicates that the attenuation of UHF signals within the transformer was not excessive. A relatively

simple physical model of the internal structure of the transformer has been developed by co-workers at the University of Strathclyde to predict the propagation paths of the UHF PD signals for defect location [85]. A discussion of this model is outside the scope of this work. However, the simulation suggested that neither discharge source, PD_1 or PD_2, were associated with phase A because the UHF signal would have to arrive at $Sensor_2$ first.

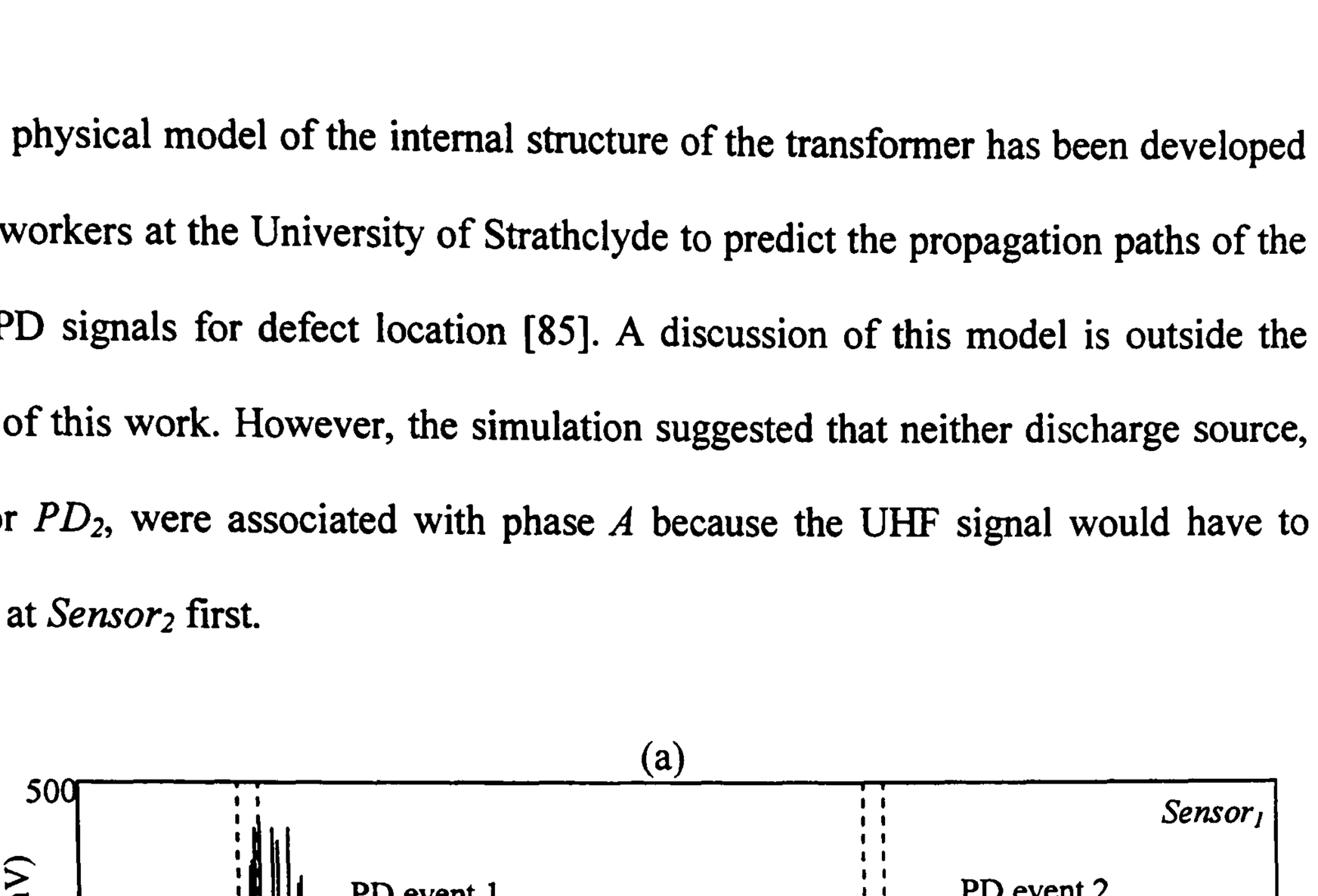

Figure 7.5 Example of UHF signals measured at (a) $Sensor_1$ and (b) $Sensor_2$.

Table 7.1 Summary of time-domain measurements.

Discharge Source	Δt	Relative Amplitudes
PD_1	~ 7.5 ns	$Sensor_1 \sim 2\ x\ Sensor_2$
PD_2	~ 10 ns	$Sensor_1 \sim 5$ x $Sensor_2$

7.3.2 Phase-resolved measurements

Figure 7.6 shows an example of a '*snapshot*' recorded at $Sensor_1$. These signals were measured relative to the phase voltage *B*. An inspection of this plot confirms the presence of two groups of discharges, labelled PD_1 and PD_2, both of which are separated in phase by 180°. PD signals from both sources are correlated with the power frequency.

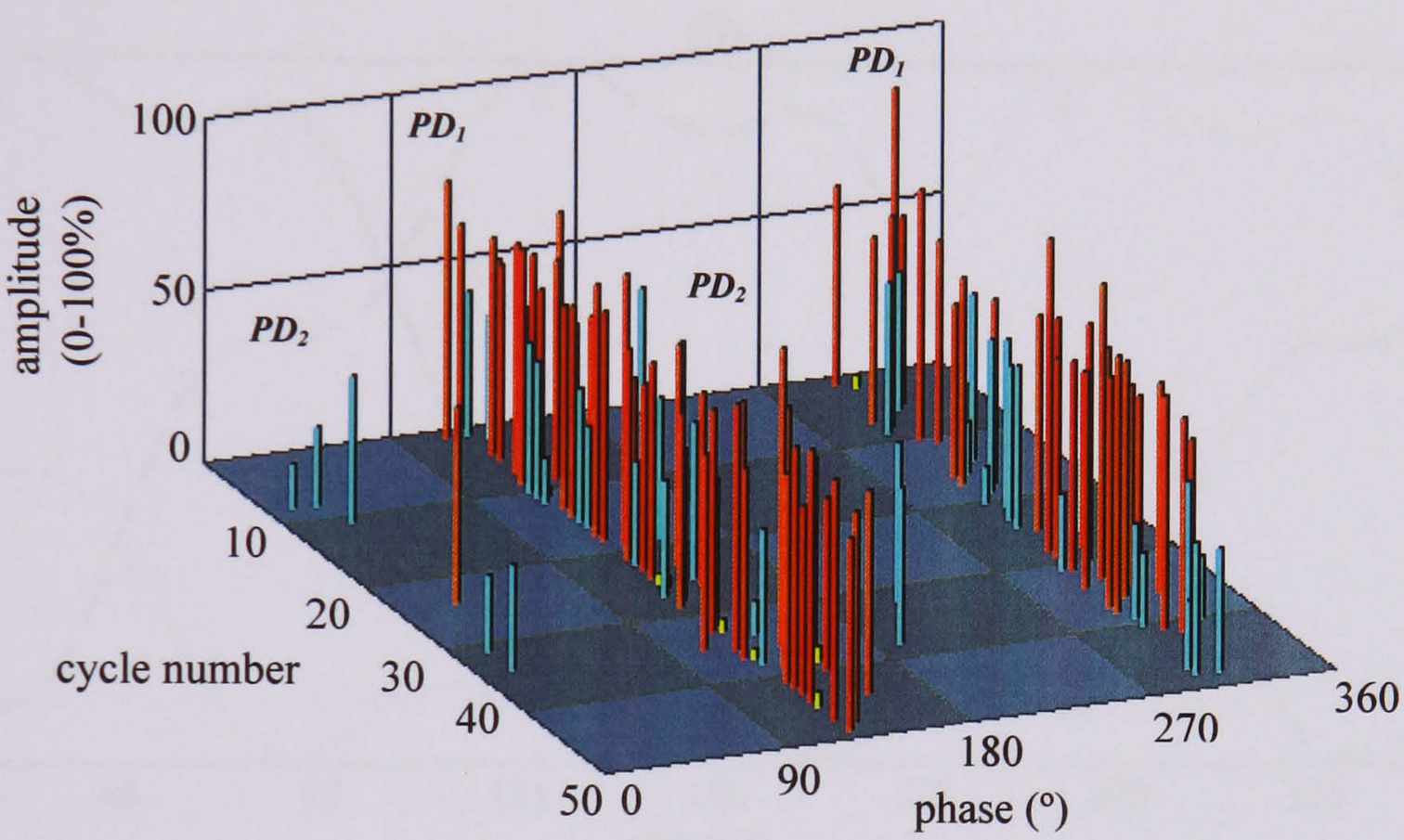

Figure 7.6 An example of UHF signals measured at $Sensor_1$ relative to the phase voltage *B*.

During a 20-minute test, a total of 993 cycles of phase-resolved measurements were recorded for each sensor. In Figure 7.7, the $H(\theta)$ distribution relating all of the PD pulses signals detected by $Sensor_1$ are shown. Since the analysis of time-of-flight measurements suggested that neither discharge source PD_1 or PD_2 could be associated with phase *A*, only the occurrence of PD events relative to the instantaneous phase voltages of *B* and *C* will be considered. Figure 7.7(b) shows that the instantaneous phase-to-ground voltages were severely distorted and this will make interpretation difficult. This was due to saturation of the step-up transformer between the generator and the tertiary winding.

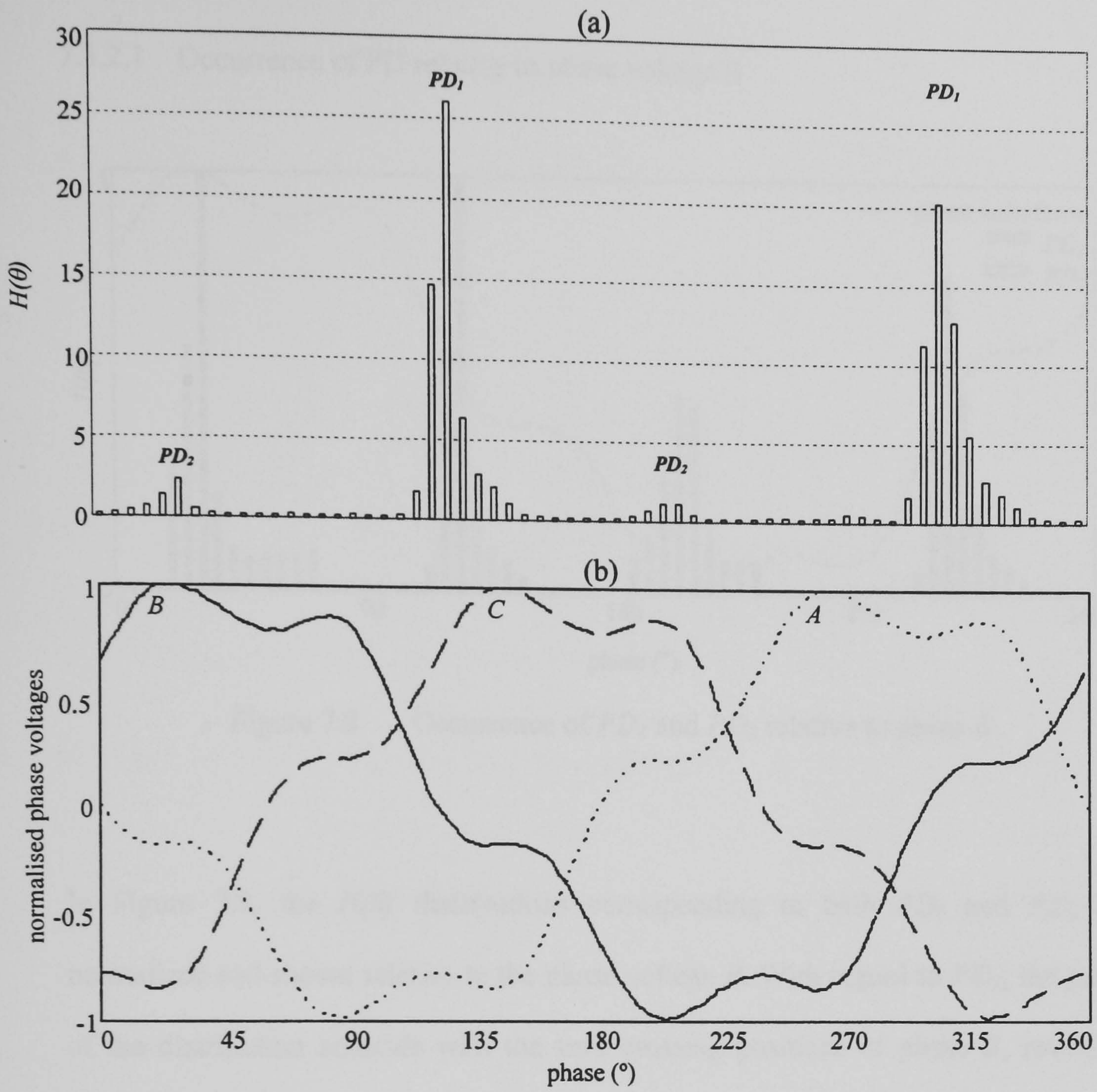

Figure 7.7 Phase-resolved PD signals recorded during a 20 minute test (115% of nominal voltage, 60 Hz)
(a) mean pulse height, $H(\theta)$ and
(b) instantaneous phase-to-ground voltages.

7.3.2.1 Occurrence of PD relative to phase voltage B

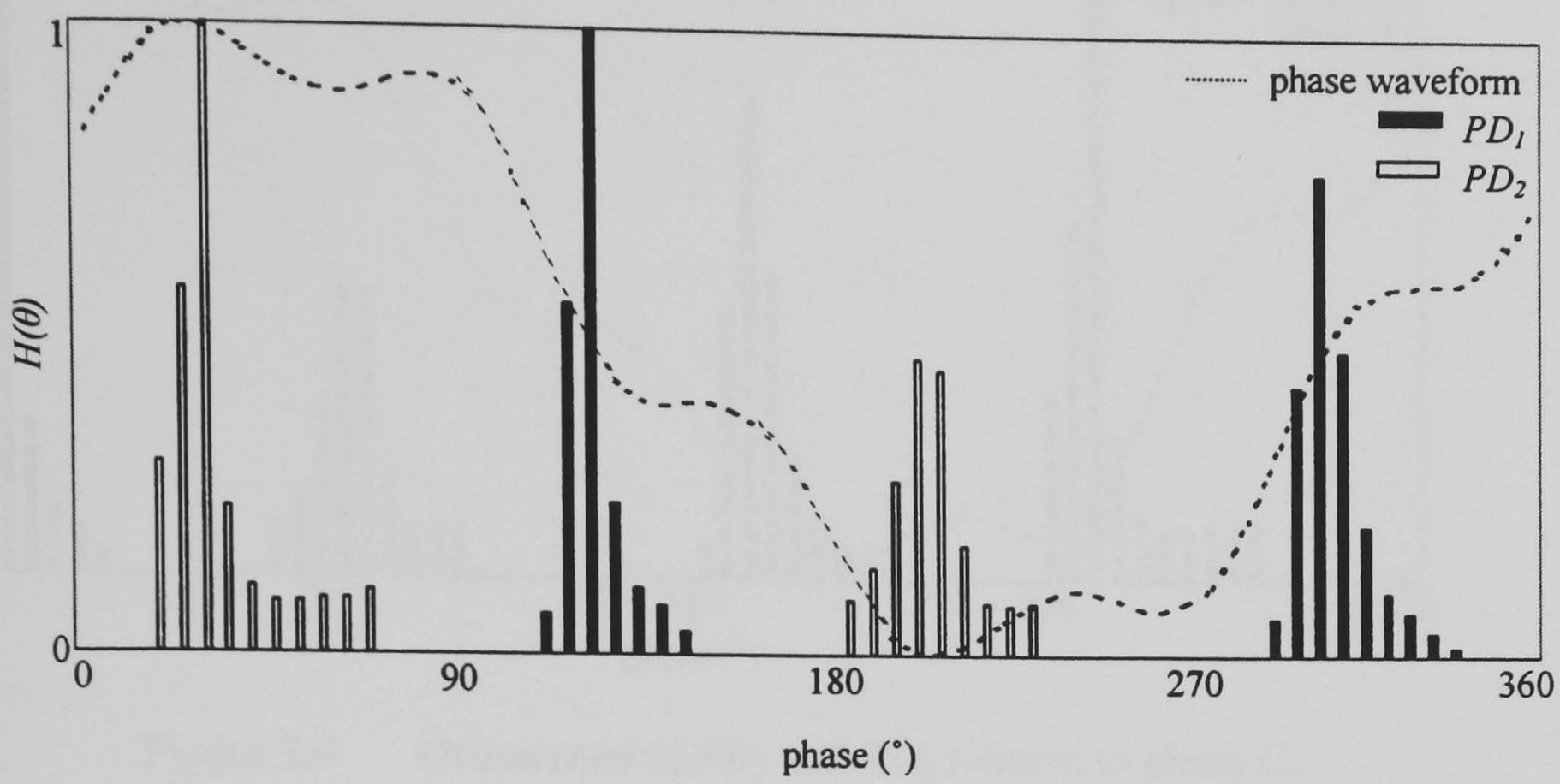

Figure 7.8 Occurrence of PD_1 and PD_2 relative to phase B.

In Figure 7.8, the $H(\theta)$ distributions corresponding to both PD_1 and PD_2 are normalised and shown relative to the phase voltage B. With regard to PD_1, the peaks of the distribution coincide with the zero crossing positions of phase B, revealing similar characteristics to the bad contact (Section 6.3.4) and the free particle (at inception voltage) that was described in Section 6.3.7. In the case of PD_2, the peaks of the distribution coincide with the peaks of the voltage waveform and no PD activity was detected at the zero-crossing positions. These characteristics are similar to the protrusion that was investigated in Sections 6.3.1 and 6.3.2.

7.3.2.2 Occurrence of PD relative to phase voltage C

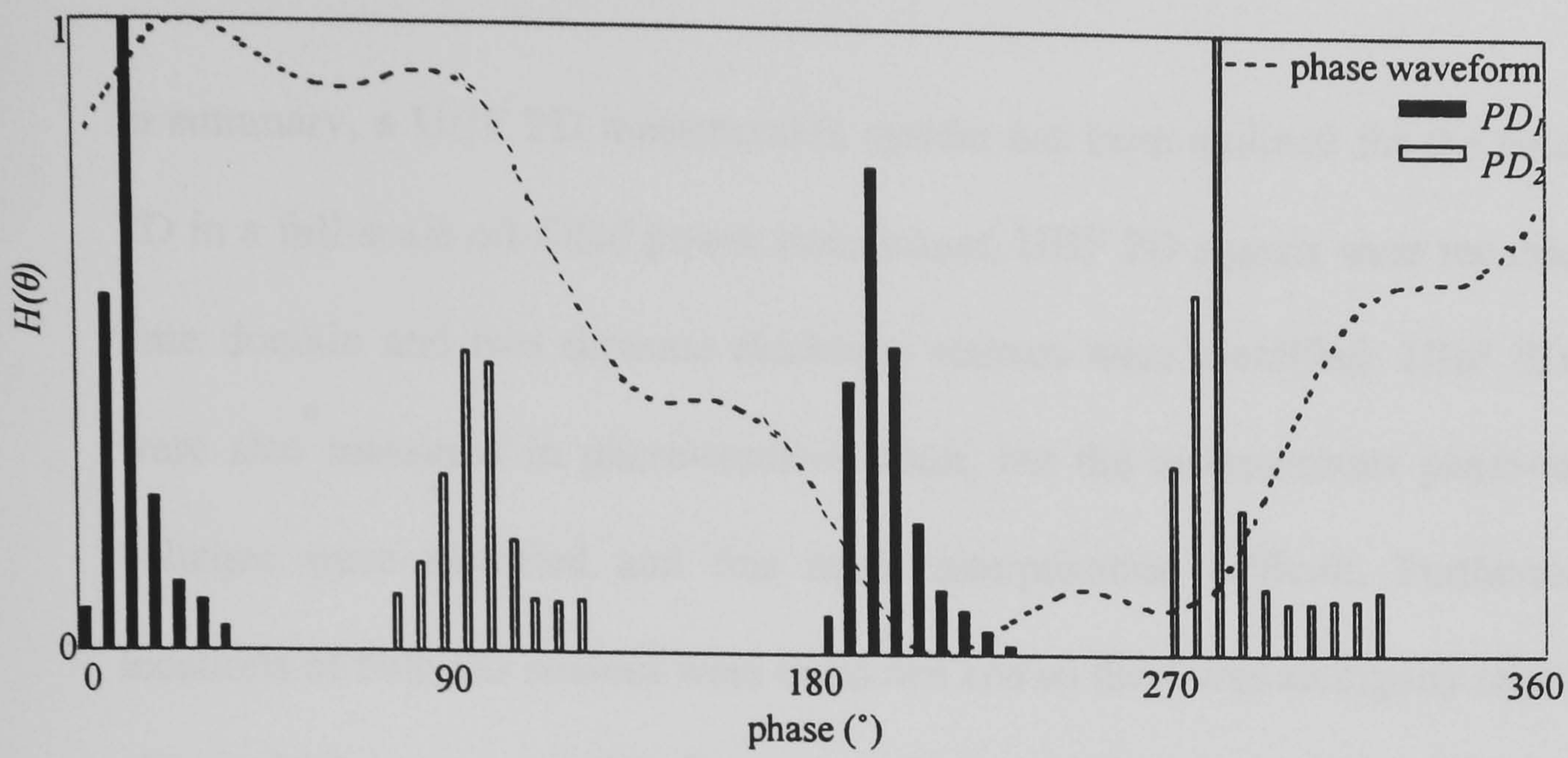

Figure 7.9 Occurrence of PD_1 and PD_2 relative to phase C.

In Figure 7.9, the $H(\theta)$ distributions corresponding to both PD_1 and PD_2 are normalised and shown relative to the phase voltage C. For PD_1, inception occurs in the first and third quadrants and decreases towards the peaks of the voltage waveform. Again, these characteristics are similar to those of the bad contact (Section 6.3.4) and the free particle (at inception voltage) of Section 6.3.7. In the case of PD_2, activity occurs following the peaks of the phase voltage C and persists until the zero-crossing positions of the power cycle. This characteristic is similar to the arcing source that was described in Section 6.3.8.

In summary, it is suggested that PD_1 is either a bad contact or a free particle (at inception voltage). This diagnosis is independent on whether PD_1 is associated with phase voltage B or C. In the case of PD_2, there is evidence to suggest that the discharge source is a protrusion when it is displayed relative to the phase voltage of B. On the other hand, if PD_2 is associated with phase voltage C then it is likely that the defect is an arcing source. However, this interpretation is somewhat limited by the severely distorted instantaneous phase-to-ground voltages.

7.4 Conclusion

In summary, a UHF PD measurement system has been outlined for the detection of PD in a full-scale oil-filled power transformer. UHF PD signals were recorded in the time domain and two separate discharge sources were identified. UHF PD signals were also measured in phase-resolved form, but the instantaneous phase-to-ground voltages were distorted and this made interpretation difficult. Furthermore, the locations of both PD sources were unknown and so there was ambiguity regarding the phase which was responsible for generating the local electric field.

The ability to locate discharge sources could be improved by adding a third sensor and by using a three-dimensional electromagnetic time-of-flight model. A suitable algorithm is currently under development by co-workers at the University of Strathclyde. This would simplify the interpretation of phase-resolved measurements because the phase voltage responsible for generating the PD would be known *a priori*.

In April 2004, ScottishPower Power Systems carried out a post-fault investigation to determine the cause of failure of SGT4. Firstly, the oil was drained from the tank and the transformer was dismantled in a controlled manner. The inspection confirmed that the magnetic circuit was in reasonable order and the windings had not suffered any significant mechanical deformation. The only evidence of overheating was on some of the upper core bolt insulating rods. However, the extent of the damage was not enough to confirm the presence of a serious discharge source. Unfortunately, the windings could not be carefully inspected because their shape was lost when they were removed from the tank. Paper samples were taken from each of the windings

and were sent to a laboratory for analysis. To date, the paper samples are awaiting furfuraldehyde analysis (FFA). It is anticipated that the results from the FFA tests will provide some evidence as to the nature of failure of SGT4.

Co-workers at the University of Strathclyde also carried out UHF measurements on an 18 MVA single phase 132/25 kV unit at St Andrew's Cross substation. This transformer was selected for monitoring because significant amounts of Hydrogen and Acetylene were found in recent DGA samples. In order to determine whether the PD was affected by load conditions, a portable UHF monitor was left on-site and data was recorded continuously in phase-resolved form for six days. Over this period the PD pattern was remarkably stable despite loading variations from 2-17MVA.

Inspection of the phase-resolved patterns suggested that the pulses were most likely to be centred on, or just before, the voltage peaks. There appeared to be no difference in the PDs whether they occurred in the positive or negative half cycles, that is, strong 180° symmetry was evident in the patterns. UHF PD signals were also recorded in the time domain. Interpretation of these results suggested that the source of the signals was just under the tap changer mechanism. During the post-fault investigation, the transformer was carefully dismantled and insulating paper on leads to the tap changer were found to be burnt in the region where the PD source was suspected. These findings confirmed that the UHF technique is suitable for detecting PD that is generated in operational power transformers.

More recently, UHF sensors have been specified for transformers at Crookston (132/33 kV) and Easterhouse (275/33 kV) substations. It is anticipated that this will provide opportunities for future UHF PD monitoring.

8. GENERAL CONCLUSIONS

In Chapter 1, a range of insulation defects that are known to cause PD in operational power transformers were reviewed. A variety of on-line measurement techniques that allow the detection of such PD were also discussed. IEC 60270-based and UHF measurements were considered to be the most suitable. The IEC 60270-based technique has the advantage that discharge magnitudes can be quantified in terms of pC. On the other hand, UHF measurements have the advantage that it should be possible to locate PD using time-of-flight techniques. The remainder of this work was concerned with assessing the efficacy of using the UHF measurement technique for detecting PD generated in transformer insulating oil.

In Chapter 2, the experimental apparatus used to generate PD was introduced. A robust HV network was constructed and used to energise the test cell and test apparatus. A capacitive divider circuit was also designed for use in monitoring the HV AC waveform. A high-frequency current transformer was investigated for measuring PD current pulses, and a broadband electric field sensor was selected to detect electromagnetic signals in the UHF range. A Diagnostics Monitoring Systems Ltd partial discharge monitor (PDM) was described and used to record UHF PD signals in phase-resolved form.

In Chapter 3, some of the physical processes involved when PD occurs in a liquid were reviewed. PD current pulses convey information relating to the PD process, so current pulses were measured at both inception and higher voltages.

At inception voltage, PD current pulses were measured directly using a high-frequency measurement system and were found to lie on sub-nanosecond timescales. At test voltages well above inception, a high-frequency current transformer was used to measure PD current pulses. The risetimes of the current pulses measured during the positive half cycle were found to lie on a sub-nanosecond duration. However, the negative current pulses consisted of shorter pulse bursts that were superimposed on an underlying pulse with a 10 μs duration. When these shorter pulse bursts were inspected they were found to lie on a sub-nanosecond timescale and cause the excitation of UHF signals. On the basis of these findings, the UHF technique can be considered to offer an effective means of PD detection.

It was suggested that further research should involve the simultaneous measurement of PD current pulse, UHF and optical measurements. In addition, chemical degradation of the oil might also be studied. This would allow current pulse and UHF measurements to be better related to the PD mechanism.

In Chapter 4, a comparative study was reported in which PD was generated in air, unused transformer oil and used transformer oil. PD current pulses were recorded simultaneously with both IEC 60270-based and UHF measurement systems. Since IEC 60270-based and UHF measurements systems operate on very different principles their responses to PD current pulses of known magnitude provide a useful basis for comparing the performance of both systems.

PD current pulses in air revealed the greatest amount of pulse-shape regularity, whereas those in used transformer oil revealed the greatest amount of pulse-shape variability. For experiments in unused transformer oil, the correlation between the charge contained in PD current pulses and IEC 60270-based measurements was found to be weaker than for air. A low correlation was also found between charge and UHF energy during the positive half cycle, and very low amounts of UHF energy were measured during the negative half cycle.

The lowest level of correlation was found in used transformer oil. This can most likely be attributed to the high impurity content associated with this transformer oil sample. Furthermore, measured current pulses were only representative of PD occurring in the oil surrounding the tip of the protrusion, but both IEC 60270-based and UHF measurement systems were additionally influenced by PD in the liquid bulk and at the pressboard barrier.

This work demonstrated that, while several PD current pulses could occur within a few nanoseconds, the IEC 60270-based measurement circuit could only respond to PD on a microsecond timescale. Therefore, individual pulses cannot necessarily be distinguished. Advantages might be gained by simultaneously recording IEC 60270-based and UHF measurements. It is anticipated that this approach will assist with the interpretation of measurements carried out on-site, and will provide a better indication of discharge severity in terms of pC. It was suggested that this should be a subject for further research.

Chapter 5 dealt with PD generated in the oil medium surrounding a protrusion, a bad contact and a free metallic particle. A high-frequency current transformer was used to measure PD current pulses and the corresponding radiated UHF signals were measured using two broadband electric field sensors mounted at different locations relative to the PD source. Discharges involving the protrusion and the bad contact revealed the greatest amount of pulses-shape variability, due to changes in the discharge process. Pulses from the free metal particle were very consistent in terms of their shape.

In the work of Chapter 5, two new ways of analysing UHF signals were presented. These are the spectral content and ratio of energies method. Both compared discharge activity during the positive and negative half cycles of the power frequency in a way that could allow different sources to be distinguished. By plotting the spectral energy during both half cycles differences in discharge mechanisms were identified. Similarly, the ratio of energies method was also used to assess variability in the pattern of radiation from the PD source.

The advantage of the two new methods is that they use only normalised data derived from the UHF signals. Therefore, these methods could be applied to the 'black box' situation which is more likely to be encountered in measurements carried out on-site. It is anticipated that these methods will complement existing techniques, such as phase-resolved measurements of PD diagnostics.

Chapter 6 covered experiments involving a variety of transformer insulation defects simulated under laboratory conditions. UHF PD signals were measured in phase-resolved form using a commercial PDM. Experiments were performed over a range of test voltages, and information was obtained on whether the PD activity was changing in character or becoming more severe.

The types of defect considered were:

- HV electrode protrusion in air
- HV electrode protrusion in oil
- Surface discharges
- Bad contact
- Floating component
- Suspended particle
- Free metallic partial
- Arcing sources

Phase-resolved measurements were evaluated, demonstrating that they provide evidence of the physical differences between the insulation defects. This involved analysing three-dimensional '*snapshots*' in the form of *phase angle*, *pulse height* and *cycle number*. In addition, the corresponding pulse-sequence distributions were also

investigated and shown to be useful for interpreting PD measurements. This work generated a valuable reference database for comparison with field measurements and is currently being used by co-workers at the University of Strathclyde to develop an expert system. This will allow defect types to be classified automatically using software.

Chapter 7 reported field tests carried out on a 1000 MVA power transformer. When the unit was operated at 60 Hz, and at voltages exceeding 115 % of its normal operating level, discharge activity was detected using the UHF technique. UHF PD signals were recorded in the time domain and this allowed two separate discharge sources to be identified. In addition, UHF PD signals were also recorded in phase-resolved form. These results were discussed with the reference database built up in Chapter 6.

This research has contributed to the knowledge base required for the development of a continuous monitoring system for oil-filled power transformers based on the UHF technique.

Following the completion of this thesis, it is recommended that further laboratory based research should be carried out in the following four main areas:

1. At present, it is widely accepted that the understanding of electrical breakdown in liquid dielectrics is still relatively modest. It is therefore recommended that the inception and development of PD in oil should be studied using high resolution optical recording systems. This will provide a better insight into the physical processes involved and will ultimately assist with the interpretation of UHF measurements.

2. Preliminary measurements showed a relationship between PD current pulse, IEC60270-based and UHF measurements. It is suggested that a better understanding between these parameters might be found by carrying out further laboratory work. Initially, PD might be generated using a relatively simple electrode geometry such as point-plane gap and experiments should be carried out under controlled conditions.

   If a strong correlation between PD current pulse, IEC60270-based and UHF measurements is found then a variety of oil grades might be tested at a range of temperatures, and oil samples might be circulated using external pumps to simulate the action of a transformer cooling system. Again, benefits might be gained by detecting PD using high resolution optical systems as the propagation of streamers will be influenced by oil grade, temperature, and flow rate. In addition, chemical degradation of the oil might also be studied.

3. In the work of Chapter 5, the spectral content method was presented as a new way of analysing UHF signals. It is recommended that advanced signal processing techniques such as wavelet analysis should also be considered and applied in a similar manner.

4. As described in Chapter 6, the commercial PDM that was used did not have sufficient resolution to detect all of the PD pulses that were likely to be generated in the oil. It is recommended that recording PD in phase resolved form should be considered further when acquisition technology with a suitably high sampling rate becomes available. Such measurements should be interpreted using analytical techniques that are related to the physics of the PD.

9. GENERAL REQUIREMENTS: AN ON-LINE UHF PD MONITORING SYSTEM FOR POWER TRANSFORMERS

This investigation has demonstrated that UHF PD measurements could assist in monitoring troublesome transformers. However, retrofitting the necessary dielectric windows to healthy transformers may be difficult to justify because an outage is required to lower the oil and replace inspection hatches. At present, transformer manufacturers are investigating a suitable design of a reliable dielectric window that will not compromise the integrity of the tank during the lifetime of a transformer. It is recommended that the procedures for fitting such UHF windows and sensors should be standardised. This will provide electrical utilities with a specification at the manufacturing stage and will allow future generations of power transformers to be monitored using the UHF technique.

As related in Chapter 7, advanced modelling techniques are currently being developed at the University of Strathclyde to allow multiple PD sources within a transformer to be located. Once UHF signals from a particular defect source have been identified, they can be recorded in appropriate phase-resolved form. In addition, the spectral content and ratio of energies methods of Chapter 5 can be used to assist with the interpretation of PD behaviour.

In this work, the UHF technique has only been considered for the detection of PD. Preliminary (unpublished) experiments have suggested that UHF sensors might also be used to simultaneously monitor the internal mechanical integrity of a transformer. The results from this work might establish whether transients from lightning activity,

geo-magnetically induced currents, switching operations or short circuit faults have caused permanent mechanical distortion of the internal structure.

Work is currently underway to produce a portable unit that will provide a development platform for integrating all of the functionality that has been outlined. This will allow engineers to remotely visualise any PD activity occurring within the suspect transformer. Ultimately, any PD monitoring system should provide information on the number of simultaneously active PD sources, their locations, their types, and whether they are changing in character or in severity.

Conventional IEC 60270-based measurements offer a standardised procedure for PD monitoring and allow discharge magnitudes to be quantified in terms of pC. However, this parameter is *apparent charge*, not *real charge*, and it is argued that the relationship between these quantities is no less complex than the relationship between *real charge* and UHF energy. The acceptance of IEC 60270-based measurements can be attributed to many years of laboratory and field experience. It is recommended that further research should involve gaining a greater understanding of the relationship between UHF energy and discharge magnitude. Techniques such as finite difference time domain (FDTD) modelling might play an important part in such an investigation [150].

It is generally accepted that the UHF technique can be used successfully for continuous remote monitoring of GIS. On this basis, the UHF technique could be a very promising technique for monitoring transformers. The use of multiple sensors to simultaneously '*look*' into a single volume of insulation allows PD activity to be

interpreted with greater accuracy. It is anticipated that this technique will have applications beyond the field of transformers, perhaps to entire substations. It is recommended that the UHF technique should now be considered for investigating the dielectric integrity of generators, and the ability of suspect circuit breakers to extinguish arcs. These are also key components of the electrical transmission network and the state of their insulation is of considerable interest to utilities.

10. Acknowledgements

This thesis is based on the project entitled '*Integrated Approach to Condition Monitoring and Plant Lifetime Modelling*', and was supported by the Engineering and Physical Sciences and Research Council under the grant number GR/M98777. I would like to thank the **EPSRC** for funding this research.

The assistance of **Mr J McKechnie, Mr D Griffin** and **Mr J Lannigan** of the Engineering Workshop of the Institute for Energy and Environment is greatly appreciated. They assisted in the construction and assembly of the experimental apparatus, and provided great encouragement throughout the project. The invaluable assistance of **Mr J Barrasford, Mr C Bennoch** and **Dr L Yang** is also greatly appreciated. The Partial Discharge Monitor was kindly supplied by **Mr J Pearson** of Diagnostic Monitoring Systems Ltd.

The constructive comments that were supplied by **Professor O Farish** and **Professor G Woolsey** during the preparation of this thesis are very much appreciated. I would also like to thank **Professor J McDonald** for the encouragement he gave me during my time at the University of Strathclyde.

I would also like thank **Dr Martin Judd** for his generous support and the constructive criticism he supplied throughout the project. His outstanding theoretical understanding and wealth of practical experience are invaluable to the field of high frequency diagnostics.

Finally, I would like to thank my wife **Alison**, my parents **Patrick and Ann Cleary**, and my **grandparents**. Their years of encouragement made this thesis possible.

11. REFERENCES

[1] 'Basic transformer theory', D. Allan, Transformers for Power Systems, EA Technology Conferences and Training, 26 – 27 November 2003

[2] M D Judd, S D J M^{c}Arthur, J R M^{c}Donald and O Farish, 'Intelligent condition monitoring and asset management – partial discharge monitoring for power transformers', Power Engineering Journal, pp. 297-304, December 2002

[3] B H Ward and S Lindgren, 'A survey of developments in insulation monitoring of power transformers', IEEE Int. Symp. on Electrical Insulation (Anaheim), pp. 141-147, April 2000

[4] E Gockenbach, 'Testing and Monitoring as basis of the dielectric diagnostic', 11th High Voltage Engineering Symp. (London), Conference Publication No. 467, pp. 1–5, August 1999

[5] B S Bernstein and E L Brancato, 'Aging of equipment in the electrical utilities', IEEE Trans. on EI-28, No.5, pp. 866-875, October 1993

[6] B Gänger and G Maier, 'On electrical ageing of oil-impregnated high-voltage dielectrics', IEEE Trans. on EI-9, No. 3, pp. 92-97, September 1974

[7] M Wang, A J Vandermaar and K.D Srivastava, 'Review of condition assessment of power transformers in service', IEEE Electrical Insulation Magazine, DEIS Feature Article, pp. 12-25, 2002

[8] M D Judd, L Yang, C J Bennoch, I B B Hunter and T Breckenridge, 'Condition monitoring of power transformers using UHF partial discharge sensors: operating principles and site testing', Euro TechCon (Manchester), November 2003

[9] W McDermid, D H Grant, A Glodjo and J C Bromley, 'Analysis of converter transformer failures and applications of periodic on-line partial discharge measurements", Electrical Insulation Conference and Electrical Manufacturing and Coil Winding Conference (Cincinnati), pp. 577-582, October 2001

[10] M Krins, H Borsi and E Gockenbach, 'Influence of ageing on the dielectric properties of carbonized transformer oil', IEEE Int. Symp. on Electrical Insulation (Quebec), pp. 546-549, June 1996

[11] CIGRE Task Force 15-302, 'Partial discharges in transformer insulation – 15-302', 2000

[12] M Krins, H Borsi and E Gockenbach, 'Influence of carbon particles on the breakdown voltage of transformer oil', Conference Record, 12th Int. Conf. on Conduction and Breakdown in Liquids (Rome), 1996

[13] M Krins, H Borsi and E Gockenbach, 'Impact of different water contents on the electric strength of oil gaps and solid/liquid interfaces in the presence of carbon particles', Proc. of the 13th Int. Conf. on Dielectric Liquids, (Nara), pp. 281-285, July, 1999

[14] T Paillat, O Moreau and G Touchard, 'Flow electrification in transformers: correlation between winding leakage current and pressboard charge accumulation', IEEE Conf. on Electrical Insulation and Dielectric Phenomena, (Victoria BC), Vol. 1, pp. 85-88, 2000

[15] E Robles, B Fruth and D W Gross, 'A high sensitivity technique to detect incipient failures on in-service high voltage bushings', Conf. Record, 9th Int. Symp. on HV Engineering (Graz), pp.1-4, August/ September 1995

[16] 'Failures and condition monitoring of power transformers', D. Allan, Transformers for Power Systems, EA Technology Conferences and Training, 26 – 27 November 2003

[17] S A Boggs, 'Electromagnetic techniques for fault and partial discharge location in gas insulated cables and substations', IEEE Trans. Power Apparatus and Systems, Vol. 101, No. 7, pp. 1935-1941, July 1982

[18] J S Pearson, O Farish, B F Hampton, M D Judd, D Templeton, B M Pryor, and I M Welch, 'Partial discharge diagnostics for gas insulated substations', IEEE Trans. on Dielectrics and Electrical Insulation, Vol. 2, No. 5, pp. 893-905, October 1995

[19] R Baumgartner, B Fruth, W Lanz and K Pettersson, 'Partial discharge – part IX: PD in gas-insulated substations – fundamental considerations', IEEE Electrical Insulation Magazine, Vol. 7, No. 6, pp. 5-13, November/December 1991

[20] E O Forster, 'Research in the dynamics of electrical breakdown in liquid dielectrics', IEEE Trans. on Electrical Insulation, Vol. EI-15, No.3, pp. 182-185, June 1980

[21] *Partial discharge measurements*, IEC Publication 60270, 2000.

[22] L G Christophorou and L A Pinnaduwage, 'Basic physics of gaseous dielectrics', IEEE Trans. on EI-25, No. 1, pp. 55-74, February 1990

[23] L Niemeyer, 'The physics of partial discharges', IEE Int. Conf. on Partial Discharge, Conference No. 378, pp. 1-4, 1993

[24] *Mineral oil-impregnated electrical equipment in service – guide to the interpretation of dissolved and free gases analysis*, IEC Publication 599, 2003

[25] M Duval, 'A review of faults detectable by gas-in-oil analysis', DEIS Feature Article, IEEE Electrical Insulation Magazine, Vol. 18, No. 3, pp. 8-17, May/June 2002

[26] L E Lundgaard, 'Partial discharge – part XIV: acoustic partial discharge detection – practical application', IEEE Electrical Insulation Magazine, Vol. 8, No. 5, pp. 34-43, 1992

[27] W R Rutgers and Y H Fu, 'UHF PD-detection in a power transformer', Conf Record, 10th Int. Symp. on HV Engineering, (Quebec), pp. 219-222, August 1997

[28] M D Judd, B M Pryor, S C Kelly, B F Hampton, 'Transformer monitoring using the UHF technique', Conf. Record, Int. Symp. on HV Engineering (London), Vol.5, pp.362-365, August, 1999

[29] B G Esp, M Carrillo and A J McGrail, "Data mining applied to transformer oil analysis data", Conf. Record, IEEE Int. Symp. on Electrical Insulation (Virginia), pp. 12-15, June 1998

[30] J B DiGiorgio, 'Dissolved gas analysis of mineral oil insulating fluids', http://www.nttworldwide.com/tech2102.html

[31] R Rogers, "IEEE and IEC codes to interpret incipient faults in transformers using gas-in-oil analysis", IEEE Transactions on EI-13, No. 5, pp. 348-354, 1978

[32] G E Power Systems, Syprotec and Harley Products, http://www.powerpoint.ie/gepower.html

http://www.nttworldwide.com/dga.ntm

[33] D G Esp and A J McGrail, 'Advances in data mining for dissolved gas analysis', Conf. Record, IEEE Int. Symp. on Electrical Insulation (Anaheim), pp. 456-459, April 2000

[34] J Lapworth, 'A novel approach (scoring system) for integrating dissolved gas analysis results into a life management system', Conf. Record, IEEE Int. Symp. on Electrical Insulation (Boston), pp. 137-143, April 2002

[35] G Zhang, Y Liv, S Ibuka, K Yasuoka and S. Ishii, 'Application of fuzzy data processing for fault diagnosis of power transformers', Conf. Record, IEE HV Engineering Symposium, (London), pp. 160-163, August 1999

[36] J. B. DiGiorgio, "Dissolved gas analysis of mineral oil insulating fluids", NTT- Technical Bulletin: Dissolved Gas Analysis, http://www.nttworldwide.com/dga.ntm

[37] M Wang, A J Vandermaar and K D Srivastava, 'Review of condition assessment of power transformers in service', DEIS Feature Article, IEEE Electrical Insulation Magazine, pp. 12-25, 2002

[38] R Blue, D Uttamchandani and O Farish, 'Infrared detection of transformer insulation degradation due to accelerated thermal aging', IEEE Trans. on Dielectrics and Electrical Insulation, Vol. 5, No. 2, pp. 165-168, April 1998

[39] R Blue, D Uttamchandani and O Farish, 'The determination of FFA concentration in transformer oil by fluorescence measurements', IEEE Trans. on Dielectrics and Electrical Insulation, Vol. 5, No. 6, pp. 892-895, December 1998

[40] M M de A Olivieri, W A Mannheimer, A P Ripper-Neto, 'On the use of acoustic signals for detection and location of partial discharges in power transformers', Conf. Record, IEEE Int. Symp. on Electrical Insulation (Anaheim), pp. 259-262, April 2000

[41] P M Eleftherion, 'Partial discharge XXI: acoustic emission-based PD source location in transformers', DEIS Feature Article, IEEE Electrical Insulation Magazine, Vol. 11, No. 6, pp. 22-26, 1995

[42] Y Lu, X Tan and X Hu, 'PD detection and localisation by acoustic measurements in an oil-filled transformer', IEE Proc. Science, Measurement and Technology, Vol. 147, No. 2, pp. 81-85, 2000

[43] A O Akumu, F Adachi, N Kawaguchi, R Ozaki, H Ihori, M Fujii and K Arii, 'A 3-D numerical simulation of partial discharge acoustic wave propagation in a model transformer', Conf. Record, IEEE Int. Symp. on Electrical Insulation (Boston), pp. 183-186, April 2002

[44] T Bengtsson, H Kols and B Jönsson, 'Transformer PD diagnosis using acoustic emission technique', Conf. Record, Int. Symp. on HV Engineering (Montréal), August 1997

[45] E Grossmann and K Feser, 'On-line PD monitoring of transformers using acoustic emission techniques', Conf. Record, Advanced Processes Testing Applications of Dielectric Materials (Wroclaw), pp. 154-157, September 2001

[46] E Grossmann and K Feser, 'Comparison of the sensitivity of an acoustical and electrical PD-measurement on transformers in the laboratory and on-site', Conf. Record, Electrical Insulation and Dielectric Phenomena (Victoria BC), pp. 690-693, October, 2000

[47] L E Lundgaard, 'Partial discharge XIII: acoustic partial discharge detection – fundamental considerations', IEEE Insulation Magazine, Vol. 8, No. 4, 1992

[48] E Lemke and P Schmiegel, 'Fundametals of the PD probe measuring technique', Radeburger Str. 47, 01468 Volkersdorf , Germany

[49] R. Lortie, J. Aubin, G H Vaillancourt and Q. Su, 'Partial discharge detection on power transformers using a multi-terminal measurement method', Conference Record, 10th International Conference on High-Voltage Engineering (Quebec), pp. 267-270, August 1997.

[50] C Boisseau, P Tantin, P Despiney and M Hasler, 'Instrument transformer monitoring', CIGRE paper 110-13, Berlin, 1993

[51] L. Jian, D. Lin, S. Caixin, L. Ruijin and C. Weigen, 'A practical PD online monitoring system for transformers', Key Laboratory of High Voltage Engineering and Electrical New Technology of Ministry of Education, Chongqing University, Chongqing 400044, China.

[52] K Feser, E Grossmann, M. Lauersdorf and T. Grun, 'Improvement of sensitivity in online PD-measurements on transformers by digital filtering', Conf. Record, IEE High Voltage Engineering Symp. (London), pp 156-159, August 1999.

[53] Z D Wang, P A Crossley, K J Cornick, D H Zhu, A J Shields and I J Kemp, 'Partial discharge location in power transformers', IEE Proceedings Science, Measurement and Technology, Vol. 147, Issue 5, pp. 249 – 255, Sept. 2000

[54] *High voltage test techniques – partial discharge measurements*, IEC Publication 42-162, 2000

[55] P. Werle, A. Akbari, H. Borsi and E. Gockenbach, 'Partial discharge localisation on power transformers using neural networks combined with sectional winding transfer functions as knowledge base', Institute of Electric Power Systems, University of Hannover, Germany.

[56] A Akbari, P Werle, H Borsi and E Gockenbach, 'Transfer function – based partial discharge localization in power transformers: a feasibility study', DEIS Feature Article, IEEE Electrical Insulation Magazine, Vol. 18, No. 5, pp. 22–32, September/October 2002

[57] A Nesbitt, B Stewart, I J Kemp and Z Richardson, 'Condition monitoring of power transformers through partial discharge measurements: problems associated with pulse distortion in the windings', Conf. Record, IEE Dielectric Materials, Measurements and Applications, pp. 270-275, 2000

[58] B H Ward, 'A survey of new techniques in insulation monitoring of power transformers', DEIS Feature Article, IEEE Electrical Insulation Magazine, Vol. 17, No. 3, pp.16-23, May/June 2001

[59] Z D Wang, P A Crossley and K J Cornick, 'Partial discharge location in power transformers using the spectra of the terminal current signals', Conf. Record, 11th Int. Symp. on High-Voltage Engineering (London), Vol. 5, pp. 58-61, August 1999

[60] W Gao and K Tan, 'Effect of pulse propagation characteristics in power transformer on partial discharge recognition', Department of Electrical Engineering, Tsinghua University, Beijing 100084, China

[61] J P van Bolhuis, E Gulski, J J Smit, T Grun and M Turner, 'Comparison of conventional and VHF partial discharge detection methods for power transformers', Conf. Record, 11th Int. Symp. on High-Voltage Engineering (London), Vol. 5, pp. 49-52, August 1999

[62] D Wenzel, H Borsi and E Gockenbach, 'A measuring system based on modern signal processing methods for partial discharge recognition and localization on-site', Conf. Record, IEEE Int. Symp. on Electrical Insulation (Virginia), pp. 20-23, June 1998

[63] H Borsi, 'A PD measuring and evaluation system based on digital signal processing', IEEE Trans. on Dielectrics and Electrical Insulation, Vol. 7, No. 1, pp 21-29, February 2000

[64] M D Judd, O Farish and B F Hampton, 'Broadband couplers for UHF detection of partial discharge in gas-insulated substations', IEE Proceedings Science, Measurement and Technology, Vol. 142, No. 3, pp. 237-243,
May 1995

[65] M D Judd, 'Dielectric windows improve the sensitivity of partial discharge detection at UHF', Conf. Record, IEEE Int. Symp. on Electrical Insulation (Anaheim), pp. 304-307, April 2000

[66] B F Hampton, R J Meats, 'Diagnostic measurements at UHF in gas insulated substations', IEE Proc., Vol. 135, Part C, No.2, pp.137-144, March 1988

[67] M D Judd and O Farish, 'A pulsed GTEM system for UHF sensor calibration', IEEE Trans. Instrumentation and Measurement, Vol. 47, No. 4, pp. 875-880, August 1998

[68] S Meijer, E Gulski and J J Smit, 'Pattern analysis of partial discharges in SF_6 GIS', IEEE Trans. on Dielectrics and Electrical Insulation, Vol. 5, No. 6, pp. 830-841, December 1998.

[69] A G Sellars, O Farish and M M Peterson, 'UHF detection of leader discharges in SF_6', IEEE Trans. on Dielectrics and Electrical Insulation, Vol. 2, No. 1, pp.143-154, February 1995

[70] A G Sellars, O Farish and B F Hampton, 'Assessing the risk of failure due to particle contamination of GIS using the UHF technique', IEEE Trans. on Dielectrics and Electrical Insulation, Vol. 1, No. 2, pp 323-331, April 1994

[71] A G Sellars, O Farish, B F Hampton and L S Pritchard, 'Using the UHF technique to investigate PD produced by defects in solid insulation', IEEE Transactions on Dielectric and Electrical Insulation, Vol. 2, No. 3, pp. 448-459, June 1995

[72] M D Judd, O Farish, J S Pearson, T Breckenridge and B M Pryor, 'Power transformer monitoring using UHF sensors: installation and testing', Conf. Record, IEEE Int. Symp. on Electrical Insulation (Anaheim), pp. 373-376, April 2000

[73] W R Rutgers and Y H Fu, 'UHF PD-detection in a power transformer', Conference Record, 10th International Symposium on High Voltage Engineering (Quebec), pp. 219-222, August 1997

[74] W R Rutgers, P van den Aardweg, A Lapp and H G Kranz, 'Transformer PD measurements: field experience and automated defect identification, Kema Consulting, Utrechtseweg, Arnhem, The Netherlands (Paper received 2000)

[75] J M Wetzer, G J Cliteur, W R Rutgers and H F A Verhaart, 'Diagnostic and condition assessment – techniques for condition based maintenance', Conf. Record, IEEE Electrical Insulation and Dielectric Phenomena (Victoria BC), pp.47-51, 2000

[76] G P Cleary, M D Judd and O Farish, 'Investigation of partial discharge current pulses in transformer insulating oil', Conf. Record, International Conference on Advances in Processing, Testing and Application of Dielectric Materials (Wroclaw), pp. 50-53, September 2001

[77] M D Judd, G P Cleary and S Meijer, 'Testing UHF partial discharge detection on a laboratory based power transformer', Conf. Record, 13th Int. Symp. High Voltage Engineering (Delft), August 2003

[78] G P Cleary, M D Judd, B G Stewart, A Nesbitt and I J Kemp, 'Simultaneous measurement of PD activity using IEC60270 and UHF detection methods', Conf. Record, Proc. XIV International Conference on Gas Discharges and their Applications (Liverpool), Vol. 2, pp. 196-199, September 2002

[79] G P Cleary, M D Judd, B G Stewart, A Nesbitt and I J Kemp 'Analysis of partial discharge activity in air and transformer insulating oil using high bandwidth measurement techniques', IEE Proceedings Science, Measurement and Technology (to be submitted).

[80] G P Cleary, M D Judd and O Farish, 'Investigation of partial discharge in water contaminated oil insulation', Conference Record, International Conference on Advances in Processing, Testing and Application of Dielectric Materials (Wroclaw), pp. 373-376, September 2001

[81] G P Cleary and M D Judd, 'UHF and current pulse measurements of partial discharge activity in mineral oil', IEE Proceedings Science, Measurement and Technology, Submitted (July 2004).

[82] G P Cleary and M D Judd, 'An investigation of discharges in oil insulation using UHF PD detection', Conference Record, Proceedings of the 14th International Conference Dielectric Liquids, (Graz), pp. 341-344, July 2002

[83] G P Cleary and M D Judd, 'Interpretation of discharge activity in transformer insulating using UHF phase-resolved measurements' IEE Proceedings Science, Measurement and Technology (to be submitted)

[84] M D Judd, G P Cleary, C J Bennoch, J Pearson and T Breckenridge, 'Power transformer monitoring using UHF sensors: separating multiple discharge sources', Proc. IEEE International Symposium on Electrical Insulation (Boston), pp. 145-149, April 2002

[85] M D Judd, G P Cleary, C J Bennoch and J S Pearson, 'Power transformer monitoring using UHF sensors: site trials' IEEE Power Engineering Review, Vol. 22, Issue 8, pp. 57-59, August 2002

[86] D Linhjell, G Berg and L E Lundgaard, 'Streamers from a metallic particle between parallel electrodes in transformer oil', Conf. Record, Proc. of 13th Int. Conf. on Dielectric Liquids (Nara), pp. 175-278, July 1999

[87] J K Nelson, 'An assessment of the physical basis for the application of design criteria for dielectric structures', IEEE Trans. on Electrical Insulation, Vol. 24, No. 5, pp. 835 – 847, October 1989

[88] K Giese, 'Electrical strength of pressboard components for transformer insulations', DEIS Feature Article, Vol. 12, No.1, pp. 29 – 33, January/February 1996

[89] Kraus, *Electromagnetics*, pp.79-81,
3rd Edition, Mc Graw Hill

[90] Schaum, *Electromagnetics*, pp. 69 – 70,
2nd Edition, J. A. Edminister

[91] F T Ulaby, *Fundamentals of applied electromagnetic*s, pp. 56-58,
Prentice Hall.

[92] Central Semiconductor Corp. Technical Specification, 1.5KE18CA, www.centralsemi.com

[93] Tektronix Technical Specification, *CT-1/CT-2,* January 1992,

[94] S. A. Boggs, 'Partial discharge – part 2: detection sensitivity', IEEE Electrical Insulation Magazine, Volume 6, No. 5, pp. 35-42, September/October 1990

[95] 'Capacitive couplers for UHF partial discharge monitoring', Technical Guidance Note TGN (T), Issue 1, January 1997

[96] Diagnostic Monitoring Systems Ltd, Partial Discharge Monitor User's Guide

[97] M D Judd, 'Contact discharges as a source of sub-nanosecond high voltage pulses', Institute of Physics, Journal of Physics D: Applied Physics, pp. 2883–2893, 2001

[98] B F Hampton, 'UHF diagnostics for gas insulated substations', 11th Int. Symp. on High Voltage Engineering (London), Vol. 5, pp. 6-16, August 1999

[99] T J Lewis, *The electrical conduction and strength of pure liquids*, pp. 111-143, Alston High Voltage Technology, Oxford University Press, 1968

[100] P K Watson, W G Chadband and M Sadeghzadeh-Araghi, 'The role of electrostatic and hydrodynamic forces in the negative-point breakdown of liquid dielectrics', IEEE Trans. on EI-26, No. 4, pp. 543-559, August 1991

[101] H Borsi, 'Study about the physical processes leading to partial discharges in insulating fluids', ETEP, Volume 9, No. 6, pp. 363-367, November/ December 1999

[102] H Okubo, A Suzuki, T Kato, N Hayakawa and M Hikita, 'Frequency component of current pulse waveform in partial discharge measurement', 9th Int. Symp. on High Voltage Engineering (Graz), pp. 1-4, August/September 1995

[103] H Okubo, N Hayakawa and A Matsushita, 'The relationship between partial discharge current pulse waveform and physical mechanisms', DEIS Feature Article, IEEE Electrical Insulation Magazine, Vol. 18, No. 3, pp 38-45, May/June 2002

[104] G Vettese, M Libotte, M Pompili, C Mazzetti and E O Forster, 'Ultrahigh frequency study of PD pulses', Conf. Record, IEEE Int. Symp. on Electrical Insulation (Pittsburgh), pp 273-276, June 1994

[105] M Pompili, C Mazzetti and R Bartnikas, 'Simultaneous ultrawide and narrowband detection of PD pulses in dielectric liquids', IEEE Trans. on Dielectric and Electrical Insulation, Vol. 5, No. 3, pp 402-407, June 1998

[106] J. M. Meek and J. D Craggs, 'Electrical breakdown of gases', Chapters 2, 3 and 6, Oxford University Press, 1995 Edition

[107] T J Lewis, 'A new model for the primary process of electrical breakdown in liquids', IEEE Trans. on Dielectrics and Electrical insulation, Vol. 5, No. 3, pp. 306-315, June 1998

[108] K Siodla, W Ziomek and E Kuffel, 'The volume and area effect in transformer oil', Conf. Record, IEEE Int. Symp. on Electrical Insulation (Boston), pp. 359-362, April 2002

[109] R Morrow, 'Theory of electrical corona in SF_6', Nuclear Instruments and Methods in Physical Research, Electrostatics (A 382), pp. 57-65, 1996

[110] R Morrow, 'A parameter study of streamer propagation in SF_6', American Institute of Physics, Journal of Applied Physics, pp. 5171-5174, 1988

[111] R Morrow, 'Properties of streamers and streamer channels in SF_6', The American Physical Society, Vol. 34, No. 4, pp 1778-1785, February 1981

[112] P K Watson, 'Electrostatic and hydrodynamic effects in the electrical breakdown of liquids', Trans. on Electrical Insulation, Vol. EI-20, No. 2, pp. 395-399, April 1985

[113] O Lesaint and R Tobazeon, 'Study of the generation by sharp electrodes of a gaseous phase in dielectric liquids subjected to high ac or step voltages', IEEE Trans. on Electrical Insulation, Vol. EI-20, No. 2, pp. 269-273, April 1985

[114] L E Lundgaard, D Lihjell and G Berg, 'Streamers/leaders from a metallic particle between parallel plane electrodes in transformer oil', IEEE Trans. on Dielectrics and Electrical Insulation, Vol. 8, No. 6, pp. 1054 – 1063, December 2001

[115] A Beroual, M Zahn, A Badent, K Kist, A J Schwabe, H Yamashita, K Yamazawa, M Danikas, W G Chadband and Y Torshin, 'Propagation and structure of streamers in liquid dielectrics', DEIS Feature Article, IEEE Electrical Insulation Magazine, Vol. 14, No. 2, pp.6-17, 1998

[116] L Lundgaard, D Linhjell, G Berg and S Sigmond, 'Propagation of positive and negative streamers in oil with and without pressboard interfaces', IEEE Trans. on Dielectrics and Electrical Insulation, Vol. 5, No. 3, pp. 388-395, June 1998

[117] R Kattan, A Denat and O Lesaint, 'Generation, growth, and collapse of vapor bubbles in hydrocarbon liquids under a high divergent electric field', Institute of Physics, Journal of Physics D: Applied Physics, pp. 4062 – 4066, November, 1989

[118] H Akiyama, 'Streamer discharges in liquids and their applications', IEEE Trans. on Dielectrics and Electrical Insulation, Vol. 7, No. 5, pp. 646-653, October 2000

[119] A Beroual, 'Electronic and gaseous processes in the prebreakdown phenomena of dielectric liquids', Institute of Physics, Journal of Physics 73(9): Applied Physics, pp. 4528-4533, May 1993

[120] P K Watson, W G Chadband and W Y Mak, "Bubble growth following a localised electrical discharge and its relationship to the breakdown of triggered spark gaps in liquids", IEEE Transactions on Electrical Insulation, Vol. EI-20, No. 3, April 1985, pp. 275-280.

[121] W G Chadband and T M Sufiani, 'Experimental support for a model of positive streamer propagation in liquid insulation', IEEE Trans. on Electrical Insulation, Vol. EI-20, No. 2, pp 239-246, April 1985

[122] K Kist, Y Julliard, R Badent and A J Schwab, 'Streamers and percolation – a new theoretical approach', Conf. Record, Electrical Insulation and Dielectric Phenomena (Victoria BC), pp. 474-477, October 2000

[123] O Lesaint and G Massala, 'Positive Streamer Propagation in large oil gaps: experimental characterisation of propagation modes', IEEE Trans. on Dielectric and Electrical Insulation, Vol. 5, No. 3, pp. 360-370, June 1998

[124] H. Debruyne and O. Lesaint, 'On the significance of PD measurements in liquids', Conf. Record, 11th Int. Symp. on High Voltage Engineering (London), Vol. 5, pp. 45–48, August 1999

[125] G Wanninger, 'Apparent charge measurement in GIS by modern diagnostic methods', ETEP Vol. 7, No. 4, pp. 251-255, July/August 1997.

[126] I Herbst and R Pietsch, 'The fast and slow signal components of partial discharges in SF_6 measurements of the electron and ion contributions to PD-signal', IEEE Electrical Insulation (Pittsburgh), pp. 283 – 287, June 1994

[127] *BS148 Class 1 – 2512,*

Electrical Oil Services Ltd, Cheshire

[128] *Oil Analysis, Report No. 0146/0003/R/02/81408*

Ingenco

[129] M D Judd and O Farish, 'Transfer functions for UHF partial discharge signals in GIS, Conf. Record, 11th Int. Symp. High Voltage Engineering (London), pp. 74-77, August 1999

[130] A Beroual and J. Fleszyński, 'Pioneering contribution of Professor J. I. Skowronski and recent developments in prebreakdown and breakdown phenomena in liquid dielectrics', Conf. Record, Advances in Processing, Testing and Application of Dielectric Materials (Wrocław), pp. 4-18, September 2001

[131] S Meijer, E Gulski, J J Smit, F J Wester, T Grun and M Turner, 'Interpretation of PD GIS using spectral analysis', Conf. Record, 11th Int. Symp. on High Voltage Engineering (London), pp. 124-127, August 1999

[132] S Birlasekaran, 'The movement of a conducting particle in transformer oil in ac fields', IEEE Transactions on EI-28, No. 1, pp. 9-17, February 1993

[133] H Kurita, O Usui, T Hasegawa and H Fujii, 'Effect of particles on partial discharge inception in oil immersed insulating system', Conf. Record, Proc. 13th Int. Conf. on Dielectric Liquids (Nara), pp. 126-131, July 1999

[134] S Strachan, G Jahn, S McArthur and J R M^{c}Donald, 'Intelligent diagnosis of defects responsible for partial discharge activity detected in power transformers', Conf. Record, Proc. Intelligent System Applications in Power (Lemnos), 2003

[135] S D J McArthur, S M Strachan and G Jahn, 'The design of a multi-agent transformer conditioning monitoring system', IEEE Trans. in Power Systems, Vol. 19, No. 4, pp. 1845-1852, November 2004

[136] F H Kreuger, E Gulski and A Krivda, 'Classification of partial discharge', IEEE Trans. on EI-28, No. 6, pp. 917-931, December 1993.

[137] E Gulski, 'Computer-aided measurement of partial discharges in HV equipment', IEEE Trans. on EI-28, No. 6, pp. 969-983, December 1993

[138] E Gulski, 'Digital analysis of partial discharges', IEEE Trans. on Dielectric Insulation, Vol. 2, No. 5, pp. 822-837, October 1995

[139] F Berton and R Patsch, 'The role of space charges in PD – process' Conf. Record, Advances in Processing, Testing and Application of Dielectric Materials (Wrocław), pp. 139-142, September 2001

[140] R Patsch, M Hoof and C Reuter, 'Pulse-sequence analysis, a promising diagnostic tool', Conf. Record, 8th Int. Symp. High Voltage Engineering (Yokohama), pp. 157-160, August 1999

[141] K Raja, F Devaux and S Lelaidier, 'Recognition of discharge sources using UHF PD signatures', DEIS Feature Article, IEEE Electrical Insulation Magazine, Vol. 18, Issue 5, pp. 8-14, September/October 2002

[142] R J Van Brunt, E W Cernyar and P von Glahn, 'Importance of unravelling memory propagation effects in interpreting data on partial discharge statistics', IEEE Trans. on EI-28, No. 6, pp. 905-916, December 1993

[143] Y L Madhavi and M N Narayanachar, 'A study of memory effect of partial discharges', Conf. Record, 11th Int. Symp. High Voltage Engineering (London), pp. 305-308, August 1999

[144] G Berg and L E Lundgaard, 'PD signatures of wedge type discharges in transformer insulation', Conf. Record, 14th Int. Conf. on Dielectric Liquids (Graz), pp. 211 – 214, July 2002

[145] G Berg and L E Lundgaard, 'Discharges in combined transformer oil/paper insulation', Conf. Record, 13th Int. Conf. on Dielectric Liquids (Nara), pp. 144-147, July 1999

[146] A G Sellars, 'Interpreting the UHF signals produced by partial discharge activity in GIS', PhD thesis, University of Strathclyde, 1995

[147] R Altenburger, C Heitz and J Timmer, 'Analysis of phase-resolved partial discharge patterns based on a stochastic process approach', Institute of Physics, Journal of Physics D: Applied Physics, pp. 1149–1163, 2002

[148] B Fruth and L Niemeyer, 'The importance of statistical characteristics of partial discharge data', IEEE Trans. on EI-27, No. 1, pp. 60 – 69, February 1992

[149] T McGrail and P Jarman, 'Condition Assessment Tests - ScottishPower Neilston, SGT4 400/275 kV, 1000 MVA, Hackbridge Hewittic Transformer, Serial Number 218184', Engineering & Technology Report, National Grid Company plc, 21 June 1997

[150] M D Judd, 'Using finite difference time domain techniques to model electrical discharge phenomena', IEEE Conf. on Electrical Insulation and Dielectric Phenomena, (Victoria BC), Vol. 1, pp. 518-521, October 2000

12. BIBLIOGRAPHY

[1] T. O. Rouse, 'Mineral insulating oil in transformers', DEIS Feature Article, IEEE Electrical Insulation Magazine, pp. 6-16, 1998

[2] R. Murray, 'How to write a thesis', Open University Press, Maidenhead, 2002

[3] P H F Morshuis, 'Partial discharge mechanisms – mechanisms leading to breakdown, analysed by fast electrical and optical measurements', PhD Thesis, University of Delft, 1993

[4] S Meijer, 'Partial discharge diagnostics of high-voltage gas-insulated systems', PhD Thesis, Delft University Press – 2001

[5] J Hyde, 'Condition monitoring of high voltage power transformer insulation systems by partial discharge measurement', PhD thesis, Glasgow Caledonian University, 2000

[6] E Kuffel, W S Zaengl and J Kuffel, 'High Voltage Engineering: Fundamentals', 2nd Edition, Butterworth-Heinemann Press, 2000

[7] D Kind and K Feser, 'High Voltage Test Techniques', 2nd Edition, Reed Educational and Professional Publishing, 2001

[8] D M Pozar, 'Microwave Engineering', Addison-Wesley Publishing Company, 1990

[9] B F Hampton and A G Newlands, 'Detecting and locating partial discharges in metalclad equipment', Chapter 10: Testing and Reliability, Central Electricity Research Laboratories (Leatherhead)

[10] D A Nattrass, 'Partial discharge measurement and interpretation', IEEE Electrical Insulation Magazine, Vol. 4, No. 3, pp. 10-22, May/June 1998

[11] W S Zaengl and K Lehmann, 'A critique of present calibration procedures for partial discharge measurements', IEEE Trans. on EI-28, No. 6, pp.1043-1049, December 1993

[12] G Vettese, M Libotte, M Pompili and C Mazzeti, 'Ultrahigh frequency study of PD pulses', Conf. Record, IEEE Int. Symp. on Electrical Insulation (Pittsburgh), pp. 273-276, June 1994

[13] M D Judd and O Farish, 'High bandwidth measurement of partial discharge current pulses', Conf. Record, IEEE Int. Symp. on Electrical Insulation (Washington), Vol. 2, pp. 436-439, June 1998

[14] G Zingales, 'Present state and prospects of standardization on PD measurements', IEEE Trans. on EI-28, No. 6, pp. 902 –904, December 1993.

[15] A Khayari, A T Perez and A Castellanos, 'The charge acquired by a spherical ball bouncing on an electrode: comparison between theory and experiment', Conf. Record, Electrical Insulation and Dielectric Phenomena (Victoria B.C.), pp. 470-473, October 2000

[16] W R Rutgers, '*Method and Device for detecting partial discharge*', International Patent Classification- GOIR 31/12, HOIF 27/40, WO 98/44356

[17] S A Stigant and H M Lacey, 'The J & P Transformer Book', Johnson and Philips Ltd

[18] *Part 1: Power transformers*, IEC Publication 76

[19] R Kuppuswamy and S Lelaidier, 'Experience with UHF partial discharge measurements', Conf. Record, Proc. 14th Int. Conf. on Dielectric Liquids (Graz), pp 239-241, 2002

[20] Y V Torshin, 'On the existence of leader discharges in mineral oil', IEEE Trans. on Dielectric and Electrical Insulation, Vol. 2, No. 1, pp. 107-179, February 1995

[21] D Koch, 'SF_6 properties and uses in MV and HV switchgear' http://www.schneider-electric.com

13. PUBLICATIONS

1) **G P Cleary**, M D Judd and O Farish, 'Investigation of partial discharge current pulses in transformer insulating oil', Proc. Int. Conf. on Advances in Processing, Testing and Application of Dielectric Materials (Wroclaw), pp. 50-53, September 2001

2) **G P Cleary**, M D Judd and O Farish, 'Investigation of partial discharge in water contaminated oil insulation', Proc. Int. Conf. on Advances in Processing, Testing and Application of Dielectric Materials (Wroclaw), pp. 373-376, September 2001

3) M D Judd, **G P Cleary**, C J Bennoch, J S Pearson and T Breckenridge, 'Power transformer monitoring using UHF sensors: Site trials', Conf. Record of the 2002 IEEE Int. Symp. on Electrical Insulation (Boston), pp. 145-149, April 2002

4) **G P Cleary** and M D Judd, 'An investigation of discharges in oil insulation using UHF PD detection', Proc. 14th IEEE Int. Conf. On Dielectric Liquids (Graz), pp. 341-344, July 2002

5) M D Judd, **G P Cleary** and C J Bennoch, 'Applying UHF partial discharge detection to power transformers', IEEE Power Engineering Review, Vol. 22, Issue 8, pp. 57-59, August 2002

6) **G P Cleary**, M D Judd, B G Stewart, A Nesbitt and I J Kemp, 'Simultaneous measurement of PD activity using IEC60270 and UHF detection methods', Proc. XIV Int. Conf. on Gas Discharges and their Applications (Liverpool), Vol. 2, pp. 196-199, September 2002

7) **G P Cleary** and M D Judd, 'UHF and current pulse measurements of partial discharge activity in mineral oil', IEE Science, Measurements and Technology Journal, Submitted (July 2004)

8) M D Judd, **G P Cleary** and S Meijer, 'Testing UHF partial discharge detection on a laboratory based power transformer', Conf. Record, 13th Int. Symp. High Voltage Engineering (Delft), August 2003

9) **G P Cleary**, M D Judd, B G Stewart, A Nesbitt and I J Kemp 'Analysis of partial discharge activity in air and transformer insulating oil using high bandwidth measurement techniques', to be submitted to IEE Science, Measurements and Technology Journal

10) **G P Cleary** and M D Judd 'Interpretation of discharge activity in transformer insulating oil using UHF phase-resolved measurements', to be submitted to IEE Science, Measurements and Technology Journal